

**A Miniature Bio-inspired Locomotion Mechanism for  
an Intra-abdominal Adhesion-reliant Robot**

Alfonso Montellano López

Submitted in accordance with the requirements for the degree of  
Doctor of Philosophy

The University of Leeds  
School of Mechanical Engineering

May, 2013

The candidate confirms that the work submitted is his own, except where work which has formed part of jointly authored publications has been included. The contribution of the candidate and the other authors to this work has been explicitly indicated in Appendix A. The candidate confirms that appropriate credit has been given within the thesis where reference has been made to the work of others.

This copy has been supplied on the understanding that it is copyright material and that no quotation from the thesis may be published without proper acknowledgement.

The right of Alfonso Montellano López to be identified as Author of this work has been asserted by him in accordance with the Copyright, Designs and Patents Act 1988.

© 2013 The University of Leeds and Alfonso Montellano López

## Acknowledgements

The fruits of human work are the result of the goodwill of a community and the creative spirit that infuses all human action. I would like to thank here all the people that made this thesis possible and I hope to make the rest of my work an acknowledgement of that creative spirit, able to turn a mere sequence of actions into an act of love.

I would like to thank Anne Neville for her generosity and inspiration, and Rob Richardson and Abbas Dehghani for their supervision. Thanks also to Tony Wiese, Dave Readman, Abbas Ismail, Andrew Marsden and Graham Brown for their help. My fellow doctorands and friends have been a source of support and inspiration: مرسى Ali, Babak and Sina; شكرا Mohammed and Amr; 谢谢 Tee and Yusheng.

A mis padres les agradezco su constante apoyo y dedicación. Sin el espíritu culturalmente inquieto de mi madre, Gloria, y su pasión por el saber tal vez nunca hubiera sentido la curiosidad de la investigación. Sin la mentalidad serena e ingenieril de mi padre, Mariano, tal vez nunca hubiera aplicado tal curiosidad al desarrollo tecnológico. Y sin el amor paciente de ambos, tal vez nunca hubiera apreciado el valor de poner el conocimiento al servicio del ser humano y del bien común. A mi hermana, Cristina, y hermanos, Alejandro y Javier, les agradezco el haber crecido juntos.

With my friends I shared the joys and toils of PhD life: thank you Gwen, merci Omar, grazie Davide.

And with Ruth I shared the wonders and the beauty of life, thank you for your presence and your love.

*After having stated his three famous Laws of Robotics, Isaac Asimov felt they were insufficient to protect society at large. In 1985, Isaac Asimov created the Zeroth Law of Robotics, to which all other laws are subordinate:*

*“A robot may not injure humanity, or,  
through inaction, allow humanity to come to harm.”*

## **Abstract**

This thesis presents, explains and analyses a novel design of a locomotion mechanism for a miniature robot envisaged for assisting surgeons during minimally invasive procedures in abdominal surgery. Minimally invasive procedures have proved to be beneficial for hospitals and patients and are currently applied successfully in many surgical operations. Robotic arms mounted outside the body are currently used in order to move the surgical tools inside the body and some research prototypes move fully inside the abdomen. In order to fully realise the potential of minimally invasive robotic surgery, the robotic assistant should operate at a distance from intense surgical activity and attach to tissue, moving stably within the abdomen.

This thesis presents the conceptual design of a miniature robot which uses four adhesive pads to attach to the surface of the abdominal wall, a vantage point within the abdominal cavity. The adhesive pads use a micro-structured surface inspired by tree frogs in order to obtain smooth and repeatable attachment to biological tissue and enable the robot to move in inverted locomotion. The design of the locomotion mechanism of the robot also takes inspiration from tree frogs and geckoes in the way the pads are peeled off the tissue in order to detach them. Inspired by amoeboid locomotion, the robot detaches one pad at a time and changes the shape of the locomotion mechanism in the horizontal plane in order to move the pads across the tissue.

The implementation and testing of the robot resulted in a proof-of-concept prototype, able to move consistently using magnetic pads with an adhesion force similar to the bio-mimetic pads. The robot also managed to attach and move the pads while attached to tissue with the bio-mimetic pads. The analysis of the locomotion mechanism resulted in the definition of a peeling model for the adhesive pad, and a stability criterion and control strategies for adhesion-reliant robots.

## Table of Contents

<b>Acknowledgements.....</b>	<b>iii</b>
<b>Abstract.....</b>	<b>v</b>
<b>Table of Contents .....</b>	<b>vi</b>
<b>List of Tables .....</b>	<b>xiii</b>
<b>List of Figures .....</b>	<b>xiv</b>
<b>Chapter 1 Introduction.....</b>	<b>1</b>
1.1 Background .....	1
1.1.1 Laparoscopic Surgery .....	1
1.1.2 Advantages and challenges of laparoscopic surgery .....	2
1.2 Motivation.....	4
1.3 Research methodology .....	6
1.4 Aims and objectives .....	6
1.4.1 Aims .....	6
1.4.2 Objectives .....	6
1.5 Contributions of the thesis.....	7
1.6 Organisation of the thesis.....	7
<b>Chapter 2 Literature review .....</b>	<b>10</b>
2.1 Introduction .....	10
2.2 Miniature robotic systems.....	10
2.2.1 The size of robotic systems.....	10
2.2.2 Actuation technologies for miniature robots .....	12
2.2.3 Manufacturing challenges for miniature robots.....	17
2.3 Locomotion strategies for miniature robots .....	19
2.3.1 Wheels and tracks.....	19
2.3.2 Legs .....	21
2.3.3 Hybrid solutions.....	22
2.3.4 Inchworm and earthworm locomotion.....	23
2.3.5 Serpentine locomotion.....	25
2.3.6 Amoeboid locomotion.....	26
2.3.7 Climbing robots and bio-inspired attachment .....	28
2.4 Robotic systems in surgical applications .....	34
2.4.1 Surgical systems with robotic arms external to the body .....	35

2.4.1.1 Robotic holders of the laparoscope .....	36
2.4.1.2 Surgical robotic operators .....	37
2.4.1.3 Needle-guiding robots .....	38
2.4.1.4 Miniature and flexible surgical tools and cameras .....	38
2.4.2 Intra-body robots .....	41
2.4.2.1 Robots for the GI tract.....	42
2.4.2.2 The HeartLander robot for cardiac surgery .....	44
2.4.2.3 The Nebraska wheeled robot for abdominal surgery .....	45
2.5 Discussion of surgical robotic systems.....	46
2.6 Summary .....	50
<b>Chapter 3 Specifications and conceptual design of the robot .....</b>	<b>52</b>
3.1 Introduction .....	52
3.2 The environment of the robot: the insufflated abdomen .....	52
3.2.1 The human abdomen .....	52
3.2.2 The abdominal wall .....	54
3.2.3 The geometry of the insufflated abdomen .....	55
3.3 Advantages of an adhesion-reliant robot moving on the surface of the peritoneum.....	56
3.4 Challenges of intra-abdominal inverted adhesion-reliant locomotion.....	58
3.5 Design principles of a locomotion mechanism for an intra- abdominal adhesion-reliant robot .....	60
3.6 Selection of a locomotion strategy for an intra-abdominal adhesion-reliant robot .....	62
3.7 Design specifications for the intra-abdominal adhesion-reliant robot.....	67
3.8 Conceptual design of the intra-abdominal adhesion-reliant robot.....	68
3.9 Locomotion sequence of the intra-abdominal adhesion-reliant robot.....	69
3.10 Summary.....	71
<b>Chapter 4 Design and analysis of the robot .....</b>	<b>73</b>
4.1 Introduction .....	73
4.2 Kinematic design of the locomotion mechanism .....	73
4.3 Workspace of the individual pads and the robot.....	77
4.3.1 Workspace of the individual pads.....	78

4.3.2	Workspace of the robot .....	82
4.4	Dynamics of the pad moved by the locomotion mechanism.....	85
4.4.1	Dynamic model of the vertical motion of the pad.....	86
4.4.1.1	Dynamic model of the pad attached to the tissue....	86
4.4.1.2	Dynamic model of the detached pad.....	88
4.4.2	Dynamic model of the pad in the horizontal plane.....	89
4.5	Generation of the locomotion sequence.....	90
4.6	Adaptability of the locomotion mechanism to the surface of tissue.....	93
4.7	Summary .....	95
<b>Chapter 5</b>	<b>Implementation and testing of the robot .....</b>	<b>96</b>
5.1	Introduction .....	96
5.2	Miniature linear motors for the locomotion mechanism .....	96
5.3	Mechanical design and construction of the locomotion mechanism.....	99
5.3.1	Design and assembly of the components for the locomotion mechanism .....	101
5.3.2	Integration of the linear motor into the locomotion mechanism.....	103
5.4	Preliminary tests with the assembly of one prismatic joint and two prismatic joints.....	106
5.4.1	Implementation of a vertical prismatic joint.....	106
5.4.1.1	Manufacturing of the components for the prismatic joint .....	107
5.4.1.2	Miniature springs in order to provide a return force to the screw of the motor.....	118
5.4.2	Force measurements from a vertical prismatic joint .....	119
5.4.3	Force measurements from a vertical and a horizontal prismatic joint attaching and detaching the adhesive pad .....	123
5.4.3.1	Preload test with the vertical prismatic joint.....	124
5.4.3.2	Horizontal force test with the vertical and horizontal prismatic joints.....	125
5.5	First prototype of the robot .....	127
5.5.1	Walking performance of the robot following an open- loop locomotion sequence .....	128
5.5.2	System architecture for closed-loop control of the robot ..	131
5.5.3	Implementation of the closed-loop controller of the robot.....	135

5.5.4 Walking performance of the robot following a closed-loop locomotion sequence .....	137
5.5.5 Future improvements to the closed-loop controller .....	140
5.6 Second prototype of the robot .....	143
5.6.1 Enhancements to the components of the second prototype .....	144
5.6.2 Walking performance of the second prototype .....	147
5.6.3 Issues of the second prototype .....	149
5.6.4 Further improvements to the second prototype .....	150
5.6.5 Walking performance of the improved second prototype ..	153
5.7 Bio-inspired features of the locomotion mechanism .....	157
5.8 Summary .....	159
<b>Chapter 6 Peeling model of the adhesive pad .....</b>	<b>161</b>
6.1 Introduction .....	161
6.2 Premises of the peeling model .....	161
6.2.1 Young's modulus of the adhesive pad attached to tissue .....	162
6.2.2 Peeling-off of the adhesive pad .....	163
6.2.3 Bending of the adhesive pad .....	164
6.3 Formulation of the peeling model .....	165
6.3.1 Kendall's peeling theory .....	166
6.3.2 Peeling theory applied to the adhesive pad .....	167
6.3.3 Euler-Bernoulli's bending equations for a cantilever .....	170
6.3.4 Force to peel off the adhesive pad .....	173
6.3.5 Uniform load to peel off the adhesive pad .....	176
6.3.6 Moment to peel off the adhesive pad .....	179
6.3.7 Combination of uniform load and moment to peel off the adhesive pad .....	180
6.4 Calculations of peeling force, uniform load and moment for the bio-mimetic adhesive pad .....	183
6.4.1 Indentation test to calculate the work of adhesion of the pad .....	183
6.4.2 Force, uniform load and moment to peel the pad .....	186
6.4.3 Combination of uniform load and moment to peel the pad .....	189
6.4.4 Comparison between the peeling model and experimental results .....	190
6.5 Discussion and conclusion .....	192

6.6 Summary.....	193
<b>Chapter 7 Stability criterion for adhesion-reliant robots .....</b>	<b>195</b>
7.1 Introduction .....	195
7.2 Stability criteria for walking robots.....	195
7.2.1 Static stability criteria for walking robots.....	195
7.2.2 Dynamic stability criteria for walking robots.....	196
7.3 Stability criterion for adhesion-reliant robots walking upside-down .....	197
7.3.1 Supporting, moving and critical pads .....	198
7.3.2 Definition of the detachment margin of an adhesive pad..	199
7.3.3 Definition of the stability criterion for an adhesion-reliant robot .....	201
7.4 Stability analysis of a two-padded robot.....	201
7.4.1 Stability when the pad is detaching from the surface .....	203
7.4.2 Stability when the pad is detached.....	205
7.4.3 Stability when the pad moves across the surface .....	206
7.4.4 Stability when the pad moves toward or away from the surface .....	208
7.4.5 Stability when the pad is attaching to the surface .....	209
7.4.6 Design parameters for stable locomotion of the two-padded robot.....	211
7.4.7 Design parameters of a two-padded robot using the bio-mimetic adhesive pads.....	213
7.5 Stability analysis of a four-padded robot taking one step .....	214
7.6 Discussion and conclusion .....	217
7.7 Summary.....	217
<b>Chapter 8 Control strategies for adhesion-reliant robots.....</b>	<b>219</b>
8.1 Introduction .....	219
8.2 Stiffness model of the soft adhesive pad and the tissue.....	219
8.2.1 Advantages of using a soft pad to attach to tissue .....	219
8.2.2 Reference surface for the stretch and compression of the pad and tissue.....	220
8.2.3 Stiffness model of the pad attached to tissue in the vertical direction and the horizontal plane .....	221
8.3 Force and moment in the locomotion mechanism of a two-padded robot .....	224
8.3.1 Locomotion mechanism of a two-padded robot.....	224
8.3.2 Vertical force on the moving pad.....	225

8.3.3 Vertical force on the supporting pad.....	227
8.3.4 Horizontal force between the pads.....	228
8.3.5 Control strategies for a two-padded robot .....	230
8.4 Links and joints for a third pad .....	230
8.5 Force and moment in the locomotion mechanism of a robot with three pads in a line .....	231
8.5.1 Locomotion mechanism of a robot with three pads in a line .....	231
8.5.2 Vertical force on the detaching pad.....	234
8.5.3 Vertical force on the supporting pads.....	237
8.5.4 Force from the horizontal motor between the pads .....	238
8.5.5 Control strategies for a robot with three pads in a line .....	239
8.5.5.1 Strategies to reduce the force and moment on the supporting pads when the vertical motor of the detaching pad is actuated .....	239
8.5.5.2 Force and moment on the supporting pads when the vertical and horizontal motors of the robot are actuated .....	240
8.6 Force and moment in the locomotion mechanism of a robot with three pads in a triangle .....	241
8.6.1 Locomotion mechanism of a robot with three pads in a triangle .....	241
8.6.2 Vertical force on the detaching pad.....	244
8.6.3 Vertical force on the supporting pads.....	248
8.6.4 Force from the horizontal motor between the pads .....	250
8.6.5 Control strategies for a robot with three pads in a triangle .....	250
8.6.5.1 Strategies to reduce the force and moment on the supporting pads when the vertical motor of the detaching pad is actuated .....	251
8.6.5.2 Force and moment on the supporting pads when the vertical and horizontal motors of the robot are actuated .....	252
8.7 An adhesion-reliant robot with four pads forming a quadrilateral .....	254
8.8 Alternative designs for an adhesion-reliant robot with four adhesive pads forming a quadrilateral .....	256
8.9 An adhesion-reliant robot with more than four adhesive pads.....	258
8.9 Discussion and conclusions .....	259
8.10 Summary .....	260

<b>Chapter 9 Conclusions and future work .....</b>	<b>262</b>
9.1 Assessment of the research objectives .....	262
9.2 Discussion and conclusions .....	264
9.3 Future work .....	268
<b>List of references .....</b>	<b>272</b>
<b>Appendix A List of published conference papers and extended     abstracts, and journal papers in preparation .....</b>	<b>290</b>
<b>Appendix B The intra-abdominal robot in the media .....</b>	<b>292</b>

## List of Tables

<b>Table 1. Typical dimensions, force range and applications of macro-robots, miniature robots, micro-robots and nano-robots, adapted from [16].</b>	<b>11</b>
<b>Table 2. Actuation technologies for miniature robotics.</b>	<b>14</b>
<b>Table 3. Features and drawbacks of the manufacturing techniques used for miniature robots.</b>	<b>19</b>
<b>Table 4. Robotic systems reviewed for the design and implementation of an intra-abdominal miniature robot.</b>	<b>48</b>
<b>Table 5. Design specifications for the intra-abdominal adhesion-reliant robot.</b>	<b>67</b>
<b>Table 6. Tolerance validation of the front side of the mounting platform and ends supporter manufactured in Teflon<sup>®</sup> with a conventional CNC machine.</b>	<b>112</b>
<b>Table 7. Tolerance validation of the back side of the mounting platform and ends supporter manufactured in Teflon<sup>®</sup> with a conventional CNC machine.</b>	<b>113</b>
<b>Table 8. Tolerance validation of the front side of the mounting platform and ends supported manufactured in Delrin<sup>®</sup> with a precision CNC machine.</b>	<b>116</b>
<b>Table 9. Tolerance validation of the back side of the mounting platform and ends supported manufactured in Delrin<sup>®</sup> with a precision CNC machine.</b>	<b>117</b>
<b>Table 10. Blocked force obtained along the screw of the motor.</b>	<b>122</b>
<b>Table 11. Suitability of force sensing technologies for the locomotion mechanism of the robot.</b>	<b>143</b>
<b>Table 12. Comparison of the walking performance of the robot using magnetic pads on a steel surface and using adhesive pads on pig peritoneum.</b>	<b>149</b>
<b>Table 13. Walking performance of the improved second prototype of the robot using magnetic pads on a steel surface.</b>	<b>155</b>
<b>Table 14. Force and moment on the pads of a robot with three pads in a line when the vertical motor of the detaching pad is actuated.</b>	<b>236</b>
<b>Table 15. Force and moment on the pads of a robot with three pads in a triangle when the vertical motor of the detaching pad is actuated.</b>	<b>247</b>

## List of Figures

Figure 1. (a) Top view of a laparoscopic procedure compared to (b) a traditional open procedure [4]. (c) Side view of a laparoscopic operation, adapted from [5].	2
Figure 2. (a) Robotic system in the macro-scale: the iCub humanoid robot, (b) miniature robotic system: a bio-inspired flying robot [23] and (c) robotic system in the micro-scale: bacteria-inspired swimming micro-robot [30].	12
Figure 3. (a) Components of an intra-abdominal camera using DC mini-motors and (b) assembled prototype of the device [56].	15
Figure 4. (a) Miniature linear piezo-electric motor and (b) prototype of an intra-body robot using piezo-electric motors to move on the surface of the heart [59].	16
Figure 5. (a) Components of an SMA-actuated robotic endoscope and (b) the assembled robot [60].	16
Figure 6. (a) Layers of an IPMC micro-pump and (b) photograph of the micro-pump [64].	17
Figure 7. (a) The wheeled miniature robots Alice [20] and (b) a tracked miniature climbing robot [69].	20
Figure 8. (a) The miniature biped BRAT [72] and the educational miniature hexapod Stiquito [73].	21
Figure 9. (a) The robot AZIMUT combines wheel, legs and tracks and can (b) climb stairs, (c) stand on four legs and (d) move along an inclined surface [74].	22
Figure 10. Mini-whegs <sup>TM</sup> with different types of wheel-legs climbs glass (a), polystyrene (b) and concrete (c) [75].	23
Figure 11. (a) Sketch of inchworm locomotion in a robotic colonoscope and (b) prototype of the robotic colonoscope moving in an inchworm fashion, both images from [60].	24
Figure 12. (a) Sketch of earthworm peristaltic locomotion (©Pearson Education, Inc.) and (b) prototype of a robot using peristaltic locomotion [77].	25
Figure 13. (a) Schematic illustrating a flexible endoscope with seven degrees of freedom, (b) demonstration of the flexibility of the endoscope when exploring a simulated abdomen, both images are taken from [83], and (c) the snake-like robot Slim Slime [79].	26
Figure 14. (a-c) Three moments of the motion of an amoeba extending the pseudopods circled in (a) changing the shape of its central body, the three images are ©Dr. R. Wagner.	27

Figure 15. (a) Soldering climbing robot using magnets for attachment and (b) a wall climbing robot using suction pads.....	28
Figure 16. Gecko adhesive hierarchical structures [96].	30
Figure 17. (a) Snapshots of gecko attachment and (b) snapshots of gecko detachment from a glass ceiling [98].	31
Figure 18. Stickybot uses gecko-inspired adhesive pads and mimics the locomotion mechanism of geckoes [100].	31
Figure 19. The climbing robot Tankbot uses tracks with gecko-inspired adhesive belts [99] and (b) Waalbot uses whlegs with gecko-inspired adhesive pads [104].	32
Figure 20. (a) Tree frog adhesion: (b) structure found on the toes of the tree frog, (c) micro-pillars forming the structure of the toes [106] and (d) replicated micro-pillars to obtain wet adhesion [9].	33
Figure 21. (a) The laparoscopic camera holder AESOP® and (b) Freehand®	37
Figure 22. (a) The Robin Heart system for cardiac surgery [122] and (b) the MiroSurge system for laparoscopic surgery (b) [123].	38
Figure 23. The Pathfinder needle guiding robot for neurosurgery[127].	38
Figure 24. (a) An articulated laparoscopic instrument (EndoWrist, Intuitive Surgical Inc.) and (b) robotic system with miniature arms for laparoscopy [130].	39
Figure 25. (a-d) Robotic platform with flexible arms and camera operating in the abdomen [131].	40
Figure 26. (left, a-d) Photos of a miniature <i>in vivo</i> robot operating from the abdominal wall [134] (right, a-d) endoscope using magnetic levitation [90].	40
Figure 27. (a) Workstation and (b) probe of a robotic system for colonoscopy [136].	42
Figure 28. (a) Pill with a camera for exploration of the gastrointestinal tract and (b and c) stop mechanism for this kind of pills: (b) with the legs folded and (c) with the legs unfolded [62].	43
Figure 29. (a) Instrumentation boxes (left), vacuum pump (upper right), and tethered crawling robot (lower right) of the HeartLander robotic system [59] and (b) the latest prototype of the robot [143].	44
Figure 30. (a) The Nebraska wheeled robot with a camera and biopsy tweezers and (b) the robot moving around the abdominal organs [145].	45
Figure 31. (a) Muscles of the human abdomen and (b) organs in the abdominal cavity [149].	53

<b>Figure 32. (a) View of the peritoneum and abdominal organs from a laparoscopic camera and (b) view from a laparoscopic camera showing the liver and the colon. ....</b>	<b>53</b>
<b>Figure 33. (a-b) Stills from a laparoscopic camera of the abdominal cavity during an operation. ....</b>	<b>54</b>
<b>Figure 34. (a) Position of the robot inside the abdominal cavity and (b) composition of the abdominal wall, adapted from [8].....</b>	<b>54</b>
<b>Figure 35. Topography of the surface of mouse peritoneum [8].....</b>	<b>55</b>
<b>Figure 36. Geometry of the insufflated abdomen (not to scale).....</b>	<b>56</b>
<b>Figure 37. Sketch of a surgical tool inserted into the abdominal cavity through a fixed port. ....</b>	<b>57</b>
<b>Figure 38. Sketch of an intra-abdominal robot moving on the surface of the abdominal organs.....</b>	<b>58</b>
<b>Figure 39. Sketch of an intra-abdominal robot moving on the surface of the peritoneum. ....</b>	<b>58</b>
<b>Figure 40. (a) Sketch of a legged walking robot, (b) sketch of a wheeled robot and (c) sketch of a tracked robot moving in inverted adhesion-reliant locomotion on the surface of tissue.....</b>	<b>63</b>
<b>Figure 41. (a) Sketch of a Cartesian walker and (b) sketch of a polar walker for adhesion-reliant inchworm locomotion. The Cartesian walker positions the adhesive pads along X and Y coordinates; the polar walker positions the pads along r and <math>\theta</math> coordinates.....</b>	<b>64</b>
<b>Figure 42. Arrangement of the pads and motors in a Cartesian walker with four adhesive pads. ....</b>	<b>68</b>
<b>Figure 43. Locomotion sequence of the intra-abdominal robot using adhesive pads.....</b>	<b>71</b>
<b>Figure 44. (a) Locomotion mechanism with four pads and four motors in the horizontal plane and (b) rotary joint linking the horizontal motors.....</b>	<b>74</b>
<b>Figure 45. (a) Locomotion mechanism in the horizontal plane and (b) side view of the mechanism showing the vertical motors connected to the pads. ....</b>	<b>75</b>
<b>Figure 46. (a) Kinematic joints of the locomotion mechanism with hinges connecting the vertical motors to the horizontal motors, (b) detail of a hinge, (c) kinematic joints of the mechanism with rigid connections between the vertical motors and the horizontal motors, and (d) detail of a rigid connection.....</b>	<b>76</b>
<b>Figure 47. Narrowing of the width of the robot enabled by the passive rotary joints. ....</b>	<b>77</b>

Figure 48. (a) Locomotion mechanism in the horizontal plane and (b) workspace of the robot defined by the workspace of the pads.....	78
Figure 49. The locomotion mechanism moving pad 1 to a new position, supported by the other three pads. ....	79
Figure 50. Geometrical parameters used in order to calculate the workspace of the pad. ....	79
Figure 51. Workspace of pad 1 moving in the horizontal plane.....	81
Figure 52. Workspace of the robot defined by the workspace of the four pads. ....	83
Figure 53. Three-dimensional workspace of the pad of the robot. ....	85
Figure 54. Dynamic model of the locomotion mechanism in the vertical direction when pad 1 is attached to the tissue. ....	86
Figure 55. Dynamic model of the locomotion mechanism in the vertical direction when pad 1 is detached. ....	89
Figure 56. (a) Dynamic model of the locomotion mechanism in the horizontal plane when pad 1 is detached and (b) detail of the two motors moving pad 1 in the horizontal plane.....	90
Figure 57. (a 1-4) Locomotion sequence of pad 1 in the vertical direction and (b 1-4) locomotion sequence of pad 1 in the horizontal plane.....	91
Figure 58. Sequence of detachment, motion and re-attachment of the four pads of the robot in order for the robot to take a step forward.....	92
Figure 59. (a) Soft pad moulding to the irregularities of the tissue, (b) soft pad moulding to the inclination of the tissue and (c) the vertical motors move the pads to different heights. The rotation of the sketched pads is due to the passive twist of the pads in contact with an irregularity (in a) and an inclined surface (in b).....	94
Figure 60. (a) Front view, (b) top view and (c) 3D view of the Squiggle <sup>®</sup> motor [35]. ....	97
Figure 61. The piezo-electric (PZT) plates, nut and screw of the Squiggle <sup>®</sup> motor. ....	98
Figure 62. (a) Voltage signal sent to the four piezo-electric plates of the Squiggle <sup>®</sup> motor and (b) vibration caused by the voltage signal on the nut [155]. ....	98
Figure 63. (a) Top view and (b) 3D view of the linear magnetic encoder Tracker <sup>®</sup> [156]. ....	99
Figure 64. Top view of the CAD model of the robot. ....	99
Figure 65. (a) CAD model of the robot and (b) detail of one corner of the locomotion mechanism. ....	100

<b>Figure 66. (a) Prismatic and rotary joints of the locomotion mechanism and (b) housing and shaft of the linear motor in a prismatic joint moving a pad.....</b>	<b>101</b>
<b>Figure 67. (a) Sketch of a prismatic joint and (b) CAD model of a prismatic joint.....</b>	<b>102</b>
<b>Figure 68. (a) CAD model of the mounting platform of the prismatic joint controlled by the motor, (b) ends supporter of the prismatic joint and (c) assembly of the prismatic joint. ....</b>	<b>102</b>
<b>Figure 69. (a) Vertical prismatic joint connected to a horizontal prismatic joint and (b) assembly of two horizontal prismatic joints and one vertical prismatic joint.....</b>	<b>103</b>
<b>Figure 70. (a) Contact between the shaft of the motor and the ends supporter and (b) angle between the shaft and the ends supporter. ....</b>	<b>104</b>
<b>Figure 71. Contact between the surface of the holes in the mounting platform and the guiding rods. ....</b>	<b>105</b>
<b>Figure 72. Position of the springs for the return force on the shaft of the motor within the assembly of the prismatic joint. ....</b>	<b>106</b>
<b>Figure 73. CAD model of the vertical prismatic joint with a slot to attach the assembly to a load cell. ....</b>	<b>107</b>
<b>Figure 74. (a) Ends supporter (ES) and mounting platform (MP) manufactured in Teflon<sup>®</sup> with conventional CNC machining, (b) ES and MP manufactured in Teflon<sup>®</sup> with precision CNC machining and (c) ES and MP manufactured in Delrin<sup>®</sup> with precision CNC machining. ....</b>	<b>108</b>
<b>Figure 75. Drawing of the mounting platform manufactured using conventional CNC machining. The tolerances shown in the drawing were determined using an ISO table of tolerances for the type of fit required for each part of the mechanism. ....</b>	<b>109</b>
<b>Figure 76. Critical dimensions of the mounting platform. ....</b>	<b>110</b>
<b>Figure 77. Drawing of the ends supporter manufactured using conventional CNC machining. The tolerances shown in the drawing were determined using an ISO table of tolerances for the type of fit required for each part of the mechanism. ....</b>	<b>110</b>
<b>Figure 78. (a) Critical dimensions of the ends supporter and (b) critical dimensions of the mounting platform and the ends supporter affecting the alignment of the guiding rods within the assembly. ....</b>	<b>111</b>
<b>Figure 79. Drawing of the mounting platform manufactured using precision CNC machining. The tolerances shown in the drawing were determined using an ISO table of tolerances for the type of fit required for each part of the mechanism. ....</b>	<b>114</b>

<b>Figure 80. Drawing of the ends supporter manufactured using precision CNC machining. The tolerances shown in the drawing were determined using an ISO table of tolerances for the type of fit required for each part of the mechanism. ....</b>	<b>115</b>
<b>Figure 81. Position of the compression springs within the prismatic joint in order to apply a return force to the screw of the motor. ....</b>	<b>118</b>
<b>Figure 82. Experimental set-up for the blocked force test of the prismatic joint.....</b>	<b>120</b>
<b>Figure 83. Blocked force obtained from the prismatic joint for twelve points along the screw of the motor. The top figure shows the increment of force obtained when voltage is applied to the motor while the motor is blocked (blocked force) for the first six points along the screw of the motor. The figure at the bottom shows the blocked force obtained for the last six points along the screw of the motor. ....</b>	<b>121</b>
<b>Figure 84. CAD model of the set-up to test the vertical and horizontal prismatic joints attaching and detaching the adhesive pad. ....</b>	<b>123</b>
<b>Figure 85. Force applied by the vertical prismatic joint to the adhesive pad in order to test different values of preload.....</b>	<b>124</b>
<b>Figure 86. Effect of preload on the adhesion force between the adhesive pad and the tissue. ....</b>	<b>125</b>
<b>Figure 87. Force applied by the vertical and horizontal prismatic joints on the adhesive pad in order to test the effect of applying a horizontal force.....</b>	<b>126</b>
<b>Figure 88. (a) First prototype of the robot manufactured in ABS plastic with a 3D printer, (b) detail of the horizontal prismatic joint and (c) detail of the vertical prismatic joint.....</b>	<b>127</b>
<b>Figure 89. Comparison between the detachment force of the adhesive pad against rat peritoneum and the magnetic pad against steel. ....</b>	<b>129</b>
<b>Figure 90. (a-i) The first prototype of the robot walking one step, following an open-loop locomotion sequence. ....</b>	<b>131</b>
<b>Figure 91. Closed-loop control system architecture of the robot.....</b>	<b>132</b>
<b>Figure 92. Data flow and communication between the three levels of the closed-loop controller of the robot.....</b>	<b>134</b>
<b>Figure 93. The two control loops of the closed-loop controller of the robot implemented in LabVIEW.....</b>	<b>136</b>
<b>Figure 94. User interface of the closed-loop controller of the robot programmed in LabVIEW 2009.....</b>	<b>137</b>
<b>Figure 95. Prototype of the robot tested with the closed-loop controller using magnetic pads on a steel surface.....</b>	<b>138</b>
<b>Figure 96. Timing of the three levels of the locomotion controller.....</b>	<b>139</b>

<b>Figure 97. Second prototype of the robot in Nylon 6, rapid-prototyped with an SLS machine.....</b>	<b>144</b>
<b>Figure 98. Slots on one side of the ends supporter to enable self-alignment of the guiding rods.....</b>	<b>145</b>
<b>Figure 99. (a) Open holes in the mounting platform and (b) mounting platform with open holes in a horizontal prismatic joint. ....</b>	<b>146</b>
<b>Figure 100. (a) Soft backing layer of the pad using memory foam and (b) soft backing layer of the pad using three stacked layers of foam.....</b>	<b>146</b>
<b>Figure 101. (a-d) Second prototype of the robot detaching, moving and re-attaching one magnetic pad on a steel surface.....</b>	<b>147</b>
<b>Figure 102. The second prototype of the robot hanging from pig peritoneum using the bio-mimetic adhesive pads. The tissue sample was glued to a steel plate and the adhesive pads were mounted on top of the magnetic pads. The pads were tested in order to check that the magnetic force had no effect through the peritoneum sample. ....</b>	<b>148</b>
<b>Figure 103. (a) Side view of the brackets for extra support of the pads and (b) top view of the brackets. ....</b>	<b>151</b>
<b>Figure 104. The slotted holes in the mounting platform.....</b>	<b>152</b>
<b>Figure 105. (a) The two separate parts of the ends supporter, and (b) ends supporter with two separate parts in a vertical prismatic joint.....</b>	<b>152</b>
<b>Figure 106. (a-m) Walking sequence of the improved second prototype using magnetic pads on a steel plate.....</b>	<b>155</b>
<b>Figure 107. (a-g) The improved second prototype of the robot detaching and moving one adhesive pad on fresh pig peritoneum.....</b>	<b>156</b>
<b>Figure 108. (a-l) The locomotion mechanism detaching the magnetic pad by peeling it off from a steel surface.....</b>	<b>158</b>
<b>Figure 109. (a-c) The locomotion mechanism moving the pad in the horizontal plane by changing the shape of the quadrilateral formed by the horizontal prismatic joints. ....</b>	<b>159</b>
<b>Figure 110. (a) Prototype of the robot and (b) adhesive pad and soft foam moved by a linear motor within a vertical prismatic joint. ....</b>	<b>162</b>
<b>Figure 111. (a-f) Locomotion mechanism of the robot peeling off the pad. ....</b>	<b>164</b>
<b>Figure 112. (a) Pad detaching from the surface and (b) sketch of the pad peeling off the surface and bending like a cantilever. ...</b>	<b>165</b>
<b>Figure 113. Kendall's peeling test [167]. ....</b>	<b>166</b>

Figure 114. Vertical motor of the robot applying a force to the edge of the adhesive pad. ....	168
Figure 115. Vertical motor of the robot applying a uniform load to the adhesive pad.....	169
Figure 116. Horizontal motor of the robot applying a moment to the adhesive pad.....	169
Figure 117. Combination of a uniform load applied by the vertical motor and a moment applied by the horizontal motor to the adhesive pad. ....	170
Figure 118. Force applied at the free end of a cantilever.....	171
Figure 119. Uniform load applied along the length of a cantilever. ....	171
Figure 120. Moment applied at the free end of a cantilever.....	172
Figure 121. (a) Vertical motor of the robot applying a force to the edge of the pad and (b) sketch of the pad peeling when a force is applied to the edge of the pad.....	174
Figure 122. Variation of the polynomial $lFx, L$ along the length of the adhesive pad for a total length of the pad of $L = 1\text{ cm}$ .....	175
Figure 123. (a) Vertical motor of the robot applying a uniform load to the pad and (b) sketch of the pad peeling when a uniform load is applied to the pad. ....	177
Figure 124. Variation of $lqx, L$ along the length of the pad for $L = 1\text{ cm}$ . ....	178
Figure 125. (a) Horizontal motor of the robot applying a moment to the pad and (b) sketch of the pad peeling when a moment is applied to the pad. ....	180
Figure 126. (a) Combination of uniform load and moment applied to the adhesive pad and (b) sketch of the pad peeling when uniform load and moment are applied to the pad. ....	182
Figure 127. Work of adhesion of the pad from the force-distance graph of an indentation test taken from [8]. ....	184
Figure 128. (a-f) Events of an indentation test for the adhesive pad shown below a force-displacement graph from [8].....	185
Figure 129. Comparison of the force required in order to peel off the pad with a uniform load (see configuration in Figure 123), a force at the edge of the pad (see configuration in Figure 121) and a moment: force at 2cm from the pad (see configuration in Figure 125). The weight of the pad is shown as a reference value, as it is the minimum force the adhesive pad must support.....	187
Figure 130. Uniform load to peel off the pad when only the adhesive surface is bending for several values of thickness of the pad.....	188

Figure 131. Uniform load to peel off the pad when only the tissue is bending for several values of thickness of the tissue. ....	189
Figure 132. Combination of peeling uniform load and moment applied to the pad. ....	190
Figure 133. (a) Force-displacement graph comparing the peeling force and peeling uniform load of the bio-mimetic adhesive pad, and (b) force-displacement graph comparing the peeling force at 0° and 45°, adapted from [169]. ....	191
Figure 134. Sketch of the support polygon and stability margin of a walking robot with one leg in the air. ....	196
Figure 135. Supporting pads and moving pad of the robot.....	198
Figure 136. Sketch of a robot with two adhesive pads. ....	202
Figure 137. (a-g) Locomotion sequence of the two-padded robot.....	202
Figure 138. Force and moment on the pads of the robot when one pad is detaching from the surface. The force shown on the sketch is the force applied at the bottom of the detaching pad by the right vertical motor. The moment shown on the sketch is the moment felt at the top of the supporting pad.....	204
Figure 139. Force and moment on the pads of the robot when one pad is detached from the surface. ....	205
Figure 140. Force and moment on the pads of the robot when the horizontal motor is moving the pad across the surface.....	206
Figure 141. Force and moment on the pads of the robot when the vertical motor is moving the pad toward or away from the surface. ....	208
Figure 142. Force and moment on the pads of the robot when the vertical motor is preloading the pad in order to re-attach it to the surface.....	210
Figure 143. Calculation of the design parameters for a two-padded robot.....	212
Figure 144. (a-e) Locomotion sequence of a four-padded robot. ....	214
Figure 145. Theoretical simulation of the force applied to the pads, detachment margin of the pads and the stability margin of the robot during the locomotion sequence of the four-padded robot.....	216
Figure 146. (a) Soft pad making contact with tissue and (b) hard pad making contact with tissue.....	220
Figure 147. (a) Force-displacement graph from an indentation test of the adhesive pad, (b) pad and tissue on the force sensor for the indentation test, and (c) pad and tissue on the abdominal wall. ....	221

Figure 148. (a) Model of the soft pad and tissue as a linear spring in the vertical direction; $F_z$ is the vertical force applied to the pad. (b) Model of the soft pad and tissue as two torsion springs in the horizontal plane; $M_x$ and $M_y$ are the moments applied around the two directions of the horizontal plane.....	222
Figure 149. (a) Soft pad attached to the tissue, (b) linear springs modelling the stiffness of the pad and the tissue in the vertical direction, (c) torsion springs modelling the stiffness of the pad and the tissue in the horizontal plane.....	223
Figure 150. (a) Sketch of a two-padded robot, (b) model of the soft pad attached to tissue in the vertical direction and (c) model of the soft pad attached to tissue in the horizontal plane.....	225
Figure 151. (a) Free body diagram of the force on the supporting pad and the detaching pad when vertical force is applied to the moving pad, and (b) free body diagram of the moment on the supporting pad and the detaching pad when vertical force is applied to the moving pad.....	226
Figure 152. Free body diagram of the forces (a) and moments (b) in a two-padded robot when the vertical motor of the supporting pad is actuated. ....	228
Figure 153. (a) Torsion springs modelling the moving pad and the supporting pad and (b) free body diagram of the moment on the supporting pad and the detaching pad when the horizontal motor is actuated. ....	229
Figure 154. (a) Radial link between the third pad and the moving pad, (b) perimetric link between the third pad and the supporting pad, and (c) revolute joint connecting the links between the third pad and the moving and supporting pad. ....	231
Figure 155. (a) Sketch of the robot with three pads in a line, (b) three springs in parallel modelling the three pads in the vertical direction, and (c) three torsion springs modelling the bending of the pads in the horizontal plane.....	232
Figure 156. (a) Stretch caused on supporting pad 2 by the bend on supporting pad 1 when the vertical motor of the detaching pad is actuated and (b) stretch caused on supporting pad 1 by the bend on supporting pad 2 when the vertical motor of the detaching pad is actuated.....	234
Figure 157. (a) Free body diagram of the force on the supporting pads and the detaching pad when vertical force is applied to the moving pad, and (b) free body diagram of the moment on the supporting pads and the detaching pad when vertical force is applied to the moving pad.....	235

<b>Figure 158. (a) Force applied to the detaching pad and supporting pads when the vertical motor of the detaching pad is actuated and (b) moment applied to the detaching pad and supporting pads when the vertical motor of the detaching pad is actuated.....</b>	<b>236</b>
<b>Figure 159. (a) Sketch of a robot with three pads in a triangle, (b) two-padded mechanism formed by pads 1 and 3, (c) two-padded mechanism formed by pads 1 and 2 and (d) two-padded mechanism formed by pads 2 and 3.....</b>	<b>242</b>
<b>Figure 160. (a) Linear springs modelling the stiffness of the pads in the vertical direction, (b) torsion spring modelling the bending of pad 3 and (c) torsion springs modelling the bending of pad 2. ....</b>	<b>243</b>
<b>Figure 161. (a) Free body diagram of the force on the supporting pads when vertical force is applied to the moving pad, and (b) free body diagram of the moment on the supporting pads when vertical force is applied to the moving pad. ....</b>	<b>245</b>
<b>Figure 162. (a) Force applied to the pads and when the vertical motor of the detaching pad is actuated, (b) moment applied to the supporting pads in the X direction and (c) moment applied to the supporting pads in the Y direction.....</b>	<b>248</b>
<b>Figure 163. (a) Sketch of a robot with four pads, (b) a robot with four pads can be analysed as a robot with three pads in a line and (c) a robot with four pads can be analysed as a robot with three pads in a triangle.....</b>	<b>255</b>
<b>Figure 164. Prototype of a robot with two pads detaching one pad... </b>	<b>256</b>
<b>Figure 165. (a) Sketch of a four-padded robot with diagonal links unconnected at the centre of the quadrilateral, (b) four-padded robot with diagonal links connected at the centre of the quadrilateral, (c) prismatic joint at the connection of the diagonal links, and (d) prismatic and revolute joint at the connection of the diagonal links. ....</b>	<b>257</b>
<b>Figure 166. (a) Sketch of a robot with five pads, (b) sketch of a robot with six pads, (c) diagonal links for a five-pads robot and (d) diagonal links for a six-pads robot.....</b>	<b>258</b>
<b>Figure 167. (a) A robot with asymmetric diagonal links, (b) a robot with a pad in the centre of the mechanism, (c) a robot with satellite pads and (d) a robot with concentric rings of pads.....</b>	<b>259</b>

# Chapter 1

## Introduction

### 1.1 Background

Machines and robots have contributed to the well-being of society by facilitating the development of human activity in many fields, from industrial production to healthcare. Robots can enhance the skills of human beings and extend them beyond the limits of their capability, for example, into the fields of space exploration or nano-manipulation. In an era where technology is becoming omnipresent and society more reliant on it, it is an important and often difficult task to set the limits and purpose of this rapidly advancing technology. Human-centred technology seeks to enhance human relations within society and with the environment rather than substitute these relations. In this way, human-centred technology provides a frame of reference in which robots can help humans and share their space in harmony with nature. The role of robotic assistants in Medicine [1] is a perfect example of the significant potential of human-robot interaction.

Nature has always been a great source of inspiration for humans in artistic and scientific expression. Over the last decade, copying nature has evolved from a trend in engineering design to an established methodology to provide solutions to technological challenges [2, 3]. The natural world gives ideas for engineering solutions in challenging environments like inside the human body. One field that requires innovative solutions due to the characteristics of its environment and application and therefore can greatly benefit from bio-inspiration is laparoscopic surgery.

#### 1.1.1 Laparoscopic Surgery

In conventional surgery, the surgeon cuts an incision and clamps it open in order to expose the surgical area. The surgeon then uses conventional tools (scalpel, clamp, scissors) to perform the operation and, when the operation is finished, sutures the incision to close it. In this type of intervention the surgeon can directly see the operating area and can freely manoeuvre the tools around it.

A different way of performing a surgical operation is laparoscopic surgery. Laparoscopic surgery is performed through small incisions in the abdominal wall. The abdomen is filled with carbon dioxide to create an operating space

and the tools are long and thin to fit through the small incisions and reach the organs in the abdomen. A camera, or laparoscope, is also inserted in the abdomen to guide the operation.

Prof David G. Jayne explains the benefits of reducing the size of the surgical incision: “The bigger the surgical incision the more trauma is caused to the skin and tissue of the patient. In clinical practice this is evident in the pain experienced by patients following conventional open surgery as compared to laparoscopic surgery. Reduction in the size of the surgical access wound also has benefits in terms of reduction in wound complications; the incidence of wound infection and incisional herniation are much reduced following laparoscopic surgery as compared to open surgery. This translates into enhanced recovery for the patient and reduced costs for healthcare providers in treating wound complications.”

Figure 1 compares the set-up of a laparoscopic procedure (Figure 1a) to a conventional one (Figure 1b). In Figure 1a, the laparoscope is inserted through the umbilicum in order to provide visual feedback of the abdominal cavity and the tools are inserted through the ports placed around the surgical target. Figure 1b shows the open incision exposing the surgical target used in conventional surgery. Figure 1c illustrates the operation of the tools and laparoscope inside the insufflated abdomen. In Figure 1c, the operation is performed through three small incisions. The laparoscope is inserted through one of the incisions and the tools manipulate the organs through the other two incisions.

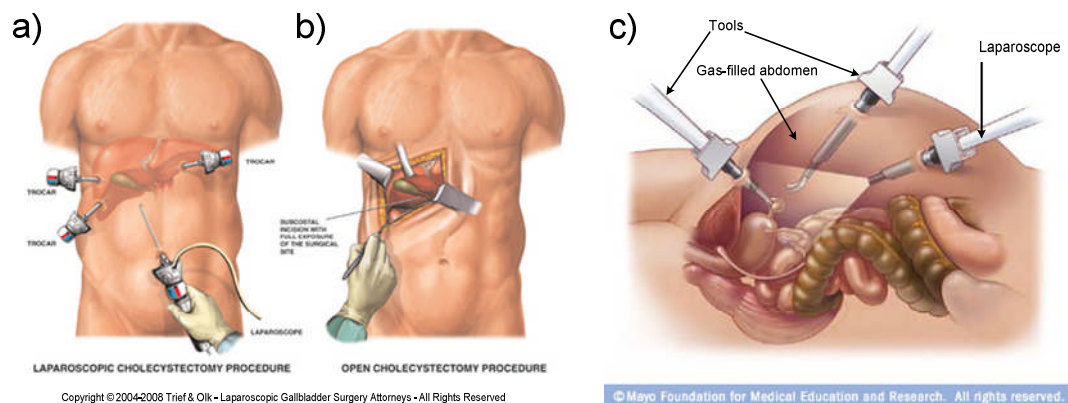


**Figure 1. (a) Top view of a laparoscopic procedure compared to (b) a traditional open procedure [4]. (c) Side view of a laparoscopic operation, adapted from [5].**

### **1.1.2 Advantages and challenges of laparoscopic surgery**

Laparoscopic surgery is increasingly becoming a standard approach in modern surgical interventions because it has clear advantages for patients

and hospitals. Smaller incisions mean less trauma, better cosmesis, quicker recovery and less post-operative pain [6, 7]. In the words of Prof David G. Jayne: "As a result [of laparoscopic surgery], patients benefit from a quicker return to normal function. In addition, there are cost-savings to healthcare providers through shorter hospital stays and efficiency savings through a higher throughput of patients."

Again, Prof David G. Jayne explains the evolution of minimally invasive surgery: "The logical evolution of laparoscopic surgery is to try and maximize its benefits through a further reduction of the surgical trauma inflicted on the patient. One attempt at this has been Single Port Laparoscopy (SPL), otherwise known as Single Incision Laparoscopic Surgery (SILS). In SPL the multi-port laparoscopic approach to the abdominal cavity is replaced by a single, centrally located port through which a laparoscopic camera and instruments are passed to effect the operation. Whilst this reduces abdominal access to a single 2 – 3cm incision, it introduces other complexities. "Crowding" of the camera and instruments through one port, leads to impaired surgical dexterity and often the surgeon has to resort to crossing of the instruments to gain the necessary triangulation to perform operative manoeuvres. This makes the procedure technically more challenging and leads to increased operative times. In addition, to date there has been no evidence that SPL results in improved patient outcomes as compared to multi-port laparoscopy, except perhaps for marginally improved cosmesis. As a consequence, SPL has been slow to gain clinical acceptance as a technique for routine application.

A further attempt to reduce surgical access trauma has been the development of natural orifice trans-luminal endoscopic surgery (NOTES). In NOTES, an abdominal wall incision is avoided with surgical access gained by passing a laparoscopic camera and instruments through a natural orifice e.g. the stomach, rectum, vagina, or bladder. In this manner, truly scarless surgery is possible. However, the procedures become increasingly more difficult to perform as the access becomes more restricted and there are legitimate concerns about the safety of access and closure techniques through internal, often contaminated, body cavities. Although an interesting and innovative concept, NOTES is still mainly restricted to the research environment due mainly to technique problems with inadequate instruments that can work effectively under such demanding conditions.

The application of robotic-assistance to surgery in the 1990's offered to overcome some of the technical limitations of conventional laparoscopic

instrumentation enabling surgeons to perform complex laparoscopic interventions with more dexterity and precision. Currently, there is still only one commercially available robotic surgical system, the Da Vinci<sup>®</sup> robot (Intuitive Surgical Inc. Sunnyvale, California). Initially aimed at cardiothoracic surgery, it has found its niche predominantly in urology (radical prostatectomy), gynaecological oncology (radical hysterectomy), and colorectal (rectal cancer) surgery; all procedures performed in the confines of the bony pelvis that necessitate precision operating. Despite its technological advantages, which include intuitive instrument handling, 3-dimensional operative field of vision, Endowrist<sup>®</sup> instrumentation with 7-degrees of freedom of movement, and digital compensation (image magnification, tremor elimination etc.), the da Vinci has failed to show marked benefit in terms of improved patient outcomes, and at a cost-price of around £1.5M it is unlikely to demonstrate cost-effectiveness. In addition, the da Vinci is still a multi-port laparoscopic device, so there are no gains derived from reduced access trauma as compared to conventional laparoscopy.”

## **1.2 Motivation**

Prof David G. Jayne explains the clinical motivation of the project: “The above approaches [laparoscopic surgery, SPL, NOTES, robotic surgery] all have their theoretical advantages but each suffers its own limitations, either from a lack of suitably advanced instrumentation (SPL and NOTES) or from a failure to reduce surgical access trauma (da Vinci<sup>®</sup> robot). A possible solution is to amalgamate the best features of each of these approaches and to develop a device for laparoscopic surgery that can function through reduced abdominal access (SPL or NOTES) with the benefits of robotic-assistance to overcome the limitations of inadequate instrumentation. Based on this premise, the concept for a miniaturized intra-abdominal surgical robot was proposed, which can be deployed through a small abdominal incision, manoeuvre around the abdominal cavity, and undertake surgical procedures with robotic precision.”

The research carried out in this project focuses on the development of a robot for a SPL or NOTES procedure. The development of the locomotion mechanism of the robot seeks to enable more precise and convenient exploration of the abdomen and access to the surgical target for the surgeon. A more convenient and precise procedure for the surgeon ultimately benefits the patient.

The vision of this project is that the ultimate solution to make an SPL/NOTES procedure more convenient for the surgeon would be a miniature intra-body robot able to move along the surfaces inside the abdominal cavity. This robot would integrate all the functionality of current surgical robots in one small portable device, initially carrying a camera for visualization of the abdominal cavity and eventually carrying tools.

This miniature robot for a SPL/NOTES procedure moving freely on all the surfaces of the abdomen would enable a panoramic view of the abdominal organs and easier access around the surgical target by operating from a vantage point. Within the insufflated abdomen, this vantage point could be the internal wall of the abdomen (the peritoneum), situated at about 5 to 6 cm above the abdominal organs.

Working towards the implementation of such a miniature robot for SPL/NOTES, the motivation for this project is to develop a miniature locomotion mechanism able to move along the peritoneum. In order to hang from the abdominal wall and move along the peritoneum, the locomotion of the robot will resist the pull of gravity using adhesive pads. This type of locomotion will be referred to in this thesis as “inverted adhesion-reliant locomotion” or simply “inverted locomotion”.

Inverted adhesion-reliant locomotion enables motion along the wall of the abdomen using an attachment method that, compared to magnets or suction cups, does not require any external equipment in order to be activated. However, this type of locomotion makes the design of the robot significantly challenging as it poses the question of how to ensure the robot can stably move along the peritoneum without falling.

The adhesive pads for the robot have been developed in the larger project this thesis is part of. This larger project (NIHR NEAT L066) is concerned with providing adhesion between the robot and the peritoneum so that the robot can hang from the abdominal wall. This adhesion is provided through a bio-mimetic surface developed at the University of Leeds [8-10]. These adhesive pads have a micro-structured surface which follows a pattern inspired by the toes of tree frogs which allows strong and repeatable adhesion to wet surfaces. This is particularly suitable for attachment to biological tissue like the internal walls of the human body which are covered in a layer of fluid. Details on these bio-mimetic pads will be given later in Section 2.3.7.

### **1.3 Research methodology**

This thesis proposes and develops a new robotic approach for motion inside the body: inverted adhesion-reliant locomotion along a biological surface. The robot moves along a surface that is difficult to model and test because of its biological nature. Biological tissue is visco-elastic [11] and becomes stiffer the drier the tissue sample. The tree frog pads used by the robot are also a new development within the field of bio-mimetic adhesives. Extensive work has been carried out in studying and mimicking the attachment mechanism of geckoes for dry surfaces [12-15], which is similar to tree frogs, but not specifically on tree frogs for wet surfaces.

Aware of the novelty of the type of locomotion and adhesive pads, as well as the challenge posed by motion along the peritoneum, the research methodology of this project was mainly empirical and followed these steps:

1. Design of a prototype of the robot based on previous knowledge about mobile and climbing robots, incorporating bio-inspiration into the design given the bio-mimetic nature of the adhesive pads. This part of the research can be found in Chapters 3 and 4.
2. Testing of the prototype, noticing the difficulties of the environment and application and learning how to overcome them through experience. This part of the research relates to Chapter 5.
3. Analysis of the locomotion mechanism in order to provide a critical assessment of the prototype that feeds into the overall conclusions and discussion surrounding further work. Chapters 6, 7 and 8 contain these theoretical analyses of the robot.

### **1.4 Aims and objectives**

The aims and objectives of this thesis are defined as follows:

#### **1.4.1 Aims**

1. Design, build and test a miniature robot to move in inverted locomotion in an intra-abdominal environment, using micro-structured adhesive surfaces to interact with biological tissue.
2. Investigate and define control strategies to enhance the stability of the locomotion mechanism of the robot.

#### **1.4.2 Objectives**

1. Review existing literature on robotic surgery, robotic intra-body devices and miniature climbing robots using bio-inspired adhesives.

2. Design a miniature mechanism for the robot to apply a controllable set of forces to the adhesive pads.
3. Identify suitable actuation and sensor technologies along with manufacturing techniques to develop a controllable miniature locomotion mechanism for the robot.
4. Analyse the kinematics and dynamics of the locomotion mechanism relevant to the motion of the robot and its interaction with the tissue.
5. Implement a miniature robot following the previous conceptual design and using the identified actuation and sensor technologies and an appropriate locomotion strategy.
6. Create engineering models of the mechanical and adhesive interaction of the locomotion mechanism of the robot and the tissue.
7. Define the main parameters involved in the control of adhesion and develop strategies for stable motion of the robot.
8. Test and evaluate the developed prototype of the robot.

## **1.5 Contributions of the thesis**

The novel contributions of this thesis can be summarised as:

1. Development of a bio-inspired design methodology for adhesion-reliant robots interacting with living tissue.
2. Proposing and development of a novel design for a surgical intra-body robot walking in inverted locomotion inside the insufflated abdomen.
3. Definition of a peeling model for the detachment of the adhesive pads of the robot and a stability criterion for inverted adhesion-reliant locomotion.
4. Proposal of control strategies to enhance the stability of the robot.

Part of the research carried out for this thesis has been presented in international conferences. The list of published papers and extended abstracts can be found in Appendix A.

## **1.6 Organisation of the thesis**

This thesis is divided into nine chapters including this introduction. The first five chapters present the background (Chapter 1), context (Chapter 2), design (Chapters 3 and 4) and the implementation and performance (Chapter 5) of the robot. The following three chapters (Chapters 6, 7 and 8) present the theoretical work and analysis carried out after testing and

evaluation of the prototype. The last chapter presents the conclusions of the thesis and suggestions for future work.

Specifically, Chapter 2 presents the literature review carried out to identify the gaps of knowledge and development of current intra-body robots. The first focus of this review is small-size climbing robots using gecko-inspired attachment. The design and development of these robots is important for the intra-abdominal robot because its locomotion is inverted and relies on adhesion. The second focus of this literature review is the evolution of surgical robots from the first camera holders to the latest miniature robots. In this way, the advantages and disadvantages each robot represents are explained in relation to the development of an intra-abdominal mobile robot.

Chapter 3 presents the conceptual design of the robot, following the specifications of operation inside the insufflated abdomen. In this chapter the environment of the robot (the human abdomen) is presented. The advantages and challenges of operation from a vantage point (the abdominal wall) are explained together with the principles to follow for a successful design. Accordingly, the type of locomotion for the intra-abdominal robot is selected and its method of locomotion defined.

In Chapter 4, the conceptual design of the robot is analysed. The kinematics and dynamics involved in the motion of the adhesive pads are presented. The chapter also characterises the robot as a walker, explaining the way the gait sequence of the robot is generated and how its design can adapt to uneven terrain.

Chapter 5 presents the process of implementation and testing of the robot. The selection of miniature motors, construction of the mechanism and testing of the assembly for one pad are presented as the first step in the implementation of the robot. Then the performance of the first prototype is presented together with the improvements that led to the second prototype. To control the motion of the prototype open-loop and closed-loop controllers were implemented and evaluated. The performance and enhancements of the second prototype are also discussed for locomotion of the robot with magnetic pads on a steel surface, and with the bio-mimetic pads on biological tissue *in vitro*.

After testing the prototype of the robot, research focused on analysing the interaction between the locomotion mechanism and the tissue supporting the motion of the robot. Better understanding of this interaction provides the basis of control strategies for the adhesion-reliant intra-abdominal robot.

Thus, in Chapter 6 a mathematical model is proposed in an attempt to explain how the pad peels off when actuated by the locomotion mechanism. This model considers the bending on the pad together with the energy required to peel the pad. In this way, the model enables calculation of the maximum value of force or moment to peel the pad. This maximum value is used for the definition of a stability criterion for adhesion-reliant walking robots presented in the next chapter.

Chapter 7 reviews the stability criteria used in the literature for walking robots and defines a new criterion specifically suitable for adhesion-reliant robots. This new criterion considers how close each adhesive pad is to detachment and how many pads are required to support the gait sequence. This chapter also illustrates how the criterion can be applied to the gait sequence of the developed robot.

The penultimate chapter, Chapter 8, looks into the ways the locomotion mechanism can be constructed, controlled and actuated in order to enhance the stability of the robot. Enhancement of stability is based on the stability margin defined for the previous stability criterion for adhesion-reliant robots. Firstly, a model of the soft pad is presented and then used in order to analyse the forces and moments that detachment of one pad causes on a robot with two pads. Building up on this two-padded configuration, the effect of adding a third pad in line with the other two and forming a triangle is analysed. This chapter also shows how the increase in stability margin achievable with these two three-padded configurations can be combined in a robot with four pads.

A summary of the achievements of the research work carried out for this thesis, along with the conclusions and future work are presented in the last chapter, Chapter 9.

## **Chapter 2**

### **Literature review**

#### **2.1 Introduction**

The literature review for the development of the intra-abdominal robot encompasses the fields of miniaturisation and locomotion for robotic systems as well as robotic systems in surgical applications. In the first place, this chapter discusses robotic systems according to their size, focusing on the actuation and manufacturing challenges of miniature robotic systems. After this, locomotion strategies for miniature robotic systems are reviewed with an emphasis on climbing robots and biological inspiration due to the use of tree frogs pads in inverted adhesion-reliant locomotion for the intra-abdominal robot. Next, robotic systems developed for surgery are reviewed, focusing on the advantages these systems bring to laparoscopy and how they can be further improved. Robotic systems for surgery range from floor-mounted robotic arms to intra-body miniature devices. Then, these surgical robots are discussed, identifying the gap of knowledge and implementation in intra-body robots. Lastly, a summary of the reviewed technologies is presented.

#### **2.2 Miniature robotic systems**

##### **2.2.1 The size of robotic systems**

The size of a robotic system determines the precision of its motion and the force the robot can generate. Thus, the size of the robot determines the actuation and sensing technology required for its operation and control as well as the manufacturing technique employed for its fabrication. With respect to size, robotic systems can be classified into conventional or macro-robots, miniature or meso-scale robots, micro-scale robots and nano-robots [16].

Table 1 summarises the typical dimensions, force range and applications of robotic systems according to their size.

**Table 1. Typical dimensions, force range and applications of macro-robots, miniature robots, micro-robots and nano-robots, adapted from [16].**

<b>Size of the robotic system</b>	<b>Typical dimensions</b>	<b>Typical force range</b>	<b>Examples</b>
<b>Macro-robots</b>	> 10 cm	> 1 N	Robots for transportation Industrial manipulation robots
<b>Miniature robots</b>	1 mm - 10 cm	1 mN - 1 N	Robotic colonoscopes
<b>Micro-robots</b>	1 $\mu$ m - 1 mm	< 1 mN	Drug delivery robots
<b>Nano-robots</b>	100 nm - 1 $\mu$ m		Cell manipulation robots Nano-scale assembly robots

Conventional robots of a size similar to humans or larger and use conventional mechanical actuators like DC motors and hydraulic pistons.

Miniature robots are conventional robotic systems scaled down to a volume of a few cubic centimetres [16]. Another name for miniature robots is meso-scale robots because their dimensions are in-between conventional robots and microscopic robots (meso is Greek for middle). The dimensions of miniature robots range from 1 mm to 10 cm [16]. Miniature robots use the same actuation technology and mechanical components as larger robots but scaled down to fit in a few cubic centimetres [16]. Miniature robots are used for research in sensor networks and distributed robotics [17-19], swarm robotics [20-22] and robots whose design is inspired by biological systems [23-25]. Miniature robots can move and operate in constrained spaces which are too small for humans or larger robots. For example, miniature robots can be used in search and rescue operations to look amongst the rubble of collapsed buildings [19, 21] and in medical applications for exploration of body cavities [26-29]. Miniature robots use smaller versions of conventional actuators, for instance DC mini-motors and miniature piezo-electric actuators, which are explained in the next section, Section 2.2.2.

Micro-robots require the use of a microscope to be seen. Forces such as surface tension or electrostatic forces that can be neglected at the macro-scale become important at the micro-scale [16]. Nano-robots are the size of biological cells and use electro-chemical forces. The actuation technology used for micro-robots and nano-robots is especially developed to generate forces of the range and nature required at the micro-scale and nano-scale.

Figure 2a shows an example of a macro-scale robot: the humanoid iCub, Figure 2b shows an example of a miniature flying robot and Figure 2c shows an example of a swimming micro-robot.

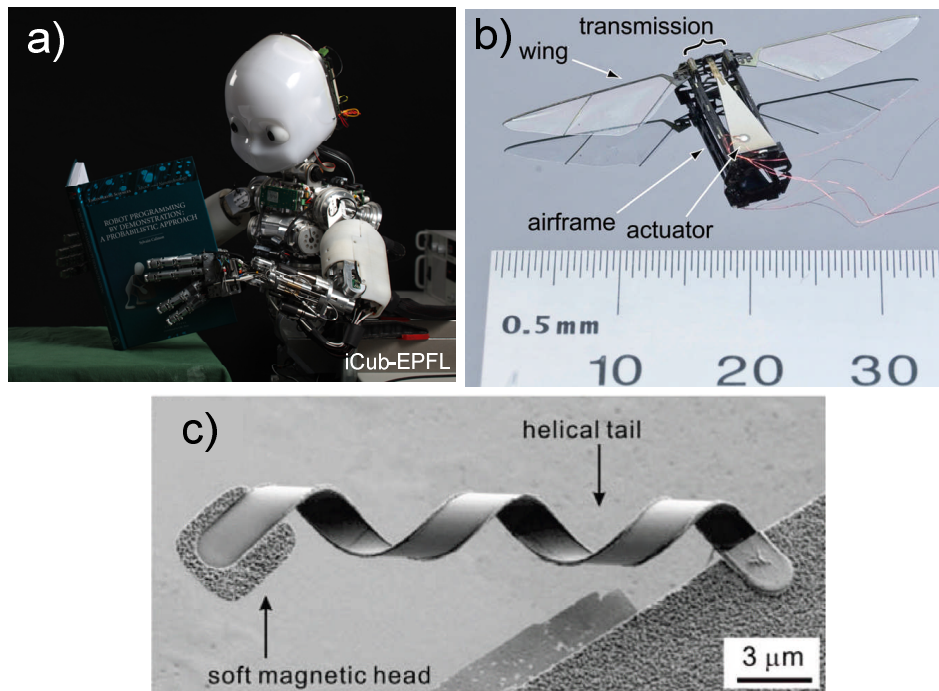


**Figure 2. (a) Robotic system in the macro-scale: the iCub humanoid robot, (b) miniature robotic system: a bio-inspired flying robot [23] and (c) robotic system in the micro-scale: bacteria-inspired swimming micro-robot [30].**

### 2.2.2 Actuation technologies for miniature robots

Miniature robots require small and compact motors able to generate the type of motion and range of force required for the application of the robot. Miniature robots are usually required to generate forces between 1 mN and 1 N. In a miniature climbing robot using adhesion to attach to the surface of support, another important specification is the weight of the actuators. The weight of the actuators will largely determine the weight of the robot which will be limited by how much load the adhesive pads can hold.

An actuation force between 1mN and 1N can be obtained through several technologies: DC mini-motors, piezo-electric miniature motors, electro-active polymers, like Ionic Polymer Metal Composites (IPMCs), and Shape Memory Alloys (SMAs).

DC mini-motors are a long established technology for robotic applications and can be purchased as ready-to-use motors. For a miniature robot, sufficient force and displacement can be obtained with DC mini-motors. In terms of the size, rotary DC mini-motors can be found in the market in very small sizes: Ø2.4mm and 8.5mm length [31], but linear DC mini-motors are

usually much larger:  $47.5 \times 21.5 \times 15 \text{ mm}^3$  [32]. If a linear motor of a smaller size than found in the market is required for the mechanism of the miniature robot, a DC mini-motor can be integrated into a lead screw. However, the previous option would require the manufacturing of a miniature lead screw suitable for the mini-motor which can be challenging given the miniature size and would increase the size of the overall actuation system.

Piezo-actuators are also a long-established technology as they are usually employed in mechatronic applications that require precise positioning. Piezo-actuators can generate forces of up to 1N, but their displacement is about 0.2% of the total length of the actuator. Rotary piezo-motors in the market are larger than DC-minimotors:  $\text{Ø}17\text{mm}$  and 33.5mm length, however, there are a few linear off-the-shelf piezo-electric motors of a compact size [33-35]. The size of the smallest of these linear piezo-motors is  $6 \times 6 \times 3 \text{ mm}^3$  with a 12mm shaft and weighs 0.160 grammes [35], that is, it is a 20% lighter than the smallest rotary DC mini-motor found [31] and 94 times lighter than the smallest linear DC mini-motor found [32].

SMAAs can be found in two forms: as wires and as springs. Both forms can deliver sufficient force for a miniature robot: up to 35N for SMA wire and up to 5N for SMA springs. For a standard length of 1cm, suitable for a miniature robot, the achievable displacement for SMA wire is small, up to 0.8 mm, but SMA springs can obtain up to 2cm of displacement. Due to their thermodynamic response, SMA actuators are slower than the other actuation technologies considered. SMAAs are not as mature a technology as DC mini-motors or piezo-electric motors and their availability as ready-to-use motors for robotic applications is limited. Nonetheless, linear and rotary motors built with SMAAs are commercially available, their dimensions and weight being:  $35 \times 6.3 \times 5.3 \text{ mm}^3$  and 1.1 grammes for the linear SMA motor [36];  $50 \times 11 \times 7.5 \text{ mm}^3$  and 5.5 grammes for the housing of the rotary SMA motor [37].

IPMCs are commercially found in the form of sheets and require integration into a mechanism to be used as a motor for a robotic application. The force they can generate is low compared to other actuation technologies, typically 10mN, and the displacement they can deliver is also low compared to the other options considered, typically a few millimetres. Actuation of IPMCs is famously difficult to control amongst robotic researchers, making IPMCs not the ideal candidate for a robot compared to the other available actuation technologies.

The features of these technologies are summarised and compared in Table 2 using data from [16, 31-34, 36-47].

**Table 2. Actuation technologies for miniature robotics.**

<b>Actuator</b>	<b>Typical force</b>	<b>Typical voltage</b>	<b>Size of the smallest commercial motor</b>
	<b>Typical displacement</b>	<b>Typical current</b>	<b>Weight of the smallest commercial motor</b>
<b>DC mini-motors</b>	3-10 N	1-3 V	Rotary: Ø2.4mm x 8.5mm Linear: 47.5x21.5x15 mm <sup>3</sup>
	20-120 mm (for a linear motor)	>32 mA	Rotary: 0.19g Linear: 15g
<b>Piezo-actuators</b>	10 mN-1 N	2.5-200 V	Rotary: Ø17mm x 33.5mm Linear: 12x3x3 mm <sup>3</sup>
	9 mm (for a linear motor)	15 mA	Rotary: 35g Linear: 0.16g
<b>SMA wire</b>	70 mN-35 N	2-5 V	Rotary: 50x11x7.5 mm <sup>3</sup> Linear: 35x6.3x5.3 mm <sup>3</sup>
	0.1-0.8 mm (for a 1cm-long actuator)	50-200mA	
<b>SMA spring</b>	1-5 N	2-5V	Rotary: 5.5g Linear: 1.1g
	0.2-2 cm (for a 1cm-long actuator)	100 mA-3A	
<b>IPMC</b>	10 mN	3-10V	No motors found in the market
	1mm (for a 1cm-long actuator)	100 mA	

The smallest and lightest rotary motor found in the market is a DC mini-motor: SBL02-06, Namiki Precision Jewel Co., a linear piezo-motor of similar size and slightly lighter weight can also be found commercially: SQL-RV-1.8, New Scale Technologies Inc.

In terms of safety inside the body, all the previous technologies can use low current: from 15mA in piezo-electric actuators up to 200mA in SMA wire, although some SMA springs consume up to 3A. Another risk of SMAs for operation inside the body is the fact that SMAs can reach a high temperature of up to 60°C during operation [48]. If a powered part of the actuator was to come into contact with human tissue, and considering the impedance of the tissue determines the current circulating through the tissue, all the previous actuators can work with low voltage (1-10 V). Piezo-actuators usually require a very high voltage, up to 200V, however, the piezo-motor SQL-RV-1.8 is specifically designed to use low voltage and operates within a range of 2.5-5V.

The four actuation technologies for miniature robots considered have been used for medical and surgical applications. Brushless DC mini-motors have been used for a number of medical applications: implantable blood pumps [49, 50], the actuation mechanism of an intra-abdominal camera [51, 52] and intra-body robots. In intra-body robots, DC mini-motors have been used to provide locomotion to endoscopes using legs [53-55] and wheeled robots moving in the abdominal cavity [56, 57]. As an example of the use of DC mini-motors in medical applications, Figure 3 a shows an actuated camera that is placed on the surface of the abdominal organs for visualisation of the abdominal cavity. A DC mini-motor is used in this intra-abdominal camera to obtain a pan and tilt motion of the camera. Figure 3 b shows the assembled prototype of the camera.

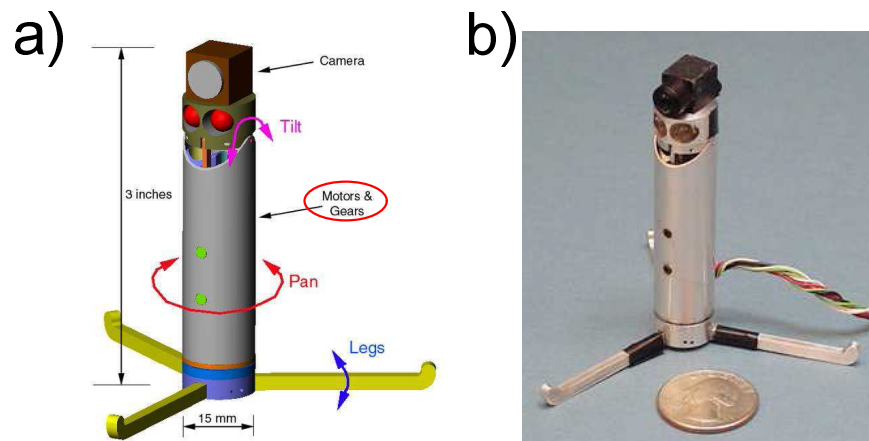


**Figure 3. (a) Components of an intra-abdominal camera using DC mini-motors and (b) assembled prototype of the device [56].**

Miniature piezo-electric motors have been used for the motion of surgical tools [58] and intra-body robots [27]. For example, miniature linear piezo-electric motors are used for the inchworm locomotion of a robot that crawls over the surface of the heart in order to deliver drug [59]. Figure 4 a shows the miniature linear piezo-electric motor used by the crawling robot shown in Figure 4 b.

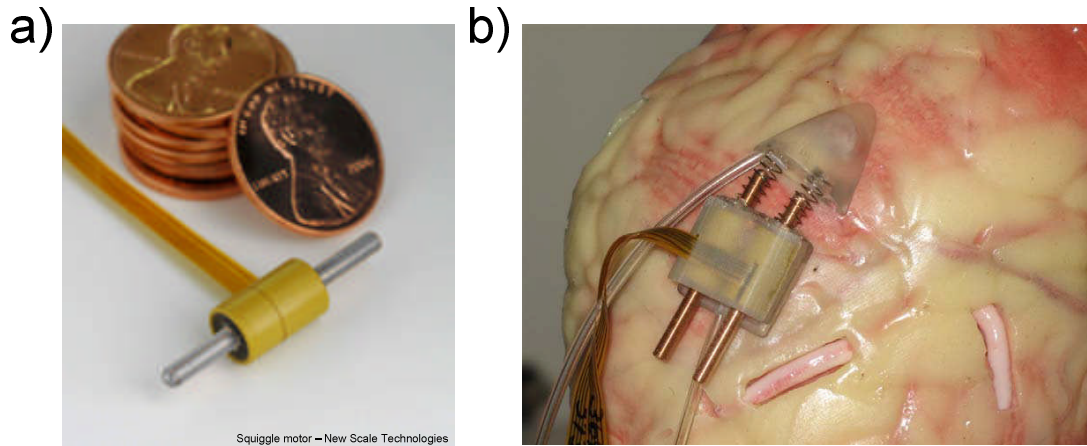


**Figure 4. (a) Miniature linear piezo-electric motor and (b) prototype of an intra-body robot using piezo-electric motors to move on the surface of the heart [59].**

SMA's have been used in the design of actuated endoscopes that crawl inside the colon [29, 60] and for the stop mechanism of capsule endoscopes [61, 62]. Some robotic endoscopes for the colon use inch-worm locomotion and SMA wires and springs are used to provide the extension and contraction that provides locomotion of the robot. Figure 5 a shows the components of a robotic endoscope using SMA wires. Figure 5 b shows the prototype of a robotic endoscope.

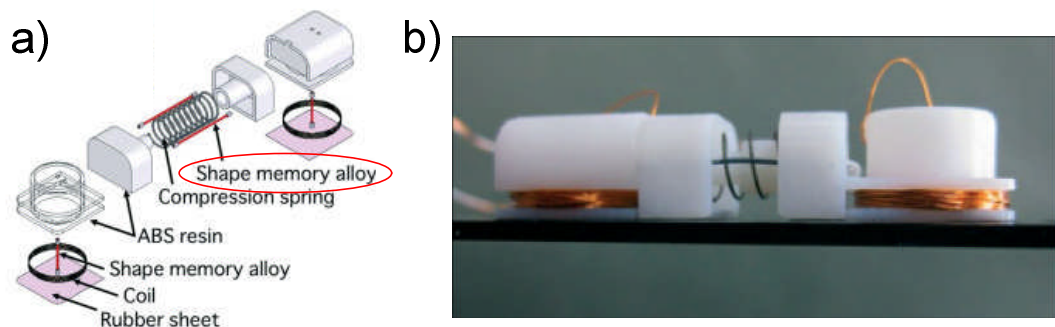


**Figure 5. (a) Components of an SMA-actuated robotic endoscope and (b) the assembled robot [60].**

IPMCs have been used to build implantable micro-pumps [63, 64]. In an IPMC micro-pump, the pumping motion of the fluid is obtained through the expansion and contraction of the IPMC material. Figure 6a shows the

components and an implantable micro-pump; one of these components is a layer of IPMC material. Figure 6b shows the prototype of the micro-pump.

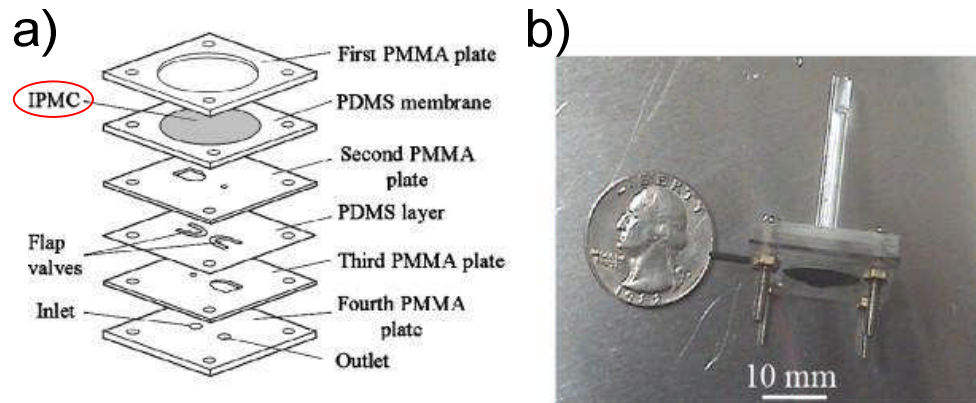


**Figure 6. (a) Layers of an IPMC micro-pump and (b) photograph of the micro-pump [64].**

DC mini-motors (SBL02-06, Namiki Precision Jewel Co.) [31], piezo-electric motors (SQL-RV-1.8, New Scale Technologies Inc.) [35], SMA wire (SmartFlex<sup>®</sup>, SAES Getters S.p.A.) [48] and SMA springs (BioMetal Helix, Toki Corporation) [65] were acquired and tested for the project in order to fully realise the potential of using each technology for the locomotion mechanism of the robot.

The ideal characteristics of an actuator for a miniature climbing robot inside the abdomen are: compact size, low weight, low voltage and current and available as a ready-to-use motor. After consideration of these characteristics, the DC rotary mini-motor SBL02-06 and the linear piezo-motor SQL-RV-1.8 were deemed the most suitable actuators for the locomotion mechanism, depending on whether rotary or linear motion is required.

### **2.2.3 Manufacturing challenges for miniature robots**

The manufacturing challenges for the components of a miniature robotic system are linked to the size and the material required for the application of the robot. The dimensions of the mechanical components of a miniature mechanism are usually a few millimetres. For dimensions of a few millimetres, the manufacturing tolerances for typical mechanical fits, for example a sliding fit, are a few microns. These tight tolerances required for miniature components make the manufacturing of miniature robots especially challenging. In miniature climbing robots the weight of the robot limits the load that the adhesive pads can hold and therefore lightweight materials are preferable. These lightweight materials are usually light metals like aluminium or plastics like Nylon or ABS.

The most widely-used manufacturing technique for small plastic pieces is injection moulding. For injection moulding liquid plastic is injected into a metallic mould with the shape of the piece to be manufactured. With injection moulding, high detail and tight tolerances of the pieces can be obtained. However, precision injection moulding requires precise machining of the mould which can be costly. Injection moulding is only cost-effective if a high volume of pieces is manufactured because a large amount of pieces to manufacture compensates for the cost of machining the mould.

CNC micro-machining can be used to manufacture pieces for miniature robots in metal or hard plastics. CNC micro-machining uses traditional CNC tools like drills and cutters in miniature size. The positioning of the tools in CNC micro-machining stations is precisely controlled in order to obtain tight tolerances. In order to make CNC micro-machining cost-effective, a high volume of the pieces to be manufactured is usually required because of the high cost of setting up the machine. CNC machining of plastics to very tight tolerances also requires specialised staff given that, compared to metals, plastics have lower stiffness and they are more sensitive to temperature and pressure during the manufacturing process.

A number of rapid prototyping techniques have been developed in recent years. Rapid prototyping machines generate solid objects by stacking layers of material that follow the shape of the piece to be manufactured. In general, the materials used in rapid prototyping are metals and thermoplastics. There are several rapid prototyping techniques; the most widely available are: Fused Deposition Modelling, Selective Laser Sintering and Stereolithography. The difference between these three rapid prototyping techniques is the way the layers of material are formed. In Fused Deposition Modelling the material is initially solid and it is melted and extruded from a nozzle that deposits the material on the layer. In Selective Laser Sintering the material is initially dust and is melted by a laser beam to form the layers. In Stereolithography the material is initially liquid and solidified with a laser beam to form the layers. Generally, Selective Laser Sintering achieves better finishing of the pieces than Fused Deposition Modelling and Stereolithography achieves better finishing than the other two techniques.

For the manufacturing of the prototype of a miniature robot, Precision Injection Moulding and CNC Micro-machining offer high manufacturing precision but are only cost-effective for a high volume of pieces. Rapid prototyping techniques are envisaged for industrial and domestic use and are generally less expensive than other manufacturing techniques for low

manufacturing volumes. However, the manufacturing tolerances achievable with Rapid Prototyping are lower than with the other two techniques.

Table 3 summarises the features of Precision Injection Moulding, CNC Micro-machining and Rapid Prototyping, along with the drawbacks of using these techniques to manufacture the prototype of a miniature robot. The features of Table 3 are based on the machines and manufacturing companies available to this project which are mentioned in Chapter 5.

**Table 3. Features and drawbacks of the manufacturing techniques used for miniature robots.**

<b>Manufacturing technique</b>	<b>Features</b>	<b>Drawbacks</b>
<b>Precision Injection Moulding</b>	<ul style="list-style-type: none"><li>• Plastics</li><li>• High precision</li><li>• Industrial use</li></ul>	Only cost-effective for high volume
<b>CNC Micro-machining</b>	<ul style="list-style-type: none"><li>• Hard plastics and metals</li><li>• High precision</li><li>• Industrial use</li></ul>	Costly for low volume
<b>Rapid Prototyping</b>	<ul style="list-style-type: none"><li>• Plastics and metals</li><li>• Fast</li><li>• Inexpensive</li><li>• Industrial and domestic use</li></ul>	Lower precision

## **2.3 Locomotion strategies for miniature robots**

The simplest and most common locomotion strategy for robots is the wheel but designers have gradually introduced more complex systems generally inspired by biological systems, like legged and snake-like robots. This variety of locomotion strategies enables the use of robotic systems in multiple environments and applications as explained in this section.

### **2.3.1 Wheels and tracks**

Wheels are the locomotion system most often used for robots because of their simple design and control. In wheeled robots motors are usually connected, either directly or through gears, to the wheels. Wheeled robots are typically controlled open-loop or with a PID controller in order to control

the motion of the wheels more precisely. Wheeled robots present the following control and navigation issues [66, 67]:

- The controllable degrees of freedom in a wheeled robot are usually fewer than the actual degrees of freedom of the robot (non-holonomic robots).
- The wheels of a wheeled robot might slip if there is insufficient friction between the wheels and the ground or when the robot is turning.
- Wheeled robots are often considered unable to climb over obstacles taller than half of the wheel radius [68].

These control and navigation issues of wheeled robots can be tackled with a more complex mechanical and/or control system.

Tracked robots are also simple to build and control and can overcome higher obstacles than wheeled robots. However, they are less often used than wheeled robots because of their higher cost and because they can only turn by allowing slippage on the ground causing the threads to wear quickly [66]. Wheeled and tracked robots perform best on flat terrain with few obstacles. Figure 7a shows an example of a pair of wheeled miniature robots and Figure 7b shows an example of a tracked miniature climbing robot.

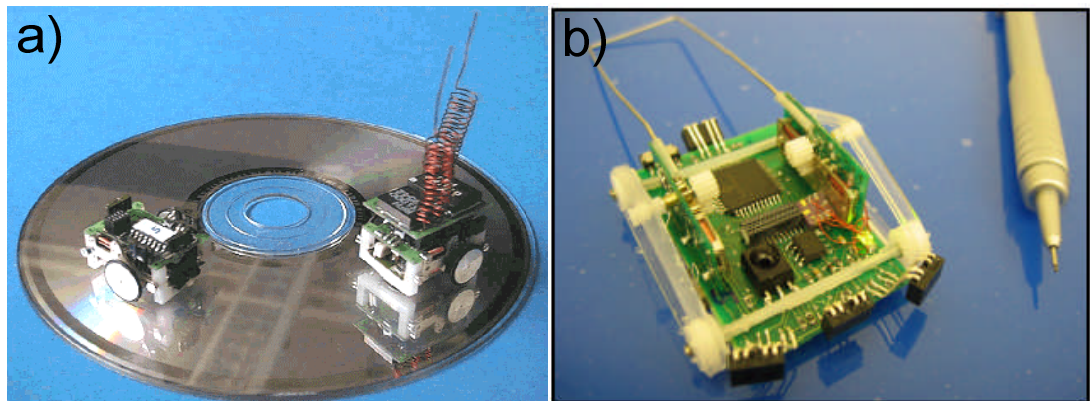


**Figure 7. (a) The wheeled miniature robots Alice [20] and (b) a tracked miniature climbing robot [69].**

For inverted adhesion-reliant locomotion, wheels and tracks offer the advantage of a simple and compact mechanism requiring only a few motors. However, the potential skidding of the wheels and tracks when turning can make a robot in inverted adhesion-reliant locomotion lose adhesion and fall off. Also, having more degrees of freedom in the robot can help to move the adhesive pads more precisely enhancing the stability of the locomotion.

### 2.3.2 Legs

Robots have been built with two legs inspired by human locomotion; four legs inspired by the locomotion of quadrupeds; and with six and eight legs inspired by insects [66]. On even terrain wheels are usually faster than legs, however, on uneven ground, legs adapt better to terrain irregularities and can achieve higher average speed than wheels [67, 70, 71]. Legs can cause less environmental damage than wheels because wheels can slip and leave a continuous track on the ground [67]. Legged robots usually have a high number of degrees of freedom and require a control system more complex than wheeled robots in order to coordinate the motion of the joints and the legs. Figure 8a shows the commercially available miniature biped BRAT (Lynxmotion) and Figure 8b shows the educational miniature hexapod Stiquito<sup>®</sup>.

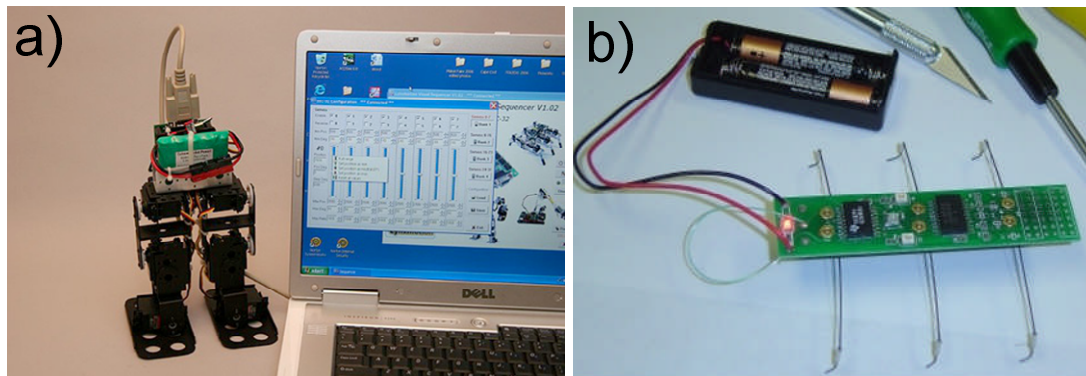


**Figure 8. (a) The miniature biped BRAT [72] and the educational miniature hexapod Stiquito [73].**

For inverted adhesion-reliant locomotion, a legged design with each leg moving an adhesive pad enables to move the pads individually, keeping as many pads in contact with the tissue as required to ensure stability of the robot. However, in a tight space like the insufflated abdomen, the motion of the legs might interfere with the walls of the abdomen or the organs. Also, in order to control the motion legs, 2-3 degrees of freedom are required per leg which might unnecessarily increase the complexity of the mechanism and its implementation. Ideally, the motion of the legs should be kept as close to the peritoneum as possible and the number of degrees of freedom should be kept to the minimum required to ensure stability of the robot. This minimum of degrees of freedom cannot be determined a priori and will be dictated by the experience and testing of the adhesive pads within the locomotion mechanism.

### 2.3.3 Hybrid solutions

The features of wheels, tracks and legs can be combined providing a robotic system with several types of locomotion. Hybrid locomotion systems seek to enhance the simple design and control of a wheeled robot with the advantages of having legs. A remarkable example of these hybrid solutions is the robot AZIMUT [74]. This robot features four legs with a thread along the edge of each leg. The orientation of the legs with respect to the body of the robot can change in order to use the thread on the edge of the legs as wheels or tracks. Figure 9 shows the different locomotion modes of the hybrid robot AZIMUT.

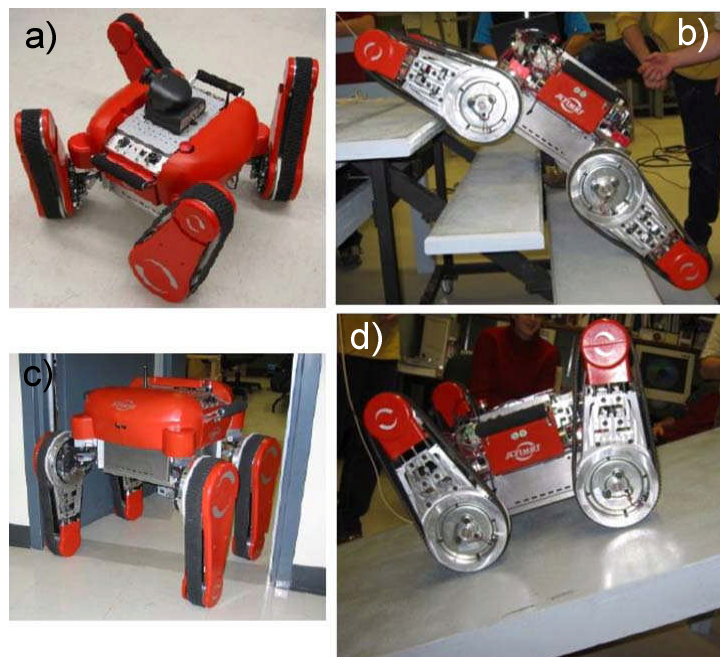


**Figure 9. (a) The robot AZIMUT combines wheel, legs and tracks and can (b) climb stairs, (c) stand on four legs and (d) move along an inclined surface [74].**

Whegs, or wheel-legs, are another important combination of locomotion features. Whegs combine wheels and legs resulting in a number of spokes rotating around an axle controlled by a motor. Whegs have the advantage of being simple to move and control like wheels and, at the same time, being able to walk over obstacles like legs. The robot Mini-whegs<sup>TM</sup> is a good example of a robot using whegs for locomotion on an inclined surface [75]. Mini-whegs<sup>TM</sup> is shown in Figure 10 climbing the surface of several materials with different designs for the whegs.

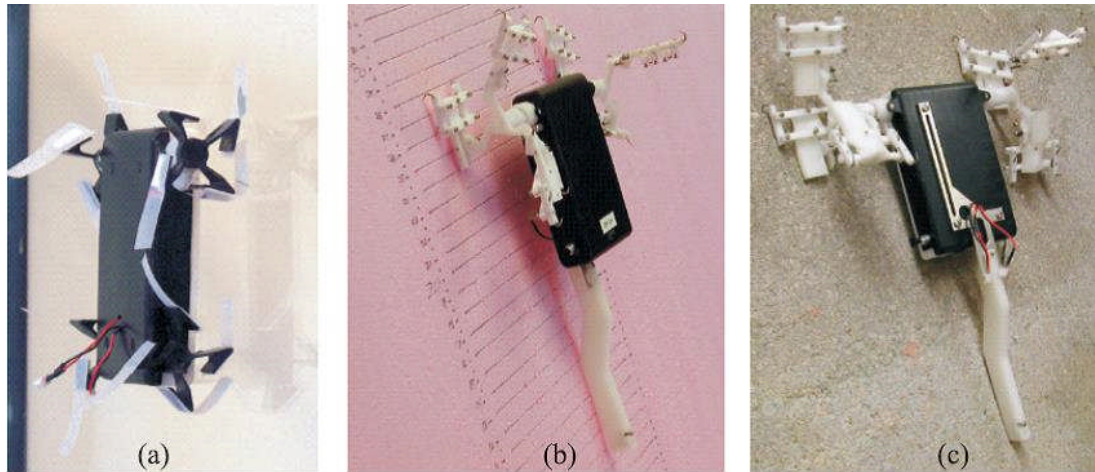


**Figure 10. Mini-whegs™ with different types of wheel-legs climbs glass (a), polystyrene (b) and concrete (c) [75].**

A combination of features from different locomotion systems seems an appropriate design methodology for a challenging application like inverted adhesion-reliant locomotion. However, for a miniature robot moving along the peritoneum there is no clear advantage to implementing a hybrid mechanism like in the AZIMUT robot because there is no change of terrain that justifies a change of locomotion type. In inverted adhesion-reliant locomotion along the peritoneum, whegs present the same risk of skidding as wheels and along the peritoneum there are no obstacles that the whegs could help clear.

### **2.3.4 Inchworm and earthworm locomotion**

Inchworms move by clamping one end of their tubular body to the ground and elongating their body to push the free end of the body forward. There is always part of the body of an inchworm attached to the surface along which they are travelling, while the other part of the body reaches for a new position. Inchworm locomotion has been implemented in miniature medical robots travelling along the gastro-intestinal tract [60, 76]. The sequence of steps followed by an inchworm robotic colonoscope is illustrated in Figure 11a. In Figure 11a, the robot detaches the trailing part of the robot's body first and contracts the body bringing the trailing part close to the leading part. Then the robot detaches the leading part of its body and extends the body making the entire mechanism travel a distance. Figure 11b shows a series of stills of the prototype of the robotic colonoscope moving a distance of 5mm approximately, following the previous sequence.

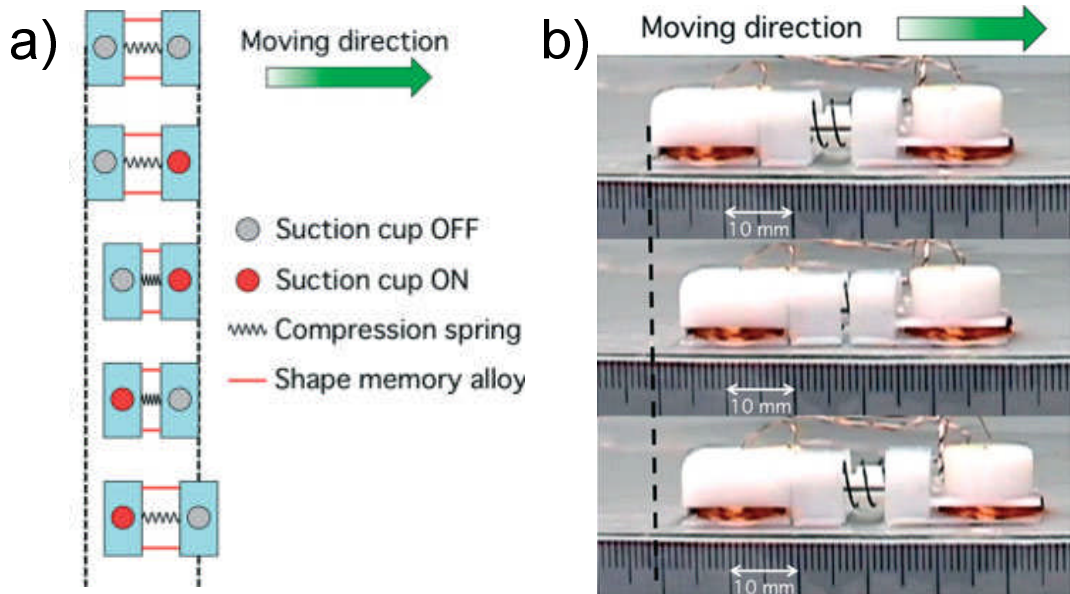


**Figure 11. (a) Sketch of inchworm locomotion in a robotic colonoscope and (b) prototype of the robotic colonoscope moving in an inchworm fashion, both images from [60].**

Earthworms move using peristaltic locomotion which is very similar to the mechanism employed by the human intestine to move food. The body of an earthworm is formed of a succession of rings that can contract or relax. The outside of these rings are covered in bristles which anchor the rings to the ground when the rings are relaxed; the contracted rings stretch out advancing the body of the earthworm. Worms can change their direction of motion by bending their flexible body towards the new direction. This type of locomotion is illustrated in the sketch of Figure 12a and Figure 12b shows a robot built in order to move following peristaltic locomotion. The rotary motor at one end of the robot in Figure 12b pulls several wires connected to the mesh that forms the body of the robot, making the segments of the mesh contract and expand. The locomotion control system used by worms has also been studied and implemented in robotic systems envisaged for search and rescue in collapsed buildings [77, 78].

Stability of a robot in inverted adhesion-reliant locomotion depends upon losing as little adhesion on the adhesive pads as possible with each motion of the mechanism. For inverted adhesion-reliant locomotion, the idea of keeping part of the body solidly in contact with the surface while the rest of the robot moves, like in inchworm and peristaltic locomotion, is promising. This is so because it means that the surface where adhesion takes place can be divided and each part controlled independently, enhancing the stability of the robot. The motion in worm-like locomotion happens mainly in the direction of motion, that is, there are no extremities wiggling around the

space along which the robot moves. This is an advantage for an application in a tight space like inside the human abdomen, making worm-like locomotion very relevant for the choice of locomotion mechanism of the robot. Ideally, the body of the robot should extend over an area, rather than stretch along a line like in worm-like locomotion, in order to maximise contact and therefore adhesion with the peritoneum.

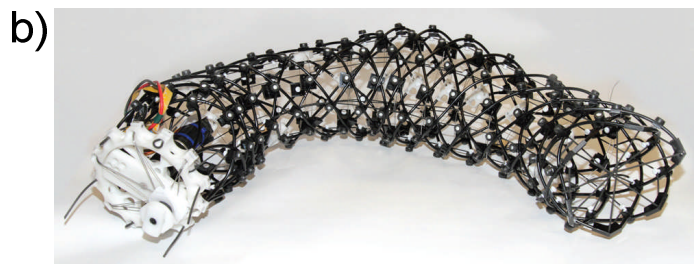
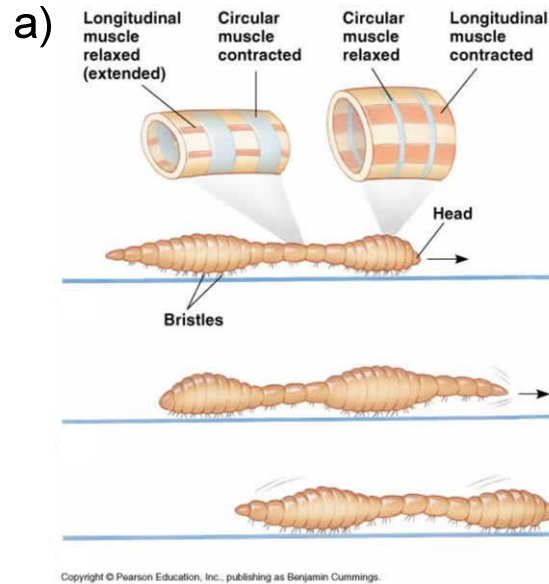
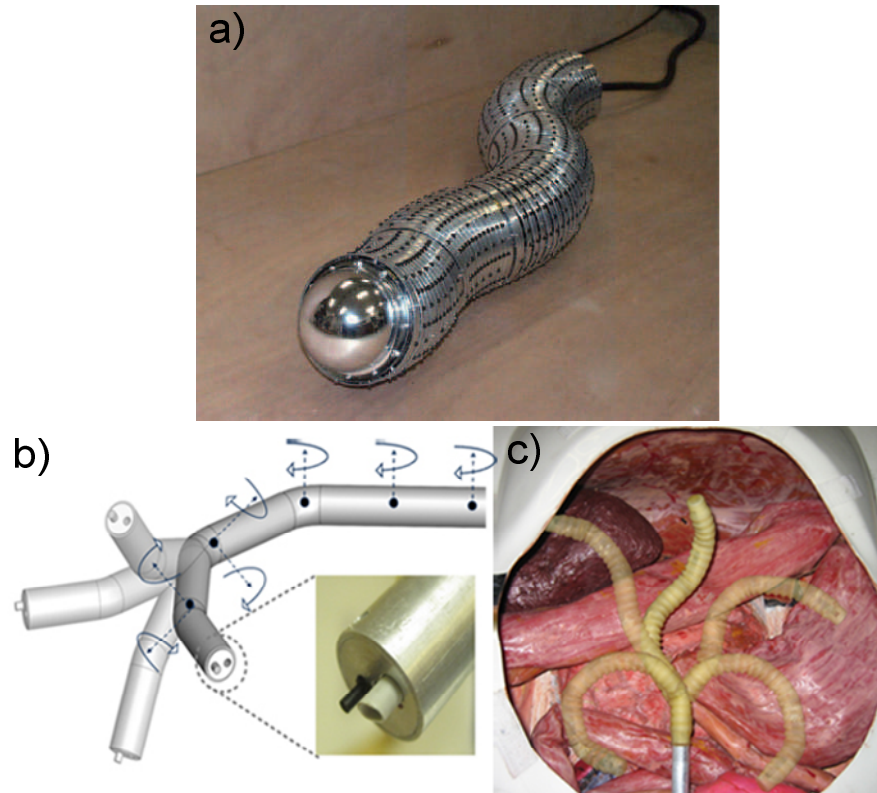


Figure 12. (a) Sketch of earthworm peristaltic locomotion (©Pearson Education, Inc.) and (b) prototype of a robot using peristaltic locomotion [77].

### 2.3.5 Serpentine locomotion

Snake-like robots mimic the snake skeleton and are made up of a number of segments connected together. These segments are moved following a wave-like pattern to obtain locomotion [79, 80]. Snake-like robots can be especially useful to crawl over rubble in search and rescue applications [81]. By way of example of this kind of robots, Figure 13a shows the snake-like robot Slim Slime which can perform a variety of movements by elongating and bending its body [79]. For medical applications, snake-like mechanisms have been built to provide flexible steering of endoscopes in SILS and NOTES applications [82]. Figure 13b shows a schematic showing the seven degrees of freedom of a flexible endoscope whose mechanism is inspired by

snake-like locomotion. Figure 13c demonstrates the use of the flexible endoscope inside a simulated abdomen.



**Figure 13. (a) Schematic illustrating a flexible endoscope with seven degrees of freedom, (b) demonstration of the flexibility of the endoscope when exploring a simulated abdomen, both images are taken from [83], and (c) the snake-like robot Slim Slime [79].**

For inverted adhesion-reliant locomotion of a miniature robot a snake-like mechanism seems a rather complex mechanism compared to other options like wheels or inchworm. In addition to that, the sliding motion of the segments in a snake-like robot can make the robot lose contact with the peritoneum putting its stability at risk.

### **2.3.6 Amoeboid locomotion**

Unicellular organisms use three main systems of locomotion: flagella, cilia or pseudopods [84]. A flagellum is a tail that the cell moves to propel itself, cilia are small hairs around the edge of the cell which the cell can use to swim or crawl and pseudopods are extensions of the body of the cell similar to feet (pseudo is Greek for fake and pod is Greek for foot). Amoebas are able to adhere to a surface and use the latter unicellular locomotion system, pseudopods, in order to move along the surface [85]. To obtain locomotion over a solid surface an amoeba extends an exploratory pseudopod first which does not stick to the surface. From this central exploratory pseudopod smaller pseudopods are formed which stick to the surface supporting the

amoeba. The amoeba then moves by changing the shape of its body and, eventually, those supporting pseudopods are detached and incorporated into the part of the body that is moving [85]. Figure 14 a-c shows three moments of the locomotion of an amoeba along a surface. Note the deformation of the body and the expansion of the pseudopods circled in Figure 14a. The motion of amoebas has been used as inspiration for the locomotion of robotic systems, focusing on the use of the surface of the skin of the robot to obtain traction forces [86].

© Dr. R. Wagner

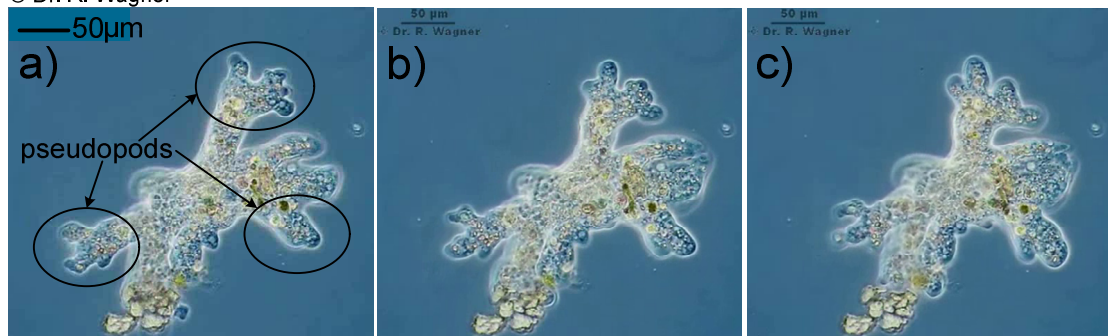


**Figure 14. (a-c) Three moments of the motion of an amoeba extending the pseudopods circled in (a) changing the shape of its central body, the three images are ©Dr. R. Wagner.**

For a miniature robot, inspiration from the locomotion of a unicellular organism can only be at a conceptual level given the very different scale of the two systems: amoebas are approximately 300µm long (see Figure 14) and a miniature robot is a few centimetres long. In an intra-body application the space for locomotion is tight and the mechanism of a robot working in it needs to be compact. For inverted adhesion-reliant locomotion, amoeboid locomotion is relevant because it uses adhesion and enables the organism to move along the surface of attachment without extremities interfering with the space underneath. Ideally, the motion of the robot should interfere as little as possible with the space underneath it and the fluidity of amoeboid locomotion enables the robot to constraint its movement to the surface of attachment. This idea is explained in more detail and illustrated in Chapter 4, Section 4.3.2, where it is shown that the workspace of the robot is mainly constrained to an area on the surface of the peritoneum.

Despite the obvious biological differences and purely from the point of view of robotic locomotion, amoeboid locomotion can be regarded as two-dimensional inchworm locomotion. This is so because amoeboid locomotion alternates the attachment of different parts of the body and extends the detached part of the body while the attached part of the body supports the

motion. However, the body of an amoeba extends over a surface rather than along a line like in worms. In worm-like locomotion, if the robot wants to change direction of motion it needs to bend the body towards the new direction. If the body of the robot extends over a surface, it can change direction of motion without bending the body, simply starting to move the part of the body closer to the new position the robot is required to go. This is illustrated later in Chapters 3 and 4, Sections 3.9 and 4.5 , where the locomotion sequence of the robot is explained.

### 2.3.7 Climbing robots and bio-inspired attachment

Climbing robots move against gravity and therefore require attachment to the surface on which they are moving. The most challenging situation for a climbing robot is a totally inverted surface. The previous locomotion strategies: wheels, tracks, legs, whegs, worm-like and snake-like, can be used for climbing a surface with the added challenge of providing attachment between the robot and the locomotion terrain. The most usual attachment methods for climbing robots are suction cups for non-metallic surfaces and for ferrous surfaces: electro-magnets, permanent magnets or a hybrid of the two. Robots using suction cups and magnets have been developed for applications such as window-cleaning, inspection of large structures and welding of ships [87-89]. Figure 15a shows a climbing robot using electro-magnets and Figure 15b shows a window-cleaning climbing robot using suction pads.

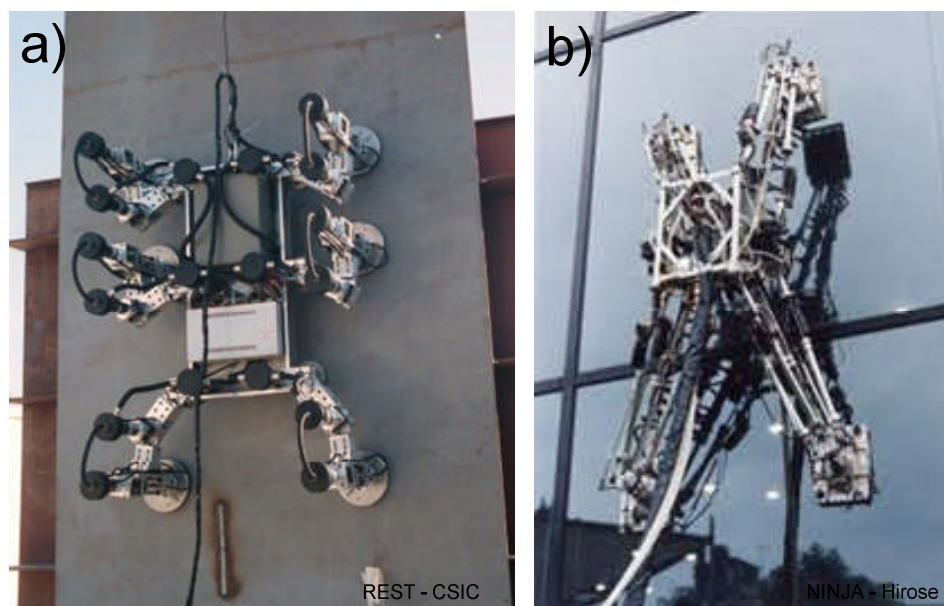
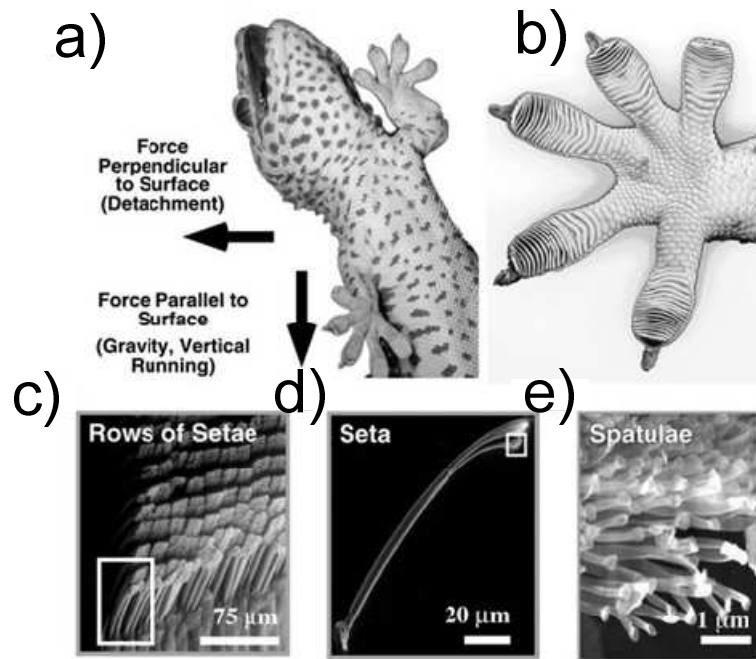


Figure 15. (a) Soldering climbing robot using magnets for attachment and (b) a wall climbing robot using suction pads.

Using magnets or suction pads for a climbing robot requires a vacuum pump to obtain suction force on the pads and electro-magnets require extra equipment in order to energise them. For an intra-body application using suction pads [27, 60], in order to make the design of the robot as compact as possible, the vacuum pump needs to be external to the body. If the intra-body robot uses magnets, an external metallic surface is required in order to keep the robot attached to the surface of the tissue [90]. An alternative to using suction pads and magnets for a climbing robot inside the body is bio-inspired adhesives. Using bio-inspired adhesives, attachment is obtained by pressing them onto the surface of attachment without the need of external equipment to maintain adhesion. Bio-inspired adhesive are the attachment method considered for this project.

Bio-inspired adhesives have been developed recently and used in order to provide attachment to climbing robots [91, 92]. The development of bio-inspired adhesive surfaces began with the discovery of the micro-structure present on the toes of geckoes [93] and the legs of insects [94] and other animals. Geckoes are the animal whose adhesive microstructure has been most extensively researched and studied [95, 96]. On the toes of the gecko, a hierarchical structure of tiny hair-like fibres increases the contact area between the foot and the surface of support [12, 95, 96]. Each tiny fibre creates a weak molecular link, called Van der Waals link, with the surface of support. These weak links between each tiny hair and the support surface result in strong attachment because of the high number of hairs in contact with the surface [93]. As a result, geckoes are capable of supporting the weight of their body with just one of their toes [97]. Figure 16 shows the adhesive structure on the foot of the gecko. Figure 16a shows the forces taking place in the climbing motion of the gecko. Figure 16b shows a detail of the posterior side of the gecko's foot, where the adhesive micro-structure is found. Figure 16c-e shows the structure of the tiny hairs found in the toes, called setae, and the even smaller fibres composing these hairs, called spatulae.



**Figure 16. Gecko adhesive hierarchical structures [96].**

The ability of geckoes to climb a variety of surfaces is due to the way geckoes control attachment and detachment as well as to the micro-structure on their toes [15]. The forces geckoes apply to their feet are parallel to the surface of support (shear force), and perpendicular to the surface of support (pull force) that result in fast and efficient attachment and detachment [15, 96]. These forces are applied to the toes during the locomotion sequence of the gecko. Geckoes unfold their toes, preloading the micro-structured area on their toes by pushing them into the surface of attachment in order to ensure good contact and obtain attachment. When geckoes require to detach their feet, they peel off their toes by curling up their fingers. This way of peeling off the toes makes detachment fast and efficient because a lower value of force is required to detach the adhesive micro-structure when peeling off than when pulling. The foot of the gecko unfolding its toes in order to attach to the surface is shown in Figure 17a and detachment of the gecko curling up its toes is shown in Figure 17b.

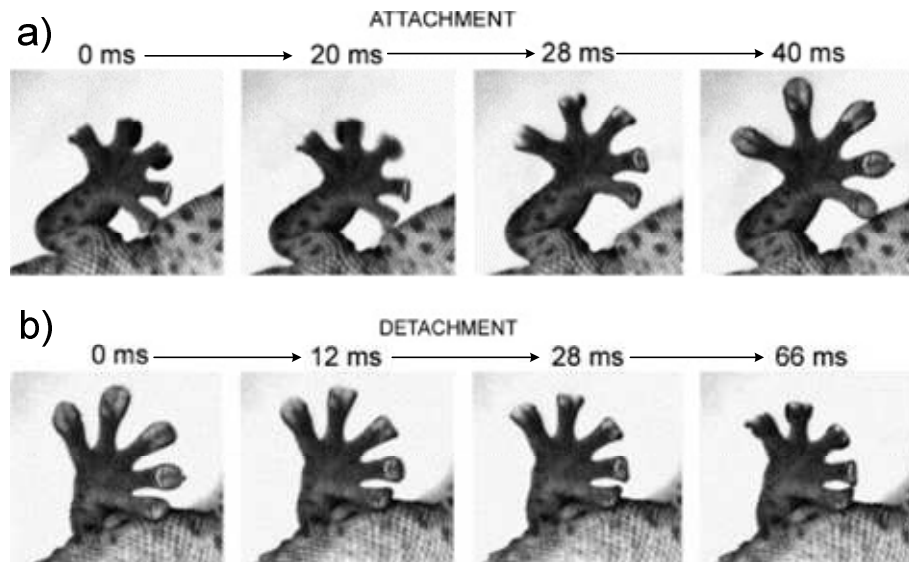


**Figure 17. (a) Snapshots of gecko attachment and (b) snapshots of gecko detachment from a glass ceiling [98].**

These micro-structured surfaces enable smooth and repeatable attachment to all kinds of dry surfaces and have been replicated for small climbing robots using a tracked design, legs and whegs [99-101]. The robot Stickybot was developed in order to replicate the attachment and detachment mechanism of geckoes [92, 100]. The design of Stickybot uses gecko-inspired adhesives on its toes and actuated cables to curl up and peel off its toes [92, 100]. Stickybot was able to climb a variety of dry surfaces: glass, ceramic tile and acrylic with a maximum speed of 4 cm/s [100]. Figure 18 shows the prototype and the main features of Stickybot.

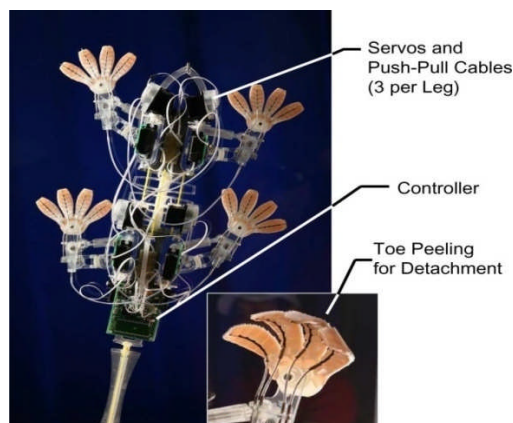


**Figure 18. Stickybot uses gecko-inspired adhesive pads and mimics the locomotion mechanism of geckoes [100].**

Several types of micro-structured surfaces have been fabricated and applied to other small climbing robots [91, 99, 101-103]. For instance, the robot Tankbot uses a tracks with gecko-inspired adhesive treads on its two belts. Tankbot can move at a maximum speed of 12 cm/s and steer, climb steep slopes, climb inverted surfaces and go over obstacles [99, 103]. The

prototype of Tankbot is shown in Figure 19a. Another example is the robot Waalbot which uses whegs to obtain locomotion. Waalbot uses two whegs with three footpads each; each footpad has a gecko-inspired adhesive surface [91, 101, 104]. Waalbot integrates on-board power and wireless communication and is able to climb 90° slopes at 6 cm/s. The locomotion of the latest prototype of Waalbot is enhanced by including force sensors on its two tails. This latest prototype of Waalbot rocks the pads in order to recover adhesion when the force sensors on the two tails of Waalbot sense insufficient attachment force [101, 104]. The latest prototype of Waalbot is shown in Figure 19b.

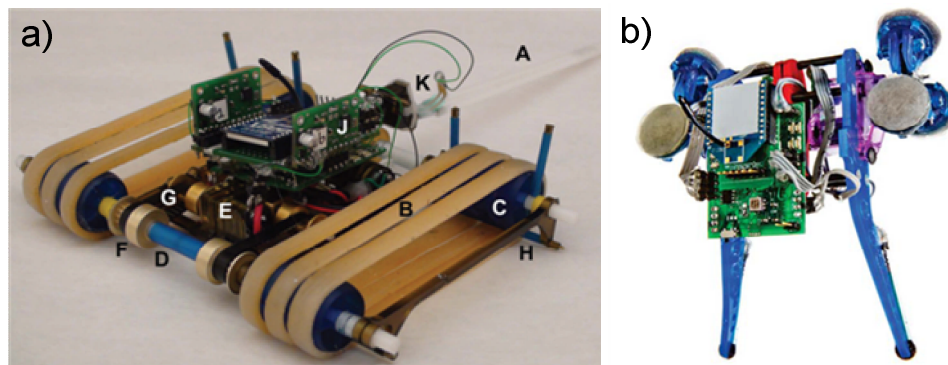


**Figure 19. The climbing robot Tankbot uses tracks with gecko-inspired adhesive belts [99] and (b) Waalbot uses whegs with gecko-inspired adhesive pads [104].**

These adhesion-reliant miniature robots demonstrate the potential of using biologically inspired adhesion and control for climbing robots moving on a dry surface. For a wet surface like the peritoneum inside the abdomen, inspiration for the development of adhesive micro-structures can be taken from the toes of the tree frog. The micro-structure of tiny hair-like fibres found on the toes of the gecko can also be found in tree frogs [105]. The micro-structure on the toes of the tree frog is adapted to wet environments. The micro-structured surface on the toes of the tree frogs uses weak molecular links and capillary forces to provide strong adhesion to wet surfaces [106-108]. Figure 20a shows a tree frog, the microstructure on the toes of the tree frog consists of a hexagonal array of cells separated by channels as shown in Figure 20b. These cells have finer micro-pillars and a smaller-scale channel structure between the pillars, the scale of these pillars and channels is shown in Figure 20c. These micro-pillars provide the first contact with the attachment surface that causes adhesion [105, 106]. This structure of micro-pillars has been replicated on the surface of a bio-compatible polymer to provide attachment to biological tissue [8, 9]. The channel structure found on the tree frog's toes was not replicated because the channels do not provide adhesion by themselves but by means of the

fluid secreted from glands into the channels [106]. Therefore, the adhesion of the replicated micro-structure on the adhesive pads for the robot comes exclusively from the contact and the capillary forces between the pillars and the wet surface of support. Figure 20d shows the micro-structured surface fabricated for the adhesive pads of the intra-abdominal robot.

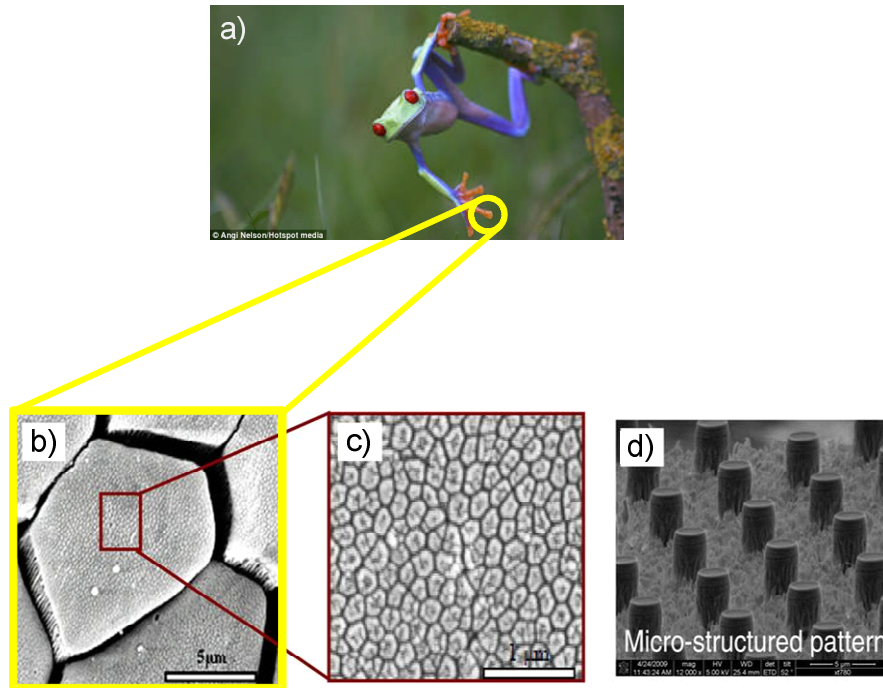


**Figure 20. (a) Tree frog adhesion: (b) structure found on the toes of the tree frog, (c) micro-pillars forming the structure of the toes [106] and (d) replicated micro-pillars to obtain wet adhesion [9].**

In order to control a robot in inverted adhesion-reliant locomotion, it is important to understand the attachment and detachment process of the pads when force from the actuators of the robot is applied to the adhesive pads. This control of the attachment and detachment process requires a model of how the force from the actuators of the locomotion mechanism affect the adhesion of the pads. This model would consider the mechanical actions at the macroscopic scale, that is, it would look into how the detachment force of an adhesive pad changes depending on the horizontal and vertical forces applied to it. Such a model would not require modelling of the microscopic contacts between the individual fibres of the adhesive micro-structure and the surface of support. Given the parameters of adhesion of the adhesive pads: preload, detachment force and work of adhesion, a model of adhesion on the macro-scale would determine the value of force applied by the robot that makes the pads detach.

To the best of the author's knowledge, a macro-scale model of an adhesive pad interacting with the locomotion mechanism of a climbing robot has not

been developed to date. Micro-scale models of gecko fibres and the fibres of other animals have been developed mainly in order to understand and improve the fabrication of bio-mimetic adhesives [14, 95, 96, 109-113]. However, no micro-scale models of the tree frog fibres have been found in the literature. Having a model of how the adhesion force changes according to the forces applied by the robot enables to define the stability of the robot, that is, how close the robot is to falling. From this definition of stability, control strategies can be determined so that the locomotion mechanism of the robot enhances attachment or detachment of the pads as required by the locomotion sequence. A model of how the adhesion force from the tree-frog pads responds to the force from the locomotion mechanism of the robot is developed in Chapter 6, explaining the relevant theoretical principles behind the model. This adhesion model is used in Chapter 7 in order to define a stability criterion for inverse adhesion-reliant locomotion. This stability criterion enables the definition of control strategies of different configurations of the locomotion mechanism presented in Chapter 8.

## **2.4 Robotic systems in surgical applications**

Minimally invasive surgery is a significant advancement of modern surgery because it brings benefits to patients and hospitals by reducing the number of scars and trauma and shortening recovery times [6, 7, 114, 115]. In these procedures, the surgeon inserts and manoeuvres the tools through small incisions with the visual feedback of a camera, inserted in the body in the same way.

However beneficial these procedures are for the patient, the surgeon loses the direct contact of an open procedure and, therefore, the precision and sensorial feedback enabled by direct access to the surgical target. In conventional laparoscopy, the motion of the surgical tools is counterintuitive as the tools are manoeuvred through holes and rotate around the point of insertion. Moving the tool through a hole makes the motion of the hand of the surgeon in one direction translate into a motion of the tool in the opposite direction (fulcrum effect). The point of insertion of the tools is fixed and cannot be easily repositioned along the operating area of the body. In addition to that, the surgeon has to see the surgical cavity on a screen, losing the three dimensional quality of the real image. Furthermore, the surgeon can no longer use their hands to palpate the tissues and organs they are operating on.

Specialised training of surgeon is provided and the insertion ports for the tools are carefully planned before the operation in order to benefit from the advantages of laparoscopic surgery and overcome its disadvantages. Three dimensional cameras are used in the latest laparoscopic systems and tools integrating haptic feedback are under development and likely to become widely available in the near future.

New technology has been developed over the last decades to make minimally invasive operations more precise and comfortable for the surgeon. The first improvement to laparoscopic operations is the use of robotic arms in order to control the surgical tools inserted in the body. More recently, the idea of miniaturising the surgical system, making the robot operate from inside the body, has posed the challenge of intra-body locomotion [1].

The robotic systems for surgery presented next are divided into two groups:

- Surgical systems with robotic arms operating from outside the body and
- Intra-body robots moving and operating inside the body.

#### **2.4.1 Surgical systems with robotic arms external to the body**

One solution proposed to improve the precision and usability of laparoscopic tools is the use of robotic arms to manoeuvre them inside the body. These robotic arms are floor-mounted or mounted on the operation table and controlled by the surgeon from a console in a master-slave fashion. The use of robotic arms makes the motion of the tools more intuitive (no fulcrum effect) and smoother, removing the lack of precision that may arise from the tiredness of the surgeon or the trembling of the hand. This kind of robotic systems have been extensively used with very successful results [114, 115] and can currently perform a wide range of operations in abdominal, spinal, cardiac, bone and brain surgery. The range of exploratory and operating tools they can handle includes cameras, scissors, needles and drills.

Surgical systems with robotic arms external to the body can be divided into four groups:

- Robotic holders of the laparoscope,
- Surgical robotic operators,
- Needle guiding robots and
- Miniature and flexible surgical tools and cameras.

The main difference between these four groups of surgical robotic systems is the degree of interaction of the system with the tissue and the organs of the patient.

Robotic holders of the laparoscope hold the camera for the laparoscopic operation, something that had been done traditionally by a member of the surgical team. Thus, the motion of this type of surgical robots requires very little interaction with the tissue.

Surgical robotic operators include more arms than the robotic holders of the laparoscope in order to control not only the camera but also the tools for the operation. The tools moved by the robotic arms and controlled by the surgeon manipulate the tissue. Therefore, this group of robots has a higher degree of interaction with the tissue than the robotic holder of the laparoscope.

Needle-guiding robots typically use one arm only but interact with the tissue very intensely as they have to make a surgical needle follow a specific path through the soft tissue.

Robotic holders of the laparoscope, robotic operators and needle-guiding robots are composed of floor-mounted robotic arms bearing tools inserted in the body through small incisions. The set-up of these robots is probably inspired by the surgeon standing by the patient and using their arms and hands to operate the tools. These robotic systems occupy a significant portion of the space around the operating table and their big dimensions and heavy weight mean that they are cumbersome, difficult to move and hinder access to the patient. Economically speaking, they require a large capital cost.

In order to reduce the unwieldiness of the surgical tools moved by big, external robotic arms, the surgical tools and camera have been miniaturised and made more flexible. Miniature and flexible tools and cameras have to interact with the tissue in the same way as the robotic holders of the laparoscope and the robotic operators. These miniature tools and cameras are attached to the surgical ports or the surface of the tissue.

#### **2.4.1.1 Robotic holders of the laparoscope**

Robotic holders of the laparoscope replace the surgical assistant that traditionally holds the camera (called laparoscope) during a laparoscopic operation. These robots are able to move the camera around the point of insertion following the surgeon's commands and enabling them to see the abdominal cavity. Commercial versions of these robots exist and are widely

available and used. A good example of this type of robots is Freehand<sup>®</sup>, featuring several joints to move the laparoscope like an industrial robot [116]. Freehand<sup>®</sup> is actuated by the head movements of the surgeon if the surgeon is pressing a pedal at the same time. Freehand<sup>®</sup> is a further development of EndoAssist [117, 118]; other robots of this kind include the voice-controlled AESOP<sup>®</sup> system [119, 120]. Figure 21 shows the Freehand and AESOP<sup>®</sup> laparoscope holders.

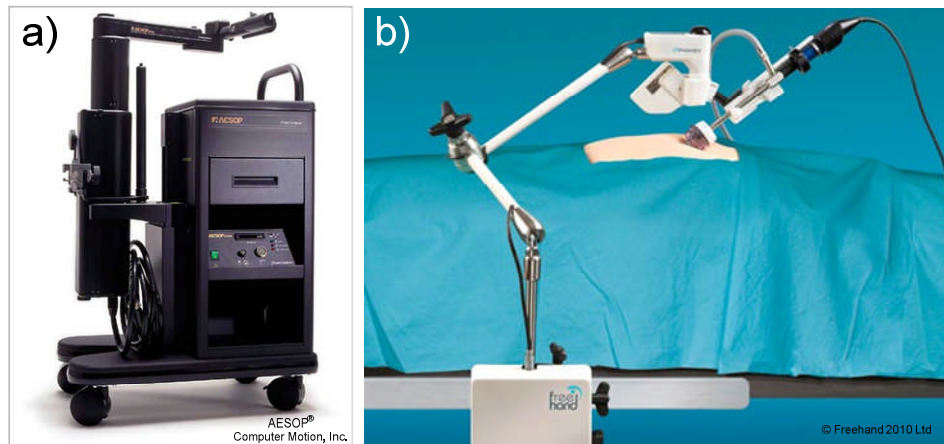


Figure 21. (a) The laparoscopic camera holder AESOP<sup>®</sup> and (b) Freehand<sup>®</sup> .

#### 2.4.1.2 Surgical robotic operators

Robotic operators for surgery are composed of several arms placed around the patient and remotely controlled by the surgeon. The surgeon controls the operation from a console where the image from the laparoscope is shown. Commercial robotic operators for surgery are available, the da Vinci<sup>®</sup> system being the most popular of these robots. In the latest development of the da Vinci<sup>®</sup> system the image from the camera is high definition 3D and the tools to operate include small graspers which replicate the movement of a human wrist [121]. Other robotic operators of this kind are the Polish Robin Heart system for cardiac surgery [122] and MiroSurge, from the German Aerospace Centre (DLR) [123, 124]. The MiroSurge robotic system uses the industrial robot KUKA, a robotic arm designed for interaction with humans [125]. Figure 22 shows the surgical robotic operators Robin Heart and MiroSurge.

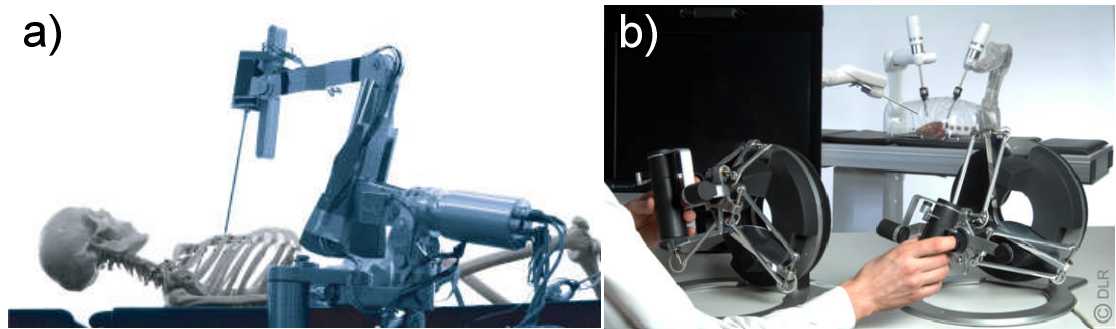


Figure 22. (a) The Robin Heart system for cardiac surgery [122] and (b) the MiroSurge system for laparoscopic surgery (b) [123].

### 2.4.1.3 Needle-guiding robots

A large number of minimally invasive interventions, like biopsy, placing therapeutic agents or stone removal, involve needle driving [126]. Several needle-guiding robots have been developed in order to increase the precision of reaching the target with the needle and minimise collateral damage. For example, the robot Pathfinder for neurosurgery scans the brain of the patient, computing a safe trajectory for the needle to reach the target [127, 128]. Figure 23 illustrates the application of the robot Pathfinder in neurosurgery.



Figure 23. The Pathfinder needle guiding robot for neurosurgery[127].

### 2.4.1.4 Miniature and flexible surgical tools and cameras

Smaller tools and cameras enable the use of fewer and smaller incisions for a laparoscopic operation and take less space inside the body cavity and around the operating table. For instance, a miniature camera that can be placed on the surface of the abdominal organs has been built and tested [51, 52]. This intra-abdominal miniature camera has several degrees of freedom, providing a view of the entire abdominal cavity [51, 52].

More flexible surgical tools can improve the precision of a laparoscopic procedure enhancing the dexterity of the surgeon controlling the tools. One

way to make laparoscopic tools more dexterous is to include miniature joints, or more degrees of freedom, in the design of conventional laparoscopic tools. For example, tools that are able to closely mimic the motion of the human hand are commercially available [129]. Another example of flexible laparoscopic tools is a robotic system with two miniature arms inserted through a single laparoscopic port [130]. Figure 24 a shows an articulated laparoscopic tool and Figure 24 b shows a robotic system for laparoscopic surgery with miniature robotic arms and cameras.

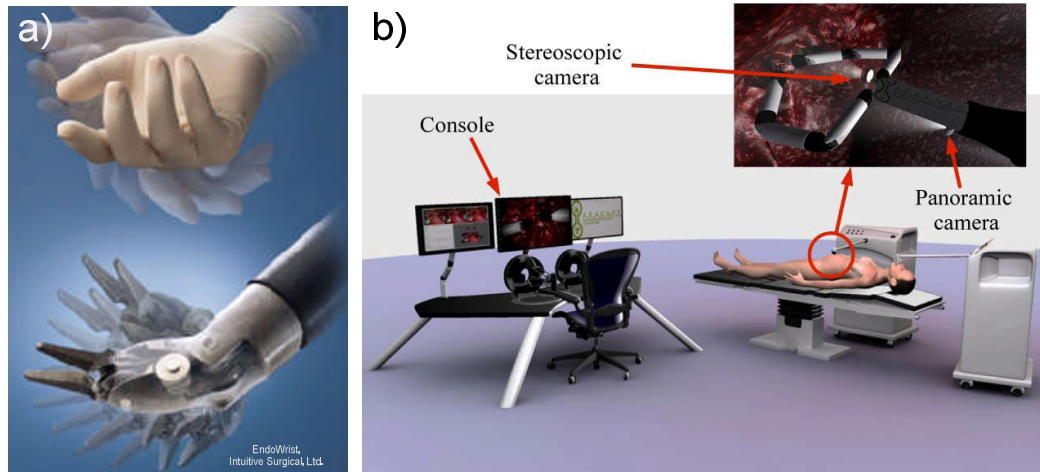


**Figure 24. (a) An articulated laparoscopic instrument (EndoWrist, Intuitive Surgical Inc.) and (b) robotic system with miniature arms for laparoscopy [130].**

Snake-like motion is a promising technology to develop flexible endoscopes. A robotic device that follows this design paradigm is the i-Snake<sup>®</sup> robot which combines multiple articulated segments to steer an endoscope inserted through its hollow centre [82]. More recently, a miniature robotic platform has been developed with flexible arms holding instruments and a head with lights and a camera [131]. This miniature robotic platform is inserted through a standard port in the abdomen [131]. Figure 25a-d shows a miniature robotic platform with flexible arms and a camera operating on the abdominal organs.

Miniature and flexible tools are fixed to a specific location and can enhance the manoeuvrability of the surgical tools and the access to the organs around that location. However, the range of motion of the tools is still limited by the surgical port through which they are inserted because they lack mobility to relocate inside the surgical cavity.

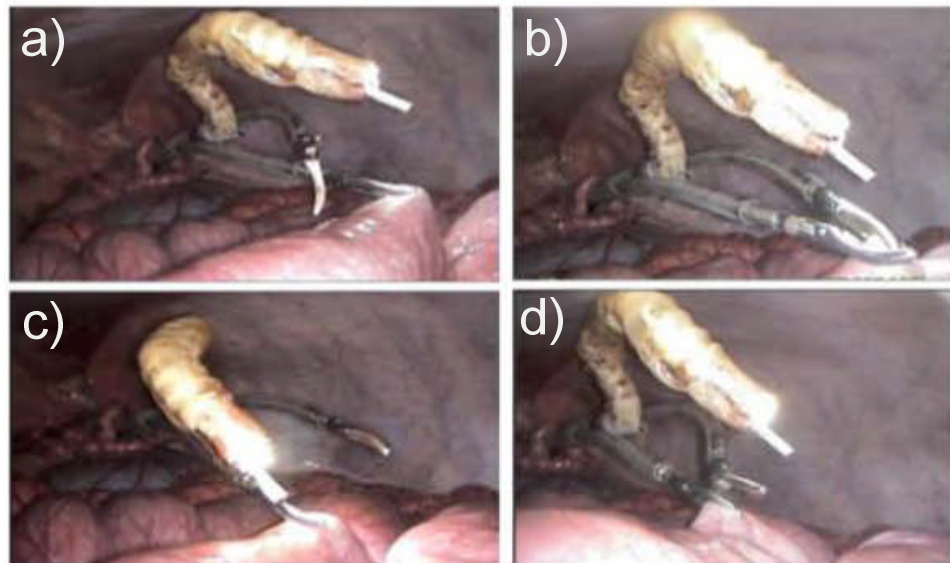


**Figure 25. (a-d) Robotic platform with flexible arms and camera operating in the abdomen [131].**

Magnetic technology has been used in order to move devices along the abdominal wall. A system with two miniature robotic arms that can be magnetically anchored to the abdominal wall has been developed [132]. A small device, magnetically fixed to the abdominal wall and able to change the tilt angle of an onboard camera has also been developed [90]. Commercial applications using magnets to manoeuvre a laparoscopic camera on the surface of the abdominal wall are available [133]. Figure 26 shows a miniature surgical robot mounted on the abdominal wall and an endoscope using magnets to attach to the abdominal wall.

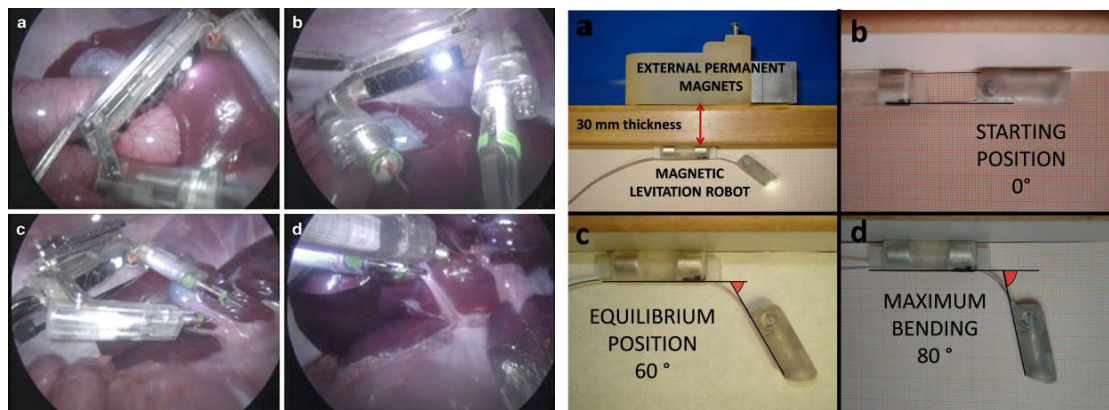


**Figure 26. (left, a-d) Photos of a miniature *in vivo* robot operating from the abdominal wall [134] (right, a-d) endoscope using magnetic levitation [90].**

Magnetic anchoring for robots inside the body extends the use of a well-known attachment technology to intra-corporeal mobility but requires external equipment to generate the magnetic field and handle the camera.

These magnetic devices drag the camera and tools using equipment outside the body and therefore they are not provided with autonomous mobility.

A different approach from making the tools more flexible or dragging them with magnets is to build a robotic device able to move around the surgical cavity carrying the tools. There are trends in current research to provide miniature surgical systems with a locomotion mechanism that enables these systems to move freely inside the body cavities.

### **2.4.2 Intra-body robots**

Intra-body robots are miniature devices able to fit inside a body cavity and perform an operation offering functionality akin to robotic holders of the laparoscope or robotic operators. For example, a mobile intra-body robot could carry a camera and the tools necessary for a surgical operation, moving fully inside the body cavity of interest. Using an intra-body robot further reduces the number of incisions as the robot could carry everything required for the operation and would need only one surgical port to get inside the cavity.

Not only does an intra-body robot have to operate on the organs, it also has to move on their surface. Locomotion on the surface of the organs means a higher degree of interaction with the tissue than robotic operators. Interaction with the tissue is more intense in an intra-body robot than in a robotic operator because the motion of an intra-body robot no longer relies on an external, solid frame of reference. Instead of having a solid frame of reference like in robotic operators, the motion of an intra-body robot depends on the interaction between the robot and the biological tissue.

The environment of an intra-body robot is the body cavity where it has to perform an operation. Body cavities have different shapes and impose a variety of design constraints depending on where in the body the procedure takes place and what type of intervention it is. For instance, in laparoscopic surgery, the environment is created by inflating the abdomen and results in a fairly open space. In minimally invasive cardiac surgery, however, the space around the heart is very tight. Accordingly, an intra-body robot to move around the heart needs to incorporate features to separate the pericardium from the surface of the heart.

Intra-body robots can be classified according to the body cavity where they operate. The body cavities where an intra-body moves can be classified into two groups:

- Tubular (or luminal) cavities like the gastro-intestinal (GI) tract,
- Non-tubular cavities like the insufflated abdomen and the tight space around the heart.

Tubular cavities are meant to be hollow as part of the human anatomy and belong to the digestive system (gastro-intestinal tract) from the mouth to the rectum.

Non-tubular cavities are not meant to be hollow as part of the human anatomy and therefore need to be created for the surgical intervention. For instance, these cavities are created by inflating the abdomen in the case of laparoscopy or separating the tissue around the heart for minimally invasive cardiac surgery.

#### 2.4.2.1 Robots for the GI tract

Robotic devices for tubular organs have been developed over the last decades [76, 135-137]. These devices are mainly designed for exploration of the colon (colonoscopy). These robotic devices move using inchworm locomotion and reduce the pain and the risk of tissue damage traditionally caused by manual steering of the colonoscope. They are a few centimetres wide, to fit the lumen comfortably, and carry lights and a camera on their head to provide an image of the internal walls of the colon. Commercial applications of these robotic systems are available [138, 139]. Figure 27 shows the components of a robotic system for colonoscopy: the workstation of the colonoscope with the screen where the images of the colon are shown (Figure 27a) and the probe to be inserted in the colon (Figure 27b).

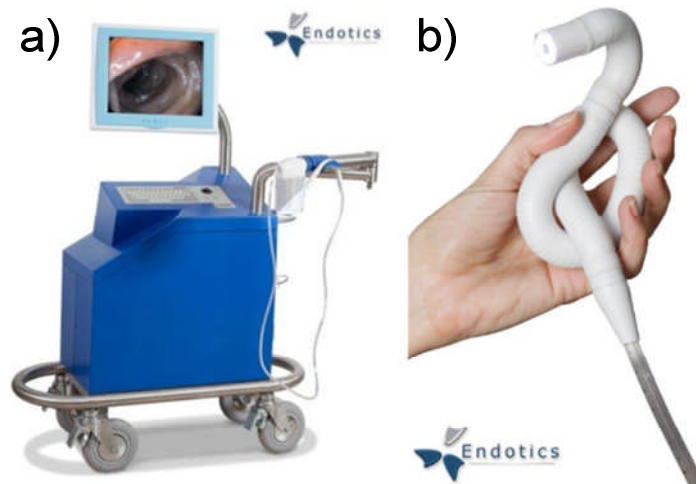
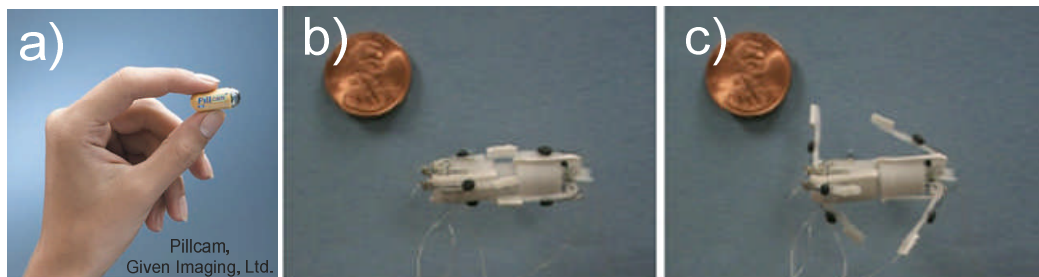


Figure 27. (a) Workstation and (b) probe of a robotic system for colonoscopy [136].

Pills that incorporate a camera to explore the GI tract are also available in the market of medical devices [140]. These pills are swallowed by the patient and take pictures as they travel through the GI tract, sending them to a computer where the doctor can check them. The pills move with the natural motion of the GI tract (peristalsis).

The commercially available versions of these pills have no capability to stop at a specific location along the GI tract. If these pills could be stopped at a specific location, they would allow more detailed exploration of specific areas of the GI tract, enabling better diagnosis of the condition. For this reason, several stop mechanisms for these pills have been developed [60, 62, 141, 142]. These mechanisms are miniaturised in order not to increase the volume of the pill significantly and some of them use bio-inspired adhesion technology to grip to the walls of the GI tract [62, 141].

Figure 28a shows one of the commercially available pill cameras for the GI tract. Figure 28b and c show a stop mechanism for this type of pills using beetle-inspired adhesive surfaces like those discussed in Section 2.3.7.



**Figure 28. (a) Pill with a camera for exploration of the gastro-intestinal tract and (b and c) stop mechanism for this kind of pills: (b) with the legs folded and (c) with the legs unfolded [62].**

The motion of a miniature robotic system inside a luminal organ is facilitated by the shape of the organ because there is only one direction to follow, forward or backward along the lumen. The design challenges of this type of locomotion focus on negotiating the intricate bends of the gastro-intestinal tract and obtaining enough grip to move along the walls of the tubular organ. In a non-tubular cavity, the locomotion mechanism of the robotic system has to enable motion of the robot in all directions of the surface of support.

The next two robots move in non-tubular cavities: around the heart and along the abdominal organs, and are the most relevant robots to the intra-abdominal robot of all the robotic systems reviewed in this chapter.

### 2.4.2.2 The HeartLander robot for cardiac surgery

The Heart Lander robot was developed in order to crawl over the surface of the beating heart and deliver drug to the location previously specified to its navigation algorithm [27, 59]. For the locomotion of this robot, two vacuum suction cups alternate attachment of the head and tail of the robot to the surface of the heart in an inchworm fashion. The main issue with this system is to ensure the seal around the cups has been formed for the suction force to be effective [27].

The locomotion mechanism of the robot is remotely actuated with a set of motors pulling and pushing a pair of cables to obtain separation between the head and tail of the robot. The mechanism can also bend the head of the robot to enable it to steer. Figure 29a shows the boxes of motors and controls of the HeartLander robotic system and Figure 29b shows the prototype of the robot.

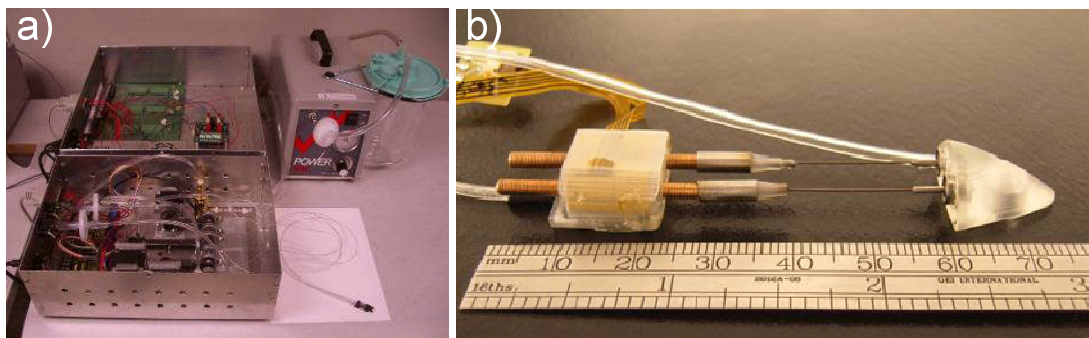


**Figure 29. (a) Instrumentation boxes (left), vacuum pump (upper right), and tethered crawling robot (lower right) of the HeartLander robotic system [59] and (b) the latest prototype of the robot [143].**

The external transmission of force through remote actuation makes the control of the robot stiff, that is, lacking in precision, and to tackle this the newest prototype includes on-board motors [143]. The size of the latests prototype is 76 x 15.5 x 9 mm (L x W x H). The HeartLander robot is designed to navigate and position on the beating heart and a series of porcine trials showed its feasibility *in vivo* [27]. In those tests the robot reached the target within 97s on average, the total relative positioning accuracy being 1.7 mm. The locomotion efficiency was 40% because of slippage; the robot designers expect to improve locomotion efficiency by synchronising the robot's motion with respiration and heartbeat [27].

### 2.4.2.3 The Nebraska wheeled robot for abdominal surgery

The Nebraska wheeled robot is designed to move around the abdominal organs with two metallic wheels driven by two independent DC motors [56]. Power to the motors of the prototype is supplied through a tether, although a wireless prototype has also been tested [56]. The robot can carry a camera and biopsy tweezers [28, 144].

Several profiles of the wheels of the robot were tested experimentally on bovine liver. The helical profile was able to provide the best traction and was chosen for the prototype of the robot. During *in vivo* tests, the robot was able to achieve a maximum speed of 2 cm/s with sufficient manoeuvrability around the abdominal organs [57, 145-147]. The wheels have an outer diameter of 15 mm to fit through a trocar port, the length of the robot is 75 mm and its mass is 50 grammes [56].

The use of micro-patterned treads on the wheels, instead of a metallic profile, has been recently investigated by the authors. The *in vivo* performance of a smooth and a micro-patterned wheel were compared and the micro-patterned wheel outperformed the smooth one [148].

The prototype of the Nebraska wheeled robot with a camera and biopsy tweezers is shown in Figure 30a. Figure 30b shows the Nebraska wheeled robot moving on the surface of the abdominal organs.

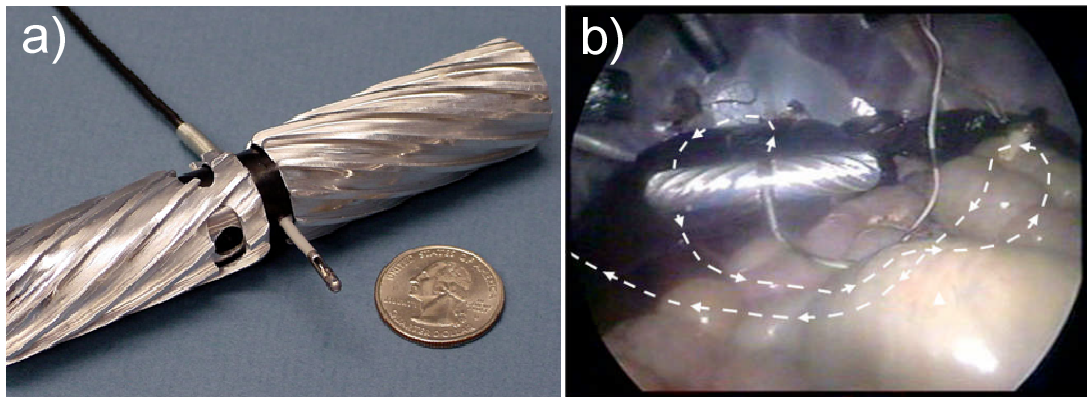


**Figure 30. (a) The Nebraska wheeled robot with a camera and biopsy tweezers and (b) the robot moving around the abdominal organs [145].**

The aluminium wheels of the Nebraska robot provide traction on visco-elastic tissue but are unable to attach to the surface of the organs and climb internal walls. The steadiness of the motion of the robot is limited by the wheels of the robot having to follow the hilly surface of the abdominal organs.

The development of these intra-body robots prove the potential of carrying out exploratory and surgical procedures with a mobile robotic platform inside the body. The design of these miniature robots adapts to the specific requirements of the environment in which they operate. To obtain intra-body locomotion, these robots, use a combination of miniature actuators and technology to move efficiently in a soft and wet environment. In this way, robots inside the colon adopt a tubular shape and their actuation mechanism follows the walls of the lumen. The hardware of the Heart Lander robot is specially designed to compensate for the motion of the heart and move between the surface of the heart and the layer of tissue covering the heart. The profile on the wheels of the Nebraska robot is optimised to move over highly compliant abdominal organs. In conclusion, for intra-body mobility it is crucial to provide the robotic system with a mechanism able to obtain locomotion on the surface of biological tissue.

## **2.5 Discussion of surgical robotic systems**

Compared to manual laparoscopy, robotic surgical systems improve the precision of the procedure, making it more comfortable for the surgeon. In externally actuated robotic systems, floor-mounted robotic arms move the tools inside the patient while the surgeon controls the tools from a console with a high definition image of the abdominal cavity. These systems are successfully used and commercialised but they are cumbersome and costly. Like in the manual procedure, the tools in an externally actuated surgical robot cannot be repositioned along the abdominal wall and can only move around the point of insertion.

Commercial applications and research prototypes of smaller and bendable laparoscopic cameras and tools are currently available. Some of these systems make use of miniature robots inserted in the abdominal cavity and fixed to the abdominal wall through a single port. These robots reduce the unwieldiness of the robotic system and the number of incisions required to insert the tools. Their flexible actuation makes access to the organs and manipulation easier but they are fixed to a position on the abdominal wall.

Other small and flexible robots use magnetic technology to fix and move the tools and camera along the wall of the abdomen. These systems enable repositioning of the tools and camera along the abdominal wall but they require external equipment to generate the magnetic field that provides attachment to the abdominal wall.

A different approach to make operation of the tools and camera more flexible is to build a small robot able to fit through an incision and move inside the cavity of interest. Following this approach, a crawling robot using suction cups and remote actuation has been developed to deliver drug to the surface of the beating heart. This robot is able to inject drug at a specific position on the heart but remote actuation makes control of the robot stiff and its performance is hindered by slippage. In addition to that, suction cups are difficult to seal around tissue and require an external vacuum circuit.

Also, a wheeled robot has also been implemented and tested moving on the surface of the abdominal organs. This robot is able to carry a camera and small tools. However, this robot cannot attach to tissue, it does not operate at a vantage point and the control of the robot is hindered by the irregular surface of the abdominal organs.

With respect to power requirements, all intra-body robots developed to date are tethered given the difficulties of integrating a power source within the mechanism of the robot without significantly increasing their size and/or weight. A wireless prototype of the Nebraska wheeled robot was tested *ex vivo* and *in vivo*; the wireless version was larger and required a larger tail in order to match the performance of the tethered prototype [56]. Some miniature climbing robots using bio-inspired adhesives, such as Waalbot [101], carry the batteries to power their motors but their size is significantly larger than required for an intra-body application: Waalbot is 10cm long. Taking into account these considerations, the prototype of the intra-abdominal robot will be tethered for the sake of simplifying the power system of the robot and in order to keep its mechanism as lightweight and compact as possible. Future development of the robot could be wireless as smaller and lighter batteries become available for intra-body applications.

Table 4 summarises the advantages and disadvantages of current surgical robotic systems, including externally actuated robots and intra-body robots. The table also includes miniature climbing robots whose size, locomotion and attachment mechanism is relevant for the design of an intra-abdominal miniature robot.

**Table 4. Robotic systems reviewed for the design and implementation of an intra-abdominal miniature robot.**

Technology	Type of Robot	Type of locomotion	Attachment	Stage of development	Advantages for inverted adhesion-reliant locomotion	Disadvantages for inverted adhesion-reliant locomotion
Externally Actuated Robotic Systems	Camera holders	Set of actuators on rigid frame	External, floor-mounted	Commercial	<ul style="list-style-type: none"> <li>• Precision of motion</li> <li>• Unaffected by tiredness</li> </ul>	Camera fixed to insertion point
	Operators and needle-guiding	Set of robotic arms	External, floor-mounted	Commercial	<ul style="list-style-type: none"> <li>• Precision of motion</li> <li>• Unaffected by tiredness</li> </ul>	Camera and tools fixed to insertion point
	Miniature and flexible tools and cameras	Articulated links or moved with external magnets	Incision-mounted or fixed to magnet	Research and Commercial	<ul style="list-style-type: none"> <li>• Better access</li> <li>• Better manoeuvrability</li> </ul>	Fixed to insertion point or external magnet
Intra-body Robots	Intra-luminal (inside GI tract)	Worm-like (follows the lumen)	To the walls of the lumen (pressure, adhesion)	Research and Commercial	<ul style="list-style-type: none"> <li>• Better access</li> <li>• Reduced pain</li> </ul>	Only for one-directional environment
	HeartLander	Inch-worm (polar walker)	To the heart with suction cups	Research	Precise positioning on the beating heart	<ul style="list-style-type: none"> <li>• Requires vacuum pump</li> <li>• Vacuum suction inefficient on tissue</li> <li>• Remote, stiff actuation</li> </ul>
	Nebraska Wheeled Robot	Wheels (metallic or micro-threaded)	Moves on the organs with profile on metallic wheels or micro-threads	Research	Repositioning of camera and tools on the surface of the abdominal organs	<ul style="list-style-type: none"> <li>• No operation from a vantage point</li> <li>• Uncontrolled locomotion on unstructured terrain</li> </ul>

Technology	Type of robot	Type of locomotion	Attachment	Stage of development	Advantages for inverted adhesion-reliant locomotion	Disadvantages for inverted adhesion-reliant locomotion
Adhesion-reliant Miniature Robots	Gecko-shaped	Legs	Bio-inspired adhesion	Research	<ul style="list-style-type: none"> <li>• Strong attachment</li> <li>• Controllable adhesion</li> </ul>	<ul style="list-style-type: none"> <li>• Complex design</li> <li>• Slow</li> <li>• No adhesion to wet surfaces</li> </ul>
	Tank-like	Tracks	Bio-inspired adhesion	Research	<ul style="list-style-type: none"> <li>• Strong attachment</li> <li>• Simple design</li> <li>• Fast</li> </ul>	No adhesion to wet surfaces
	Wheel-leg	Wheel-legs	Adhesion (some bio-inspired)	Research	<ul style="list-style-type: none"> <li>• Strong attachment</li> <li>• Simple design</li> <li>• Fast</li> <li>• Adhesion recovery</li> </ul>	No adhesion to wet surfaces

The surgical robot of the future will combine the advantages of the technologies and improvements for laparoscopic surgery reviewed in this chapter and summed up in Table 4.

Such a robot will have autonomous locomotion inside the cavity while being comfortably controlled by the surgeon from a console. This future robot will also carry flexible tools, using controllable adhesion to climb the wall of the abdomen and move in inverted locomotion. In addition to that, the robot could also include magnets as a back-up attachment system.

In order to develop a robot with all these features, intra-body robots require autonomous motion, operating from the wall of the abdomen without any external equipment to keep them attached. A locomotion mechanism able to control adhesion to the surface of the peritoneum would be a significant contribution to the development of this surgical robot of the future.

## **2.6 Summary**

Robots have been developed in conventional, miniature, micro and nano dimensions. In order to provide locomotion to robots a number of strategies have been used: wheels, tracks, legs, wheel-legs, worm-like and snake-like locomotion. Robot also use different attachment methods, like magnets, suction pads or adhesion, in order to climb a surface and move in inverted locomotion.

Miniature robots are conventional robots scaled-down to a few cubic centimetres. The main challenges of a miniature robot are: manufacturing in a small scale and actuation for low forces. Current actuation technologies for miniature robots include DC mini-motors, piezo-electric motors, SMA actuators and IPMCs. Current manufacturing techniques for miniature robots include injection moulding, CNC micro-machining and rapid prototyping. Miniature climbing robots using bio-inspired adhesion have been developed using a variety of locomotion strategies: legs, tracks and whegs.

Inspiration from nature has been used to improve the performance of robotic systems and can be useful to resolve the challenges posed by intra-body locomotion. Three particular features found in nature are relevant to inverted adhesion-reliant locomotion for an intra-abdominal robot: control of attachment in geckoes, adhesion to wet surfaces in tree-frogs and amoeboid locomotion. Geckoes obtain strong attachment through tiny hairs on their toes and can control adhesion by preloading and peeling off their toes. Tree frogs have a micro-structured pattern on their toes that enables them to

attach strongly to wet surfaces. Amoebas move along a plane changing the shape of their body and alternating locomotion between different parts of their body.

Laparoscopic surgery is beneficial for patients and hospitals but makes the operation more difficult for surgeons because they have to operate with long tools inserted through incisions, watching the organs on a screen. Robotic systems with robotic arms moving the laparoscopic tools make the procedure more precise and comfortable for the surgeon. These systems are actuated from outside the body and include camera holders, robotic operators and needle guiding robots.

Miniature and flexible tools and cameras have been developed in order to make surgical robots less cumbersome and further reduce the number of incisions used in laparoscopy. Miniature cameras can be mounted on the abdominal organs or attached with magnets to the abdominal wall. Flexible tools use snake-like mechanisms to improve manoeuvrability and access inside the abdomen.

Fully internalised mobile robots have also been developed in order to further reduce the size of surgical robots and enhance their mobility inside the body. These intra-body robots are used for exploration of the digestive system and for operation on the heart and inside the abdomen. Colonoscopy robots use inch-worm locomotion in order to reduce the pain caused by the manual procedure. Stop mechanisms for pill endoscopes use gecko-inspired adhesion and enable the doctor to stop the pill at a specific location. The HeartLander robot uses inch-worm locomotion to crawl over the surface of the beating heart with suction pads, delivering drug to a specific location on the surface of the heart. The Nebraska wheeled robot uses two wheels with a profile or micro-treads that enable motion on the surface of the abdominal organs, carrying a camera and small surgical tools.

## **Chapter 3**

### **Specifications and conceptual design of the robot**

#### **3.1 Introduction**

The literature review on miniature robots for intra-body operation showed the great potential of internalising the operation of robotic assistants for surgery. Alongside with this, it also made clear that a new paradigm of intra-abdominal operation and locomotion is required to advance the development of technology for minimally invasive surgery. Accordingly, a novel design for an intra-body robot is presented in this chapter. In order to understand the constraints imposed by the environment on the design of the intra-abdominal robot, a brief description of the abdominal cavity is given in the first place.

After this, the advantages of using a robot hanging from the top of the abdominal cavity are explained together with the challenges of intra-abdominal operation in inverted locomotion. Several design principles are drawn from the considerations of the environment and the application of the robot and the type of locomotion is selected accordingly. The design of the locomotion mechanism and the locomotion sequence of the robot are explained in the last sections before summarising the contents of the chapter.

#### **3.2 The environment of the robot: the insufflated abdomen**

In laparoscopic surgery, the space for the surgical operation is created by insufflating the abdomen. The insufflated abdomen provides space for the surgeon to insert and manoeuvre the tools and see the abdominal organs with the help of a camera and lights. This section first explains what the abdomen is and then describes the surface on which the robot moves: the inside wall of the abdomen or peritoneum. Lastly, the section summarises the geometrical aspects of the abdomen and the surface properties of the peritoneum relevant to the motion of the robot.

##### **3.2.1 The human abdomen**

The abdomen is the part of the body between the chest and the pelvis, where most of the gastro-intestinal organs are placed. The main organs of interest for surgery in this part of the body are: the stomach, the liver, the

small bowel, the gall bladder, the colon and the sexual organs. In Figure 31a the muscular layer of the abdominal area is shown. Figure 31b shows the complexity and uneven surface of the abdominal organs.

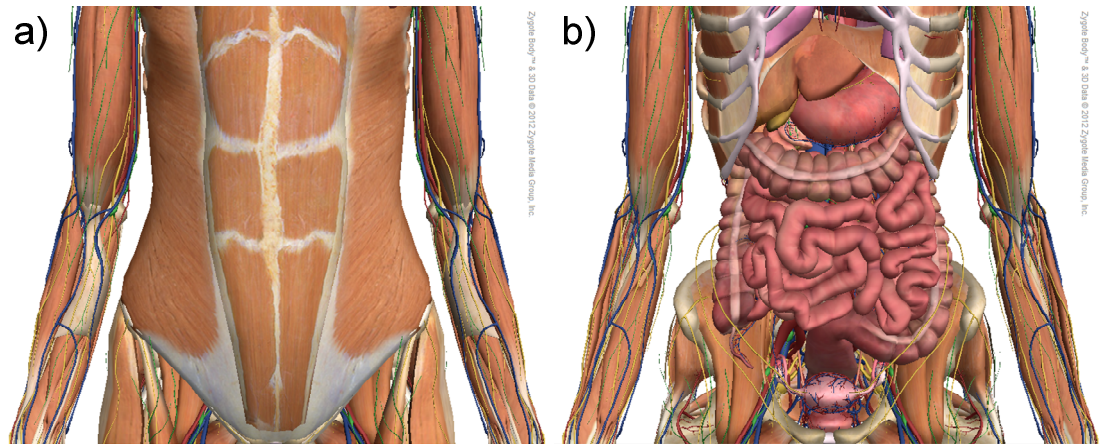


**Figure 31. (a) Muscles of the human abdomen and (b) organs in the abdominal cavity [149].**

Inside the abdomen, the abdominal organs are covered by a layer of fat. The inside wall of the abdomen, the peritoneum, is situated above the abdominal organs. Figure 32a shows a view of the peritoneum and the abdominal organs covered by the layer of fat (the yellow substance) from a laparoscopic camera. Figure 32b shows a view of the colon and liver from a laparoscopic camera.

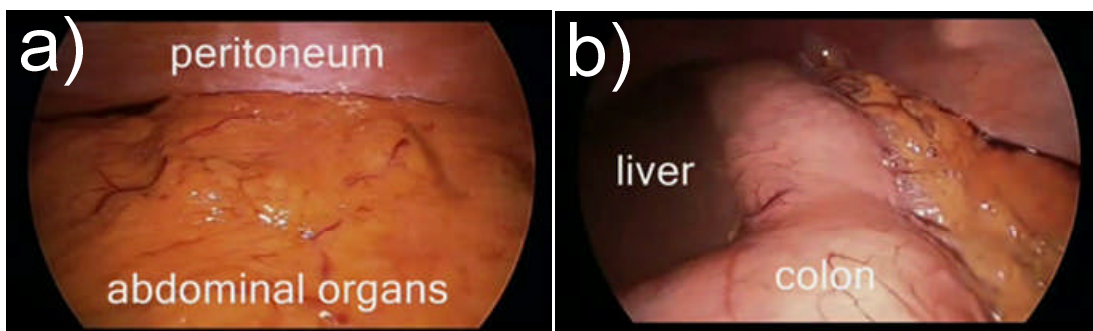


**Figure 32. (a) View of the peritoneum and abdominal organs from a laparoscopic camera and (b) view from a laparoscopic camera showing the liver and the colon.**

The surgical tools and endoscopic camera are inserted into the abdominal cavity through the abdominal wall and peritoneum. During the operation, the surgeon uses the laparoscopic tools in order to move the layer of fat out of the way and gain access to the organs. Using the laparoscopic tools, the surgeon moves the organs around in order to find the surgical target. Figure

33a and Figure 33b show the aspect of the abdominal cavity during a laparoscopic operation.

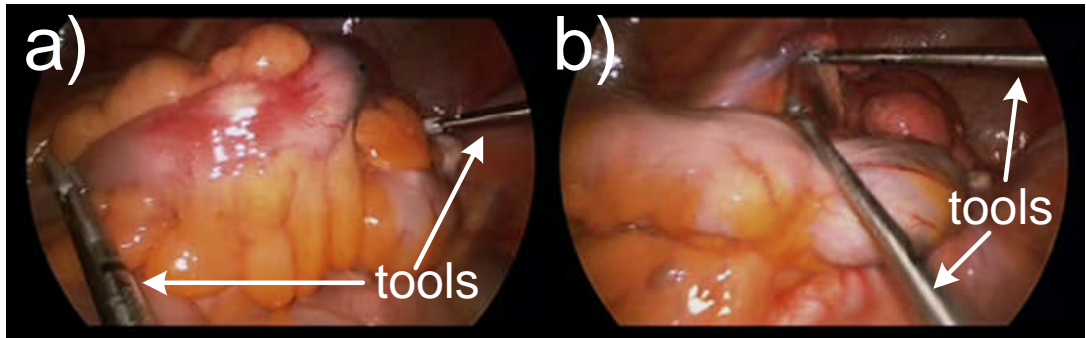


**Figure 33. (a-b) Stills from a laparoscopic camera of the abdominal cavity during an operation.**

The abdominal wall is the surface that will be used by the intra-abdominal robot to support itself and is described in detail next.

### 3.2.2 The abdominal wall

The abdominal wall is composed of skin, a layer of fat, a layer of muscle and the peritoneum, the peritoneum being the most internal layer. The proposed intra-abdominal robot will attach to the inside wall of the abdomen in order to operate from a vantage point inside the insufflated abdomen. Figure 34a shows the position of the robot inside the abdominal cavity and Figure 34b shows the layers that compose the abdominal wall.

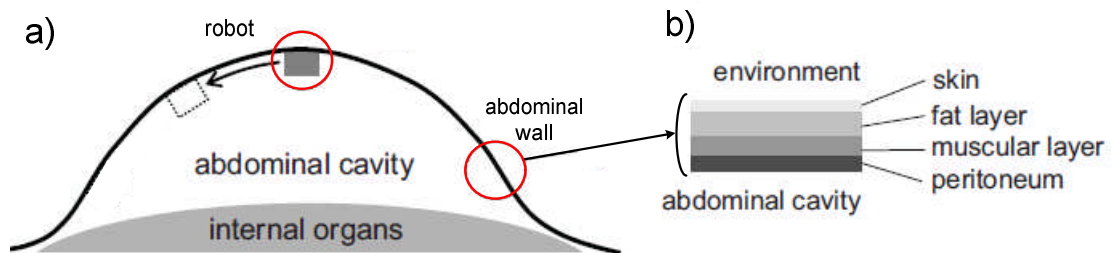


**Figure 34. (a) Position of the robot inside the abdominal cavity and (b) composition of the abdominal wall, adapted from [8].**

The peritoneum is composed of a thin layer of cells that forms the internal surface lining of the abdominal wall and covers the surface of the abdominal organs. The peritoneum is covered by a thin layer of fluid which is secreted continuously from specialised cells, ensuring that the peritoneum remains wet at all times and lubricates the organs [150]. The presence of this fluid will be exploited by the adhesive pads used for the intra-abdominal robot because these pads use capillary forces to enhance the attachment of the

robot to the peritoneum. Dehydration damages the peritoneal tissue and lowers the weight that the adhesive pads can support [10].

Mouse peritoneum is very similar to human peritoneum; the topography of mouse peritoneum has been investigated and shown to be a relatively flat surface [8]. An image of mouse peritoneum obtained in this investigation is shown in Figure 35.

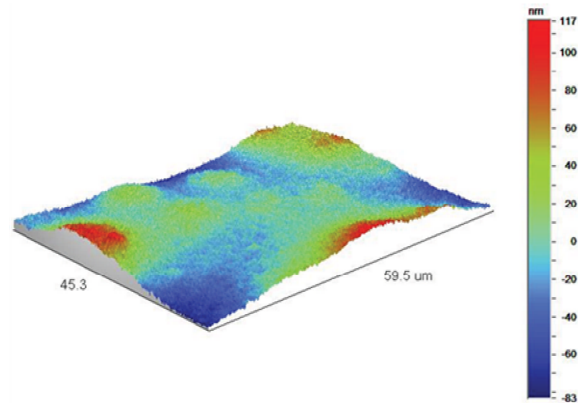


**Figure 35. Topography of the surface of mouse peritoneum [8].**

The intra-abdominal robot operates inside the abdominal cavity, attached to the peritoneum. The geometry of the insufflated abdomen as the environment for the intra-abdominal robot is explained next.

### **3.2.3 The geometry of the insufflated abdomen**

The peritoneum surface is held up, away from the abdominal organs, by the pressure of the carbon dioxide used to insufflate the abdomen, which causes the peritoneum to be slightly vaulted. Inside the insufflated abdomen, the space between the raised peritoneum and the surface of the abdominal organs is 5-6 cm. The maximum inclination between the horizontal and the curvature of the peritoneum is about 60°. The maximum length of the transversal section (from the left to the right side) of the human abdomen is approximately 30 cm. For this project, based on the experience of the surgical team, the area of interest for the operation of the robot is considered a square of 10cm x 10cm at the centre of the abdomen. Drawing from the experience of Prof David G. Jayne: “Preliminary observations undertaken during laparoscopic surgery showed that a working range of 10cm x 10cm was seen to provide sufficient intra-abdominal coverage to enable most surgical procedures to be performed”. Figure 36 illustrates the geometry of the insufflated abdomen and the position of the robot within it.

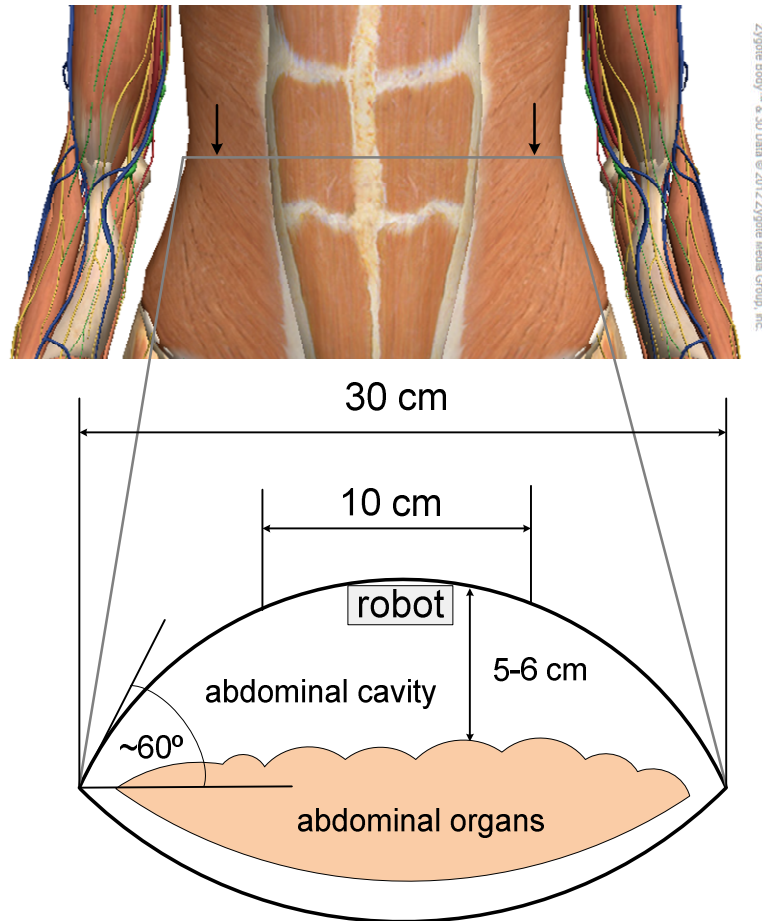


**Figure 36. Geometry of the insufflated abdomen (not to scale).**

As shown in Figure 36, the robot will move on the surface of the peritoneum at a distance from the abdominal organs.

### **3.3 Advantages of an adhesion-reliant robot moving on the surface of the peritoneum**

An adhesion-reliant robot moving on the abdominal wall could potentially carry a laparoscopic camera and tools. The advantages of having an adhesion-reliant robot moving on the surface of the peritoneum are:

- Repositioning of the camera or tools carried by the robot along the surface of the peritoneum, which means:
  - Better view of the organs from the camera carried by the robot and
  - More convenient interaction with the surgical target from the tools carried by the robot.
- Enhanced manoeuvrability around the surgical target.
- No external equipment required for the attachment system.

The camera and tools carried by the robot can be repositioned along the peritoneum because the motion of the robot is not limited to the insertion port. A completely internalized device could work at any location and orientation within the abdominal cavity, moving out of the way of other operating instruments. Thus, an intra-abdominal robot could obtain a better view of the organs by changing the position of the camera on the peritoneum. Likewise, an intra-abdominal robot carrying surgical tools enables the tools to reach the surgical target and interact with it more comfortably because the position of the robot on the peritoneum can be adjusted. This is an advantage over current surgical robotic systems where the tools and camera are inserted through a fixed port and moved by actuators outside the body cavity [121, 123, 131]. Robotic systems operating through a fixed port enable vision and manipulation within a defined area, but the motion of the laparoscope and tools is limited to an arc around the point of insertion [151]. This limitation of surgical robotic systems with actuation external to the abdomen is illustrated in Figure 37.

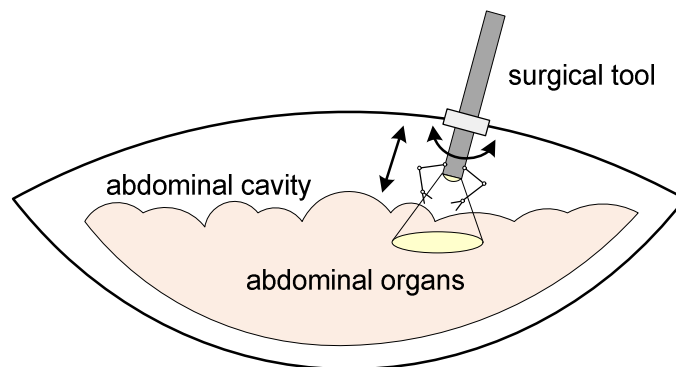


**Figure 37. Sketch of a surgical tool inserted into the abdominal cavity through a fixed port.**

Compared to motion on the surface of the abdominal organs, from a vantage point within the abdominal cavity like the peritoneum, it is easier to move to a position where a better view and clearer access to the surgical target is obtained. The peritoneum is a smooth surface so mobility on the peritoneum is not hindered by the roughness of the surface. This is an advantage over intra-abdominal robots that move on the surface of abdominal organs [56, 57] (see Figure 38) because the surface of the abdominal organs is highly unstructured as shown earlier in Figure 33. Therefore, it is difficult to control the motion of a miniature robot on the surface of the abdominal organs. Figure 38 shows a sketch of a miniature mobile robot moving on the surface of the abdominal organs.

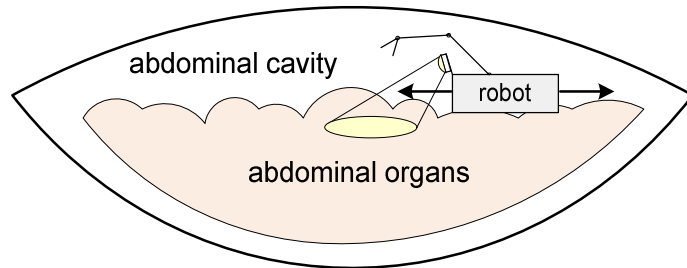


**Figure 38. Sketch of an intra-abdominal robot moving on the surface of the abdominal organs.**

Unlike other attachment technologies, bio-inspired adhesive pads do not require any additional components to ensure the pads are attached and detached. This is an advantage over other intra-abdominal devices that use suction pads or electromagnets to attach to tissue [27, 90, 133, 134, 152]. For example, for a robot using suction cups, a vacuum circuit is required to attach and detach the robot to the tissue. For electro-magnetic attachment, an external magnetic field generator is required to control the attachment and detachment of the robot to the tissue. No external equipment is required for the bio-mimetic adhesive pads because the locomotion mechanism of the robot can be used in order to preload the pads to attach and peel them off to detach.

A mobile robot operating from the peritoneum can focus on and reach virtually every place inside the abdominal cavity, moving on a smooth and stable surface. A sketch of an intra-abdominal robot operating from the peritoneum is shown in Figure 39.

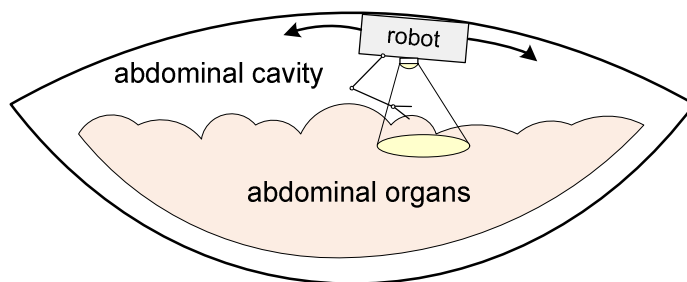


**Figure 39. Sketch of an intra-abdominal robot moving on the surface of the peritoneum.**

### **3.4 Challenges of intra-abdominal inverted adhesion-reliant locomotion**

The challenges of intra-abdominal locomotion on the surface of the peritoneum are set by the environment (the human abdomen), the inverted adhesion-reliant locomotion and the requirements to make operation of the robot medically safe:

- The environment (the human abdomen):
  - Miniature size of the robot,
  - Compact motion of the robot,
- Inverted adhesion-reliant locomotion:
  - Weight of the robot,
  - Control of the adhesion of the pads,
- Medical safety:
  - Minimal tissue damage,
  - Safe temperature of operation,
  - Low voltage of operation,
  - Sterilisation of the robot,
  - Bio-compatibility.

The robot would be inserted into the abdomen through one of the incisions used for the laparoscopic procedure. Laparoscopic ports range from less than 12 mm to up to 2 cm in diameter [153]. For Single Incision Laparoscopic Surgery (SILS) ports can be up to 3 cm in diameter because they are used for the extraction of the surgical specimen. The robotic device has to fit through a SILS port and therefore the maximum width of the robot should be 3 cm. The distance between the abdominal wall and the abdominal organs is 5-6 cm (see Figure 36) so the robot should be able to fit and manoeuvre comfortably within that space. The robot should occupy as little volume as possible during locomotion, so that the mechanism of the robot does not interfere with the tools and tissue around the robot.

An area of 1 cm<sup>2</sup> of the tree frog adhesive pads used to support the robot against gravity (see Section 2.3.7) can hold a weight of 8-14 grammes [10]. The weight of the robot should be lower than the total weight the pads of the robot can support. The adhesive pads need a preload force of around 10 mN [10] to attach to the tissue and can be detached by applying their maximum load or by peeling them off. The design of the robot requires a locomotion mechanism able to apply sufficient force on the pads to attach and detach them.

In medical terms, the locomotion of the robot inside the abdomen should cause as little tissue damage as possible. The robot should not cause harmful friction or pressure on the tissue. The temperature of the parts of the robot touching the tissue must be within the range of temperature tolerable by the tissue; the normal temperature of the body is 36.9°C and up to 45°C

can be tolerated for up to one minute [154]. The parts of the robot touching tissue must be electrically insulated. The materials of the robot in contact with human tissue must be free from harmful chemicals and bio-compatible. The robot should undergo some sterilization procedure before and the parts of the robot in contact with tissue should be ideally disposable.

The material used for the pads is a bio-compatible soft elastomer: MacDermid Autotype™ [10]. The mechanism of the robot can be designed so that the pads are the only part of the robot in contact with the tissue and can be disposed of after each intervention. The mechanism of the robot can be insulated and protected with a case of a bio-compatible material that can also be disposable.

### **3.5 Design principles of a locomotion mechanism for an intra-abdominal adhesion-reliant robot**

Considering the previous challenges of the application and environment of the robot, what design principles should be followed?

The first design principle to follow is simplicity of the design; this is true of any engineering system and it is especially important in a robot where the size and weight are critical factors to determine its functionality. Too big a size of the robot would make it impossible to fit inside the abdomen and too heavy a weight cannot be withstood by the adhesive pads and would make the robot fall down.

A locomotion mechanism with as few components as possible is required to obtain a compact design of the robot. The addition of mechanical components, like links and joints, and control components, like sensors and actuators, is only justified if these additional components offer a clear qualitative or quantitative advantage over a simpler design. For instance, if the addition of a pad enables the robot to carry a higher payload, this would be an important quantitative improvement and the addition of the pad would be justified. An example of a relevant qualitative improvement would be if the addition of a pad changes the distribution of moments on the pads of the robot in a way that benefits the stability of the robot. More details on how the different configurations of the pads can affect the stability of the robot are given in Chapter 8. In terms of the power supplied to the robot and the communication between the robot and the surgeon, the weight and size of the robot can be kept to a minimum by using a tethered design. This tether will carry the power for the motors of the mechanism as well as the control

signal for the motors. This control signal will follow the commands of the surgeon who monitors and decides on the motion of the robot from a computer console. In this way, the batteries and drivers of the robot can be kept off-board, reducing the size and weight of the robot.

The design of the robot can be more compact if the number of actuators is reduced by using the same motor for different purposes within the locomotion mechanism. For example, a rotary motor can apply a moment to the pad in order to peel off the adhesive pad but cannot control the separation between the pad and the tissue. A linear motor can apply a force to peel the pad off and can also control the separation between the pad and the tissue. Therefore, in this case, a linear motor is preferable to a rotary motor because the linear motor can control the distance between the pad and the tissue, which is a desirable feature of the mechanism. As explained in Section 2.2.2., another reason to prefer linear motors over rotary motors is that the smallest and lightest linear motors found in the market are more compact and lightweight than the smallest commercial rotary motors.

Symmetry of motion makes the design of the robot more robust by simplifying the locomotion mechanism as well as the implementation and control of the robot. Symmetry of motion means that all the pads of the robot are detached, attached, moved and supported during motion in exactly the same way. Symmetry of motion involves geometrical symmetry of the locomotion mechanism as well as identical support conditions for each pad. The theory behind this design principle of motion symmetry is further explored in Chapter 8.

The second design principle regards the stress that the robot can apply to the tissue. Locomotion on the surface of the peritoneum should be smooth in order to ensure minimal tissue damage. Smooth locomotion on the surface of the peritoneum means diminishing the rubbing between the adhesive pads and the tissue that may cause damage. For instance, shearing or twisting the pad in order to detach it makes the adhesive surface rub against the tissue, causing a more intense contact than peeling the pad off. Therefore, in this case, peeling the pads off is preferable to other detachment methods in order to minimise tissue damage. Peeling off the adhesive pads also requires less detachment force than other methods.

The third design principle is concerned with the stability of the robot, that is, how much control the locomotion mechanism can have on the pads in order to prevent a fall. Attachment and detachment of the adhesive pads should be controllable in order to prevent the robot from falling from the peritoneum.

Control of the adhesion of the pads diminishes tissue damage because it enables control of the preloading and peeling forces applied on the tissue. Locomotion is more efficient with control of adhesion because the locomotion controller knows whether the pads are detached and can move or whether the pads are attached and can support the robot.

In all, the design principles for the locomotion mechanism are:

- Simplicity. The complexity, size and weight of the mechanism and control system must be kept to a minimum by:
  - Using as few mechanical and control components as possible,
  - Using the actuators for different purposes within the locomotion sequence of the robot,
  - Making the motion of the robot symmetrical for all directions of locomotion and
  - Supplying the power and control signal of the motors via a tether, tele-operating the robot from a computer console.
- Minimal tissue damage. Locomotion over the surface of the peritoneum must be as smooth as possible,
- Stability. Attachment and detachment of the adhesive pads must be controllable and repeatable.

### **3.6 Selection of a locomotion strategy for an intra-abdominal adhesion-reliant robot**

Of the locomotion strategies considered in Section 2.3 the simplest to implement are wheels, tracks and inchworm locomotion. However, legs offer the advantage over wheels and tracks of more controllable mobility and interaction with the environment at the cost of higher complexity and a significantly lower speed [67]. Wheels and tracks leave a continuous mark on the surface which can cause more tissue damage than the individual steps of a walking robot. Wheels and tracks also damage the tissue when turning because they rub the surface of the tissue. Legs do not leave a continuous mark and can turn without rubbing the tissue, although they exert higher local pressure. A wheel is a remarkably simple mechanism but lacks the versatility of legs when it comes to changing the direction of motion and negotiating irregularities or obstacles. Wheels can slip when turning to change the direction of motion and are more likely to jam into the tissue than

legs. Lower achievable speed is not considered an important impediment to the performance of the robot because the robot is not expected to change location within the abdomen frequently. During operation inside the abdomen the robot is expected to reach the position of the surgical target and stay there for most of the operation. Figure 40 shows the sketch of a legged walking robot (Figure 40a), a wheeled robot (Figure 40b) and a tracked robot (Figure 40c).

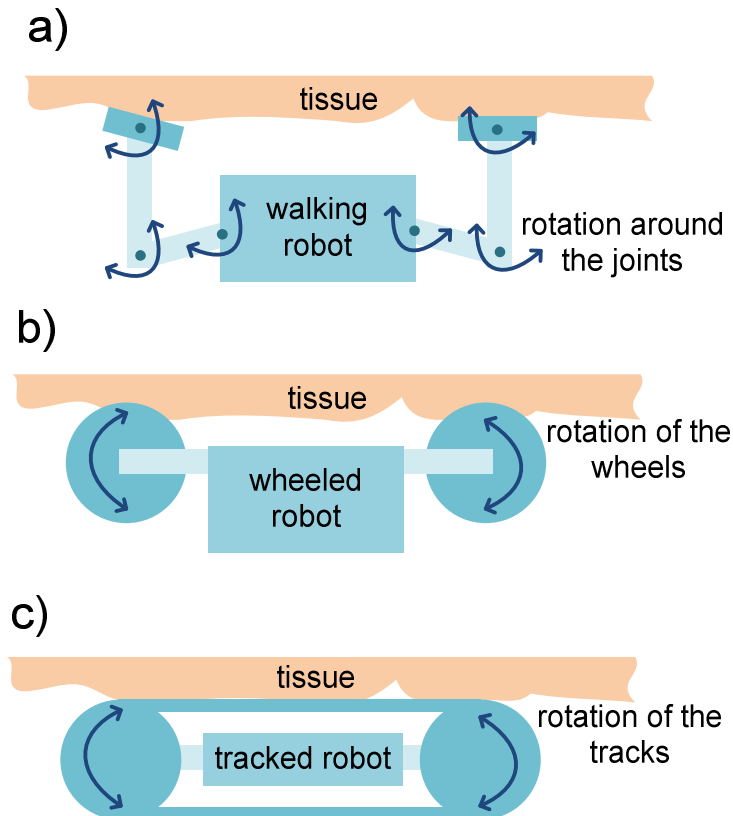


**Figure 40. (a) Sketch of a legged walking robot, (b) sketch of a wheeled robot and (c) sketch of a tracked robot moving in inverted adhesion-reliant locomotion on the surface of tissue.**

Inchworm locomotion offers the same advantages of legs over wheels and tracks in terms of controllability and tissue damage but can be implemented with a mechanism simpler than a legged robot. Inchworm locomotion can be implemented following a polar walker configuration or a Cartesian walker configuration. A inchworm polar walker can be implemented using rotary and linear motors and an inchworm Cartesian walker can be implemented using linear motors only. In a polar walker with two pads, positioning of the pads along the surface of the tissue is obtained by rotating one pad around the other and increasing or decreasing the distance between the pads. Figure 41a shows a sketch of the polar walker with the degrees of freedom to position the pads along a surface: the distance between the pads and rotation of the pads with respect to each other. In a Cartesian walker with

two pads, positioning of the pads along the surface of the tissue is obtained by increasing or decreasing the horizontal distance and the vertical distance between the pads. Figure 41b shows the sketch of a Cartesian walker with the degrees of freedom to position the pads along a surface: the vertical distance between the pads and the horizontal distance between the pads.

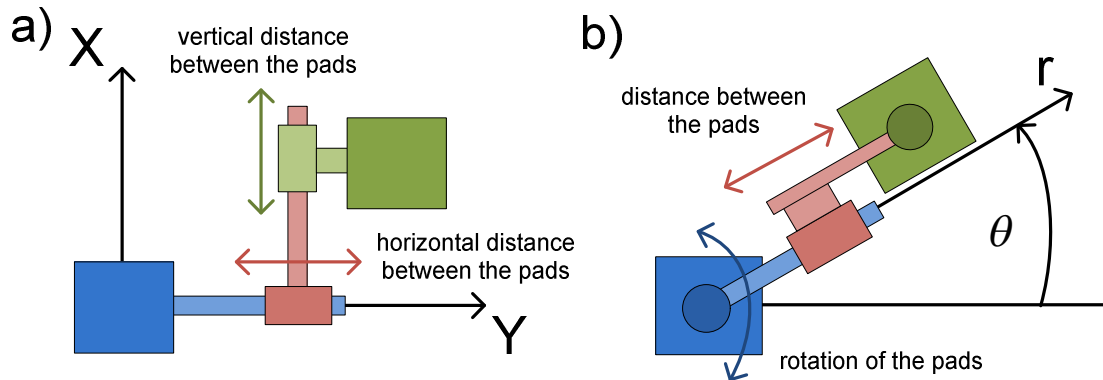


**Figure 41. (a) Sketch of a Cartesian walker and (b) sketch of a polar walker for adhesion-reliant inchworm locomotion. The Cartesian walker positions the adhesive pads along X and Y coordinates; the polar walker positions the pads along  $r$  and  $\theta$  coordinates.**

In an inchworm polar walker with two pads, when one pad detaches, the other pad withstands the twist of the rotary motor at the attached pad in order to rotate the detached pad. This twist on the supporting pad can cause movement between the pad and the surface of the tissue and damage the tissue. The twist on the supporting pad can also cause sudden detachment of the pad. A rotary motor on the supporting pad enables rotation of the detached pad, however, a rotary motor on the detached pad does not enable control of the distance between the pad and the tissue. The distance between the pad and the tissue can be controlled with a linear motor. In a Cartesian walker with two pads, when one pad is detached, the other pad withstands a force parallel to the surface of the pad in order to move the pad along the surface of the tissue. Linear motors can be used in order to change the vertical and horizontal distance between the pads as well as to peel off the pads and control the separation between the pads and the tissue.

The preferred actuator for the robot is a linear motor: Squiggle<sup>®</sup> RV motor as explained in Section 2.2.2. This Squiggle<sup>®</sup> RV is very compact and lightweight and its position can be controlled with a linear encoder which is also very compact and lightweight and will be presented in Chapter 5 Section 5.2. Thus, an inchworm Cartesian walker is preferred over a polar

inchworm walker because the first can be built with linear motors only. A Cartesian inchworm walker can be implemented with only two pads. For the intra-abdominal robot, using two tree frog adhesive pads means that the robot should weigh between 8 and 12 grammes because that is the weight each pad can support [10]. A weight of the robot of 30 grammes was estimated at the beginning of the project and, therefore, more pads can be considered in an inchworm Cartesian walker design. With three pads the robot can weigh between 16 and 24 grammes, a value closer to the estimated weight of the robot. However, when one of the pads is detached the two remaining pads feel a moment from the detached pad that can peel them off easily; this also happens in the two-padded robot when one pad is detached. With four pads, the weight of the robot can be between 24 and 36 grammes and the peeling-off moment on the three remaining pads when one pad is detached can be cancelled. Thus, with four pads a strong base of three pads attached to the tissue can be kept while each pad moves to a new position. These configurations of two, three and four pads were tested prior to the construction of the robot with a mock-up structure of the locomotion mechanism. This test with the mock-up structure verified the beneficial effect of the fourth pad in cancelling the peeling-off moment on the attached pads when one pad is detached. Chapter 8 analyses these two, three and four pads configurations showing the force and moment applied to the pads for each configuration.

In all, based on the actuators available in the market and design principles defined in the previous section, the selected locomotion system is an inchworm Cartesian walker with four adhesive pads using linear motors exclusively. How can all these requisites be combined in a compact locomotion mechanism able to move in all directions of the abdominal wall? How can the number of degrees of freedom (motors) be kept to a minimum while ensuring sufficient controllability of the robot? The answer to these questions can be found in one of the biological locomotion systems reviewed in Section 2.2.2: amoeboid locomotion.

Amoebas alternate adhesion between different parts of their body and only the part of the body that is detached moves while the rest of the body stays attached to the surface. The intra-abdominal robot can move one pad at a time while the rest of the pads support the weight of the robot. If only one pad moves at a time, two adjacent pads can share the same actuator for the same degree of freedom of both pads. For example, for one linear motor between two pads, when the first pad is attached the linear motor moves the

second pad and, when the second pad is attached, the same linear motor moves the first pad. The detached part of the body of an amoeba is moved to a new position by changing the shape of the body of the amoeba. Inspired by this aspect of amoeboid locomotion, the actuators of the robot can connect the four adhesive pads forming a quadrilateral, the body of the robot. When the motors between the pads are actuated, the shape of the robot changes moving the detached pad to a new position.

The number of degrees of freedom depends on the degree of controllability required for the robot to minimise tissue damage and maximise stability. Ideally, the fewer motors the better in order to keep size, weight and the complexity of the design to a minimum. On the other hand, the more degrees of freedom the better in terms of controllability because both horizontal and vertical forces can be applied to the adhesive pads mimicking the adhesion control observed in geckoes (see Section 2.3.7). A trade-off solution will be required between having few degrees of freedom to keep the design simple and having a sufficient number of degrees of freedom to move and apply force to the pads in different directions. Nonetheless, a very compact actuator like the Squiggle<sup>®</sup> RV motor (0.16grammes and 3x3x12 mm<sup>3</sup>) enables the use of several actuators within the locomotion mechanism without significantly increasing the size or weight of the robot. Inspired by amoeboid locomotion, the robot can move one of the four pads at a time and have the four pads interconnected in a central quadrilateral that changes shape during locomotion. Thus, the same motor can be used for the same direction of motion of the two pads sharing the motor and, therefore, some actuators can be saved without reducing the number of degrees of freedom of each individual pad. This concept of shared degrees of freedom is further explained in Section 3.8 when talking about the conceptual design of the robot. The idea of amoeba-inspired locomotion is further explained in Section 4.3 when talking about the workspace of the robot.

### 3.7 Design specifications for the intra-abdominal adhesion-reliant robot

Table 5. Design specifications for the intra-abdominal adhesion-reliant robot.

<b>Intra-abdominal adhesion-reliant miniature robot for laparoscopic surgery</b>	
Description:	A miniature robot is to be designed, fabricated and tested using bio-mimetic adhesive pads in order to move in inverted locomotion on the surface of peritoneal tissue.
Size:	The robot is required to fit through an incision of 2-3cm and move comfortably within a volume of 10cm x 10cm x 5cm.
Weight:	The maximum weight of the robot is determined by the maximum adhesion force provided by the bio-mimetic pads: each pad can hold a weight of 8-12 grammes [10]. The robot should be manufactured in lightweight materials.
Actuators and sensors:	The actuators of the robot are required to be very compact and their motion should be controllable integrating sensors in the locomotion mechanism. The actuators are required to operate at low voltage and at a temperature between 36.9°C and 45°C in order not to damage the tissue.
Locomotion strategy:	The locomotion strategy of the robot should ensure repeatable and stable motion of the robot against gravity with minimal tissue damage. A Cartesian walker has been identified as an appropriate choice for the locomotion strategy.
Power:	The robot will be powered off-board via a tether.
Control:	The robot will be tele-operated by the surgeon through a computer console. The drivers of the locomotion mechanism will be connected to the robot with a tether which will carry the control signal for the motors.

### 3.8 Conceptual design of the intra-abdominal adhesion-reliant robot

For the design of the intra-abdominal robot, a Cartesian walker is chosen. The locomotion mechanism of the Cartesian walker for the intra-abdominal robot uses four adhesive pads interconnected by linear motors. One pad is moved at a time, providing a strong base of support of three pads for the motion of each pad. The linear motors between the pads increase and decrease the distance between the pads in the horizontal plane, parallel to the surface of the tissue. The linear motors in the horizontal plane are connected with rotary joints forming a quadrilateral; the adhesive pads are situated at the corners of the quadrilateral formed by the horizontal motors. In addition to the horizontal motors, each pad has a linear motor for vertical motion towards and away from the tissue, controlling the separation between the pads and the tissue.

Figure 42 illustrates the arrangement of the pads and motors in the design of the robot for the horizontal plane (XY) and the vertical direction (Z).

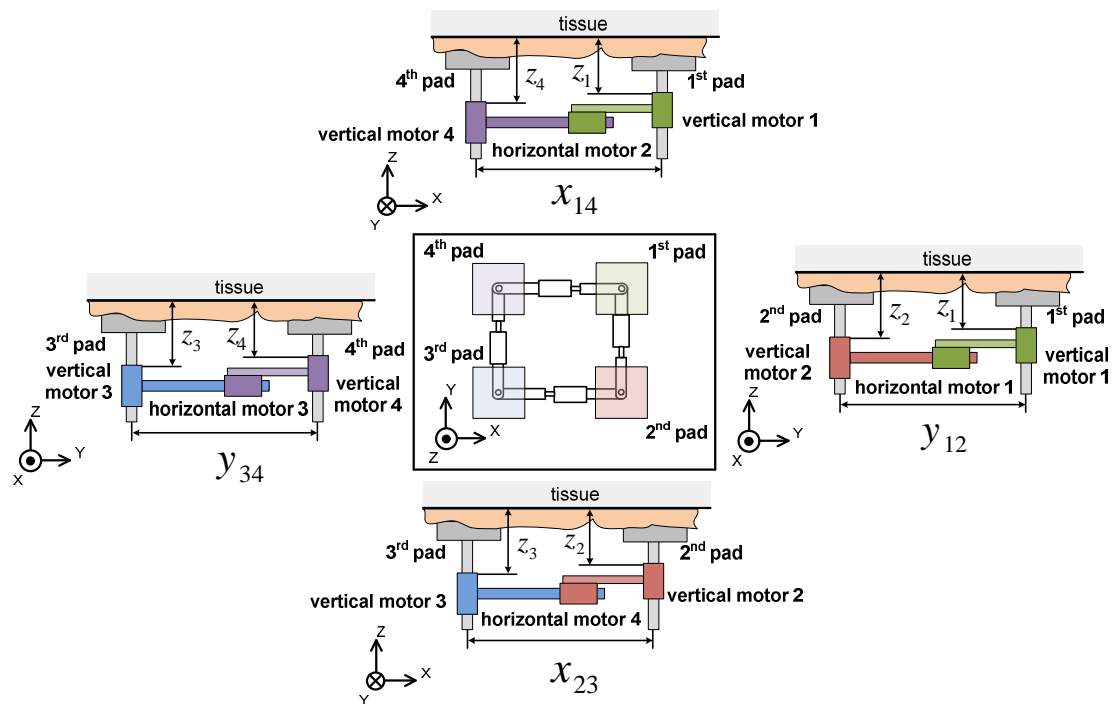


Figure 42. Arrangement of the pads and motors in a Cartesian walker with four adhesive pads.

In the locomotion mechanism of the robot in Figure 42, when one pad is detached and supported by the other three, the detached pad has three degrees of freedom:

- Motion along the X direction in the horizontal plane defined by the variables  $x_{23}$  and  $x_{14}$  for the four pads in Figure 42.
- Motion along the Y direction in the horizontal plane defined by the variables  $y_{12}$  and  $y_{34}$  for the four pads in Figure 42.
- Motion along the vertical direction Z defined by the variables  $z_1, z_2, z_3$  and  $z_4$  in Figure 42.

Each degree of freedom in the robot is controlled by a linear motor. Only four motors are required to control the motion of the four pads in the horizontal plane (XY) because the pads are moved one at a time, alternating their role of moving and supporting pads. Thus, the motors in the horizontal plane are shared between adjacent pads. For this design of the robot, the required number of actuators is:

$$n_{actuators} = n_{pads} \cdot n_{dof} - n_{dof}^{shared} \quad (1)$$

Where  $n_{actuators}$  is the number of actuators,  $n_{pads}$  is the number of pads,  $n_{dof}$  is the number of degrees of freedom for each pad and  $n_{dof}^{shared}$  is the number of degrees of freedom shared by adjacent pads.

For the intra-abdominal robot with four pads, three degrees of freedom are required for each pad and there are four pairs of adjacent pads in the horizontal plane (see Figure 42). Therefore, according to Equation ( 1 ), the number of motors for the intra-abdominal robot is:  $n_{actuators} = 4 \cdot 3 - 4 = 8$ .

The locomotion mechanism of the robot should avoid detachment of the pad when the pad is supporting and favour detachment of the pad when the pad is required to move. Keeping a base of three pads supporting the motion of each pad enables the locomotion mechanism to detach the pads when required, avoiding detachment of the supporting pads.

### **3.9 Locomotion sequence of the intra-abdominal adhesion-reliant robot**

The locomotion sequence of the robot is the same for all directions of the horizontal plane. The four pads are arranged symmetrically in the locomotion mechanism and the four pads are moved and supported by the mechanism in the same way. Figure 43 shows the locomotion sequence of the robot in the X direction of the horizontal plane following these steps:

- a) Initially, the four pads are attached to the surface of the tissue (Figure 43 a),

- b) The vertical motor of the first pad detaches the first pad (Figure 43 b),
- c) The first pad is moved to a new position by actuating the two horizontal motors joined at the first pad (Figure 43 c),
- d) The vertical motor of the first pad re-attaches the first pad and the vertical motor of the second pad detaches the second pad (Figure 43 d),
- e) The second pad is moved to a new position actuating the two horizontal motors joined at the second pad (Figure 43 e),
- f) The vertical motor of the second pad re-attaches the second pad and the vertical motor of the third pad detaches the third pad (Figure 43 f),
- g) The third pad is moved to a new position actuating the two horizontal motors joined at the third pad (Figure 43 g),
- h) The vertical motor of the third pad re-attaches the third pad and the vertical motor of the fourth pad detaches the fourth pad (Figure 43 h),
- i) The fourth pad is moved to a new position actuating the two horizontal motors joined at the fourth pad. The vertical motor of the fourth pad re-attaches the fourth pad completing a step of the robot (Figure 43 i).

The locomotion sequence of Figure 43 results in motion of the robot along the positive direction of the X axis. The robot can move along the negative direction of the X axis or along the Y direction following the same locomotion sequence but moving the pads in a different order.

The motion of the detached pad requires the combined actuation of the two horizontal motors joined at the pad. This combined motion of the horizontal motors can move the detached pad to a new position along the X direction, the Y direction or diagonally.

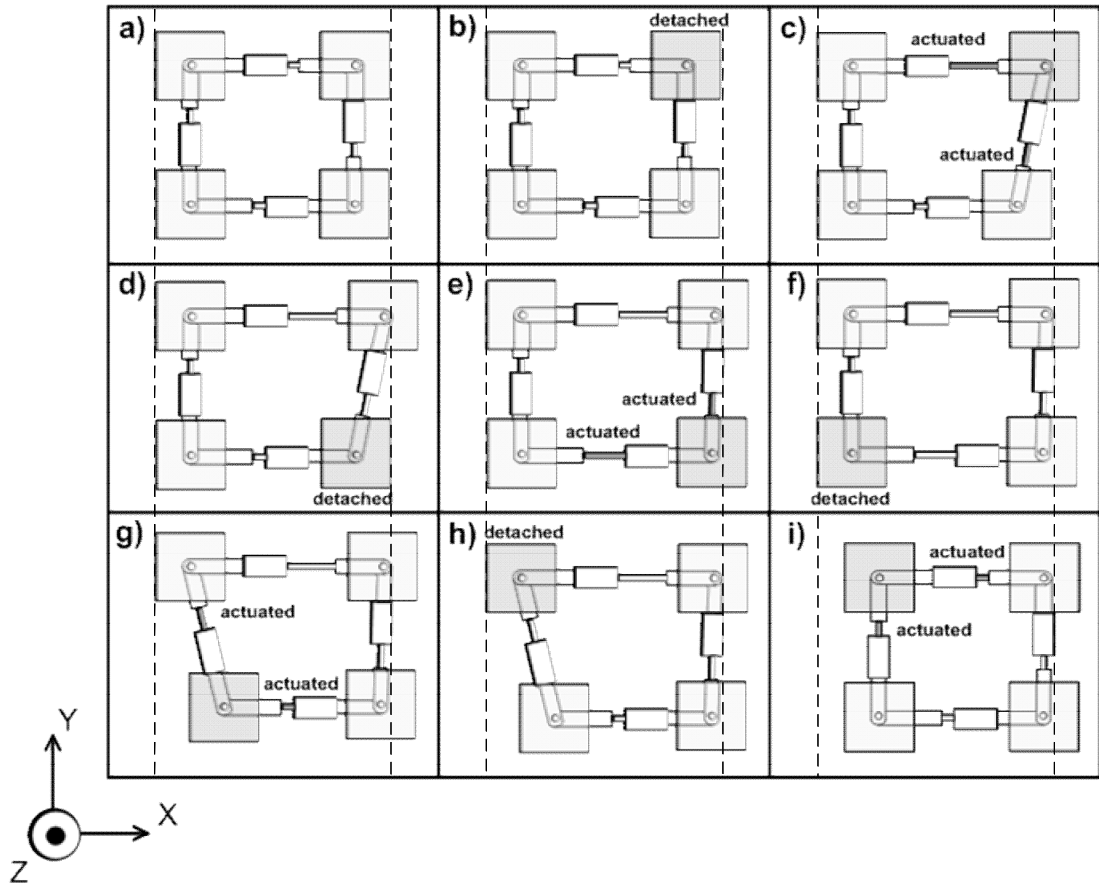


Figure 43. Locomotion sequence of the intra-abdominal robot using adhesive pads.

### 3.10 Summary

The intra-abdominal robot moves in inverted locomotion inside the insufflated abdomen, attaching to the surface of the abdominal wall (peritoneum). Inside the insufflated abdomen, the peritoneum is a vantage point, raised several centimetres above the abdominal organs.

Motion on the surface of the peritoneum should provide a good view of the organs if the robot is carrying a camera and comfortable interaction with the organs if the robot is carrying tools. Operation from the peritoneum enhances manoeuvrability around the surgical target and no external equipment is required for the bio-mimetic adhesive pads of the robot.

The constrained space inside the insufflated abdomen requires the robot to be very small and move in a compact way. The weight of the robot should be low and the locomotion mechanism should control the adhesion of the pads in order to enable the robot to move in inverted locomotion. The robot

shouldn't cause tissue damage to the peritoneum, should operate at a safe temperature and voltage and should be sterilisable and bio-compatible.

For the robot to fit in the abdomen and move safely on the peritoneum, the locomotion mechanism of the robot should be simple and the interaction with the tissue should be smooth and controllable.

For the motion of the intra-abdominal robot, legged locomotion is preferable to wheeled locomotion because of the controllability and minimal tissue damage achievable with legs. The locomotion strategy chosen for the robot is a Cartesian walker with a compact locomotion mechanism inspired by amoebas in which the adhesive pads are interconnected and moved one at a time.

For the design of the robot, four adhesive pads are arranged forming a quadrilateral, interconnected by four motors in the horizontal plane and with another four motors providing vertical motion to the pads (see Figure 42).

The locomotion sequence of the robot is the same for all directions in the horizontal plane and follows a series of steps detaching, moving and re-attaching the pads one by one (see Figure 43).

## **Chapter 4**

### **Design and analysis of the robot**

#### **4.1 Introduction**

The previous chapter showed the conceptual design of the intra-abdominal robot: a Cartesian walker featuring four adhesive pads interconnected with linear motors. This chapter presents the design and analysis of the locomotion mechanism. Thus, the kinematic design of the robot is presented first, explaining the kinematic joints and links of the robot. Then, the workspace of the robot is presented, analysing the positioning of the pads within the horizontal plane. After that, a dynamic model of the pad attached to the tissue and also moving freely is explained for motion in the vertical direction and along the horizontal plane.

The locomotion sequence of the robot, moving one pad at a time, was shown in Figure 43. This chapter explains how the locomotion sequence is generated in order to move the robot in any direction of the horizontal plane. Then, the chapter shows how the locomotion mechanism can adapt to the surface of the tissue and to the inclination of the abdominal wall. After that, the last section presents a summary of the chapter.

#### **4.2 Kinematic design of the locomotion mechanism**

The locomotion mechanism uses four adhesive pads to attach to the tissue and moves the pads in the two directions of the horizontal plane parallel to the surface of the tissue, and the vertical direction perpendicular to the surface of the tissue. Figure 44a shows the four motors in the horizontal plane of the locomotion mechanism forming a quadrilateral. Figure 44b shows the rotary joint linking the horizontal motors.

In order to move the pads in the two directions of the horizontal plane, the locomotion mechanism uses four linear motors. Each motor in the horizontal plane controls the motion of a prismatic joint. The four horizontal motors form a quadrilateral and are connected to each other with rotary joints. The pads are placed at the corners of the quadrilateral formed by the horizontal motors.

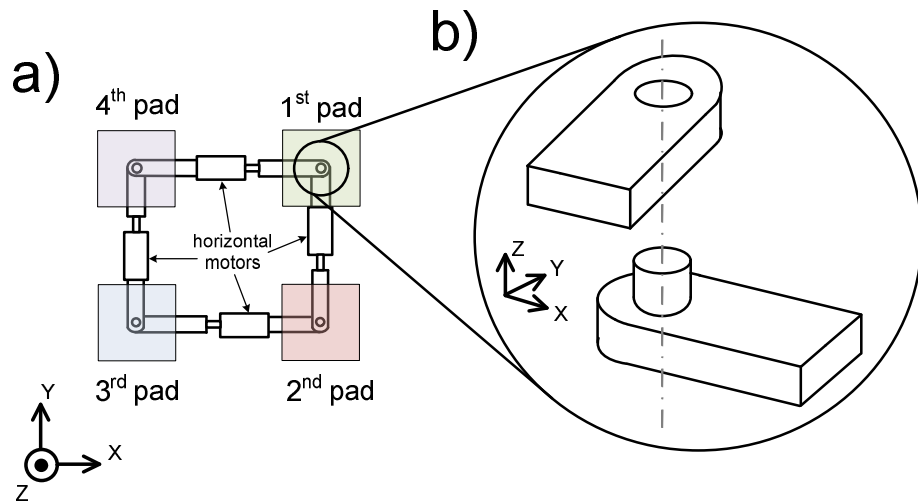


**Figure 44. (a) Locomotion mechanism with four pads and four motors in the horizontal plane and (b) rotary joint linking the horizontal motors.**

As shown in Figure 44a, the locomotion mechanism in the horizontal plane is an articulated quadrilateral. In this articulated quadrilateral, there is a linear motor on each side of the quadrilateral and they are linked to each other with the rotary joint shown in Figure 44b. This articulated quadrilateral has extensible sides because the motors can change the length of each side of the quadrilateral, thus changing the shape of the locomotion mechanism. The adhesive pads are placed at each corner of the quadrilateral, therefore, the position of the corners of the mechanism is fixed when the pads are attached. When three pads are attached and one pad is detached, the position of the detached pad is controlled by the combined motion of the two linear motors joined at the pad.

In order to move the pads in the vertical direction, perpendicular to the tissue, the locomotion mechanism uses another four motors. Each motor in the vertical direction controls the motion of a prismatic joint. The vertical motors are placed at each corner of the quadrilateral formed by the horizontal motors. The pads are connected to these vertical motors. Figure 45a shows the locomotion mechanism in the horizontal plane and Figure 45b shows the view of one side of the locomotion mechanism with two vertical motors connected to the pads.

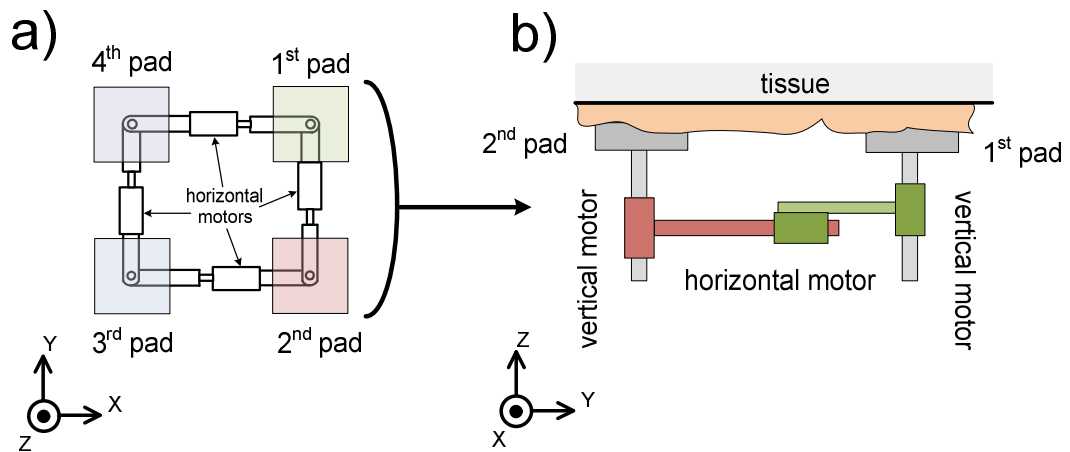


**Figure 45. (a) Locomotion mechanism in the horizontal plane and (b) side view of the mechanism showing the vertical motors connected to the pads.**

There are two possibilities for the connection between the vertical motors and the horizontal motors:

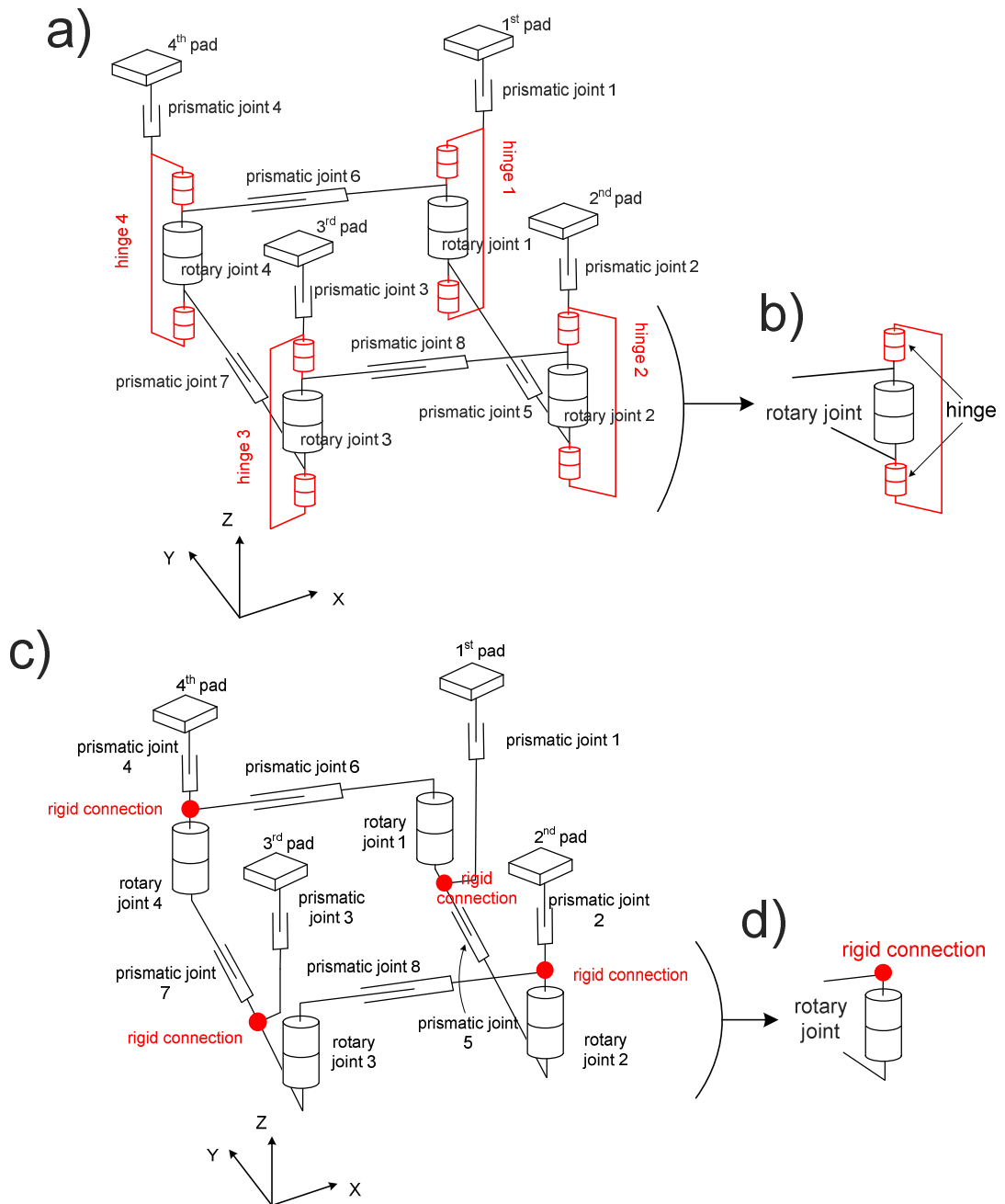
- a hinge between each vertical motor and each corner of the quadrilateral formed by the horizontal motors, or
- a rigid connection between each vertical motor and each horizontal link.

Figure 46a shows the kinematic joints of the locomotion mechanism with four hinges connecting the vertical motors to the horizontal motors and Figure 46b shows a detail of a hinge. Figure 46c shows the kinematic joints of the locomotion mechanism with rigid connections between the vertical motors and the horizontal motors and Figure 46d shows a detail of a rigid connection.

In Figure 46a, the pads supporting the detached pad are isolated from the horizontal motion of the detached pad by the hinges, because there is no moment transmitted from the horizontal motors to the pads. The hinges enable the horizontal motors to rotate freely around the supporting pads without causing any twist on the supporting pads. However, when the pads are detached the hinges enable the pads to rotate freely because the motion of the hinges is not controlled. This uncontrolled motion can interfere with the locomotion mechanism, hindering the walking performance of the robot. In order to avoid this interference, springs can be fitted at the hinges to constrain their motion.

In Figure 46c, a rigid connection between the vertical link and the horizontal links prevents the detached pad from rotating freely. Thus, rigid connections prevent the detached pad from interfering with the locomotion mechanism.

Rigidly connecting the vertical and the horizontal motors is simpler than using springs to control the motion of the hinges. However, it means that the horizontal motors cause a twist on the supporting pads when the horizontal motors are moving the detached pad. This twist on the supporting pads can be diminished with a soft backing layer on the adhesive surface. A soft backing layer on the pads also favours contact between the adhesive surface and the tissue.



**Figure 46. (a) Kinematic joints of the locomotion mechanism with hinges connecting the vertical motors to the horizontal motors, (b) detail of a hinge, (c) kinematic joints of the mechanism with rigid connections between the vertical motors and the horizontal motors, and (d) detail of a rigid connection.**

When the robot is not attached to tissue the shape of the robot can change to make the width of the robot narrower. Figure 47 shows the shape of the robot with a narrower width.

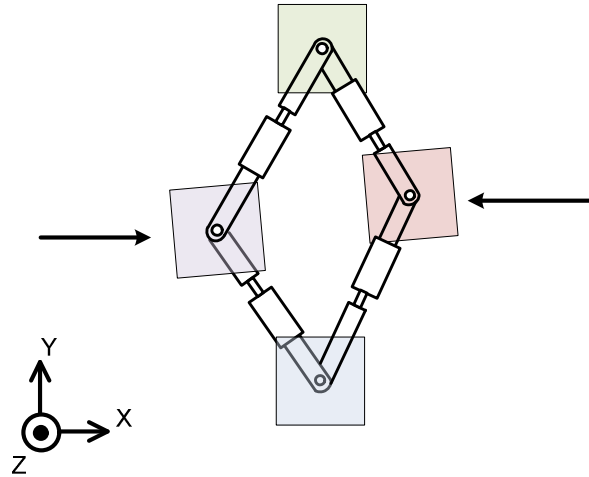


**Figure 47. Narrowing of the width of the robot enabled by the passive rotary joints.**

In Figure 47, narrowing of the locomotion mechanism is possible because the rotary joints between the horizontal motors are passive. Making the width of the robot narrower is beneficial for an intra-body application because it makes the robot fit through the surgical incision more comfortably. Once the robot is inside the abdominal cavity, the locomotion mechanism can be reshaped.

The drawback of having passive rotary joints between the horizontal motors is that the supporting pads might drift apart during locomotion of the robot. In this case, rotary encoders can be used at the rotary joints in order to measure the separation of the supporting pads. Alternatively, springs between non-adjacent pads can be used in order to help reshape the mechanism.

The kinematic joints determine the dexterity of the locomotion mechanism and the area the pads can cover from a specific position. The area the pads can cover defines the workspace of the individual pads and the workspace of the whole robot.

### **4.3 Workspace of the individual pads and the robot**

When one pad of the robot is detached and three pads of the robot are attached, supporting the motion of the detached pad, the robot can be considered a manipulator. The detached pad would be the end-effector of the manipulator. The end-effector, the detached pad, is moved by the

vertical motor that control the distance between the pad and the tissue and the two horizontal motors that connect the detached pad to the rest of the mechanism. Following this analogy with a robotic manipulator, the term 'workspace' is defined and explained in this section and applied to the pads of the robot.

The workspace of a robot is the region of space made up of all the points the robot can reach. This region is defined by the limit of motion of all the joints in the mechanism of the robot. The workspace of the intra-abdominal robot is the region of space where the robot can position the adhesive pads. Figure 48a shows the initial position of the locomotion mechanism where all the horizontal motors are at the position of minimum extension. From this initial position, the locomotion mechanism can move the pads to the regions of space shown in Figure 48b.

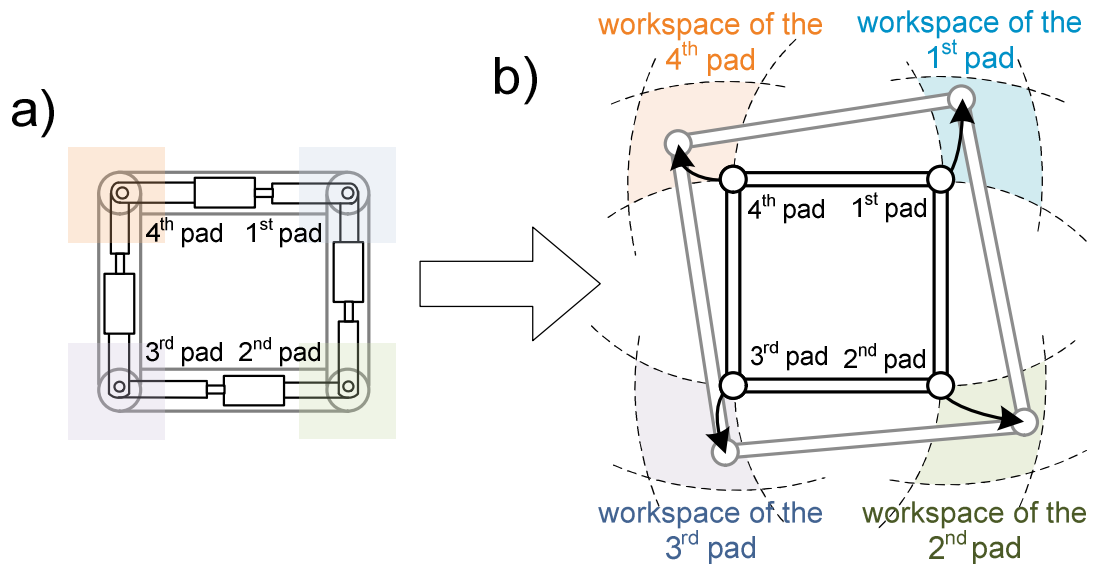


**Figure 48. (a) Locomotion mechanism in the horizontal plane and (b) workspace of the robot defined by the workspace of the pads.**

The workspace of the robot is made up of the workspace of the individual pads.

### 4.3.1 Workspace of the individual pads

The workspace of the individual pads in the horizontal plane is defined by the motion of the horizontal links. The pads are moved one at a time, supported by the other three pads. Two horizontal motors move simultaneously in order to position the pads in the region of the horizontal plane shown in Figure 48b. These two horizontal motors are the motors joined at the corner of the moving pad. Figure 50 shows pad 1 moving to a new position  $(x_1, y_1)$ , supported by pads 2, 3 and 4. In Figure 50 the

horizontal links moving pad 1 are the links between pads 1 and 2, and between pads 1 and 4.

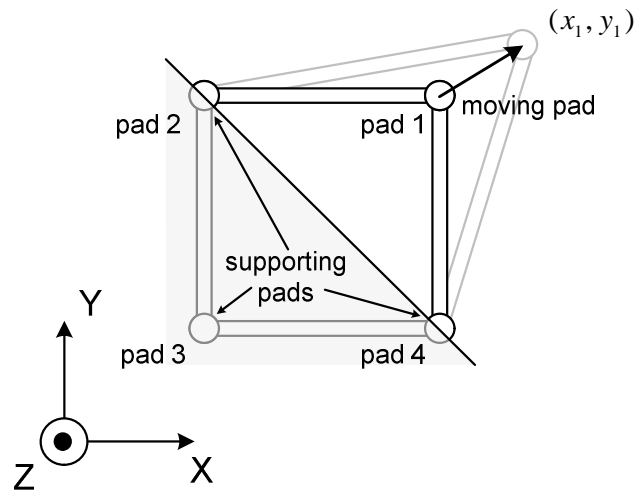


**Figure 49. The locomotion mechanism moving pad 1 to a new position, supported by the other three pads.**

The motion of the two horizontal links joined at the corner of the moving pad defines the workspace of the pad. The relation between the length of these two horizontal links defines the position of the pad in the horizontal plane and thus, the workspace of the pad. Figure 50 shows the geometrical parameters used in order to calculate the workspace of the pad.

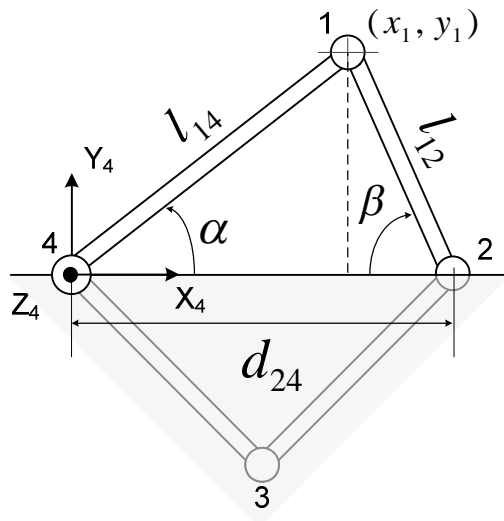


**Figure 50. Geometrical parameters used in order to calculate the workspace of the pad.**

According to the parameters in Figure 50, the following equations define the relation between the length of the two horizontal links:

$$l_{14} \cdot \cos(\alpha) + l_{12} \cdot \cos(\beta) = d_{24} \quad (2)$$

$$l_{14} \cdot \sin(\alpha) = l_{12} \cdot \sin(\beta) \quad (3)$$

Where:

- $l_{14}$  is the length of the horizontal link between pads 1 and 4,
- $l_{12}$  is the length of the horizontal link between pads 1 and 2,
- $\alpha$  is the angle between the line joining pads 2 and 4 and the horizontal link between pads 1 and 4,
- $\beta$  is the angle between the line joining pads 2 and 4 and the horizontal link between pads 1 and 2,
- $d_{24}$  is the distance between pads 2 and 4, the two pads adjacent to the moving pad (pad 1).

The upper and lower limits of the angles  $\alpha$  and  $\beta$  will be determined by the construction of the locomotion mechanism.

The previous parameters:  $(l_{14}, l_{12}, \alpha, \beta, d_{24})$  determine the position of the moving pad. The new position of pad 1 with respect to the system of coordinates  $(X_4, Y_4)$  at the position of pad 4 (see Figure 50), is given by the following equations:

$$x_1 = l_{14} \cdot \cos(\alpha) = d_{24} - l_{12} \cdot \cos(\beta) \quad (4)$$

$$y_1 = l_{14} \cdot \sin(\alpha) = l_{12} \cdot \sin(\beta) \quad (5)$$

Where  $(x_1, y_1)$  are the coordinates of the new position of the pad as indicated in Figure 50.

The distance  $d_{24}$  can be directly measured on the locomotion mechanism or it can be measured initially and its variation calculated as the robot moves. The length of the horizontal links:  $l_{14}$  and  $l_{12}$ , can be measured with a linear encoder. Therefore,  $(x_1, y_1)$  and  $d_{24}$  are known and the unknowns are the lengths:  $l_{14}$  and  $l_{12}$ , and the angles:  $\alpha$  and  $\beta$ .

The relation between the lengths of the horizontal links moving the pad:  $l_{14}$  and  $l_{12}$ , can be obtained by solving the system of equations formed by Equations ( 2 )-( 5 ) for each position of the pad  $(x_1, y_1)$ . Thus, the value of the angles  $\alpha$  and  $\beta$  is obtained by dividing Equation ( 3 ) by Equation ( 2 ):

$$\alpha = \text{atan}\left(\frac{y_1}{x_1}\right) \quad (6)$$

$$\beta = \text{atan}\left(\frac{y_1}{d_{24} - x_1}\right) \quad (7)$$

With the value of the angles  $\alpha$  and  $\beta$ , the length of the links  $l_{14}$  and  $l_{12}$  are:

$$l_{14} = \frac{y_1}{\sin(\alpha)} = \frac{x_1}{\cos(\alpha)} \quad (8)$$

$$l_{12} = \frac{y_1}{\sin(\beta)} = \frac{d_{24} - x_1}{\cos(\beta)} \quad (9)$$

When all the horizontal links are at minimum extension, for any given position of three pads, the workspace of the fourth pad is the area within the intersection of the four arcs shown in Figure 51.

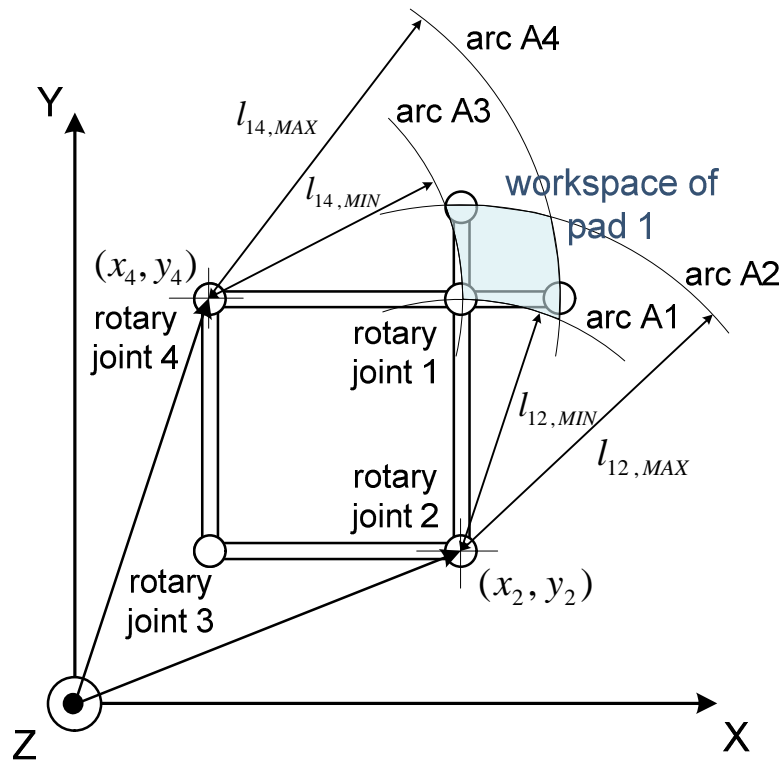


Figure 51. Workspace of pad 1 moving in the horizontal plane.

The four arcs marking out the workspace of the pad in Figure 51 are defined as follows:

1. The centre of arc A1 is at rotary joint 2 and the radius of arc A1 is the minimum length of the link between pads 1 and 2. Rotary joint 2 is one of the two rotary joints adjacent to the moving pad.

2. The centre of arc A2 is at rotary joint 2 and the radius of arc A2 is the maximum length of the link between pads 1 and 2.
3. The centre of arc A3 is at rotary joint 4 and the radius of arc A3 is the minimum length of the link between pads 1 and 4. Rotary joint 4 is the other rotary joint adjacent to the moving pad.
4. The centre of arc A4 is at rotary joint 4 and the radius of arc A4 is the maximum length of the link between pads 1 and 4.

The workspace of pad 1 represented in Figure 51 can be mathematically expressed as:

$$W_1: (x, y) \in \{A_1^1 \cap A_1^2 \cap A_1^3 \cap A_1^4\} \quad (10)$$

$$A_1^1: (x - x_4)^2 + (y - y_4)^2 \geq l_{14,MIN} \quad (11)$$

$$A_1^2: (x - x_4)^2 + (y - y_4)^2 \leq l_{14,MAX} \quad (12)$$

$$A_1^3: (x - x_2)^2 + (y - y_2)^2 \geq l_{12,MIN} \quad (13)$$

$$A_1^4: (x - x_2)^2 + (y - y_2)^2 \leq l_{12,MAX} \quad (14)$$

Where Equation ( 10 ) defines the workspace  $W_1$  of the pad 1  $(x, y)$  as the intersection of the four regions of the horizontal plane  $A_1^1$ ,  $A_1^2$ ,  $A_1^3$  and  $A_1^4$  defined in Equations ( 11 )-( 14 ).

In Equations ( 11 ) and ( 12 ):

- $(x_4, y_4)$  are the coordinates of rotary joint 4,
- $l_{14,MIN}$  is the minimum length of the link between pads 1 and 4, and
- $l_{14,MAX}$  is the maximum length of the link between pads 1 and 4.

Similarly, in Equations ( 13 ) and ( 14 ):

- $(x_2, y_2)$  are the coordinates of rotary joint 2,
- $l_{12,MIN}$  is the minimum length of the link between pads 1 and 2, and
- $l_{12,MAX}$  is the maximum length of the link between pads 1 and 2.

Following similar calculations, the workspace of the other three pads can be calculated, obtaining the workspace of the whole robot.

### 4.3.2 Workspace of the robot

The workspace of the robot is defined by the workspace of the four pads in the locomotion mechanism. From a position where all the horizontal links are at minimum extension, the workspace of the four pads is shown in Figure 52.

The workspace of the robot is mathematically expressed as:

$$W_{robot}: (x, y) \in \{W_1 \cup W_2 \cup W_3 \cup W_4\} \quad (15)$$

$$W_1: (x, y) \in \{A_1^1 \cap A_1^2 \cap A_1^3 \cap A_1^4\} \quad (16)$$

$$W_2: (x, y) \in \{A_2^5 \cap A_2^6 \cap A_2^7 \cap A_2^8\} \quad (17)$$

$$W_3: (x, y) \in \{A_3^9 \cap A_3^{10} \cap A_3^{11} \cap A_3^{12}\} \quad (18)$$

$$W_4: (x, y) \in \{A_4^{13} \cap A_4^{14} \cap A_4^{15} \cap A_4^{16}\} \quad (19)$$

$$A_i^j: (x - x_m)^2 + (y - y_m)^2 \geq l_{im,MIN} \quad (20)$$

$$A_i^k: (x - x_m)^2 + (y - y_m)^2 \leq l_{im,MAX} \quad (21)$$

Where Equation ( 15 ) defines the workspace of the robot:  $W_{robot}$  as the union of the workspace of each individual pad:  $W_1, W_2, W_3$  and  $W_4$ .

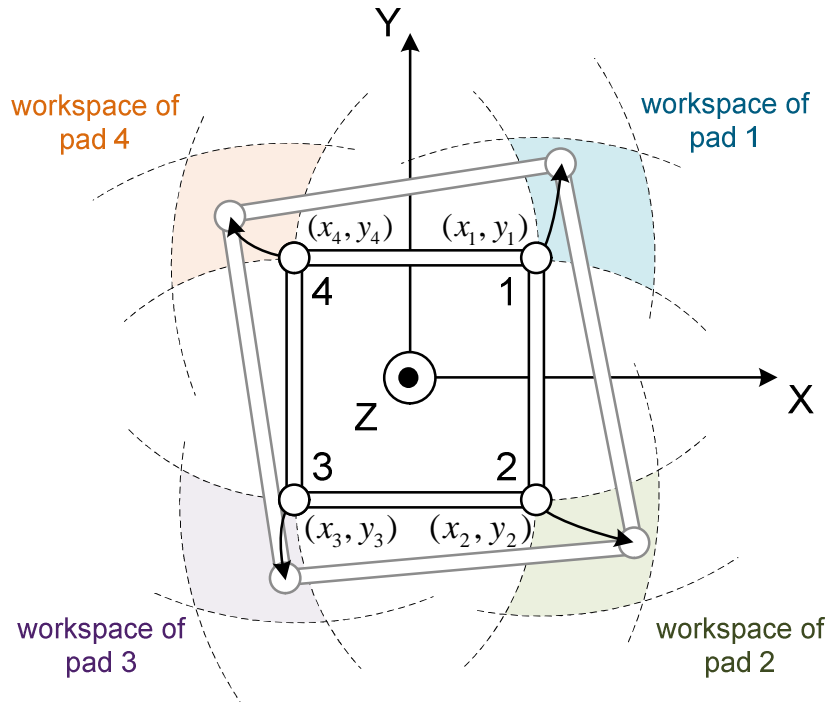


**Figure 52. Workspace of the robot defined by the workspace of the four pads.**

The workspace of each pad is defined in Equations ( 16 )-( 19 ) as the intersection of the four regions of the horizontal plane:  $A_1^1, A_1^2 \dots A_4^{16}$ . Equations ( 20 ) and ( 21 ) define these regions of the horizontal plane, where the indexes  $i, j, k$  and  $m$  take the following values depending on the pad:

- For pad 1:  $i = 1, j = 1, 2, k = 3, 4, m = 2, 4$ .
- For pad 2:  $i = 2, j = 5, 6, k = 7, 8, m = 1, 3$ .

- For pad 3:  $i = 3, j = 9, 10, k = 11, 12, m = 2, 4$ .
- For pad 4:  $i = 4, j = 13, 14, k = 15, 16, m = 1, 3$ .

Thus,  $i$  is the moving pad and  $m$  is the number of pad adjacent to the moving pad. The index  $j$  is the number of arc with radius the minimum length of the horizontal link between pad  $i$  and  $m$ . Similarly,  $k$  is the number of arc with radius the maximum length of the horizontal link between pad  $i$  and  $m$ .

The minimum and maximum length of each horizontal link is the minimum and maximum extension of the prismatic joint in each horizontal link. The range of motion of the linear motors determine the minimum and maximum extension of the prismatic joints. The length of each horizontal link has an upper and a lower limit:

$$l_{im,MIN} \leq l_{im} \leq l_{im,MAX} \quad (22)$$

Where  $i$  is the moving pad and  $m$  is the number of pad adjacent to pad  $i$ . The length of the link between pads  $i$  and  $m$  is  $l_{im}$  and the minimum and maximum limits of  $l_{im}$  are  $l_{im,MIN}$  and  $l_{im,MAX}$  respectively.

From an initial position of the pads, each pad can move to any point within the workspace of that initial position as long as the length between the moving pad and the adjacent pads is within the limits defined by Equation ( 22 ). The workspace of the whole robot defines the area within reach of the pads and also defines the shape of the locomotion mechanism. The shape of the locomotion mechanism can change as illustrated in Figure 52. This type of locomotion resembles amoeboid locomotion: the adhesive pads are positioned within their surrounding area in the horizontal plane, changing the shape of the locomotion mechanism. The locomotion mechanism also enables the robot to steer, changing the orientation of the robot in the horizontal plane. In order to steer the pads can move to a position within their workspace that makes the robot rotate about the vertical axis. This change of orientation of the locomotion mechanism can be seen in Figure 52.

The vertical motors detach and attach the pads, changing the part of the mechanism attached to the tissue, and the horizontal motors move the pads one by one until the whole robot is at a new position. The pads can also be positioned in the vertical direction. Thus, the pads can move within a volume defined by the workspace of the pads in the horizontal plane and the motion range of the vertical motors. In order to obtain the volume within which the pads can move, the workspace in the horizontal plane can be extruded along the vertical direction a depth equal to the motion range of the vertical

motor. Figure 53 shows the three-dimensional workspace of the pad of the robot.

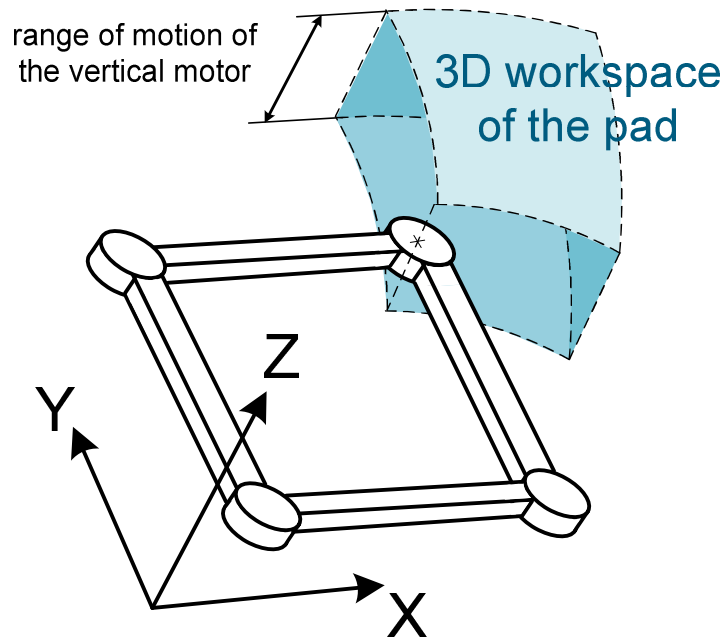


Figure 53. Three-dimensional workspace of the pad of the robot.

#### 4.4 Dynamics of the pad moved by the locomotion mechanism

In order to move the pad to a new position, the locomotion mechanism applies force on the adhesive pad, actuating the vertical and horizontal motors in this order:

- The vertical motor pulls the pad in order to detach it from the tissue,
- The horizontal motors apply a force parallel to the tissue in order to move the pad across the surface of the tissue,
- The vertical motor pushes the pad back on the surface of the tissue in order to re-attach the pad at the new position.

Therefore, the pad can be moved by one motor in the vertical direction and by one or two motors in the horizontal plane. The dynamics of the system change depending on whether the pad is attached to the tissue or detached.

This section presents a simple model of the dynamics of the robot by way of introduction to the forces present in the interaction between the robot and its environment. Chapters 6, 7 and 8 analyse in detail the forces and moments present during locomotion of the robot on the surface of tissue and elaborate on the dynamic models presented here.

#### 4.4.1 Dynamic model of the vertical motion of the pad

The vertical motors in the locomotion mechanism pull the pad in order to peel it off when the pad is attached to the tissue. In this case the vertical pad pulls the soft surface of the tissue and the pad and the motor has to overcome the adhesion force between pad and tissue in order to separate them.

When the pad is detached, the vertical motors can increase the separation between the tissue and the pad or move the pad towards the tissue in order to re-attach it. In this case, the horizontal motors are moving a free load when the pad is detached or pushing the pad against the soft surface of the tissue in order to re-attach the pad.

##### 4.4.1.1 Dynamic model of the pad attached to the tissue

The dynamic model of the vertical motor pulling the pad to detach it is shown in Figure 54. In Figure 54, the four pads are attached to the tissue through the stiffness of the pad:  $K_{pad}$  and the stiffness of the tissue:  $K_{tissue}$ . The vertical motor at pad 1 is moving the pad a distance  $\Delta z$  in order to detach it from the tissue.

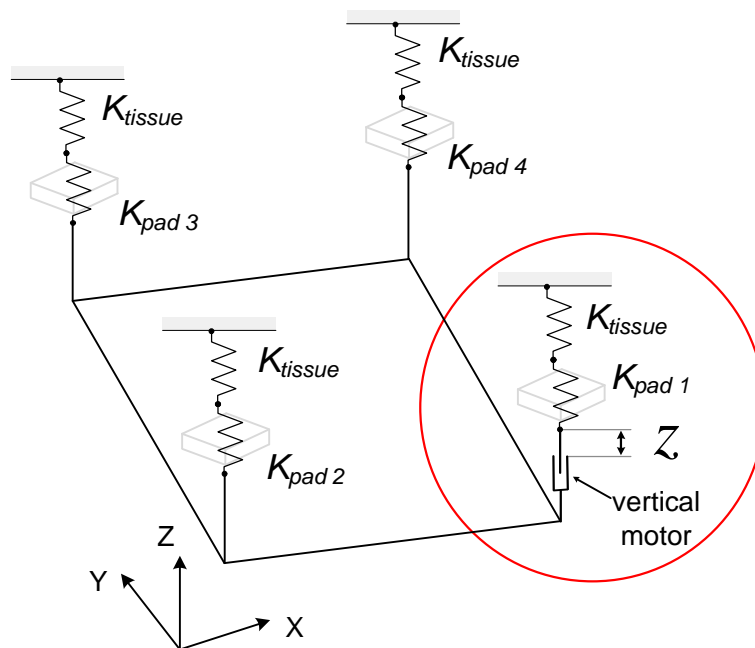


**Figure 54. Dynamic model of the locomotion mechanism in the vertical direction when pad 1 is attached to the tissue.**

The vertical motor pulling pad 1 is supported by the other three pads attached to the tissue. Therefore, the force applied by the vertical motor on pad 1 in order to detach it is also felt by the three supporting pads.

Considering as the reference of motion the quadrilateral formed by the horizontal links, pad 1 in Figure 54 moves towards this quadrilateral when the vertical motor below pad 1 is detaching it. In this case, the force from the vertical motor below pad 1 while the pad is attached to the tissue is:

$$F_{motor} = (K_{tissue+pad1}) \cdot \Delta z_{pad1} \quad (23)$$

Where:

- $F_{motor}$  is the force applied by the vertical motor,
- $K_{tissue+pad1}$  is the stiffness of the tissue:  $K_{tissue}$  in series with the stiffness of pad 1:  $K_{pad1}$ , and
- $\Delta z_{pad1}$  is the vertical displacement of pad 1 relative to the quadrilateral formed by the horizontal links; this displacement is caused by the motor.

The expression of force is the same when the vertical motor is pushing the pad against the tissue in order to re-attach the pad. The vertical displacement  $\Delta z_{pad1}$  can be positive or negative depending on the direction of motion of the vertical motor.

Considering the pad attached to tissue as the motion reference, when the vertical motor is detaching the pad, the quadrilateral formed by the horizontal links moves towards the tissue. In this case, the force from the motor on the three supporting pads (pads 2, 3 and 4) is:

$$F_{motor} = (K_{tissue+pad2} + K_{tissue+pad3} + K_{tissue+pad4}) \cdot \Delta z_{pads2,3,4} \quad (24)$$

Where:

- $F_{motor}$  is the force applied by the vertical motor,
- $K_{tissue+pad2}$  is the stiffness of the tissue:  $K_{tissue}$  in series with the stiffness of pad 2:  $K_{pad2}$ ,
- $K_{tissue+pad3}$  is the stiffness of the tissue:  $K_{tissue}$  in series with the stiffness of pad 3:  $K_{pad3}$ , and
- $K_{tissue+pad4}$  is the stiffness of the tissue:  $K_{tissue}$  in series with the stiffness of pad 4:  $K_{pad4}$ , and
- $\Delta z_{pads2,3,4}$  is the vertical compression of pads 2, 3 and 4 against the tissue caused by the motion of the vertical motor. This vertical displacement is considered the same for the three supporting pads: pads 2, 3 and 4 and is relative to the surface of the tissue.

The expression of force is the same when the vertical motor is pushing the pad against the tissue in order to re-attach the pad. The vertical

displacement  $\Delta z_{pads2,3,4}$  can be positive or negative depending on the direction of motion of the vertical motor.

When the vertical motor at pad 1 is pulling the pad, pad1 and the quadrilateral formed by the horizontal links move closer to each other. In the vertical direction, for pad 1 to detach, the stretch of pad 1 towards the horizontal links must be greater than the compression of the horizontal links pushing against the tissue. Mathematically expressed, pad 1 detaches if:

$$\Delta z_{pad1} > \Delta z_{pads2,3,4} \quad (25)$$

Where  $\Delta z_{pad1}$  is the vertical displacement of pad 1, relative to the quadrilateral formed by the horizontal links, and  $\Delta z_{pads2,3,4}$  is the vertical displacement of pads 2, 3 and 4 caused by the motor, relative to the surface of the tissue.

The force from the vertical motor is the same in Equation ( 23 ) and Equation ( 24 ).Therefore, the condition of detachment of the pad in Equation ( 25 ) can be expressed in terms of the stiffness of the pads:

$$K_{tissue+pad2} + K_{tissue+pad3} + K_{tissue+pad4} > K_{tissue+pad1} \quad (26)$$

Where  $K_{tissue+pad2}$ ,  $K_{tissue+pad3}$ ,  $K_{tissue+pad4}$  and  $K_{tissue+pad1}$  are the stiffness of the tissue and pad 2, 3, 4 and 1 respectively.

Each of the supporting pads will have a stiffness constant similar to the moving pad. The supporting pads are in parallel and therefore the equivalent stiffness is the addition of their individual stiffness constant. Thus, Equation ( 25 ) is satisfied, as there are three supporting pads and their equivalent stiffness is three times that of the moving pad.

#### 4.4.1.2 Dynamic model of the detached pad

When the pad is detached from the tissue and can move freely, the motor moves the mass of the pad along the vertical direction. Figure 55 shows the dynamic model of the vertical motor moving the mass of the detached pad ( $m_{pad1}$ ).

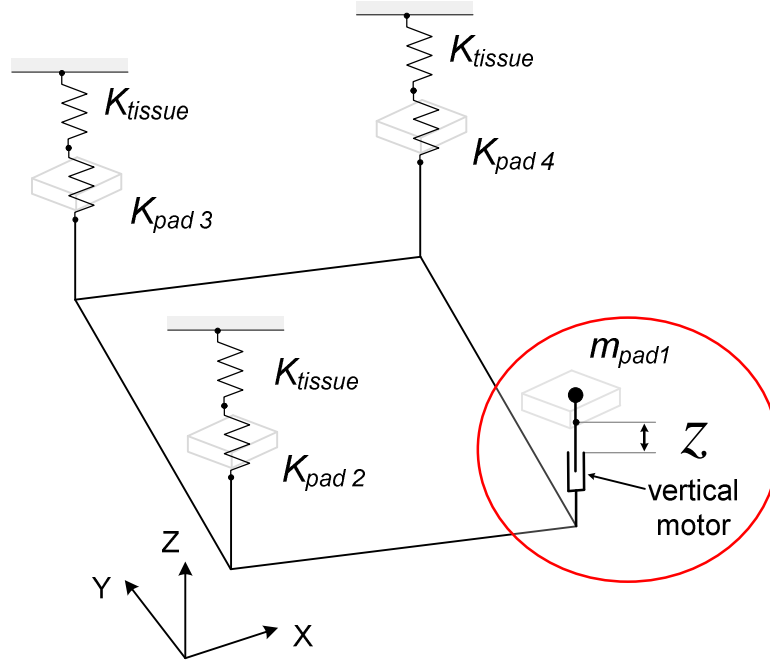


**Figure 55. Dynamic model of the locomotion mechanism in the vertical direction when pad 1 is detached.**

The vertical motor moves the pad, supported by the other three pads but without any connection between the moving pad and the tissue. In this case, the force applied by the vertical motor on the moving pad is:

$$F_{pad1} = m_{pad1} \cdot a_{pad1} \quad (27)$$

Where  $F_{pad1}$  is the force applied on the detached pad,  $m_{pad1}$  is the mass of the detached pad and  $a_{pad1}$  is the acceleration of the pad controlled by the motor, including gravity.

#### 4.4.2 Dynamic model of the pad in the horizontal plane

On the horizontal plane, the detached pad is moved by the combined actuation of the two motors adjacent to the pad. Figure 56a shows the dynamic model of detached pad 1 in the horizontal plane. Figure 56b shows a detail of the dynamic model with pad 1 moved by two motors in the horizontal plane.

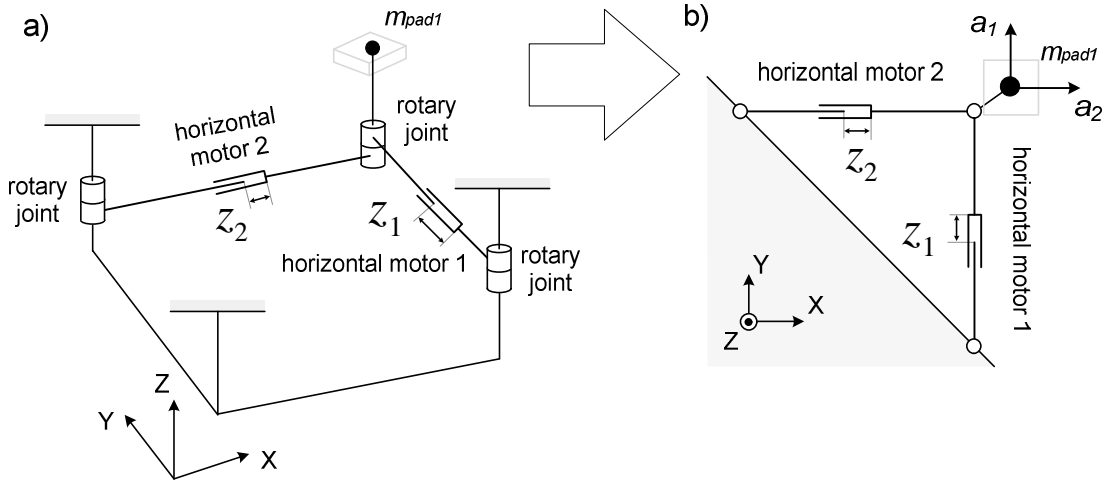


**Figure 56. (a) Dynamic model of the locomotion mechanism in the horizontal plane when pad 1 is detached and (b) detail of the two motors moving pad 1 in the horizontal plane.**

The force applied on the detached pad is the addition of the two force vectors from the horizontal motors moving the pad:

$$\vec{F}_{pad1} = \vec{F}_{motor\ 1} + \vec{F}_{motor\ 2} = m_{pad1} \cdot (\vec{a}_1 + \vec{a}_2) \quad (28)$$

Where:

- $\vec{F}_{pad1}$  is the total force applied on the detached pad,
- $\vec{F}_{motor\ 1}$  is the force from horizontal motor 1,
- $\vec{F}_{motor\ 2}$  is the force from horizontal motor 2,
- $m_{pad1}$  is the mass of pad 1, including the mass of the mechanism surrounding pad 1,
- $\vec{a}_1$  is the acceleration of the pad caused by horizontal motor 1 (see Figure 56b), and
- $\vec{a}_2$  is the acceleration of the pad caused by horizontal motor 2 (see Figure 56b).

This dynamic model considers that the pads are detached and re-attached only with the vertical motors, without using the horizontal motors in order to help peel off or preload the pads. A more detailed model and analysis of the force and moment applied by the locomotion mechanism to the pads is presented in Chapters 6, 7 and 8.

## 4.5 Generation of the locomotion sequence

From an initial position where all the pads are attached to the tissue, the locomotion mechanism moves the pads one by one, keeping three pads

attached to the tissue at all times. In this way, the locomotion mechanism detaches one pad first, moves it to a new position and re-attaches the pad to the tissue. Figure 57a shows a side view of the locomotion mechanism moving one pad in the X direction of the vertical plane and Figure 57b shows the locomotion sequence of one pad in the horizontal plane.

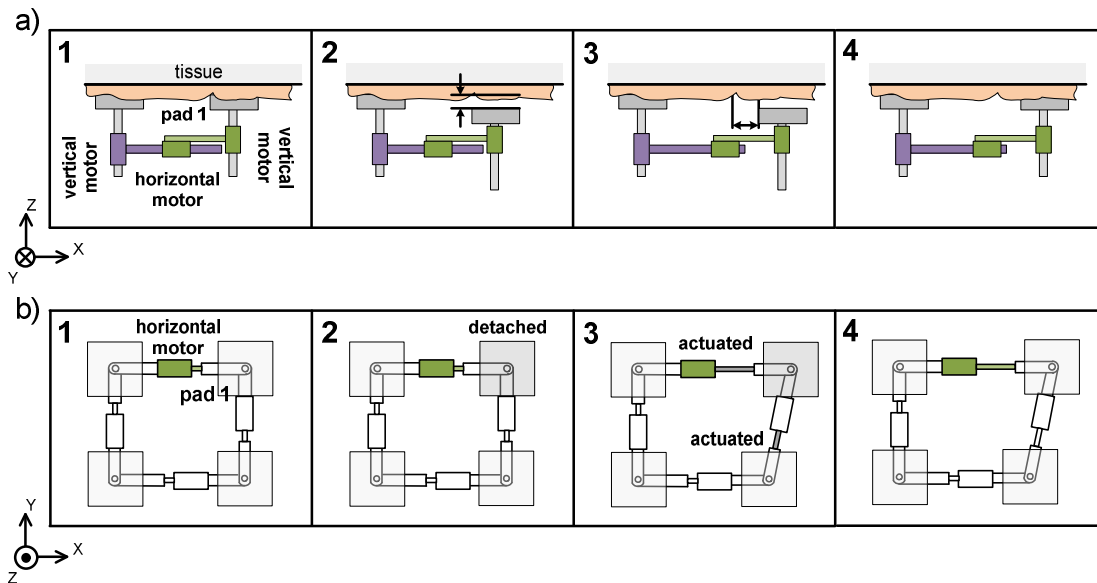


**Figure 57. (a 1-4) Locomotion sequence of pad 1 in the vertical direction and (b 1-4) locomotion sequence of pad 1 in the horizontal plane.**

The locomotion mechanism then repeats the process with the other pads until the whole robot reaches a new position. In this way, the vertical motors are used for detachment and re-attachment to the tissue and the horizontal motors move the pads across the surface of the tissue.

The locomotion sequence is generated by timing and coordinating the actuation of the vertical and horizontal motors. The time diagram in Figure 58 indicates when the vertical motors detach and re-attach the pads and shows the change in position of the horizontal motors in order to move the pads across the tissue. In Figure 58, the horizontal motors 1 and 3 move from a position of minimum extension to a position of maximum extension of the prismatic joint the motors control.

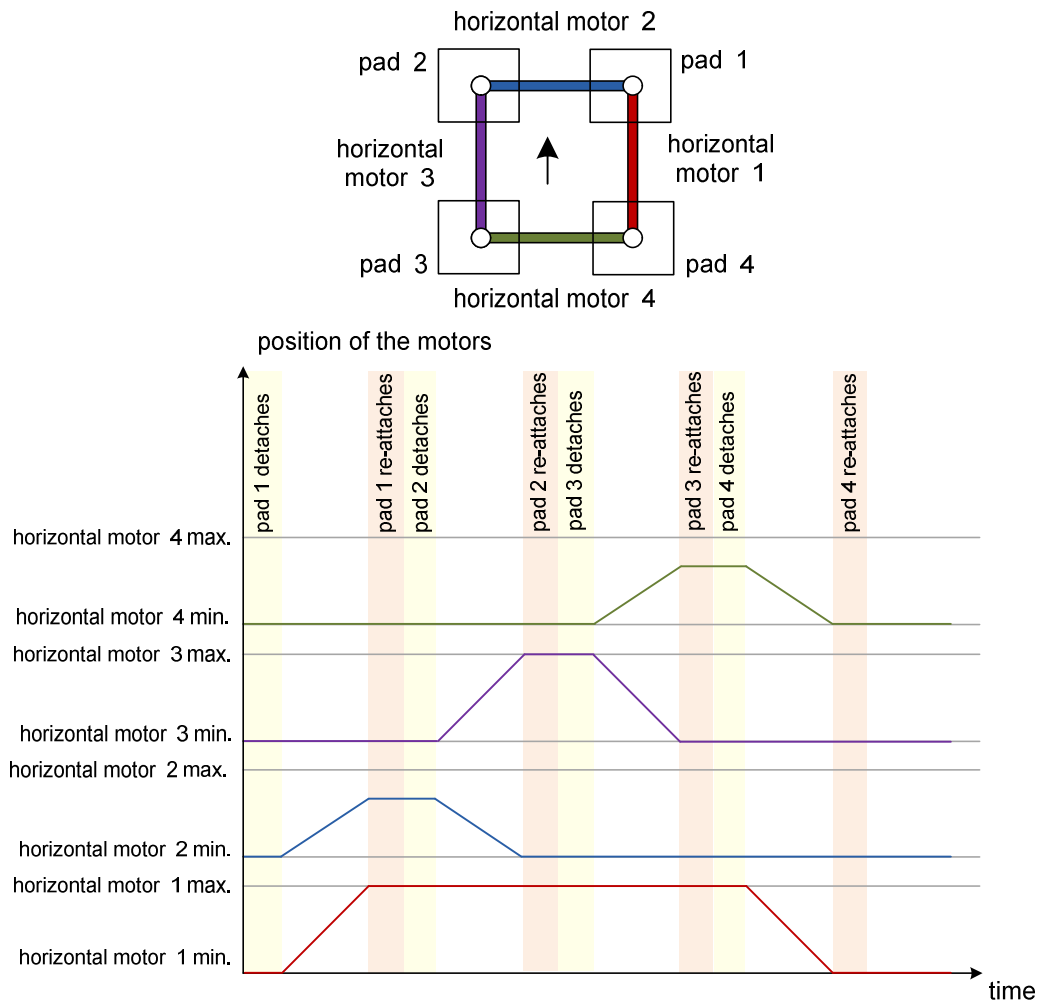


**Figure 58. Sequence of detachment, motion and re-attachment of the four pads of the robot in order for the robot to take a step forward.**

The diagram in Figure 58 shows the locomotion sequence to make the robot take one step in the direction of the arrow shown in the sketch of the robot at the top of the diagram. The diagram in Figure 58 considers that the speed of the horizontal motors is constant.

The sequence starts detaching pad 1 with a vertical motor and then pushing the pad with horizontal motor 1 up to the new position of the pad. During the time horizontal motor 1 moves the pad, horizontal motor 2 moves as well in order to enable straight motion of the pad. The relation between the motion of the horizontal motor 1 and horizontal motor 2 is given by the Equations ( 2 )-( 5 ) explained earlier. This relation between the motion of the horizontal motors determines the direction of motion of the pad along the surface of the tissue.

Once pad 1 is at a new position, the vertical motor re-attaches pad 1 and the next pad to move, pad 2, is detached. Then, pad 2 is moved forward with horizontal motor 3 and horizontal motor 2 moves along, returning to the

position of minimum extension. In this way, the two leading pads in the locomotion mechanism reach a new position in the direction of motion. For the two trailing pads, the actions of the motors are repeated until all the pads are at the new position and the robot is ready to move another step.

The symmetry of the locomotion mechanism enables the robot to take a step to the side by changing the order of actuation of the motors in the locomotion sequence. For instance, in Figure 58, to make the robot move to the right the horizontal motor 2 can be actuated first and then the horizontal motor 4. The locomotion mechanism can also steer as illustrated earlier in Section 4.3.2, Figure 52.

#### **4.6 Adaptability of the locomotion mechanism to the surface of tissue**

The locomotion mechanism of the robot can adapt to the inclination and minor irregularities of the tissue in the two following ways:

- using soft pads that mould to the curvature and irregularities of the tissue and
- changing the distance between the tissue and the horizontal links with the vertical motors in order to keep the horizontal links parallel with the horizontal.

Figure 59 shows a side view of the locomotion mechanism where the soft pads are moulding to the irregularities of the tissue (Figure 59a) and moulding to the inclination of the surface (Figure 59b). Figure 59c shows how the vertical motors can move the pads to different heights in order to keep the horizontal links parallel to the horizontal.

Soft pads mould to the curvature of the abdominal wall and the irregularities of the surface, enabling full contact between the adhesive pads and the tissue. Full contact between the pads and the tissue favours adhesion, enabling stronger attachment of the robot to the tissue.

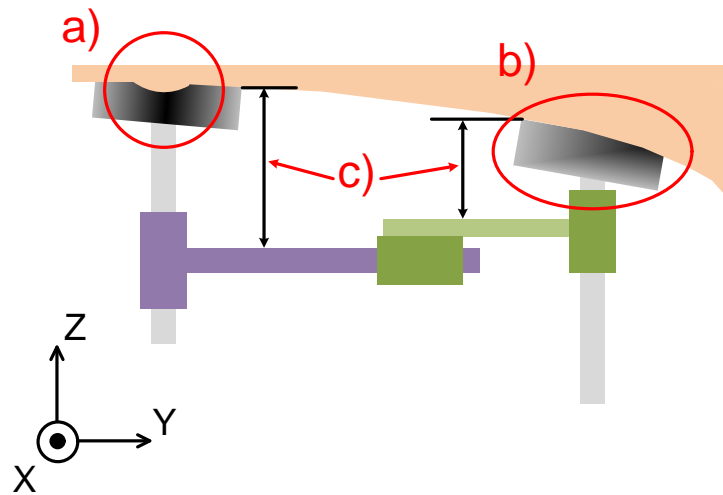


**Figure 59. (a) Soft pad moulding to the irregularities of the tissue, (b) soft pad moulding to the inclination of the tissue and (c) the vertical motors move the pads to different heights. The rotation of the sketched pads is due to the passive twist of the pads in contact with an irregularity (in a) and an inclined surface (in b).**

The vertical motors can control the distance between the corners of the quadrilateral formed by the horizontal links and the tissue. If the surface of the tissue is curved, the vertical motors can move the pads to different heights, adapting to the inclination of the tissue and keeps the quadrilateral formed by the horizontal links parallel to the ground. If the distance between the quadrilateral and the tissue could not be controlled the vertical motor could end up pushing the pads too far into the tissue and making the pads twist and peel off. The quadrilateral formed by the horizontal links in the locomotion mechanism is where the tools and camera of the robot would be mounted. Therefore, it is desirable to keep the quadrilateral formed by the horizontal links parallel to the surface of the abdominal organs.

In order to adapt to the surface of the tissue successfully, the robot should sense the contact with the tissue and should measure the force applied to the tissue. Sensing contact enables the robot to control detachment and attachment of the pads in order to follow the locomotion sequence. Sensing the force between the pads and the tissue enables the robot to control the peel off force and the preload applied to the pads. When the pad is required to move, the vertical motor applies a force to peel off the pad until the pad loses contact with the tissue, without detaching the supporting pads in the process. When contact with the tissue is sensed, the robot can apply a preload force to attach the pad and stop before pushing further into the tissue and causing the supporting pads to peel off.

Contact can be sensed directly with a force sensor, or indirectly with a position sensor or an accelerometer. Force between the pads and the tissue

can be measured directly with a force sensor. This force can also be measured indirectly when the pad is in contact with the tissue using a position sensor and a mathematical model of how the force changes with the position of the motor.

## 4.7 Summary

The kinematic joints of the locomotion mechanism are: four prismatic joints forming a quadrilateral parallel to the surface of the tissue, and one prismatic joint at each corner of the quadrilateral, perpendicular to the tissue. The extension of each prismatic joint is controlled by a linear motor and the four adhesive pads are connected to the vertical prismatic joints.

The workspace of the pads in the horizontal plane is an area around the corners of the quadrilateral formed by the horizontal links. The pad can be positioned within a volume defined by the workspace of the pads in the horizontal plane and the range of motion of the vertical motors. Positioning the four pads within their workspace enables the robot to move along any direction of the horizontal plane and change the orientation and shape of the quadrilateral formed by the horizontal links.

In the vertical direction, the pad attached to the tissue can be modelled as the stiffness of the pad in series with the stiffness of the tissue, being the stiffness of the three supporting pads in parallel. When the pad is detached, the motor simply pulls or pushes the mass of the pad.

When the pad is detached, the motion of the two horizontal motors adjacent to the pad is coordinated in order to move the pad along the horizontal plane. The horizontal motion of the pad can be modelled dynamically as two horizontal motors joined at the pad, pushing or pulling the mass of the pad in conjunction.

The locomotion sequence is generated by timing the motion of the motors so that the pads are detached, moved and re-attached one by one until the whole robot has moved to a new position.

The robot can adapt to the surface of the tissue using soft pads that mould to the irregularities and curvature of the tissue, thus favouring contact between the pads and the tissue. In order to adapt to the inclination of the tissue, the vertical motors can control the distance between the tissue and the quadrilateral formed by the horizontal links keeping this quadrilateral parallel with the ground.

## **Chapter 5**

### **Implementation and testing of the robot**

#### **5.1 Introduction**

The previous chapter presented the conceptual design of the robot, explaining the kinematic links, workspace and dynamic model of the locomotion mechanism moving the adhesive pads. This chapter presents the implementation of the locomotion mechanism, presenting the motors used for the mechanism first and then explaining how the joints of the mechanism are built, assembled and tested. After that, the chapter presents the implementation and testing of the two robot prototypes.

The previous chapter also explained how the locomotion sequence is generated and how the pads and the mechanism adapt to the surface of the tissue. This chapter presents the preliminary tests carried out with the assembly of two prismatic joints attaching and detaching one adhesive pad. After that, the chapter shows the walking performance of the robot, explaining the different improvements made to the hardware and the controller used in order to generate the locomotion sequence.

The chapter closes with a section illustrating the bio-inspired features of the locomotion mechanism and the summary of the chapter.

#### **5.2 Miniature linear motors for the locomotion mechanism**

As explained in Sections 2.2.2, 3.5 and 3.6, the miniature linear motor selected for the locomotion mechanism is the piezo-electric motor Squiggle<sup>®</sup> RV (New Scale Technologies, Inc.). The Squiggle<sup>®</sup> motor is composed of a housing and a threaded shaft (screw); the housing contains four piezo-electric plates and a nut. Figure 60 shows the components and dimensions of the Squiggle<sup>®</sup> motor: Figure 60a shows the front view of the motor, Figure 60b shows the top view of the motor and Figure 60c shows an isometric view of the motor.

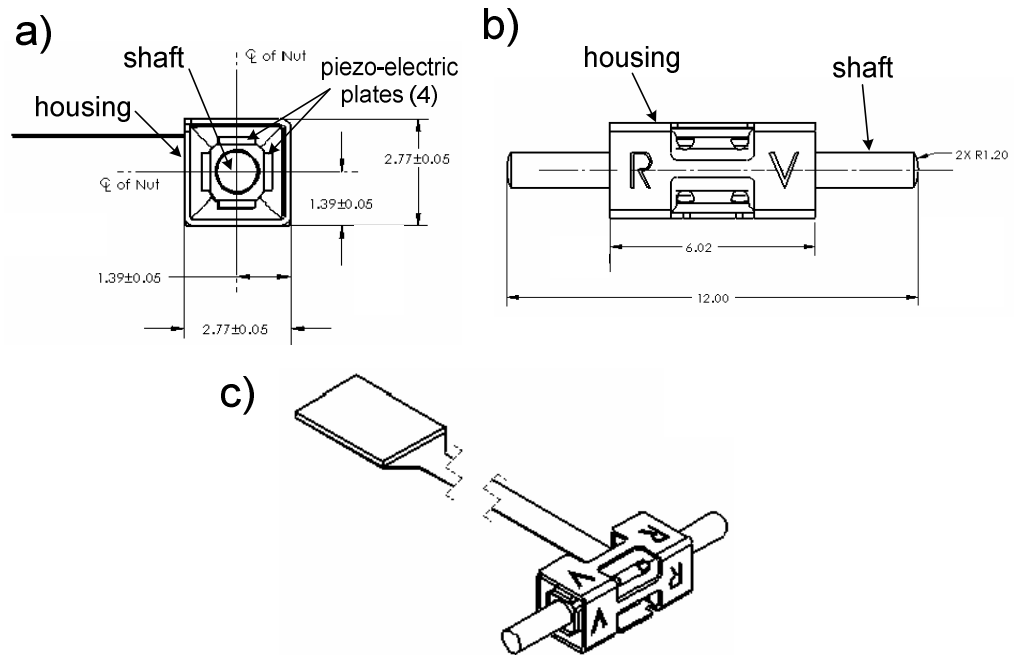


Figure 60. (a) Front view, (b) top view and (c) 3D view of the Squiggle<sup>®</sup> motor [35].

The main characteristics of the Squiggle<sup>®</sup> motor are [35]:

- very low weight: 0.16 grammes per unit,
- very compact size: the dimensions of the housing are 2.8mm x2.8mm x 6mm and the shaft is 12mm long, providing a maximum travel of 9mm.
- high force for its size: the stall force at 4.5V is 500 mN,
- high speed: typically 10 mm/s at 15 grammes load and
- the motor can be integrated in a robotic system using linear encoders specially developed for the Squiggle<sup>®</sup> motor.

The main drawback of using piezo-electric motors inside the body is the high voltage they usually require. The maximum voltage of the Squiggle<sup>®</sup> RV motor is 5.5V, making it more suitable for intra-body operation than other piezo-motors because, with reduced voltage, a lower current will circulate through the tissue if a powered part of the actuator touches it. Another important feature of the Squiggle<sup>®</sup> motor for inverted locomotion is that the motor holds the position when the power is off, preventing the robot from falling in the event of power disruption.

The Squiggle<sup>®</sup> motor is composed of four piezo-electric plates bonded to the faces of a nut that hosts a screw. Figure 61 shows the four piezo-electric plates of the motor attached to the nut, with the screw inside the nut.

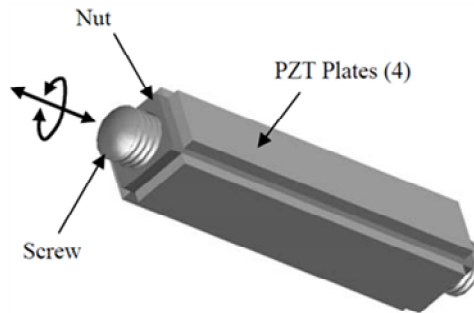


**Figure 61.** The piezo-electric (PZT) plates, nut and screw of the Squiggle<sup>®</sup> motor.

The driver of the motor applies a voltage to the piezo-electric plates at their bending resonant frequency, causing amplified strain on the plates [155]. The voltage signal applied to the piezo-electric plates causes a vibration on the nut, turning the screw inside the nut and making it move forward or backward [155]. Figure 62a shows the voltage signal applied to the piezo-electric plates and Figure 62b shows the vibration that causes the screw to move linearly.

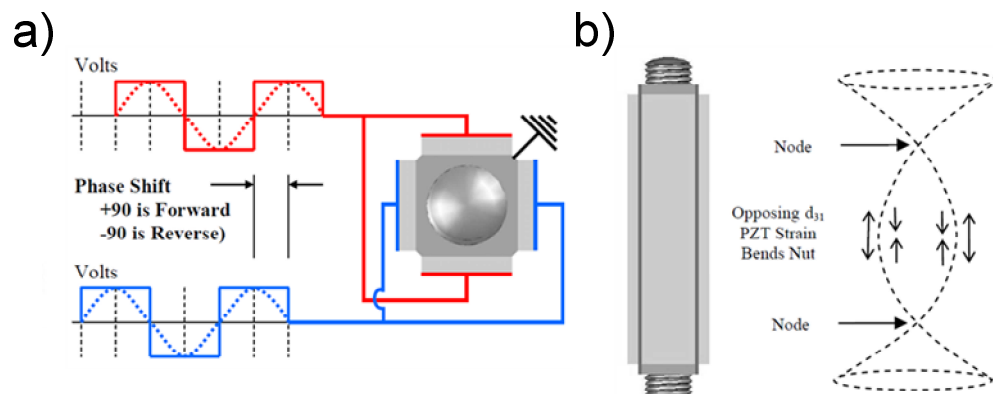


**Figure 62.** (a) Voltage signal sent to the four piezo-electric plates of the Squiggle<sup>®</sup> motor and (b) vibration caused by the voltage signal on the nut [155].

The magnetic linear encoder Tracker<sup>®</sup> NS-5310, manufactured by Austria Micro-systems, is used in order to detect the position of the Squiggle<sup>®</sup> motor. This encoder uses a multi-pole linear magnetic strip and a micro-chip in order to measure the position of the motor. The magnetic strip is attached to the part of the mechanism moved by the screw of the motor and the micro-chip is attached to the part of the mechanism connected to the nut. The micro-chip detects the change in magnetic field caused by the movement of the magnetic strip, thus tracking the position of the part of the mechanism attached to the magnetic strip. Figure 63a shows the top view of the Tracker<sup>®</sup> encoder with the magnetic strip positioned above the micro-chip and Figure 63b shows an isometric view of the Tracker<sup>®</sup> encoder.

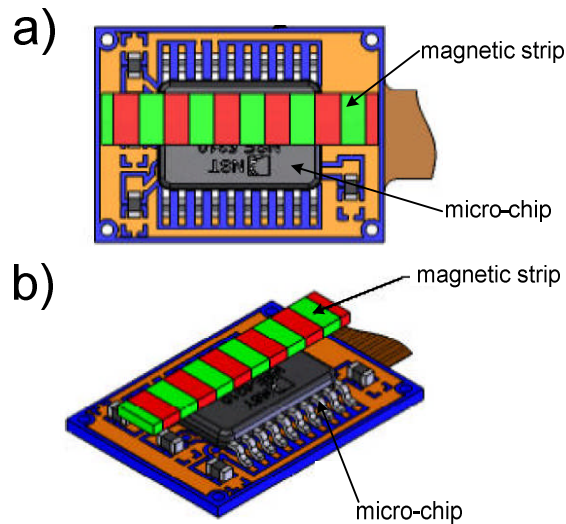


**Figure 63. (a) Top view and (b) 3D view of the linear magnetic encoder Tracker<sup>®</sup> [156].**

The Squiggle<sup>®</sup> motor and the Tracker<sup>®</sup> encoder are used in order to move the pads, controlling the extension of the prismatic joints in the locomotion mechanism.

### 5.3 Mechanical design and construction of the locomotion mechanism

The locomotion mechanism of the robot has four adhesive pads. In the horizontal plane, these adhesive pads are moved by four prismatic joints controlled by linear motors. These prismatic joints form a quadrilateral in the horizontal plane and are connected to each other with passive rotary joints. Figure 64 shows a top view of the CAD model of the robot with four adhesive pads and the four prismatic joints of the locomotion mechanism used in the horizontal plane.

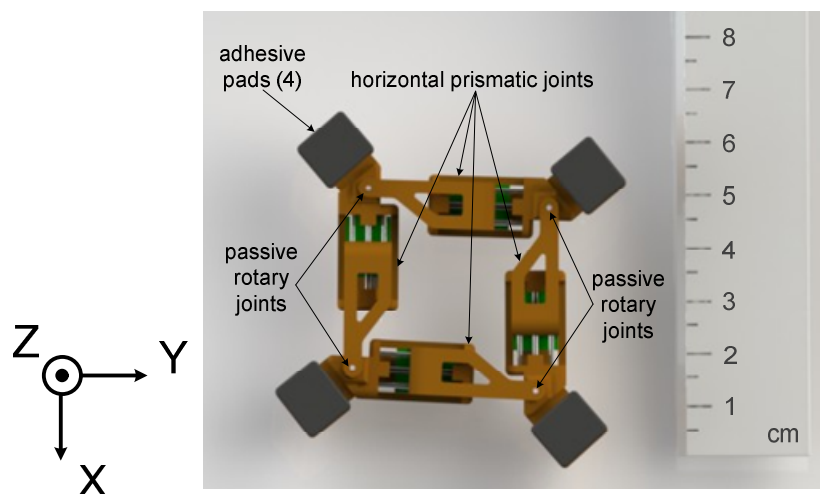


**Figure 64. Top view of the CAD model of the robot.**

In order to move the adhesive pads vertically, the locomotion mechanism has four prismatic joints attached to the corners of the quadrilateral formed by the horizontal prismatic joints. Figure 65a shows the CAD model of the robot held by a model hand for scale. Figure 65b shows a detail of the corner of the robot with the adhesive pad attached to a vertical prismatic joint.

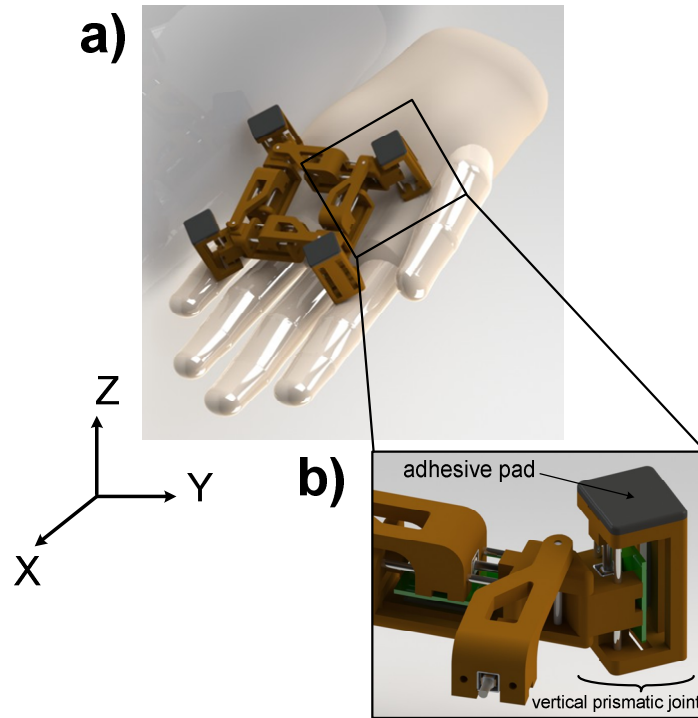


**Figure 65. (a) CAD model of the robot and (b) detail of one corner of the locomotion mechanism.**

The dimensions of the robot are 6 cm x 6 cm x 3 cm (length x width x height). The ideal width of the robot is 2 to 3 cm, so the designed prototype is a double-scale prototype. The motors occupy less than 1% of the total volume of the robot. Thus, the size of the robot is mostly determined by the size of the piece where the housing of the motor is mounted (mounting platform) and the size of the piece supporting the ends of the motor shaft (ends supporter).

The total mass of the prototype manufactured in a plastic like Nylon 6 or ABS is around 20 grammes. The mass of the robot is largely determined by the weight of the mounting platform and the ends supporter because the mass of the eight motors in the robot is only 5% of the total mass.

### 5.3.1 Design and assembly of the components for the locomotion mechanism

The locomotion mechanism of the robot is a series of prismatic joints moved by linear motors and interlinked with passive rotary joints. Figure 66a shows the prismatic and rotary joints of the locomotion mechanism. Figure 66b shows a sketch of the housing and shaft of the linear motor controlling the motion of a prismatic joint, and therefore controlling the motion of the adhesive pad attached to the prismatic joint.

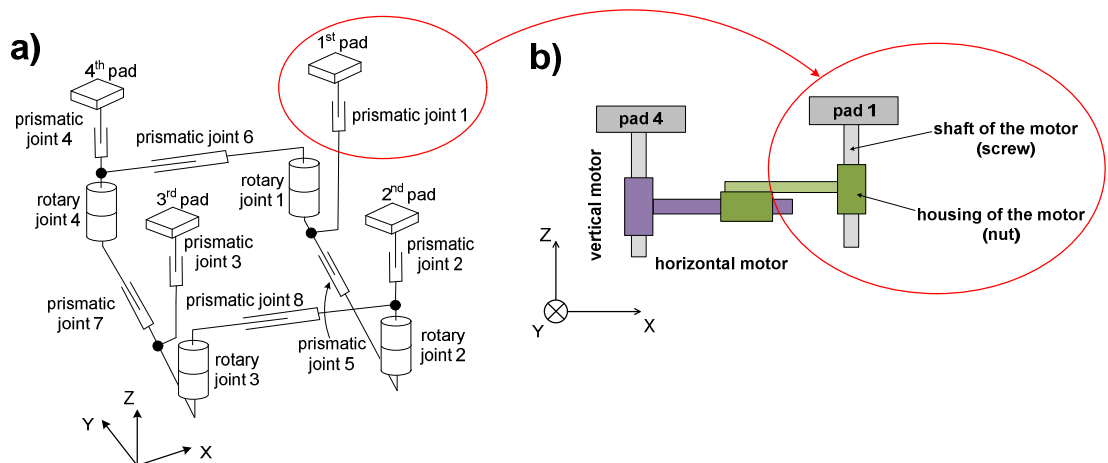


**Figure 66. (a) Prismatic and rotary joints of the locomotion mechanism and (b) housing and shaft of the linear motor in a prismatic joint moving a pad.**

The components of the mechanism of a prismatic joint are:

- one linear motor, composed of one shaft or screw and one housing or nut,
- one ends supporter: the shaft of the motor pushes against this ends supporter,
- one adhesive pad, fixed to the ends supporter,
- one mounting platform: the housing of the motor is fixed to this mounting platform, and
- two guiding rods, connecting the ends supporter and the mounting platform together.

Figure 68a shows a sketch of the components of the prismatic joint and Figure 68b shows the CAD model of the prismatic joint, indicating the components used in order to build the prismatic joint controlled by the motor.

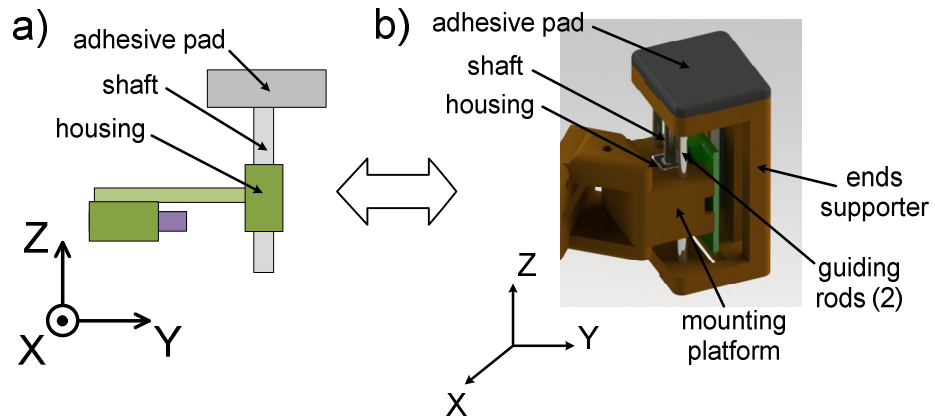


Figure 67. (a) Sketch of a prismatic joint and (b) CAD model of a prismatic joint.

The housing of the motor is fixed to the mounting platform and the adhesive pad is fixed to the ends supporter. The ends supporter is connected to the mounting platform with two guiding rods. The guiding rods are fixed to the ends supporter and slide into two holes on the mounting platform. In order to control the position of the pad, the magnetic strip of the linear encoder is fixed to the ends supporter and the micro-chip of the linear encoder is fixed to the mounting platform. Figure 68a shows the housing of the motor fixed to the mounting platform and Figure 68b shows the adhesive pad and the magnetic strip fixed to the ends supporter. Figure 68c shows the mounting platform and the ends supporter connected with the guiding rods and the micro-chip of the linear encoder attached to the mounting platform.

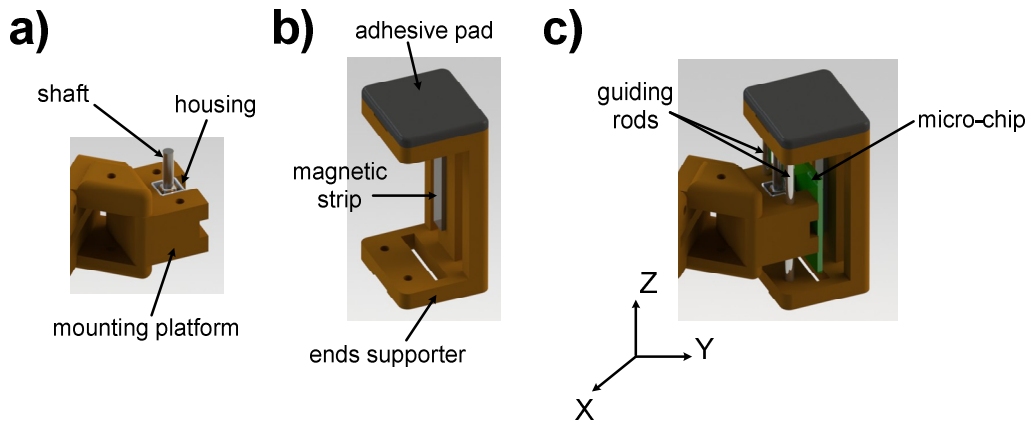


Figure 68. (a) CAD model of the mounting platform of the prismatic joint controlled by the motor, (b) ends supporter of the prismatic joint and (c) assembly of the prismatic joint.

The assembly shown in Figure 68c is for a vertical prismatic joint used in order to move the adhesive pad in the vertical direction. The prismatic joints in the horizontal plane also have one motor, one ends supporter, one mounting platform and two guiding rods. These components are assembled in the same way as shown in Figure 68c in order to obtain the horizontal

prismatic joints. A steel pin is used to build a rotary joint and connect the horizontal prismatic joints to one another. Figure 69a shows the vertical prismatic joint connected to the horizontal prismatic joint and the steel pin to connect this assembly to another horizontal prismatic joint. Figure 69b shows two horizontal prismatic joints and one vertical prismatic joint connected together, enabling motion of the pad in the horizontal plane and vertical direction.

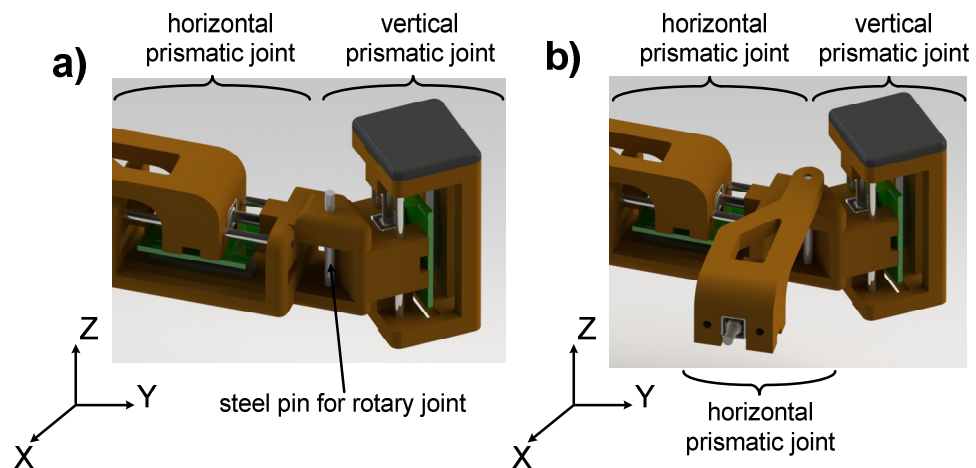


Figure 69. (a) Vertical prismatic joint connected to a horizontal prismatic joint and (b) assembly of two horizontal prismatic joints and one vertical prismatic joint.

### 5.3.2 Integration of the linear motor into the locomotion mechanism

These are the design practices to consider in order to integrate the Squiggle<sup>®</sup> motor into the locomotion mechanism [157]:

- the screw of the motor should not be side-loaded,
- a small return force opposite to the direction of motion should be constantly applied to the screw,
- the motor should not run into a hard stop and
- the friction of the mechanism connecting the motor to the load should be minimal.

The screw of the motor moves linearly because the vibration caused by the piezo-electric plates on the nut makes the screw turn inside the nut. Therefore, if the screw of the motor is side-loaded, the screw does not engage with the nut properly and this can prevent the screw from moving. A return force on the screw ensures that the nut and the screw engage properly when the motor changes direction. The motor should not run into a hard stop because this can damage the threads on the screw. The maximum load the motor can move is reduced if there is friction on the mechanism connecting the motor and the load.

In the locomotion mechanism of the robot, the load the motor has to move is the adhesive pad attached to the ends supporter. The adhesive pad cannot be directly coupled to the screw of the motor because this would prevent the screw from turning inside the nut, thus stopping the linear motion of the motor. The motion of the pad requires a mechanism that connects the motor to the adhesive pad without side-loading the screw of the motor. This mechanism to connect the motor to the pad is the prismatic joint and it should move with very little friction in order not to stall the motor.

Considering the previous design practices, these are the features of the locomotion mechanism designed in order to integrate the motor:

- the surface of the ends supporter in contact with the tip of the screw is low friction,
- the angle between the ends supporter and the screw of the motor is  $90^\circ$ ,
- compression springs can be fitted between the mounting platform and the ends supporter in order to apply a return force to the screw of the motor, and
- contact between the surface of the holes in the mounting platform and the guiding rods is low friction.

Side-loading of the screw can prevent the screw from engaging with the nut and therefore can stop the motion of the screw. In order to prevent side-loading of the screw, the surface of the ends supporter in contact with the tip of the screw is low friction and the angle between this surface and the screw is  $90^\circ$ . Figure 70a shows the contact between the tip of the screw and the ends supporter and Figure 70b shows the  $90^\circ$  angle between the screw and the surface of the ends supporter.

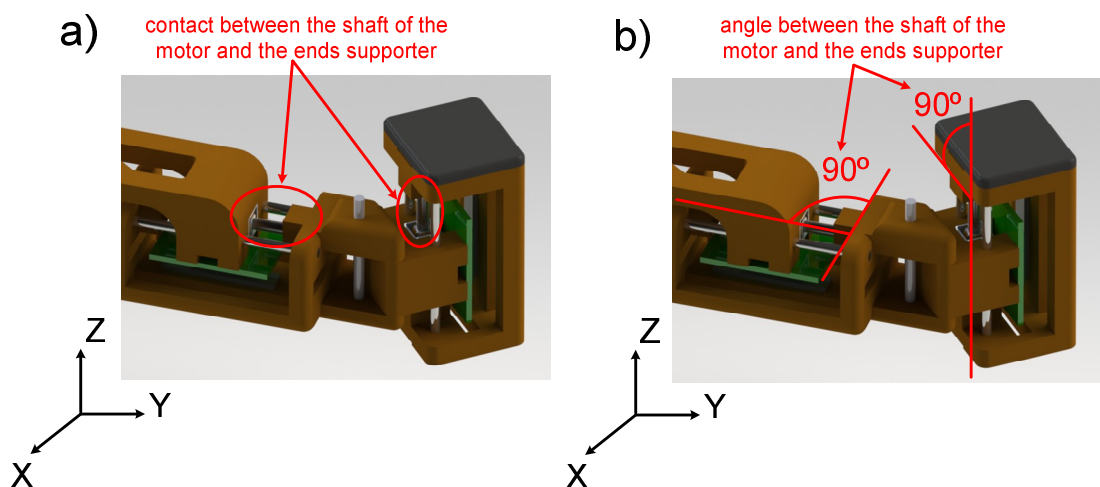
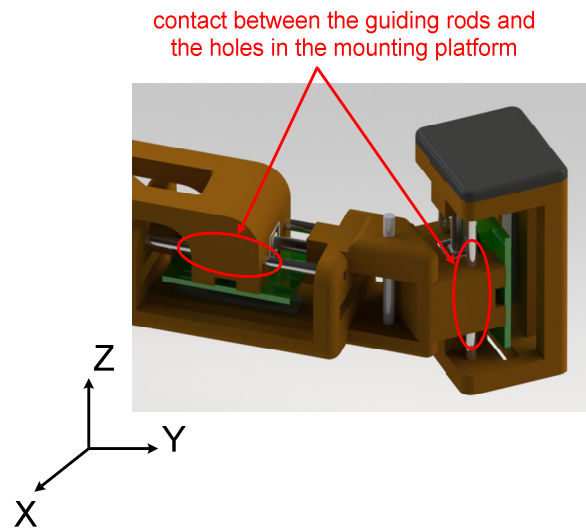


Figure 70. (a) Contact between the shaft of the motor and the ends supporter and (b) angle between the shaft and the ends supporter.

The guiding rods connecting the mounting platform and the ends supporter slide into the holes of the mounting platform in order to obtain the prismatic joint. Friction between the surface of the holes in the mounting platform and the guiding rods diminishes the load the motor can move. Thus, the contact between the surface of the holes in the mounting platform and the guiding rods is low friction. Figure 71 shows the contact between the surface of the holes in the mounting platform and the guiding rods.



**Figure 71. Contact between the surface of the holes in the mounting platform and the guiding rods.**

A return force can be applied to the screw of the motor by fitting compression springs on the guiding rods, between the mounting platform and the ends supporter. A set of four springs on the rods between the mounting platform and the ends supporter ensures a return force is constantly applied to the screw whether the motor is moving forward or backward. Four springs, two on each of the two guiding rods, cancel the tilt that the return force causes on the ends supporter. Figure 72 shows the position of the four springs between the mounting platform and the ends supporter.

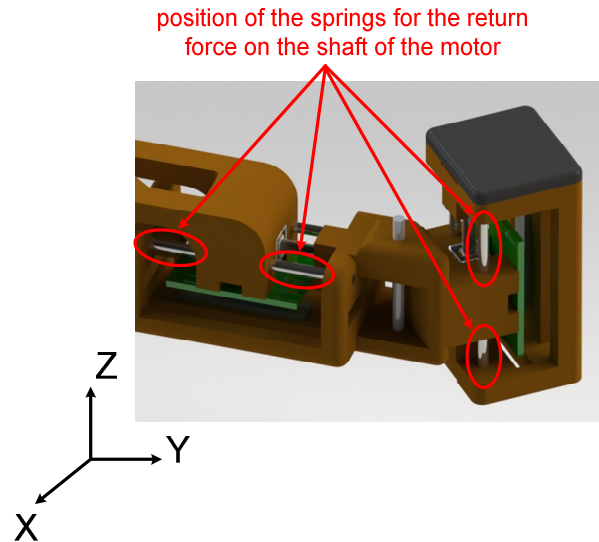


**Figure 72. Position of the springs for the return force on the shaft of the motor within the assembly of the prismatic joint.**

## **5.4 Preliminary tests with the assembly of one prismatic joint and two prismatic joints**

In order to test the motion of one adhesive pad in the horizontal plane and the vertical direction, the following prismatic joints of the locomotion mechanism were tested:

- a vertical prismatic joint, measuring the force able to be applied to the pad,
- a vertical prismatic joint connected to a horizontal prismatic joint, testing the attachment and detachment of the pad.

### **5.4.1 Implementation of a vertical prismatic joint**

The assembly of a vertical prismatic joint is made up of: one motor, one ends supporter, one mounting platform and two guiding rods and follows the design explained earlier. However, this design includes an extension of the mounting platform with a slot in order to attach the mounting platform to a load cell and measure the force applied by the prismatic joint. Figure 73 shows the CAD model of the vertical prismatic joint with the slot to attach the assembly to a load cell.

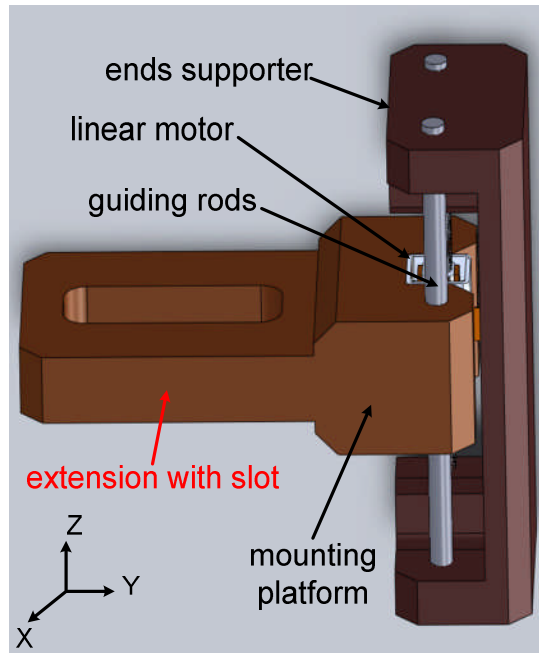


**Figure 73. CAD model of the vertical prismatic joint with a slot to attach the assembly to a load cell.**

The linear motor is a Squiggle<sup>®</sup> motor and the guiding rods are hardened stainless steel (SS 303) of 1 mm diameter and h6 tolerance. The ends supporter and mounting platform are manufactured in low friction, hard plastic.

#### **5.4.1.1 Manufacturing of the components for the prismatic joint**

Three sets of the ends supporter (ES) and the mounting platform (MP) were manufactured using the following manufacturing techniques and materials:

- conventional CNC machining in Teflon<sup>®</sup>,
- precision CNC machining in Teflon<sup>®</sup> (able to machine tolerances of microns for dimensions smaller than 3mm) and
- precision CNC machining in Delrin<sup>®</sup> 500 AF, a type of Acetal<sup>®</sup> resin with a percentage of Teflon<sup>®</sup>.

Figure 74a shows a picture of the ends supporter and the mounting platform manufactured in Teflon<sup>®</sup> using conventional CNC machining. Figure 74b shows a picture of the ends supporter and the mounting platform manufactured in Teflon<sup>®</sup> using precision CNC machining. Figure 74c shows a picture of the ends supporter and the mounting platform manufactured in Delrin<sup>®</sup> 500 AF using precision CNC machining.

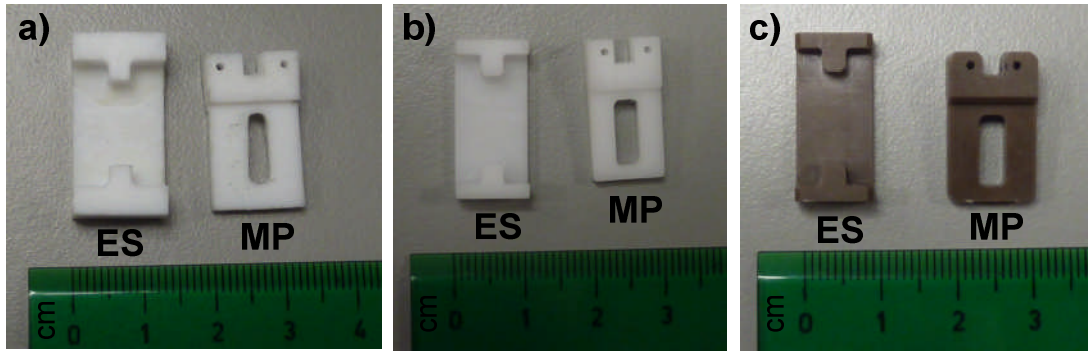


**Figure 74. (a) Ends supporter (ES) and mounting platform (MP) manufactured in Teflon<sup>®</sup> with conventional CNC machining, (b) ES and MP manufactured in Teflon<sup>®</sup> with precision CNC machining and (c) ES and MP manufactured in Delrin<sup>®</sup> with precision CNC machining.**

These three sets of components for the prismatic joint were manufactured in order to investigate the most suitable material and manufacturing technique available to the budget of the intra-abdominal robot. In order to check the friction of the prismatic joint and the play between the components of the assembly, each assembly was tested with the motor, and the dimensions of the components were validated. The achievable tolerances for the manufactured components of the prismatic joint depend on the machine used for manufacturing, the material and the skill of the technician operating the machine.

The first set of components for the prismatic joint was manufactured in Teflon<sup>®</sup> using conventional CNC machining. Figure 75 shows the dimensions and tolerances of the mounting platform of this first set of components. The critical dimensions of the mounting platform are marked on Figure 75 with the circled numbers 1-4.

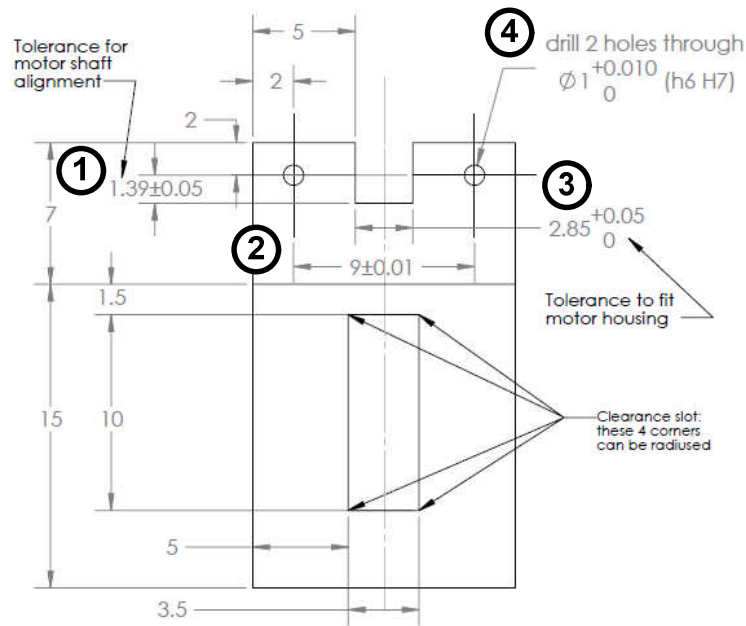


**Figure 75. Drawing of the mounting platform manufactured using conventional CNC machining. The tolerances shown in the drawing were determined using an ISO table of tolerances for the type of fit required for each part of the mechanism.**

The critical dimensions of the mounting platform are:

1. the distance between the base of the motor's housing and the holes for the guiding rods in the mounting platform (see ① in Figure 75),
2. the distance between the holes in the mounting platform where the guiding rods are inserted (see ② in Figure 75),
3. the width of the gap to fit the motor's housing (see ③ in Figure 75), and
4. the diameter of the holes in the mounting platform in order to insert the guiding rods with a sliding fit (see ④ in Figure 75).

The distance between the base of the motor's housing and the holes for the guiding rods ensures that the two guiding rods and the screw of the motor are all at the same height.

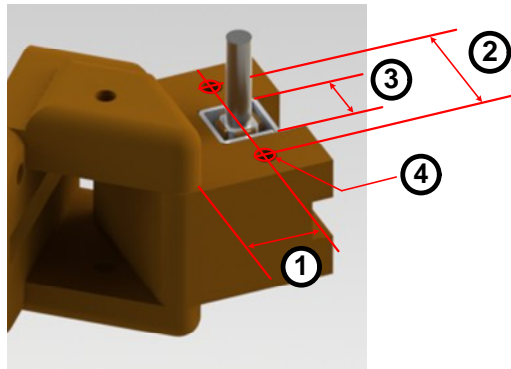
The distance between the holes in the mounting platform corresponds to the distance between the holes at both ends of the ends supporter. The tolerance for this distance ensures that the holes for the guiding rods in the mounting platform are aligned with the holes in the ends supporter.

The width of the gap to fit the motor's housing determines how parallel the screw of the motor and the two guiding rods are.

The sliding fit between the holes in the mounting platform and the guiding rods ensures that the fit is not too tight or too loose. If the fit between the holes and the guiding rods is too tight it causes interference between the

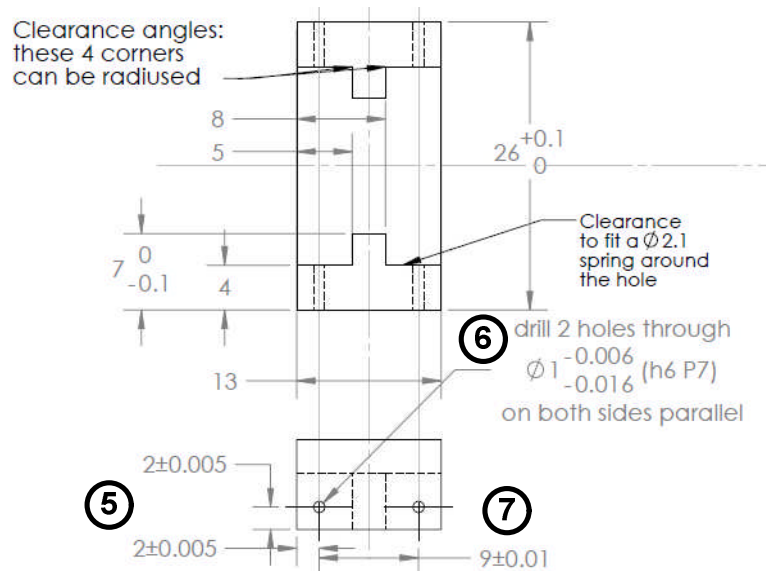
guiding rods and the mounting platform when the motor is moving. If the fit between the holes and the guiding rods is too loose, the angle between the screw of the motor and the ends supporter changes when the motor is moving.

Figure 76 shows the critical dimensions of the mounting platform on the CAD model of the mounting platform and the motor.



**Figure 76. Critical dimensions of the mounting platform.**

Figure 77 shows the dimensions and tolerances of the ends supporter manufactured in Teflon<sup>®</sup> using conventional CNC machining. The critical dimensions of the ends supporter are marked on Figure 77 with the circled numbers 5-7.



**Figure 77. Drawing of the ends supporter manufactured using conventional CNC machining. The tolerances shown in the drawing were determined using an ISO table of tolerances for the type of fit required for each part of the mechanism.**

The critical dimensions of the ends supporter are:

5. the position of the holes in the ends supporter in order to fix the guiding rods to both ends of the ends supporter (see ⑤ in Figure 77),
6. the diameter of the holes in the ends supporter in order to insert the guiding rods with an interference fit (see ⑥ in Figure 77),
7. the distance between the holes in the ends supporter where the guiding rods are inserted (see ⑦ in Figure 77).

The position of the holes in the ends supporter determines how parallel the guiding rods are to each other when the guiding rods are fixed to the ends supporter.

The interference fit between the guiding rods and the holes in the ends supporter ensures that the rods are fixed at both ends of the ends supporter.

The distance between the holes in the ends supporter and the holes in the mounting platform should be the same in order to ensure that the guiding rods are parallel to each other in the assembly.

Figure 78a shows the critical dimensions of the ends supporter on the CAD model of the ends supporter. Figure 78b shows the critical dimensions affecting the alignment of the guiding rods within the assembly of the mounting platform and the ends supporter.

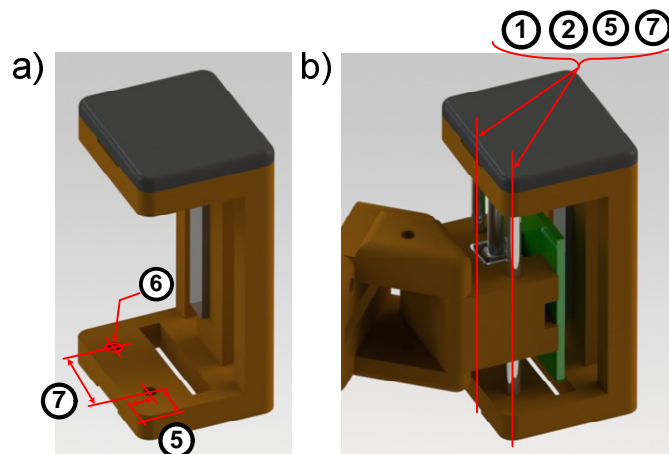


**Figure 78. (a) Critical dimensions of the ends supporter and (b) critical dimensions of the mounting platform and the ends supporter affecting the alignment of the guiding rods within the assembly.**

The tolerances of the three sets of components for a prismatic joint were validated in order to investigate the most suitable manufacturer available to the project. A precision profile projector was used to validate the dimensions and tolerances of the mounting platform and the ends supporter. In a precision profile projector the profile of the manufactured component is projected and amplified on a screen. The dimensions of the component are

measured on the projected image using an electronic micrometer. The error of the measurements due to manual positioning was estimated to be  $\pm 3$  microns, this error was estimated by repeating several measurements and calculating the maximum variation between these measurements. Table 6 and Table 7 show the measurements of the critical dimensions of the mounting platform and ends supporter, indicating whether they are in or out of tolerance. Table 6 shows the measurements for the front side of the mounting platform and ends supporter and Table 7 shows the measurements for the back side.

**Table 6. Tolerance validation of the front side of the mounting platform and ends supporter manufactured in Teflon<sup>®</sup> with a conventional CNC machine.**

		Critical dimension	Measurement	In or out of tolerance
<b>Mounting Platform</b>	①	1.39 ± 0.05 RIGHT	1.365	OUT
		1.39 ± 0.05 LEFT	1.428	OUT
	②	9 ± 0.01	8.902	OUT
	③	2.85 + 0.05	2.639	OUT
	④	∅1+ 0.010 RIGHT	1.097	OUT
		∅ 1+ 0.010 LEFT	1.076	OUT
<b>Ends Supporter</b>	⑤	2 ± 0.005 RIGHT WEST	1.938	OUT
		2 ± 0.005 RIGHT SOUTH	1.993	OUT
		2 ± 0.005 LEFT EAST	1.996	IN
		2 ± 0.005 LEFT SOUTH	1.978	OUT
	⑥	1 - 0.006 -0.016 RIGHT	1.193	OUT
		1 - 0.006 -0.016 LEFT	1.996	OUT
	⑦	9 ± 0.01	8.995	IN

**Table 7. Tolerance validation of the back side of the mounting platform and ends supporter manufactured in Teflon<sup>®</sup> with a conventional CNC machine.**

		<b>Critical dimension</b>	<b>Measurement</b>	<b>In or out of tolerance</b>
<b>Mounting Platform</b>	①	1.39 ± 0.05 RIGHT	1.361	OUT
		1.39 ± 0.05 LEFT	1.328	OUT
	②	9 ± 0.01	8.959	OUT
	③	2.85 + 0.05	2.521	OUT
	④	∅1+ 0.010 RIGHT	1.130	OUT
		∅ 1+ 0.010 LEFT	1.082	OUT
<b>Ends Supporter</b>	⑤	2 ± 0.005 RIGHT WEST	1.996	IN
		2 ± 0.005 RIGHT SOUTH	2.085	OUT
		2 ± 0.005 LEFT EAST	1.965	OUT
		2 ± 0.005 LEFT SOUTH	1.931	OUT
	⑥	1 - 0.006 -0.016 RIGHT	1.157	OUT
		1 - 0.006 -0.016 LEFT	1.965	OUT
	⑦	9 ± 0.01	8.954	OUT

For the mounting platform of the first set of components, 100% of the critical dimensions were out of tolerance. For the ends supporter, 79% of the critical dimensions were out of tolerance.

The linear motor was tested within the assembly of this first set of components. Motion of the prismatic joint was obtained but the fit between the mounting platform and the guiding rods was loose. This loose fit caused the angle between the screw of the motor and the ends supporter to change significantly during motion, thus causing side-loading of the screw and

stalling the motor. The guiding rods mounted on the ends supporter were not parallel, increasing the interference between the guiding rods and the mounting platform and further causing the motor to stall.

The second set of components for the prismatic joint was manufactured in Teflon<sup>®</sup> using precision CNC machining. The size of the components of this second set is smaller than the size of the first set, however, the critical dimensions are the same. Figure 79 shows the dimensions and tolerances of the mounting platform of this second set of components. The critical dimensions of the mounting platform are marked on Figure 79 with the circled numbers 1-4.

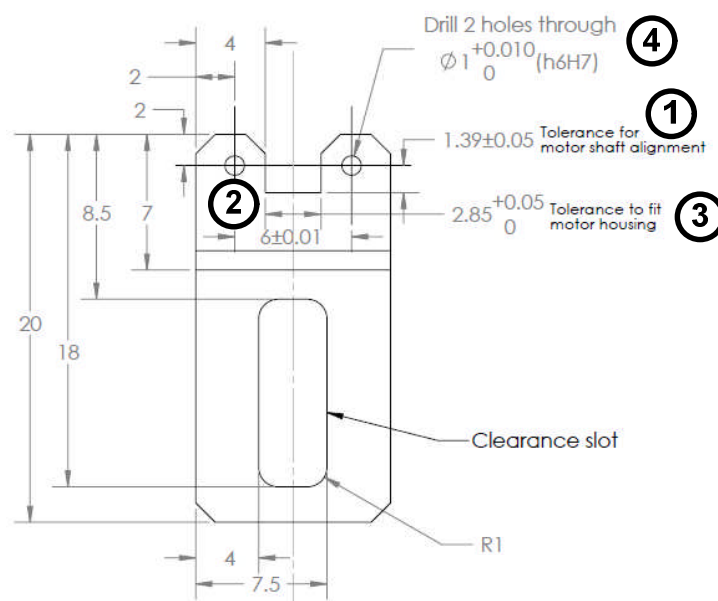


**Figure 79. Drawing of the mounting platform manufactured using precision CNC machining. The tolerances shown in the drawing were determined using an ISO table of tolerances for the type of fit required for each part of the mechanism.**

Figure 80 shows the dimensions and tolerances of the ends supporter manufactured in Teflon<sup>®</sup> using precision CNC machining. The critical dimensions of the ends supporter are marked on Figure 80 with the circled numbers 5-7 and are the same as the first ends supporter.

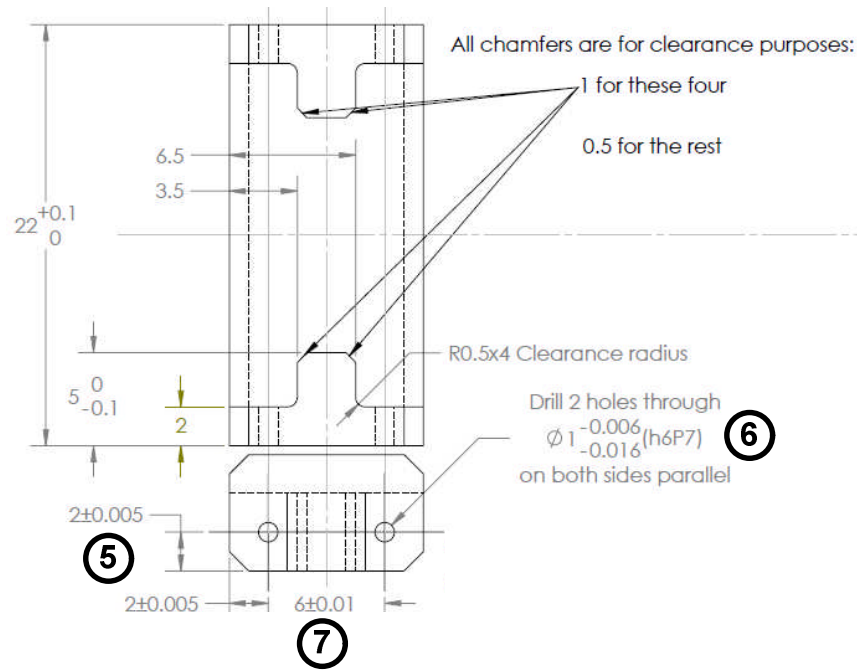


**Figure 80. Drawing of the ends supporter manufactured using precision CNC machining. The tolerances shown in the drawing were determined using an ISO table of tolerances for the type of fit required for each part of the mechanism.**

The linear motor could not move within the assembly of this second set of components because the fit between the guiding rods and the holes of the mounting platform was too tight.

The third set of components for the prismatic joint was manufactured in Delrin<sup>®</sup> using precision CNC machining. The dimensions and tolerances of this third set of components are the same as the second set: see Figure 79 for the specifications of the mounting platform and Figure 80 for the specifications of the ends supporter. For this set of components, the technical specifications of the components was supplied to the manufacturers together with an explanation of how the mechanism is assembled and how it is designed to work. The critical dimensions of this third set of components were measured with the precision profile projector and are shown in Table 8 for the front side of the mounting platform and ends supporter and Table 9 for the back side.

**Table 8. Tolerance validation of the front side of the mounting platform and ends supported manufactured in Delrin® with a precision CNC machine.**

	<b>Critical dimension (see Figure 79 and Figure 80)</b>	<b>Measurement</b>	<b>In or out of tolerance</b>	
<b>Mounting Platform</b>	① 1.39 ± 0.05 RIGHT	1.362	IN	
		1.39 ± 0.05 LEFT	1.370	IN
	② 6 ± 0.01	5.998	IN	
	③ 2.85 + 0.05	2.907	OUT	
	④ Ø1+ 0.010 RIGHT	1.057	OUT	
		Ø 1+ 0.010 LEFT	1.083	OUT
<b>Ends Supporter</b>	⑤ 2 ± 0.005 RIGHT WEST	1.939	OUT	
		2 ± 0.005 RIGHT SOUTH	2.058	OUT
		2 ± 0.005 LEFT EAST	1.997	IN
		2 ± 0.005 LEFT SOUTH	1.959	OUT
	⑥ 1 - 0.006 -0.016 RIGHT	1.031	OUT	
		1 - 0.006 -0.016 LEFT	1.043	OUT
	⑦ 6 ± 0.01	6.077	OUT	

**Table 9. Tolerance validation of the back side of the mounting platform and ends supported manufactured in Delrin<sup>®</sup> with a precision CNC machine.**

	<b>Critical dimension (see Figure 79 and Figure 80)</b>	<b>Measurement</b>	<b>In or out of tolerance</b>
<b>Mounting Platform</b>	①	1.39 ± 0.05 RIGHT	1.387 IN
		1.39 ± 0.05 LEFT	1.332 OUT
	②	6 ± 0.01	5.953 OUT
	③	2.85 + 0.05	2.912 OUT
	④	∅1+ 0.010 RIGHT	1.096 OUT
		∅ 1+ 0.010 LEFT	1.109 OUT
<b>Ends Supporter</b>	⑤	2 ± 0.005 RIGHT WEST	2.014 OUT
		2 ± 0.005 RIGHT SOUTH	2.001 OUT
		2 ± 0.005 LEFT EAST	2.013 IN
		2 ± 0.005 LEFT SOUTH	1.954 OUT
	⑥	1 - 0.006 -0.016 RIGHT	0.980 OUT
		1 - 0.006 -0.016 LEFT	1.021 OUT
	⑦	6 ± 0.01	6.003 IN

For the mounting platform of the third set of components, 86% of the critical dimensions were out of tolerance. For the ends supporter, 79% of the critical dimensions were out of tolerance.

The linear motor was tested within the assembly of this third set of components. The motion of the prismatic joint with the third set of components was smoother than with the first and the second because of the

expertise of the manufacturers in adjusting miniature mechanisms machined in plastic.

#### 5.4.1.2 Miniature springs in order to provide a return force to the screw of the motor

A force of 50 mN constantly applied to the screw of the motor ensures that the threads of the screw are engaged with the nut and prevent the motor from stalling or working intermittently [157]. Providing a return force to the screw of the motor is especially important when the motor has stopped and starts moving again in a different direction. In order to provide this force to the screw, four springs can be fitted around the guiding rods, in the space between the mounting platform and the ends supporter of the prismatic joint. Figure 81 shows the position of the compression springs in the vertical and prismatic joint of the locomotion mechanism.

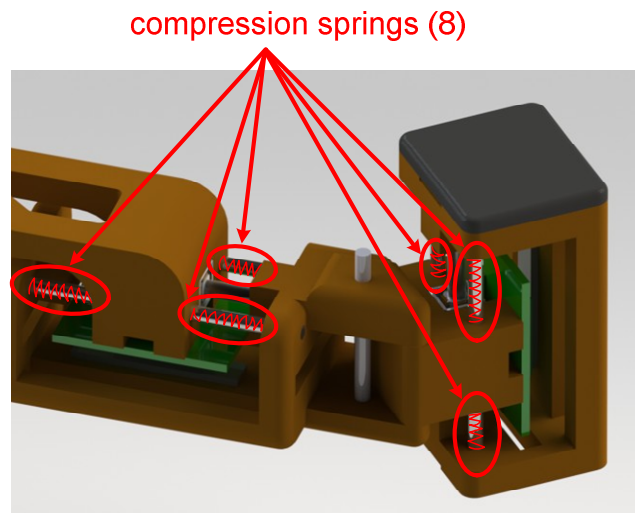


**Figure 81. Position of the compression springs within the prismatic joint in order to apply a return force to the screw of the motor.**

The specifications of the compression springs in order to provide a return force to the screw of the motor are:

- length of a few millimetres: 1-5 mm,
- inner diameter greater than 1 mm in order to fit loosely around the guiding rods, and
- a stiffness constant so that the return force applied to the screw is around 50 mN for the whole range of motion of the motor.

Commercially available springs for the size and the stiffness required are difficult to find. Off-the-shelf compression springs with constant force are much larger than the size required for the prismatic joints of the locomotion mechanism.

In terms of the size, the most suitable compression spring found off-the-shelf has a free length of 2 mm, an outer diameter of 1.2 mm, a wire diameter of 0.2 mm and a spring constant of 4.09N/mm (Ondrives Ltd., UK). The dimensions of this spring are suitable for the design of the prismatic joint but the return force this spring provides is much higher than the force required. For these springs, 1mm of compression applies a force on the screw 14 times greater than the maximum force that stalls the motor (300 mN) and 82 times the return force recommended by the manufacturers (50 mN).

In terms of the stiffness, the most suitable one found in the market has a free length of 12 mm, an outer diameter of 1.7 mm and wire diameter of 0.15 mm (Muelles Ros, Spain). This spring uses music wire and has a stiffness constant of 0.1 N/mm, providing a force twice the return force recommended by the manufacturers for 1mm of compression. However, the spring has to be cut to a shorter length because the free length of the spring is twice the length of the motor's housing. If the spring is cut to a more suitable size, like 2 mm, the spring constant increases 4.5-fold up to 0.45N/mm. For a free length of 2 mm, the return force on the screw for 1 mm of compression of this spring is 1.5 times the stall force of the motor and 9 times the recommended return force.

The Ondrives spring and the Muelles Ros spring cut to a free length of 2 mm were tested in the mechanism of the prismatic joint. The springs prevented the motor from stalling when the springs were compressed slightly at the end of the travel range. However, for further compression, a higher return force from the springs caused the motor to stall frequently. In addition to that, the length of the springs on each side of the motor is slightly different because they are cut manually. This difference of return force applied on each side of the motor changes the angle between the guiding rods and the ends supporter, side-loading the screw of the motor.

For the vertical motors, there is always a return force applied to the motor during locomotion. This is so because if the pad is detached, the motor pushes against the weight of the pad and if the pad is attached, the motor pulls against the adhesion force. For this reason and because of the lack of availability of suitable springs, compression springs to provide a return force to the screw were not included in the final design.

#### **5.4.2 Force measurements from a vertical prismatic joint**

In order to check the performance of the prismatic joint, the motor was tested measuring the force the motor applies to the ends supporter when the

motion of the prismatic joint is blocked. The components used for this test were the mounting platform and ends supporter manufactured in Delrin<sup>®</sup> using precision CNC machining. Figure 82 shows the experimental set-up for this blocked force test, which includes the following components:

- one mounting platform fixed to an aluminium structure,
- one linear motor,
- one ends supporter touching the load cell through a piece of foam in order to ensure full contact,
- one magnetic strip fixed to the ends supporter and
- one magnetic encoder fixed to the aluminium structure.

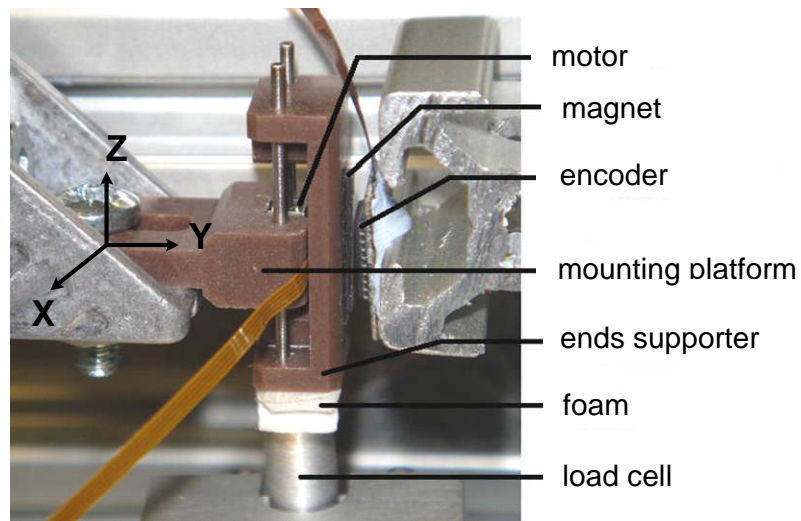


**Figure 82. Experimental set-up for the blocked force test of the prismatic joint.**

In order to simulate the prismatic joint detaching or attaching the adhesive pad, the motion of the motor within the prismatic joint is blocked with an initial load of  $150 \pm 15 \text{ mN}$ . This initial load ensures contact between the motor and the load cell. The force is measured with a GSO 100 grammes load cell manufactured by Transducer Techniques, Inc. The force delivered by the motor when the motion of the prismatic joint is blocked should be greater than the adhesion force of the pad in order to detach the pad.

The force from the motor depends on the voltage input to the drivers and the speed setting, which determine the power produced by the motor for a certain load [35]. For constant voltage and constant load on the motor, the force the motor is able to produce decreases with a lower speed setting. For this force test, the voltage is set at 3.3 V and the speed setting is 70% of the maximum.

The force delivered by the motor is checked at 12 points along the screw of the motor in order to measure how uniform the performance of the motor is along its travel range. The length of the screw is 12 mm and each point

considered for the test is at  $500 \pm 200 \mu\text{m}$  of distance between the housing and the tip of the screw. This distance between the housing and the tip of the screw is measured with the Tracker<sup>®</sup> linear magnetic encoder.

These are the steps followed to measure the force of the prismatic joint at each point along the length of the screw:

- the driving voltage is set at 3.3 V and the speed is set at 70% of the maximum,
- the motor is moved to the initial position along the length of the screw,
- the motion of the prismatic joint is blocked applying the default load of  $150 \pm 15 \text{ mN}$  and
- the driving signal is sent to the motor, measuring the force applied to the load cell.

Figure 83 shows the graph of force applied by the prismatic joint for each point along the length of the screw. The increment of force shown in Figure 83 is the increment of force obtained from the initial load applied to the prismatic joint in order to block it.

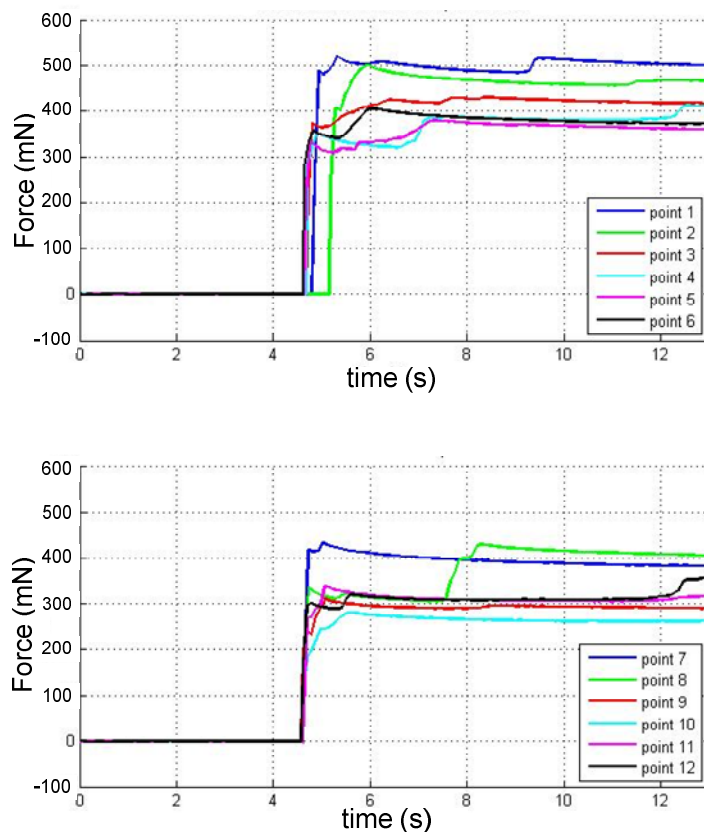


**Figure 83. Blocked force obtained from the prismatic joint for twelve points along the screw of the motor. The top figure shows the increment of force obtained when voltage is applied to the motor while the motor is blocked (blocked force) for the first six points along the screw of the motor. The figure at the bottom shows the blocked force obtained for the last six points along the screw of the motor.**

Table 10 shows the value of blocked force obtained from the prismatic joint for the 12 points considered along the screw of the motor.

**Table 10. Blocked force obtained along the screw of the motor.**

<b>Point along the screw</b>	<b>Initial load (mN)</b>	<b>Force increment (mN)</b>	<b>Point along the screw</b>	<b>Initial load (mN)</b>	<b>Force increment (mN)</b>
<b>1</b>	141.16	518.19	<b>7</b>	155.79	432.33
<b>2</b>	150.54	500.39	<b>8</b>	164.53	429.95
<b>3</b>	148.47	429.63	<b>9</b>	153.88	310.06
<b>4</b>	146.41	411.98	<b>10</b>	154.67	281.12
<b>5</b>	139.25	378.43	<b>11</b>	148.95	340.27
<b>6</b>	155.95	403.87	<b>12</b>	144.66	373.02

Looking at the values in Table 10 the force seems to diminish for the later points along the screw; this is probably due to minor deficiencies in the mechanical assembly of the prismatic joint and experimental set-up. For the bio-mimetic pads, the maximum adhesive force measured for a preload of 10 mN is 140 mN [10]. Therefore, in order to detach the adhesive pad, the prismatic joint needs to apply a block force greater than 140 mN.

The minimum force obtained from the prismatic joint is 280 mN approximately and the maximum is 520 mN depending on the point of operation along the screw. The average force obtained from the prismatic joint is 400.8 mN which is approximately 3 times the maximum adhesion force of the pad. The variability of the blocked force for the points considered along the screw is  $\pm 70.1$  mN, that is 17.5% of the average blocked force. This value of force is sufficient to apply a preload of 10 mN and a detachment force of 140 mN, enabling the intra-abdominal robot to control the adhesion of the pad and follow the locomotion sequence.

The prismatic joint manufactured in Delrin<sup>®</sup> using precision CNC machining can deliver sufficient force and moves the adhesive pad smoothly. However, precision CNC machining of the whole robot was beyond the project's budget and rapid prototyping was used instead in order to manufacture the rest of the components for the locomotion mechanism.

### 5.4.3 Force measurements from a vertical and a horizontal prismatic joint attaching and detaching the adhesive pad

In order to check the performance of the locomotion mechanism moving the pad, the vertical and horizontal prismatic joints were tested attaching and detaching the adhesive pad on tissue. Figure 84 shows the experimental set-up for this test, which includes the following components:

- one load cell connected to the mounting platform of the horizontal prismatic joint,
- one load cell above the ends supporter of the vertical prismatic joint, holding the sample of tissue,
- one assembly of a vertical and horizontal prismatic joint, including the adhesive pad backed by a layer of foam, and
- one sample of rat peritoneum.

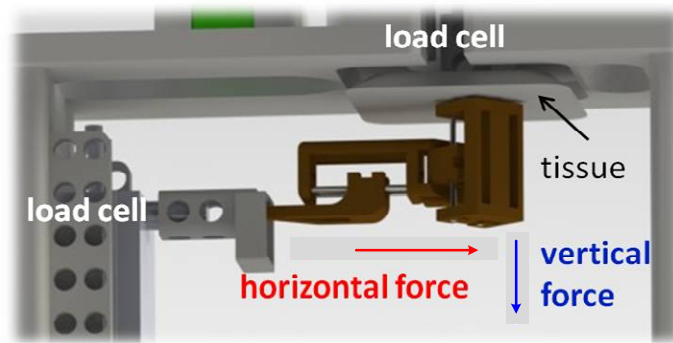


**Figure 84. CAD model of the set-up to test the vertical and horizontal prismatic joints attaching and detaching the adhesive pad.**

The load cell to measure the vertical force is a GSO 100 grammes load cell and to measure the horizontal force, a GSO 50 grammes load cell is used, both manufactured by Transducer Techniques, Inc. The stem of the load cell for vertical force is aligned with the screw of the vertical motor, applying the vertical force to the centre of the adhesive pad.

The components of the vertical and horizontal prismatic joints were rapid-prototyped in ABS plastic with a 3D printer (HP Designjet 3D Printer CQ656A). The adhesive pad is attached to the ends supporter of the vertical prismatic joint. The adhesive pad is a square of 100 mm<sup>2</sup>, connected to the ends supporter of the vertical prismatic joint through a 3.5mm-thick layer of Tempur<sup>®</sup> memory shape foam.

Rat peritoneum is used for the tissue sample because it resembles human peritoneum [10]. The force applied on the tissue by the vertical and horizontal prismatic joints was measured in the following two tests:

- preload test: a series of values of preload were applied to the adhesive pad in order to attach it and then the pad was detached in order to measure the adhesive force,
- horizontal force test: the pad was attached with the vertical motor, a force was applied with the horizontal motor and then the pad was detached with the vertical motor.

#### 5.4.3.1 Preload test with the vertical prismatic joint

The preload test shows the ability of the vertical prismatic joint to apply different values of preload, thus controlling the adhesion of the pad. These are the steps followed to measure the adhesive force for different values of preload:

- the preload is applied to the pad, ensuring attachment to the tissue; this is registered as compression force by the load cell,
- a few seconds are waited in order to enable the foam backing of the pad to comply to the pressure applied on the pad,
- a pull force is applied to the attached pad, bringing it back to the initial position and obtaining the value of adhesive force; this is registered as tension force by the load cell.

These steps are shown in Figure 85 on the graph of force obtained during the process of preloading and detaching the adhesive pad. The negative value of force in Figure 85 corresponds to compression force, obtained when preloading the pad. The positive value of force in Figure 85 corresponds to tension force, obtained when detaching the pad. The adhesive force is the maximum positive force recorded during the test.

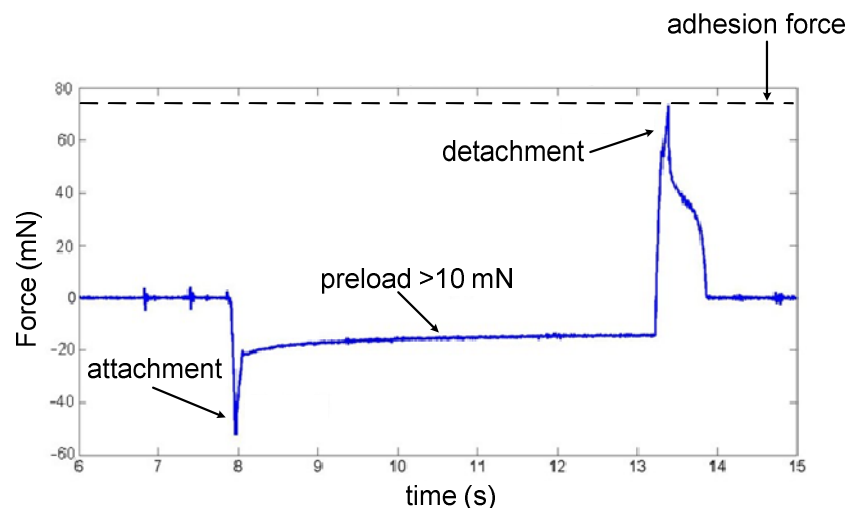


**Figure 85. Force applied by the vertical prismatic joint to the adhesive pad in order to test different values of preload.**

Following the previous steps, the pad was preloaded and detached from the tissue for five consecutive times for values of preload between 10 and 100

mN. The graph in Figure 86 shows the average and standard deviation of the adhesion force recorded for preload values between 10 and 100 mN.

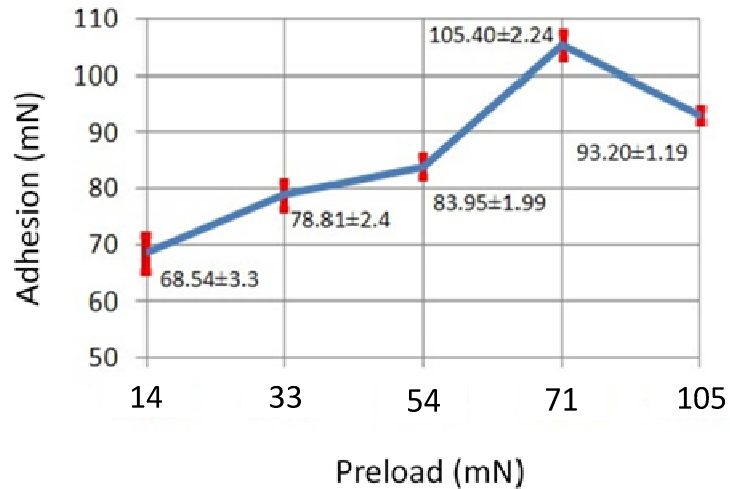


**Figure 86. Effect of preload on the adhesion force between the adhesive pad and the tissue.**

Adhesion force increases by an average of 25% for each 80% average increment of preload force applied to the pad. This direct proportionality between preload and adhesion force is true until a value of 70 mN of preload is reached. This maximum value of preload suggests that pressure on the pad favours the formation of links between the pad and the tissue until excessive force starts breaking them. Therefore, preload force between 10 and 70 mN can be used in order to control the adhesion of the pad when the pad is in contact with the tissue.

In previous research, a preload between 5 and 30 mN was tested on the adhesive pad, concluding that there is no significant increase in adhesion force for a preload between 10 and 30 mN [10]. The results of the test presented here confirms the conclusions of previous research for a preload of 10 and 30 mN and complements those results by testing values of preload up to 100 mN.

#### **5.4.3.2 Horizontal force test with the vertical and horizontal prismatic joints**

The horizontal force test shows the ability of the prismatic joints to use a horizontal force in order to control the adhesion of the pad. These are the steps followed to show the effect of a horizontal force on the adhesive force of the pad:

- the pad is attached with a preload and detached, measuring the adhesion force when no horizontal force is applied to the pad;



adhesion force of the pad decreases by 10%. This increase and decrease in the adhesion force of the pad with horizontal force is mainly caused by the compliance of the foam backing of the pad; some of this variation is probably due to the adhesion force decreasing over cycles. When a low horizontal force is applied to the pad, adhesion force increases because more intimate contact between the pad and the tissue is obtained. However, a high horizontal force can cause shearing on the surface, thus favouring detachment. A horizontal force on the pad similar to the adhesion force enhances attachment, while detachment is more effective when a horizontal force several times higher than the adhesion force is applied to the pad.

These tests show that the adhesion of the bio-mimetic pad is enhanced and diminished depending on the vertical and horizontal force applied on the pad. Controlling adhesion is useful for the locomotion of the robot because it enables to recover the adhesion force of the pad and can make detachment more efficient.

## 5.5 First prototype of the robot

The first prototype of the robot was rapid-prototyped in ABS plastic with a 3D printer (HP Designjet 3D Printer CQ656A). Figure 88a shows the first prototype of the robot composed of eight prismatic joints. Figure 88b shows a detail of the horizontal prismatic joint, indicating the position of the magnetic strip and the encoder within the mechanism. Figure 88c shows a detail of the vertical prismatic joint.

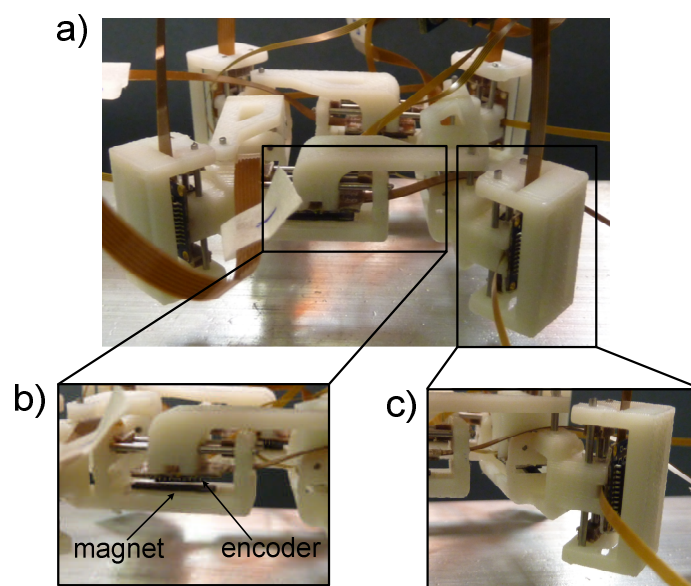


**Figure 88. (a) First prototype of the robot manufactured in ABS plastic with a 3D printer, (b) detail of the horizontal prismatic joint and (c) detail of the vertical prismatic joint.**

The dimensions of the prototype are 6 cm x 6 cm x 3 cm (L x W x H) when the horizontal prismatic joints are fully contracted and 6.6 cm x 6.6 cm x 3 cm when the horizontal prismatic joints are fully extended. The mass of the first prototype including motors and encoders is approximately 21 grammes.

The components required significant adjustment in order to obtain the sliding fit at the prismatic joints and at the passive rotary joints connecting the horizontal prismatic joints to the vertical prismatic joints. This adjustment of the components was required because of the rough finishing of the surfaces in the components obtained with the 3D printer. The adjustment of the components involved filing and drilling the holes in the mounting platform and the rotary joints in order to reduce interference. In order to diminish the friction between the screw and the ends supporter, a couple of small pieces of Delrin<sup>®</sup> were fitted on the surface where the tip of the screw touches the ends supporter.

### **5.5.1 Walking performance of the robot following an open-loop locomotion sequence**

In order to check the walking performance of the first prototype of the robot, the locomotion sequence was programmed making the motors follow open-loop commands. These open-loop commands move the motors for a length of time at a speed sufficient to make the motor reach its end of travel. For this locomotion sequence, magnetic pads and a steel surface were used instead of adhesive pads and tissue in order to minimise the handling and use of biological materials. The magnetic pads were custom made by trimming down a magnetic sheet to the appropriate size to resemble the adhesive pads. Each magnetic pad has the same area as the adhesive pad: 100 mm<sup>2</sup> and has an detachment force around 100 mN, resembling the detachment force of the bio-inspired adhesive pad [10]. The magnetic pads are flexible and backed by a 3.5mm-thick layer of Tempur<sup>®</sup> memory shape foam. Figure 89 compares the force-displacement graph of an indentation test for the adhesive pad against rat peritoneum to the same graph of the magnetic pad against steel. In Figure 89, the peak force in the plot of the adhesive pad is the adhesion force and the peak force in the plot of the magnetic pad is the detachment force of the magnet.

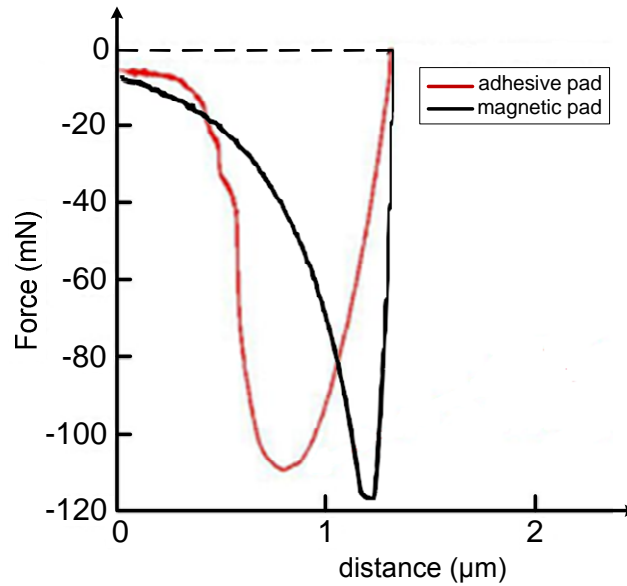


**Figure 89. Comparison between the detachment force of the adhesive pad against rat peritoneum and the magnetic pad against steel.**

In the magnetic pad, the magnetic force takes effect before contact with the surface and this makes attachment of the pad easier because no preload is required. On the other hand, detachment with the magnetic pad is more difficult than with the adhesive pad because the magnetic force is still present when the two surfaces are separated. Another difference between the magnetic pad and the adhesive pad is the work of the detachment force. The work of the detachment force is the area between the line described by the detachment force in Figure 89 and the horizontal line at zero value of force. The work of the detachment force affects the way the pad detaches and differs to some extent between the adhesive pad and the magnetic pad as shown in the graph of Figure 89.

The motion of the motors is coordinated to follow the locomotion sequence of detaching, moving and re-attaching one pad at a time. Figure 90 shows the detachment and re-attachment sequence of the pads making the robot move one step. The video of this step of the robot can be seen in [158].

The steps of the locomotion sequence shown in Figure 90 are:

- a) initial position with the four pads attached to the surface, pad 1 is commanded to move,
- b) pad 1, the pad at the back, detaches after 233 ms,
- c) pad 1 re-attaches to the surface 701 ms later,
- d) pad 2, the pad on the left-hand side, detaches 134 ms later,
- e) pad 2 re-attaches to the surface 700 ms later,
- f) pad 3, the pad at the front, detaches 367 ms later,
- g) pad3 re-attaches to the surface 534 ms later,
- h) pad4, the pad on the right-hand side, detaches 200 ms later,

- i) pad 4 re-attaches to the surface 501 ms later, completing one step of the robot.

The distance travelled by the pads is 5.5 mm, which is the range of motion of the motor within the prismatic joint and thus, the length of the robot's step. Minor deficiencies in the assembly of the prismatic joints limit the range of motion to 5.5 mm instead of the theoretical 6 mm. On average, each pad takes 233.5 ms to detach and 842.5 ms to move to its final position within the locomotion sequence. The speed of each pad is therefore 6.53 mm/s. The robot takes 3.37s to cover 5.5 mm in a straight line and thus the overall speed is 1.6 mm/s. Considering a distance of 10 cm from side to side of the operating space on the abdominal wall, the robot would take just over one minute to cross this operating space.

The robot required some trial steps until it managed to complete a step in a repeatable way. The step of the robot showed in Figure 90 is representative of four successful recorded steps that the robot was able to take. When the robot failed to complete a step it was because the vertical prismatic joints could not detach or re-attach the pads in the length of time the motors were commanded to move. This happened because each motor requires a different length of time to reach the end of its travel depending on how fast and smooth the motor moves within the prismatic joint. The motor moves more slowly or intermittently within the prismatic joint depending on the friction of the mechanism and the side-loading on the screw of the motor. This friction and side-loading in the mechanism of the prismatic joint depend on the precision of the sliding fit between the guiding rods and the mounting platform.

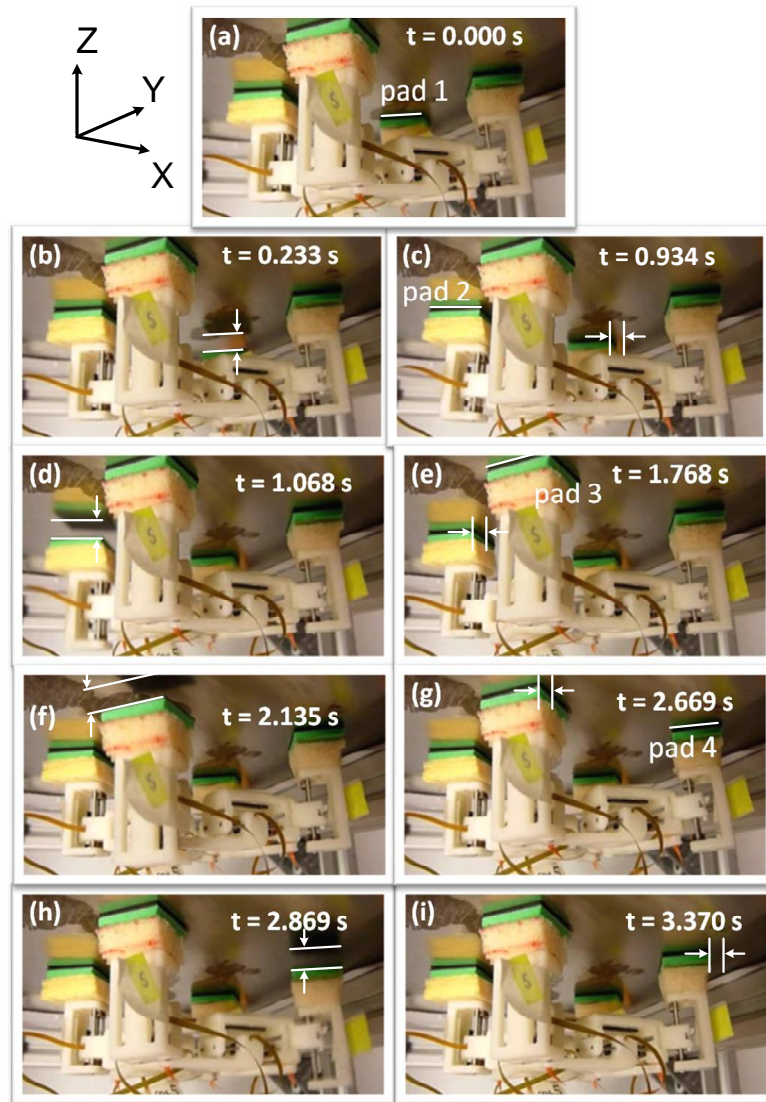


Figure 90. (a-i) The first prototype of the robot walking one step, following an open-loop locomotion sequence.

### 5.5.2 System architecture for closed-loop control of the robot

Closed-loop control of the robot ensures that the motors reach the desired position by integrating the information from the encoders into the locomotion sequence. The controller of the robot is the link between sensors and actuators, translating inputs from the sensors into outputs of the motor's drivers. The controller receives the information available from the sensors and processes it into locomotion commands.

The architecture of the closed-loop control system of the robot is made up of the following components:

- Three hierarchical levels of control:
  - The Intelligent Controller, in charge of deciding the task of the robot and how to carry out that task,
  - The Gait Planner, in charge of translating the plan of the Intelligent Controller into specific actions for the motors, and
  - The Motors' Driver, in charge of setting the parameters for the drivers of the motors to follow the actions set by the Gait Planner.
- Two communication buses between the control levels:
  - The Trajectory parameters bus, which contains the steps the robot needs to follow in order to complete a task, and
  - The Step parameters bus, which contains the actions the motors have to follow in order to complete a step of the trajectory.

When the controller starts, the system is initialised first and then the controller enters the first control level: the Intelligent Controller, followed by the other two: the Gait Planner and the Motors' Driver. The two communication buses: the Trajectory parameters bus and the Steps parameters bus enable communication between the three levels of the controller. Figure 91 shows the closed-loop control system architecture of the robot integrating the three levels of control and the two communication buses.

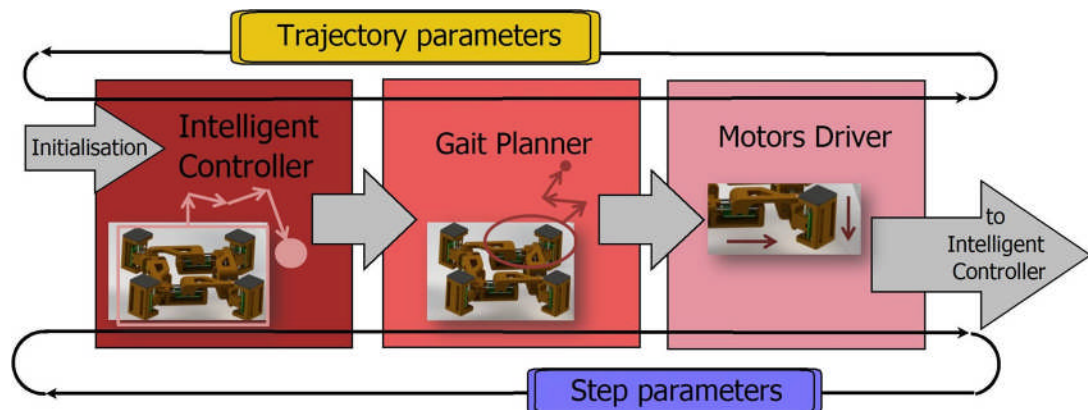


**Figure 91. Closed-loop control system architecture of the robot.**

The first level of the closed-loop controller is the Intelligent Controller. The Intelligent Controller supervises the entire locomotion mechanism, integrating all the tasks the robot carries out. The Intelligent Controller decides what the robot needs to do and how to do it. The algorithm of the Intelligent Controller can include advanced control tasks such as trajectory planning and stability calculations. Considering the information received from

the sensors of the robot, the Intelligent Controller plans how the robot is going to carry out a specific task and sends this plan to the second level.

The second level of the closed-loop controller is the Gait Planner. The Gait Planner translates the plan of the Intelligent Controller into specific actions for the motors and sends the information of these actions to the third level.

The third level of the closed-loop controller is the Motors' Driver. The Motors' Driver commands the drivers of the motors, talking directly to the motors and setting their parameters of operation. In this way, the Motors Driver sets the position reference to the PID controller of the motors. The Motors Driver also includes any reactive actions of the controller aimed at improving the performance of the motors, for instance, modifying the acceleration settings when a motor stalls.

Usually, the task of the robot is to move to a specific location. In that case, the Intelligent Controller decides how the robot moves to the new location: following a straight line or taking an alternative route if there are any obstacles in the way. Then, the Gait Planner commands the pads to follow a specific path: depending on where the robot has to move, this path can be in any direction of the horizontal plane. For the pads to reach the new position, the Motors' Driver sets the position reference of the motors.

The architecture of the controller reflects the hardware design of the locomotion mechanism. In the locomotion mechanism of the robot, motion of the robot is obtained coordinating the motion of the eight prismatic joints of the robot. In the control system architecture, the Intelligent Controller controls the motion of the whole robot. In the locomotion mechanism of the robot, one pad is moved at a time. In the control system architecture, the Gait Planner controls the pad moving at any one time. In the locomotion mechanism of the robot, one vertical motor and two horizontal motors move the pad. In the control system architecture, the Motors' Driver controls the motion of the motors connected to the pad.

The Trajectory parameters bus is set by the Intelligent Controller and is made up of the steps the robot has to follow to complete a specific task. The Gait Planner reads the steps in the Trajectory parameters bus and divides these steps into actions to be followed by the Motors' Driver. For example, if the Intelligent Controller decides that the robot needs to move in order to avoid a fall, the Intelligent Controller uploads this motion command to the Trajectory parameters bus. The Gait Planner receives the command through the Trajectory parameters bus and breaks it into a series of actions

specifying what pad needs to move where and when. These actions are uploaded to the Step parameters bus and sent to the Motors' Controller. The Motors' Controller sets the position reference and the motion parameters for each motor. Once the motor commanded by the Motors' Controller reaches the reference position, the Motors' Controller moves on to the next action in the Step parameters bus. When the last action in the Step parameters bus finishes, the Gait Planner uploads the next step to the Step Parameters bus. When the last step in the Trajectory parameters bus finishes, the Intelligent Controller uploads the next trajectory to the Trajectory Parameters bus and the process starts over.

Figure 92 shows the data flow in the controller's algorithm. The data flow starts with the information received from the sensors and passes through the three control levels until it reaches the actuators, using the communication buses. In Figure 92, some of the tasks of each control level are indicated as an example.

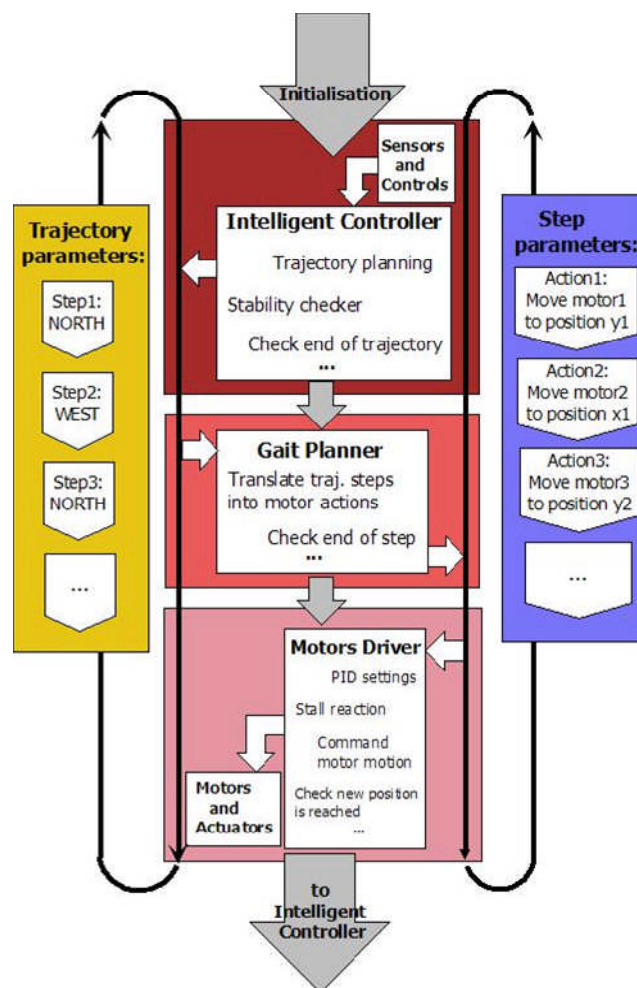


Figure 92. Data flow and communication between the three levels of the closed-loop controller of the robot.

The flow of information passing through the algorithm of the controller allows for changes in the settings of the robot when required for stability or safety reasons. The algorithm of the controller should detect priority actions, focusing on specific information and blocking the parts of the algorithm which are not required to carry out the priority actions. For instance, if the algorithm detects that the robot is going to fall, the controller can temporarily ignore the locomotion sequence and concentrate on preloading the pads in order to recover adhesion. On the other hand, the controller can focus on improving the performance of the locomotion sequence if the algorithm of the controller predicts a stable situation. For example, if the robot is following a familiar path the controller can focus on improving the speed of the robot.

### **5.5.3 Implementation of the closed-loop controller of the robot**

The closed-loop controller of the robot following the previous system architecture was implemented in LabVIEW 2009. The algorithm of the controller in LabVIEW is a state machine with one case for each level of the controller and two arrays passing information through the levels of the controller.

The algorithm of the controller programmed in LabVIEW starts by calibrating the motors and setting the parameters of the sensors and motors. Then, the algorithm executes the state machine starting with the highest level, the Intelligent Controller, and restarting the cycle when the lowest level, the Motors' Driver, is executed. The three levels of the controller are executed sequentially and the priority of control actions within the levels is set depending on the inputs received from the sensors and the user interface. The controller runs idly through the three levels of control if no action is required from the robot.

The communication buses between the levels of the controller are implemented in LabVIEW through two arrays of clusters. When the robot has to move to a new location, the array of the Trajectory parameters bus contains information about the direction of motion of the robot and the number of steps in the trajectory. The array of the Step parameters bus specifies which motor needs to move and the direction of motion of the motor.

The closed-loop controller of the robot runs on a PC and communicates with the controller board of the motors and sensors (MC-3300-RV by New Scale Technologies Inc.) via a USB interface. Thus, there are two control loops

integrated in the system: the closed-loop controller running on the PC and the PID control of the motors running on the mother board of the motors and sensors. Communication between these two control loops takes place at the Motors' Driver level of the closed-loop controller of the robot. At the Motors' Driver level, the position reference of the motors is set and the status of the motors and encoders is read from the mother board. In order for the control algorithm to talk to the mother board, the controller uses a library of ActiveX functions supplied by the manufacturers of the motor.

Figure 93 shows a sketch of the two control loops in the closed-loop controller of the robot and the way they communicate at the Motors' Driver level.

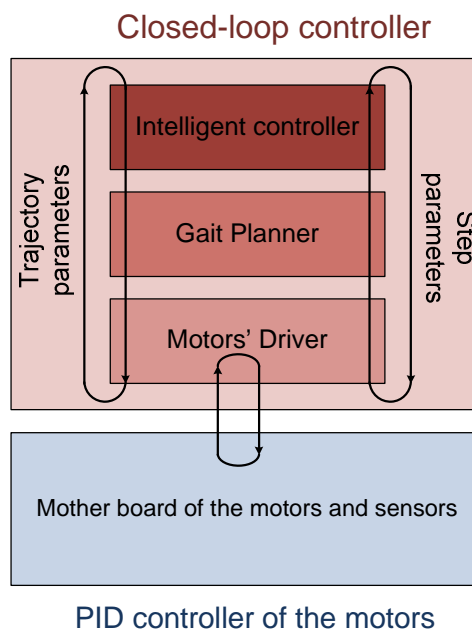


**Figure 93. The two control loops of the closed-loop controller of the robot implemented in LabVIEW.**

The user interface of the LabVIEW programme has four buttons to set the direction of motion of the robot. The user interface offers the option of a short step which is a single step of the robot of approximately 6mm, or a long step which is three consecutive single steps. Figure 94 shows the user interface of the controller including direction buttons, the length of step button and a console showing messages about the status of the robot.

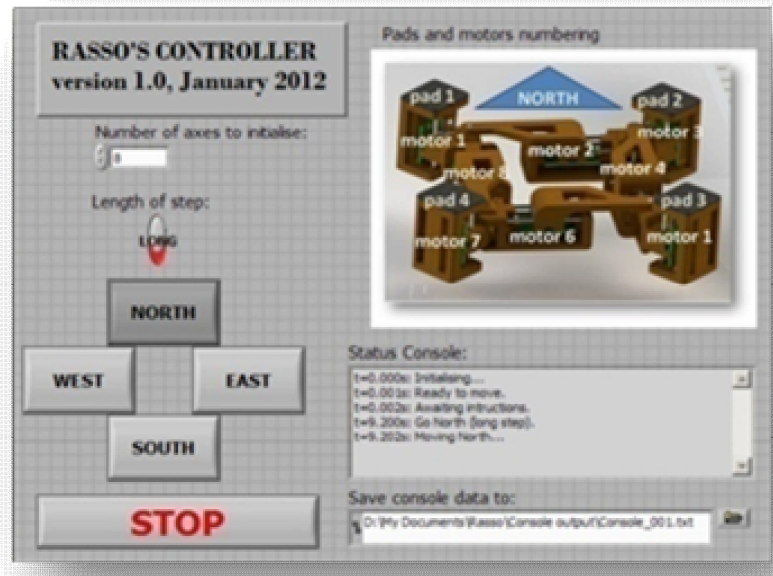
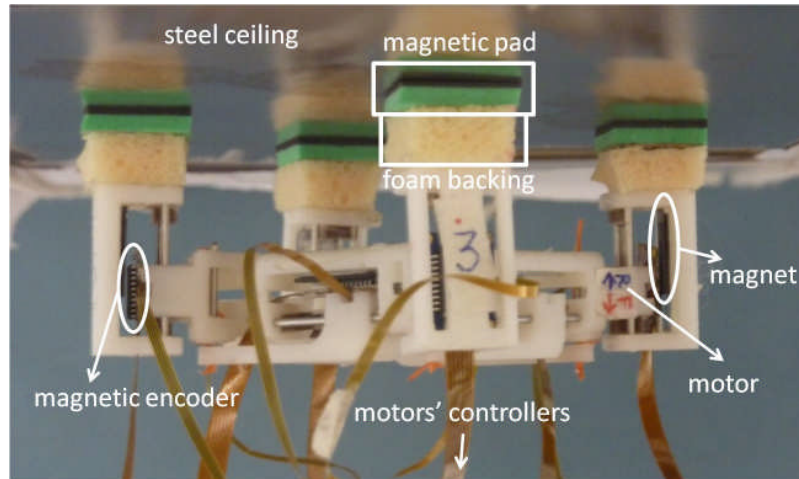


Figure 94. User interface of the closed-loop controller of the robot programmed in LabVIEW 2009.

#### 5.5.4 Walking performance of the robot following a closed-loop locomotion sequence

The walking performance of the robot with the closed-loop controller was tested using the position sensors in order to detect when the motor reached the desired position within the locomotion sequence. The position sensors also enable to detect when the motor stalls so that some action can be performed on the stalled motor to help it overcome friction and move again. When the controller detects that the motor is stalled, it increases the speed and acceleration settings of the motor or increases the proportional constant of the PID control.

The robot was preliminary tested for 19 steps using magnetic pads on a steel surface. The robot was able to complete 4 steps successfully (21%), needed gentle prodding to complete 10 steps (53%) and fell down for 5 (26%) of these preliminary steps. After this, the robot was tested again using magnetic pads on a steel surface, walking in a straight line for 60 consecutive steps. These 60 steps cover a distance of 30 cm which is approximately the cross section of the abdomen and three times the length of the operating area on the abdominal wall. The robot was able to complete 95% of the steps successfully, the unsuccessful steps took place mainly over the first eight steps while the mechanism was adjusting to the motion of the motor inside the prismatic joint. Figure 95 shows the prototype of the robot and the steel surface, indicating the components of the locomotion mechanism.



**Figure 95. Prototype of the robot tested with the closed-loop controller using magnetic pads on a steel surface.**

Videos of the robot taking several steps using the closed-loop controller during the preliminary test can be seen in [159] and [160]. In the first video (see [159]), the robot takes one step successfully and falls when attempting to take a second step. During the first step, the front pad (marked number 3 in Figure 95) does not re-attach to the surface when the motor reaches the end of its motion range. However, the pad re-attaches when lifted by the motion of the next pad in the sequence, preventing the robot from falling. The pad cannot re-attach because of the loose fit between the guiding rods and the mounting platform and the loose fit at the rotary joints. The loose fit at the guiding rods and rotary joints is due to the lack of precision of the 3D printer used to manufacture the prototype and is also due to the manual assembly process. This loose fit makes part of the mechanism come down under its own weight when the pad detaches. This increases the distance between the pad and the surface and thus prevents the pad from re-attaching when the motor moves it back to the surface.

This issue of the loose fit in the mechanism preventing the pad from re-attaching can be also observed in the second video (see [160]). Another issue can be seen in this second video: on the second step of the robot, the motor at the back stalls and the closed-loop controller is unable to make it move again. A gentle prod is required to overcome the static friction in the prismatic joint and resume motion of the motor, completing the step of the robot.

The timing of the three levels of the controller was also checked during this test. Figure 96 shows the timing of the three levels of the controller during the walking experiment from the moment the robot is commanded to walk until it completes one step. Figure 96 shows the average and standard

deviation of the time the controller spent in each of the three levels during the sixty steps of the test.

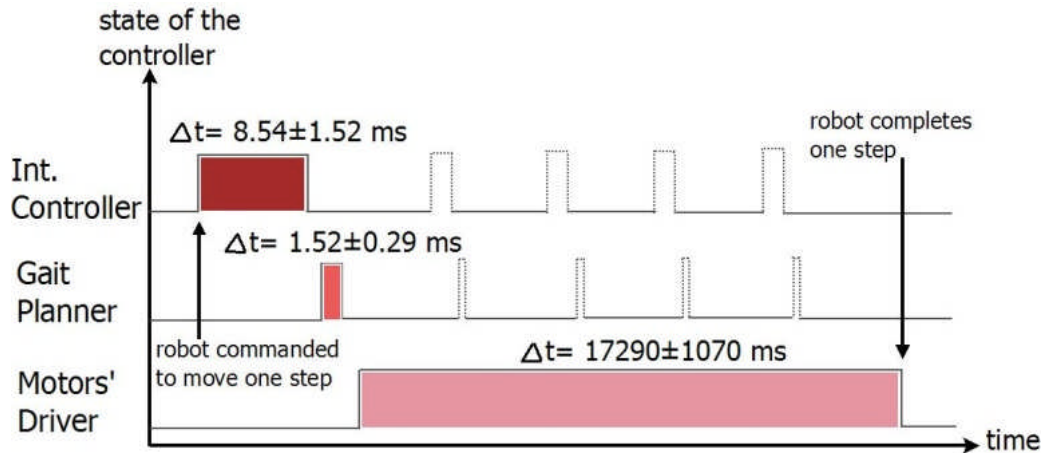


**Figure 96. Timing of the three levels of the locomotion controller.**

In Figure 96, the time spent in the Intelligent Controller includes the time spent in order to upload the trajectory parameters. In Figure 96, the time spent in the Gait Planner includes the time spent translating the trajectory parameters into motor actions.

Once the robot is commanded to move, the Intelligent Controller takes 8.5 ms in order to upload the trajectory parameters and send them to the Gait Planner. The Gait Planner then spends 1.5 ms in order to translate the trajectory parameters into motor actions, upload these actions to the Step parameters bus and send them to the Motors' Driver. When the information in the Step parameters bus reaches the Motors' Driver, the Motors' Driver requires 17 s to complete one step of the robot.

The Intelligent Controller requires communication with the user interface and this takes up most of the time spent in this level of the controller. The Gait Planner takes approximately the minimum cycle time in a PC because its only task is to convert the trajectory parameters from the Intelligent Controller into motor actions for the Motors' Driver. The Motors' Driver takes nearly all the time needed to move the robot because communication with the mother board of the motors and encoders takes place at this level.

During the time the Motors' Driver takes to complete one step, the Intelligent Controller and Gait Planner are executed as shown in Figure 96. For this test, once the robot is commanded to move there are no new control inputs for the Intelligent Controller and therefore no new actions for the Gait Planner to set for the Motors' Driver. Thus the execution of the Intelligent Controller and the Gait Planner takes much shorter while the Motors' Driver is completing the step and is not considered in the time calculations of

Figure 96. The controller runs through the Intelligent Controller and Gait Planner while the Motors' Driver is completing the step, enabling modifications on the control parameters if and whenever required. Closed-loop positioning of the motors is not interrupted during this time because the motors are directly controlled by the drivers of the mother board.

### **5.5.5 Future improvements to the closed-loop controller**

In order to fully realise the potential of the closed-loop system architecture and further enhance the walking performance of the robot, the two major improvements for the closed-loop controller are:

- customised communication with the mother board and drivers of the motors in order to enable direct control of the motors, also improving the sampling of the encoders, and
- sensors to detect important events in the locomotion sequence like pad detachment or re-attachment.

For the current version of the motors and encoders, communication with the mother board is only possible via a USB connection through a series of pre-programmed functions that command the micro-controller of the board. The time delay between the moment a command is sent to the mother board and the moment the response is received through the USB connection is typically 200 ms. In order to control the position of the motor, the controller needs to:

- query the position to the mother board, which takes 200 ms,
- wait until the reading of the position is received from the mother board, which takes 200 ms,
- calculate the control action depending on the position reading received, and
- send the control action to the mother board, which takes 200 ms.

Therefore, more than 600 ms are required in order to communicate a control action from the controller of the robot to the mother board. This communication system is too slow to register and control an event in the locomotion sequence like the detachment of the pad which takes around 200 ms.

Position sensors in the robot can detect when the motor stalls and trigger strategies like increasing acceleration, changing direction momentarily or moving the other motors in order to release the stalled motor. The controller can detect the end of the motion range of the motors with the position sensors and implement a soft stop. With a position sensor, the range of motion along which the motor does not stall can be found, preventing the motor from getting into a position where it is likely to stall during locomotion.

Force sensors can detect contact and detachment between the pad and the surface and can also measure the preload applied by the prismatic joints on the pad. Force sensors can also detect irregularities on the surface of the tissue and can determine the zone of the tissue where adhesion is higher. Unlike DC motors where the force from the motor can be inferred from the current of the windings, in order to measure the force of the piezo-electric motor an external force sensor is required.

Integration of force sensors within the locomotion mechanism was investigated but no suitable force sensor was found in the market. The requirements of the force sensor for the locomotion mechanism of the robot are:

- very compact size in order to integrate it in the locomotion mechanism without increasing the size of the robot significantly,
- lightweight, so that it does not overload the adhesive pads,
- able to detect a change of force of a few millinewtons in tension and compression.

The force sensor integrated in the locomotion mechanism should occupy a maximum volume of 10 mm x 10 mm x 5 mm and weight less than 2 grammes per unit. Each of the four pads of the robot should use an individual force sensor.

The force sensing technologies reviewed for the locomotion mechanism of the robot are:

- piezo-electric force sensors,
- pressure sensitive films,
- capacitive sensors,
- pressure sensitive polymers,
- strain gauges,
- quantum channelling composites (QTC) and
- force sensitive resistors (FSR).

Piezoelectric force sensors are very accurate and can be very compact but for the size required for the locomotion mechanism of the robot they would have to be custom-made for a very high cost.

Pressure sensitive films are found in force sensing plates for bio-mechanic measurements of a much bigger size than the robot. The pressure sensitive film alone is not commercially available and in order to use it for the robot bespoke electronics and calibration are required.

Capacitive sensors, like Flexiforce<sup>®</sup> sensors, are compact and low cost but cannot measure force continuously within the required range: 1-150 mN.

Pressure sensitive polymers, commercially known as Polypower<sup>®</sup>, can be made to the specifications of force and size required for the robot but the cost is very high for the low volume required.

Strain gauges are widely available, relatively low cost and very accurate for low ranges of force. Strain gauges can be found commercially in load cells and are also sold on their own. Integration of strain gauges in the robot would involve the development of a conditioning circuit specific to the application. This is especially challenging because the strain gauges would have to be mounted on a deformable surface like plastic. Using strain gauges on plastic requires careful mounting of the sensing surface and filtering of the noise obtained in the signal because of the deformable surface. In fact, the manufacturers of strain gauges recommend against using strain gauges on plastic due to their difficult integration.

Quantum channelling composites (Peratech's QTC pills) are very compact, light and affordable but the manufacturers have stopped selling them individually. A custom made sensor could be ordered from the manufacturers but the price is beyond the budget of the project.

Force sensitive resistors (FSR) are compact, lightweight and inexpensive but not sensitive enough within the desired range of force: 1-150 mN. These sensors were tested and the activation force required for FSR sensors is greater than the maximum force applied by the motor.

Table 11 summarises the features of the force sensing technologies reviewed for the locomotion mechanism of the robot.

The use of accelerometers can be considered instead of force sensors, detecting the attachment and detachment of the pad through the change of acceleration caused on the pad. Inclinometers can be also useful in order to measure the inclination of the pads with respect to the horizontal, inferring how close the pads are to peeling off.

**Table 11. Suitability of force sensing technologies for the locomotion mechanism of the robot.**

	Compact	Lightweight	Precision	Resolution	Easy to integrate	Low cost
Piezo-electric	✓	✓	✓	✓	✓	✗
Pressure sensitive films	✓	✓	✓	✓	✗	✗
Capacitive	✓	✓	✗	✗	✓	✓
Pressure sensitive polymers	✓	✓	✓	✓	✓	✗
Strain gauges	✓	✓	✓	✓	✗	✓
QTC	✓	✓	-	-	✗	✗
FSR	✓	✓	✗	✗	✓	✓

## 5.6 Second prototype of the robot

The second prototype of the robot was rapid-prototyped in a stronger material: Duraform<sup>®</sup> Nylon 6, in order to make the locomotion mechanism more robust and facilitate its assembly. A more precise rapid prototyping technique was employed: Selective Laser Sintering with a Vanguard HS plus HiQ machine from 3D Systems. Figure 97 shows a picture of the second prototype, held by a hand for scale.

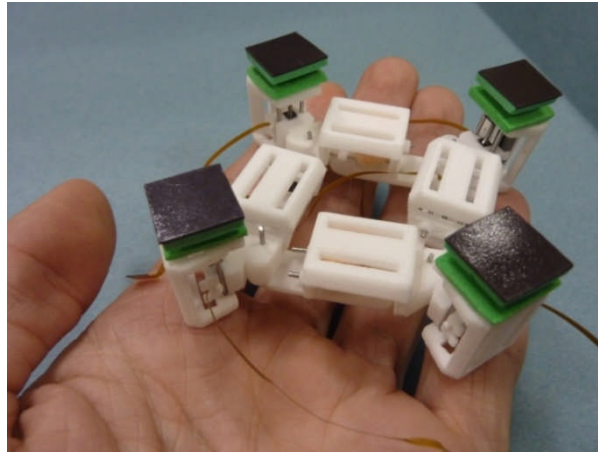


**Figure 97. Second prototype of the robot in Nylon 6, rapid-prototyped with an SLS machine.**

The dimensions of the prototype are 6.5 cm x 6.5 cm x 3 cm (L x W x H) when the horizontal prismatic joints are fully contracted and 7.1 cm x 7.1 cm x 3 cm when the horizontal prismatic joints are fully extended. The mass of the second prototype including motors and encoders is approximately 25 grammes. These dimensions are bigger than the previous prototype because thicker walls of the material used in this rapid prototyping machine are required in order to have a strong enough prototype.

The purpose of building this prototype was to improve the performance of the open-loop sequence given that closed-loop locomotion could not be explored further given the lack of suitable force sensors for the robot. Thus, the position sensors were removed from this prototype, focusing on improving the performance of the motor within the mechanism. In this way, the design of the components of the locomotion mechanism was enhanced in order to improve the open-loop walking performance of the robot and make it suitable for motion on the surface of tissue.

### **5.6.1 Enhancements to the components of the second prototype**

In order to make the mechanism more robust and improve the performance of the motor within the mechanism, the following features were included in the design of the components for the second prototype:

- slots on one side of the ends supporter in order to improve the alignment of the guiding rods,
- open holes in the mounting platform in order to reduce interference between the guiding rods and the mounting platform, and
- a soft backing layer with the same thickness for all the pads in order to keep all the pads at the same height.

On one side of the ends supporter, a slot can be used instead of a hole in order to enable self-alignment of the guiding rods during the assembly and motion of the prismatic joint. By turning the holes on one side of the ends supporter into slots, the guiding rods can align themselves with the screw of the motor when the motor is moving. These slots in the ends supporter decrease interference due to misalignments between the guiding rods but increase the play of the guiding rods within the holes of the ends supporter. Figure 98 shows the slots on one side of the ends supporter, the holes on the other side of the ends supporter can also be appreciated in the figure.

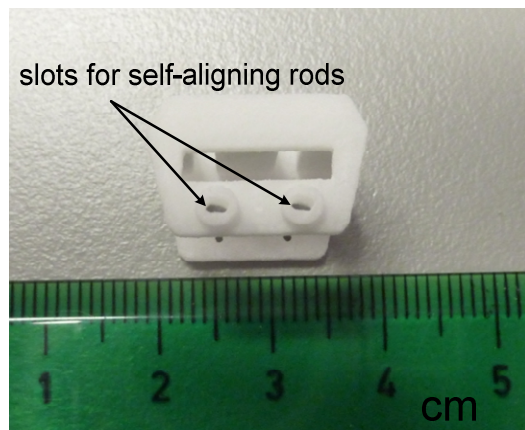


**Figure 98. Slots on one side of the ends supporter to enable self-alignment of the guiding rods.**

The holes in the mounting platform can be opened to the outside edge of the mounting platform in order to reduce the interference between the guiding rods and the mounting platform. This interference is diminished because the contact area between the guiding rods and the holes is smaller and also because with open holes the guiding rods can align themselves with each other more easily. Figure 99a shows the open holes in the mounting platform, Figure 99b shows the mounting platform integrated in the horizontal prismatic joint and Figure 99c shows the mounting platform integrated in the vertical prismatic joint.

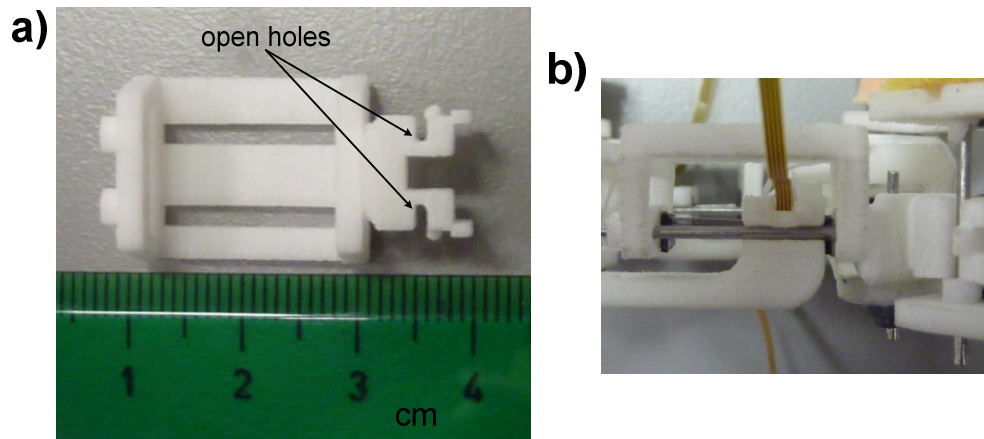


**Figure 99. (a) Open holes in the mounting platform and (b) mounting platform with open holes in a horizontal prismatic joint.**

The same thickness of the soft backing layer for all the pads ensures that there is no difference in height between the pads when in contact with the tissue. If the height of the pads is different when the pads are in contact with the tissue, the pads can twist causing the adhesive surface to come off unexpectedly.

In the first prototype, the soft backing layer of the pad was cut manually from a memory foam billet and this did not guarantee the same thickness for all the pads. In the second prototype, the soft backing layer for the pads are made stacking layers cut from a foam sheet, making sure that all the pads are the same thickness. Figure 100a shows the magnetic pad with the soft backing layer of memory foam and Figure 100b shows the magnetic pad with a soft backing layer made up of three layers of foam.

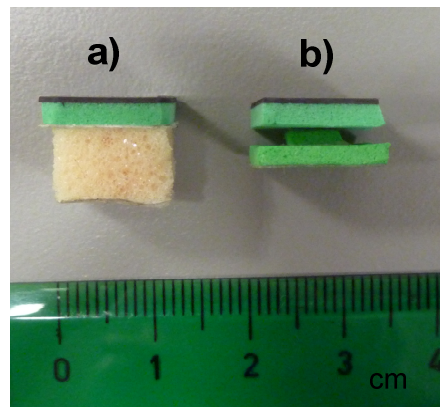


**Figure 100. (a) Soft backing layer of the pad using memory foam and (b) soft backing layer of the pad using three stacked layers of foam.**

For the pad with three layers of foam shown in Figure 100b, the compliance of the pad is determined by the area of the layer in the middle.

### 5.6.2 Walking performance of the second prototype

The second prototype of the robot was tested walking with magnetic pads on a steel surface. The magnetic pads were 1 cm<sup>2</sup> using the soft backing layer of three stacked layers of foam shown previously in Figure 100b. Each magnetic pad provides an attachment force of 120 mN approximately. In order to test the walking performance of the robot with magnetic pads, the robot followed an open-loop locomotion sequence. The time spent for each motion of the motors was recorded together with the number of times the robot fell down and the number of times the locomotion mechanism required assistance to complete a motion. Figure 101 shows the robot moving one pad on a steel surface:

- a) initial position of the robot with all the pads attached to the steel surface (see Figure 101a),
- b) the front pad of the robot is detached and moved across the steel surface to the new position (see Figure 101b),
- c) the front pad is at the new position (see Figure 101c), and
- d) the front pad is re-attached to the steel surface at the new position (see Figure 101d).

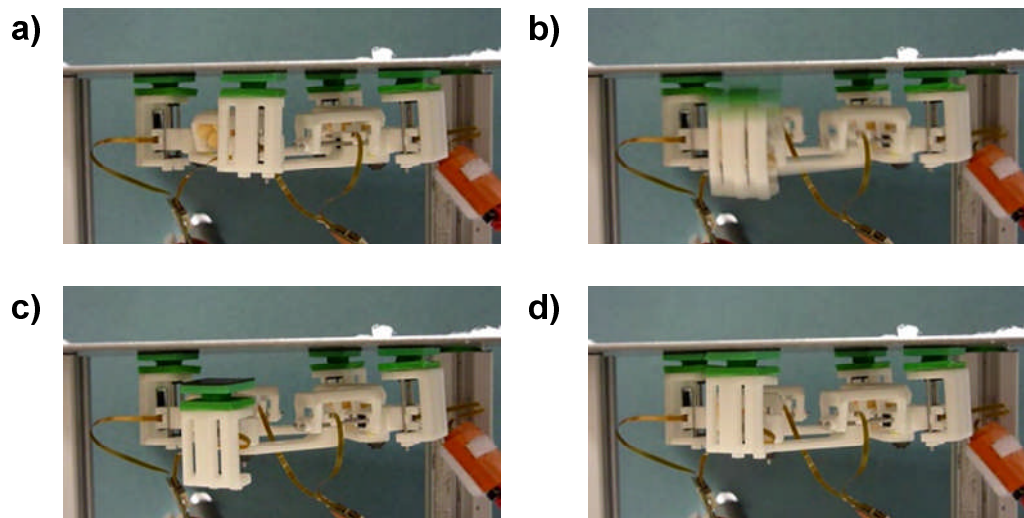


**Figure 101. (a-d) Second prototype of the robot detaching, moving and re-attaching one magnetic pad on a steel surface.**

The second prototype of the robot moving with magnetic pads on a steel surface and the issues experienced with the locomotion mechanism can be seen in the video in [161].

The second prototype of the robot was also tested walking with the bio-mimetic adhesive pads on the surface of porcine peritoneum. Porcine peritoneum was used instead of rat peritoneum in order to test the whole robot because it is more easily available and a bigger sample size can be obtained. The adhesive pads were 1 cm<sup>2</sup> using the soft backing layer of

three stacked layers of foam. The robot followed an open-loop locomotion sequence, recording the time spent for each motion of the motor, how often the robot fell and how often the robot required assistance to complete a motion. Figure 102 shows the prototype of the robot hanging from pig peritoneum during the walking test with the adhesive pads. In Figure 102, one of the pads of the robot is detached so the weight of the robot is supported by the other three adhesive pads.

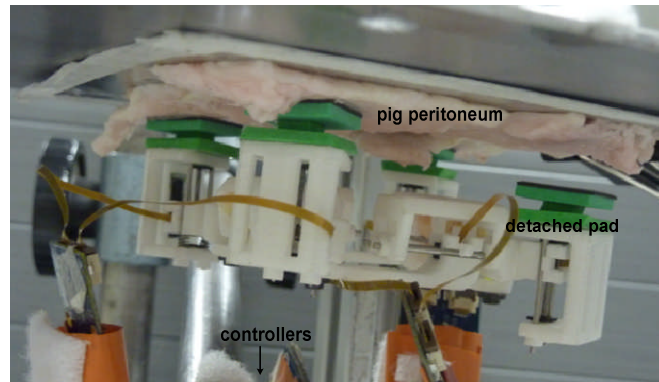


**Figure 102. The second prototype of the robot hanging from pig peritoneum using the bio-mimetic adhesive pads. The tissue sample was glued to a steel plate and the adhesive pads were mounted on top of the magnetic pads. The pads were tested in order to check that the magnetic force had no effect through the peritoneum sample.**

Table 12 summarises and compares the parameters of the walking performance of the robot moving with magnetic pads on a steel surface and moving with the adhesive pads on pig peritoneum. The parameters of the walking performance shown in Table 12 are:

- the average speed of the robot,
- the time the robot takes in order to cross the 10cm-long operating area on the abdominal wall,
- percentage of steps the robot could not complete because it fell down, and
- percentage of motions the robot could not complete because the motors failed to move the pads.

**Table 12. Comparison of the walking performance of the robot using magnetic pads on a steel surface and using adhesive pads on pig peritoneum.**

Type of Pad	Support surface	Number of steps	Average speed (mm/s)	Time to cross 10 cm (min)	Falls (% steps)	Mechanism failures (% motions)
Magnetic	Steel	30	0.24	7	17	32
Adhesive	Peritoneum	20	0.11	15.7	40	45

When the robot is walking on tissue, the adhesive pads need a preload to attach. Without force sensors, the robot cannot ensure that a preload has been applied to the pads and thus, the robot cannot ensure attachment of the pads to the tissue. This causes the robot walking with adhesive pads to fall down more often than with magnetic pads.

The mechanism failures shown in Table 12 include the number of times the motor stalls within the locomotion mechanism or is unable to bring the pad back to the surface of the tissue. These failures are caused by the imprecision of the mechanical fit of the components of the robot and the friction of the prismatic joints.

Using commercially available sleeve bearings in order to reduce the friction between the guiding rods and the mounting platform was considered. However, in order to use sleeve bearings effectively within the locomotion mechanism an assembly technique more accurate than manual assembly should be employed and this was not available to the project. Mounting the guiding rods on a couple of self-aligning bearings in order to correct the misalignments of the guiding rods was also considered. However, in order to integrate commercially available self-aligning bearings in the robot, the dimensions of the robot have to increase significantly.

### **5.6.3 Issues of the second prototype**

The Squiggle<sup>®</sup> motor used for the locomotion mechanism stalls and moves intermittently if:

- there is friction between the tip of the screw of the motor and the load pushed by the motor, preventing the screw from rotating,
- there is side load applied to the screw of the motor preventing the nut to engage with the screw,
- there is friction in the prismatic joint moved by the motor, diminishing the maximum load the motor can move.

These three causes of intermittent operation are present in the locomotion mechanism because the components of the mechanism require thorough manual adjustment due to the poor finishing obtained with rapid-prototyping. Rapid-prototyping and manual assembly of the locomotion mechanism were the only manufacturing and assembly techniques for miniature components available to the budget of the project.

The contact between the tip of the screw and the ends supporter was made low friction by covering the ends supporter with a low friction material.

The friction in the prismatic joint and the side-loading of the screw are due to the imprecision of the fit between the guiding rods and the mounting platform and the friction between the two materials. During assembly, the holes of the mounting platform are filed in order to reduce the friction of the prismatic joint. However, this loosens the fit between the guiding rods and the mounting platform, enabling sideways motion of the guiding rods inside the holes. Sideways motion of the guiding rods inside the holes of the mounting platform causes the 90° angle between the guiding rods and the ends supporter to change, thus side-loading the screw. A balance between reducing the friction of the prismatic joint by loosening the fit and reducing sideways motion of the rods by tightening the fit is difficult to achieve with manual adjustment.

A loose fit around the guiding rods also causes the mechanism to flop down when the one of the pads is detached, preventing the pad from re-attaching. The mechanism also flops down because of the loose fit at the passive rotary joints of the quadrilateral formed by the horizontal prismatic joints; this fit is also manually adjusted and assembled. When this happens, one way to re-attach the pad is to move the vertical prismatic joints of the supporting pads, lifting the quadrilateral formed by the horizontal prismatic joints and thus lifting the detached pad. However, considering the previous issues with the performance of the motors within the locomotion mechanism, it is difficult to make the motors move all at the same rate without causing detachment of the pads.

#### **5.6.4 Further improvements to the second prototype**

In order to further improve the open-loop walking performance of the robot, the following improvements were designed for the hardware of the robot:

- brackets on the adhesive pads in order to support the pads better during detachment,

- curvature at the surface of the ends supporter touching the tip of the screw in order to keep the angle between the screw and the ends supporter as close to  $90^\circ$  as possible,
- slotted holes in the mounting platform of the vertical prismatic joint in order to reduce interference with the guiding rods during detachment of the pad,
- ends supporter separated into two pieces in order to improve the alignment of the guiding rods during assembly,
- extra support at the passive rotary joints of the quadrilateral formed by the horizontal prismatic joints of the locomotion mechanism, and
- memory foam soft backing layer for the pads.

The brackets on the adhesive pads reduce the twist that the weight of the detached pad causes on the supporting pads. Figure 103a shows a side view of the four brackets fitted around the edges of the adhesive pad and Figure 103b shows a top view of the brackets.

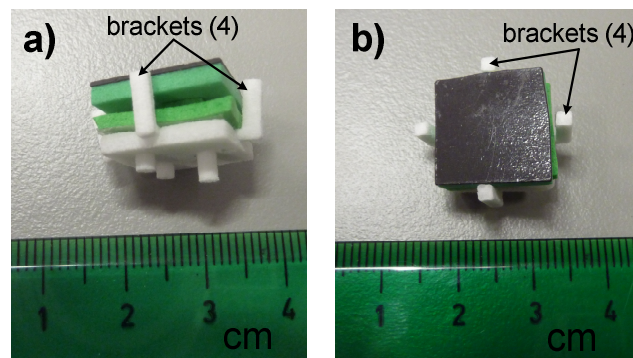


**Figure 103. (a) Side view of the brackets for extra support of the pads and (b) top view of the brackets.**

The brackets make contact with the support surface, supporting the pad and reducing the twist cause on the supporting pads by the detaching pad. However, the brackets interfered with the motion of the pads when tested in the prototype and therefore were not included in the prototype.

A dent with a slight curvature at the surface of the ends supporter touching the tip of the screw ensures a  $90^\circ$  angle between the tip of the screw and the ends supporter at all times. The tip of the screw follows the curvature on the surface of the ends supporter when the guiding rods move sideways inside the holes of the mounting platform, keeping the screw perpendicular to the ends supporter. However, the curvature of this dent on the ends supporter was too subtle for the rapid prototyping machine to print it and therefore, this feature was not included in the prototype.

The holes in the mounting platform of the vertical prismatic joint are slotted in the direction of the twist caused by the motor on the pad. These slots reduce the interference between the holes in the mounting platform and the

guiding rods when the motor is pulling the pad in order to detach it. Figure 104 shows the slotted holes in the mounting platform of the vertical prismatic joint.

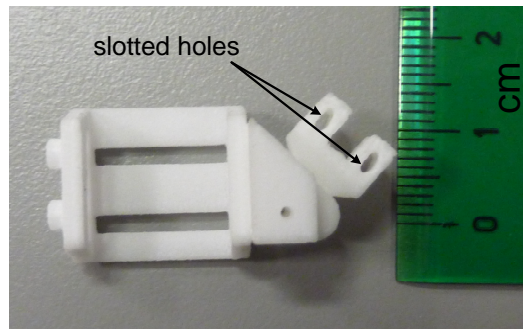


**Figure 104. The slotted holes in the mounting platform.**

These slotted holes were tested in the locomotion mechanism, resulting in easier detachment of the pad by the motor. However, the play between the slotted holes and the guiding rods causes motion of the ends supporter with respect to the mounting platform when the pad detaches, hindering the motion of the pad. Therefore, the slotted holes were not included in the prototype.

The ends supporter was printed as two separate pieces in order to improve the alignment of the guiding rods during assembly. During the assembly of the mechanism, the two pieces are joined with the two guiding rods of the prismatic joint and a third rod in order to make the assembly strong. Figure 105 shows the separate parts of the ends supporter, featuring slotted holes for two of the three rods joining the two parts of the ends supporter.

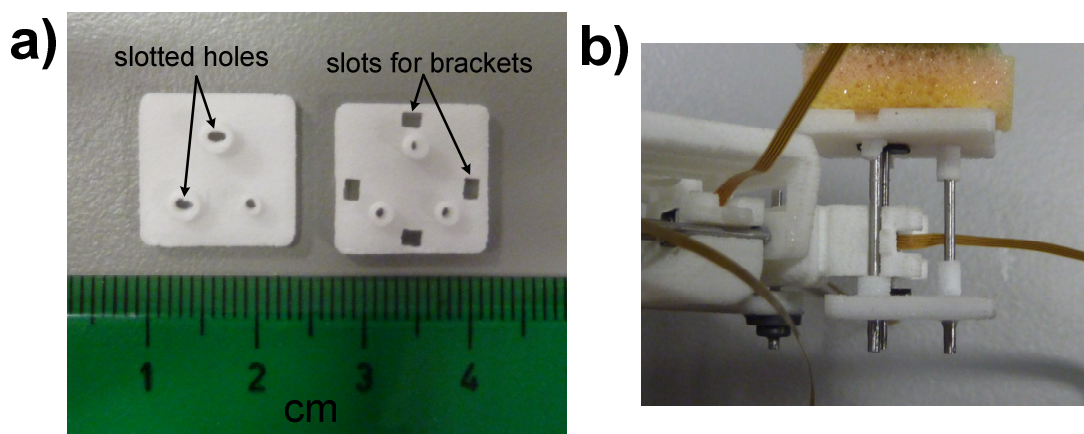


**Figure 105. (a) The two separate parts of the ends supporter, and (b) ends supporter with two separate parts in a vertical prismatic joint.**

For previous versions of the ends supporter, the ends supporter was manufactured as one piece to obtain more accurate positioning of the holes

in a CNC machine. When the manufacturing technique changed to rapid-prototyping, the ends supporter was left as one piece in order to integrate the magnet of the position sensor. This prototype of the robot runs on an open-loop locomotion sequence and does not require the position sensor, so the ends supporter can be split to facilitate the alignment of the rods with respect to the mounting platform.

In order to make sure that the rods are as precisely aligned as possible, two of the three holes in the ends supporter are slotted as shown in Figure 105. The non-slotted hole is used as a reference to join the two parts and mount them on one hole of the mounting platform. Then, the other two rods are mounted, fixed at one end and free to move at the slotted end. A position of the rods with little interference with the mounting platform is found by moving the motor within the assembly and checking for friction along the motion range of the motor. Once a position of low friction is found, the rods are fixed at the slotted end. This way of assembling the ends supporter was found helpful to improve the motion of the motors within the prismatic joint and thus was included in the prototype for the vertical prismatic joints.

Extra material was added along the passive rotary joints of the quadrilateral formed by the horizontal prismatic joints. This extra material provides support to the mechanism when the pad is detached, preventing the mechanism to flop down under the weight of the detached pad. This improvement was proved to be beneficial for the performance of the robot and therefore included in the prototype.

Memory foam pads were cut using a hot wire in order to obtain a more uniform thickness. With uniform thickness the memory foam pads proved to improve the performance of the robot over the pads with three stacked layers of foam. This improvement is due to the memory effect of the material which changes the stiffness of the pads when they are pulled or pressed against the surface. This change of stiffness is beneficial because it counteracts the stress caused on the pads by the imprecision of the assembly and the irregularities on the surface. Memory foam pads were therefore included in the improved second prototype of the robot.

### **5.6.5 Walking performance of the improved second prototype**

The improved second prototype was tested walking with magnetic pads on a steel surface, following an open-loop locomotion sequence and using a 5mm-thick memory foam backing layer for the pads. In this test, the robot crossed a 9cm-long steel plate with the motors consistently detaching,

moving and re-attaching the pads. The video showing this walking test can be seen in [162].

Figure 106 shows a step of the improved second prototype of the robot walking with magnetic pads on a steel surface:

- Figure 106a shows the initial position with all the pads attached to the surface,
- Figure 106b-c show the detachment of pad 1 and also the motion of pad 1 to the new position,
- Figure 106c-d show the re-attachment of pad 1 at the new position,
- Figure 106d-g show the detachment, motion and re-attachment of pad 2,
- Figure 106g-j show the detachment, motion and re-attachment of pad 3
- Figure 106j-m show the detachment, motion and re-attachment of pad 4 completing one step of the robot.

The robot was tested for 49 steps in total, taking an average of 20.8 s to complete each step at an average speed of 0.29 mm/s. More than three quarters (77%) of the steps were completed successfully including the twelve consecutive steps of Figure 106 shown in the video in [162]. The majority of the unsuccessful steps (64%) happened during the first thirteen steps; the locomotion mechanism failed to complete these steps because of the issues previously experienced with the other prototypes.

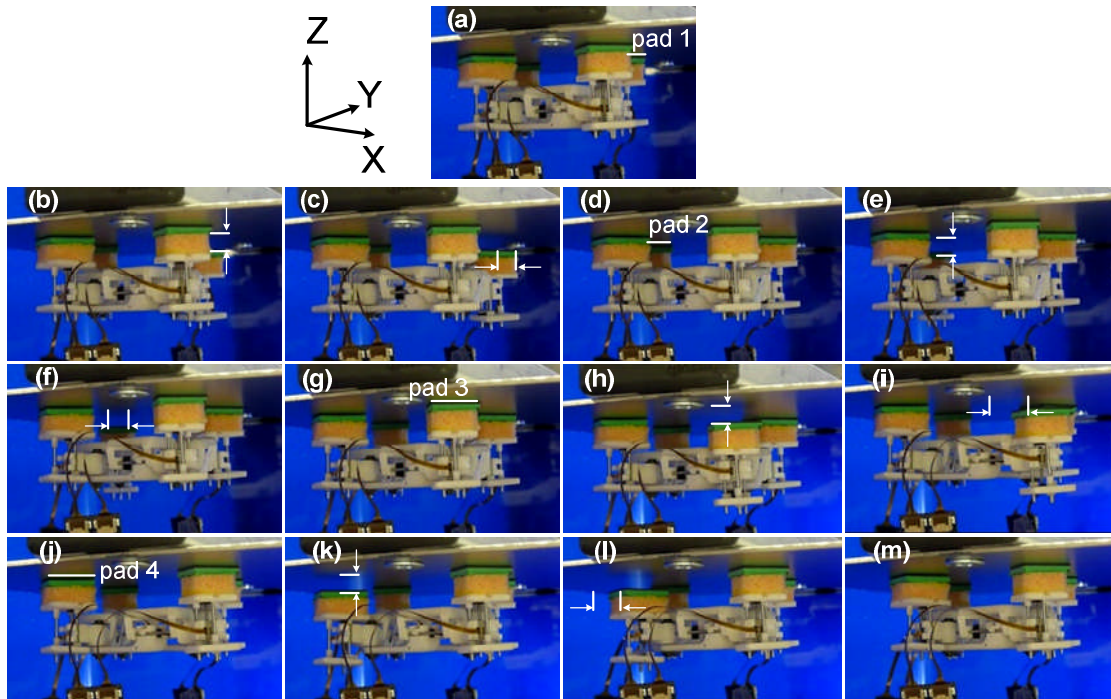


**Figure 106. (a-m) Walking sequence of the improved second prototype using magnetic pads on a steel plate.**

Table 13 summarises the parameters of the walking performance of the improved second prototype moving on a steel surface using magnetic pads. The parameters of the walking performance are: average speed, time to cross a 10cm-long operating area, falls and mechanism issues.

**Table 13. Walking performance of the improved second prototype of the robot using magnetic pads on a steel surface.**

Type of Pad	Support surface	No. of steps	Average speed (mm/s)	Time to cross 10 cm (min)	Falls (% tests)	Mechanism issues (% motions)
Magnet	Steel	49	0.29	5.7	8	14

Compared to the previous prototype, the percentage of falls is reduced to half: from 17% with the previous prototype to 8% with the improved second prototype for similar average speed of the robot. Similarly, the percentage of mechanism issues is reduced from 32% with the previous prototype to 14% with the improved second prototype.

The improved second prototype was also tested walking with the adhesive pads on the surface of fresh porcine peritoneum. The sample of peritoneum was used within the first ten minutes after being harvested. The robot followed an open-loop locomotion sequence using a 5mm-thick memory

foam backing layer for the pads. Figure 107 shows the robot detaching one adhesive pad from pig peritoneum and moving the pad to a new position:

- Figure 107a shows the initial position of the robot with the four adhesive pads attached to the sample of pig peritoneum; the mechanism and electronics of the robot are protected with plastic film,
- Figure 107b shows pad 1 detached by the vertical motor,
- Figure 107c shows pad 1 moved to the new position by the horizontal motor,
- Figure 107d shows pad 1 re-attached to the tissue sample by the vertical motor,
- Figure 107e shows pad 2 ready to detach,
- Figure 107f shows pad 2 detached by the vertical motor,
- Figure 107g shows the robot falling down.

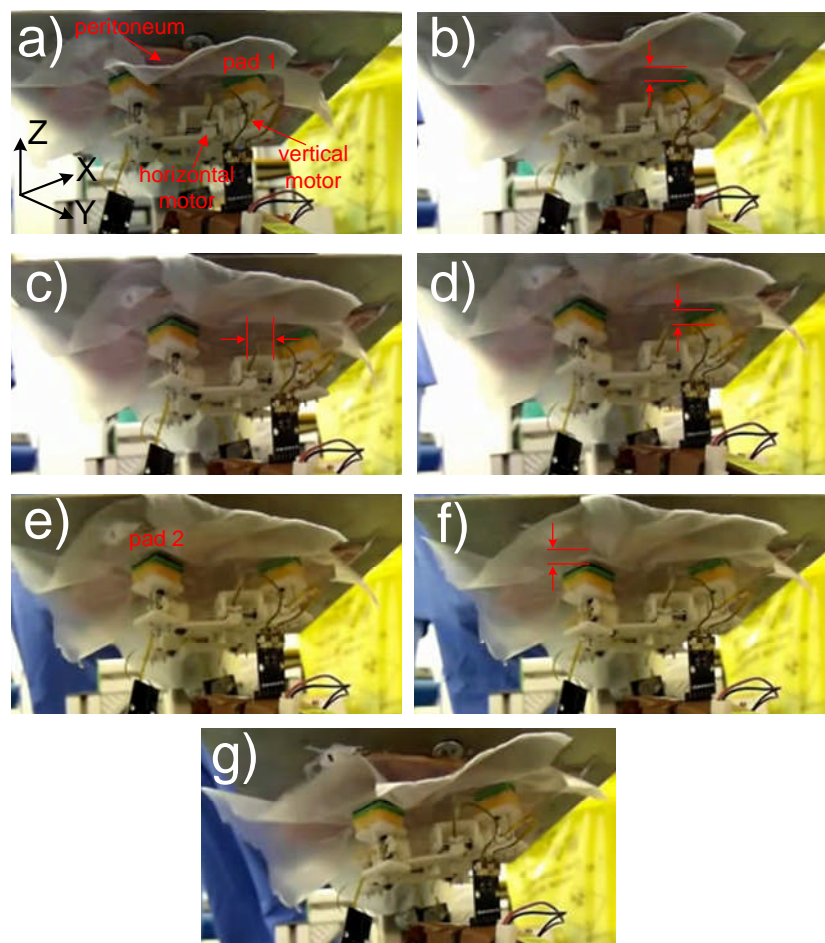


**Figure 107. (a-g) The improved second prototype of the robot detaching and moving one adhesive pad on fresh pig peritoneum.**

The video showing this walking test can be seen in [163]. In this test, the robot detached and moved the pads but could not re-attach the pads to the tissue because the robot could not detect if sufficient preload was applied to the pads. This prevented the robot from completing a successful step. In order to walk consistently on tissue, the robot requires a control system

integrating sensors able to detect contact between the adhesive pad and the tissue and the value of preload applied to the pad.

## **5.7 Bio-inspired features of the locomotion mechanism**

This section shows a series of stills illustrating the peeling-off of the pad inspired by tree frogs and geckoes, and the motion of the pad in the horizontal plane inspired by amoeboid locomotion.

Figure 108 shows the locomotion mechanism of the robot peeling off a magnetic pad from a steel surface. Initially, the pad is attached to the surface, making full contact with the surface, and the motor is ready to peel off the pad:

- Figure 108a shows the robot ready to detach the pad,
- Figure 108b shows a close-up of the vertical motor moving the pad, and
- Figure 108c shows a close-up of the pad in contact with the surface.

From this initial position, the motor starts detaching the pad and the pad starts to peel off from one edge:

- Figure 108d shows the robot detaching the pad,
- Figure 108e shows the close-up of the vertical motor pulling the pad in order to peel it off, and
- Figure 108f shows one edge of the pad detached from the surface while the other edge is still attached.

When the motor detaches the pad, the whole area of the pad comes off the surface:

- Figure 108g shows the robot detaching the pad,
- Figure 108h shows the close-up of the vertical motor pulling the pad, and
- Figure 108i shows the whole area of the pad coming off the surface.

Finally, the pad is fully separated from the surface and the motor reaches the end of its motion range:

- Figure 108d shows the robot with the pad detached from the surface,
- Figure 108e shows the close-up of the vertical motor at the end of its range of motion, and
- Figure 108f shows the pad at a distance from the tissue.

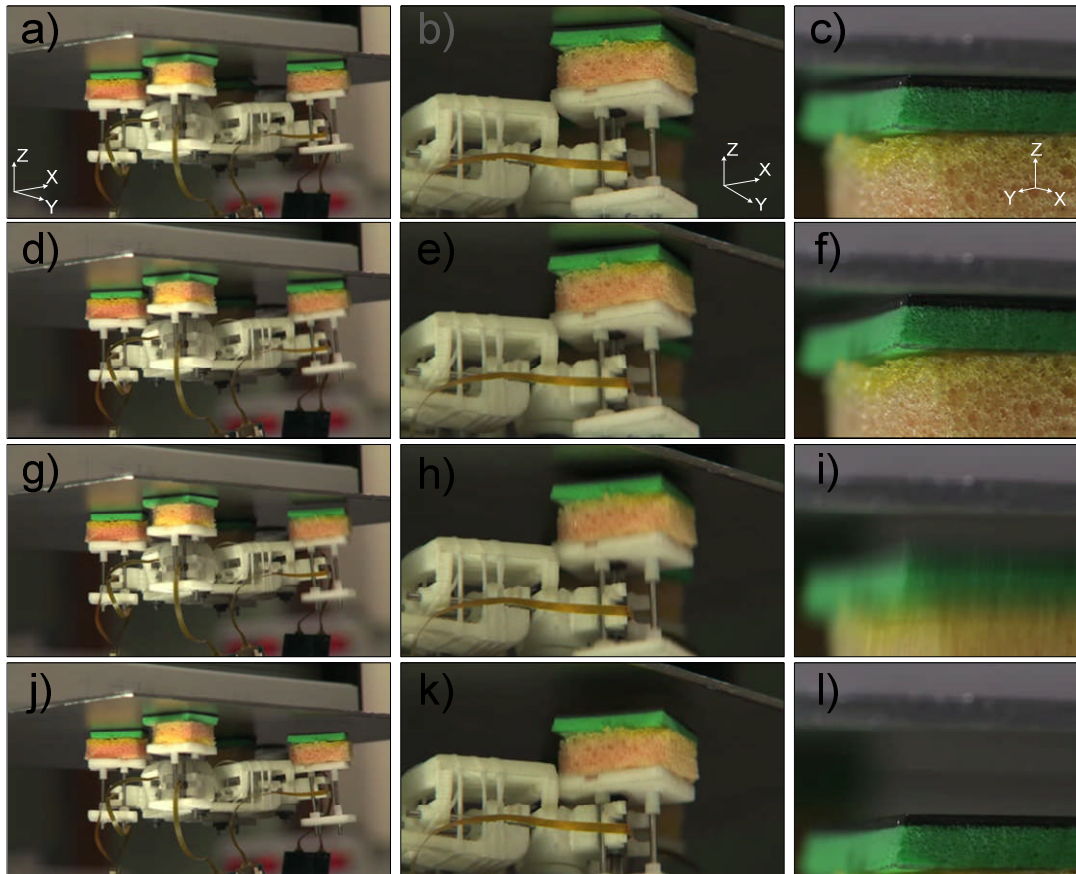


**Figure 108. (a-l) The locomotion mechanism detaching the magnetic pad by peeling it off from a steel surface.**

The stills of the locomotion mechanism peeling off the pad shown in Figure 108 were taken from a clip about the robot that featured in the BBC1 programme *The One Show* (see Appendix B).

Figure 109 shows the robot moving the pad in the horizontal plane by changing the shape of the quadrilateral formed by the horizontal prismatic joints of the locomotion mechanism. Figure 109a shows the initial position of the detached pad with the horizontal prismatic joint fully contracted. In Figure 109b the motor in the horizontal prismatic joint has moved half of its travel range, moving the pad accordingly. Figure 109c shows the final position of the detached pad with the horizontal prismatic joint fully extended.

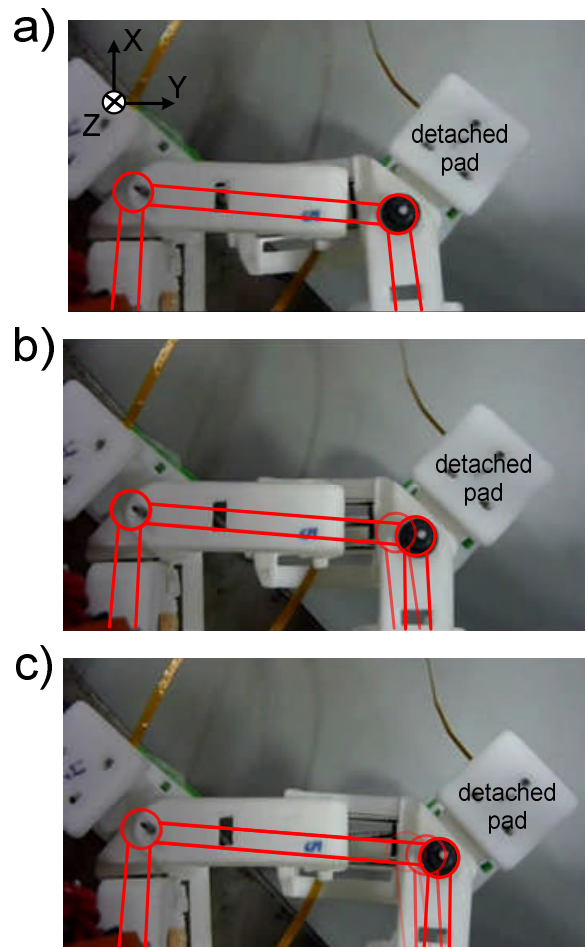


**Figure 109. (a-c) The locomotion mechanism moving the pad in the horizontal plane by changing the shape of the quadrilateral formed by the horizontal prismatic joints.**

## 5.8 Summary

The miniature piezo-electric motor Squiggle<sup>®</sup> is used for the implementation of the locomotion mechanism. The miniature linear encoder Tracker<sup>®</sup> is used in order to control the position of the motor. The prismatic joints of the robot controlled by a linear motor are built with these components: one mounting platform, one motor, one ends supporter and two guiding rods. In order to build the prismatic joint, the ends supporter and the mounting platform are connected through the guiding rods; the guiding rods are fixed to the ends supporter and slide into two holes of the mounting platform. The housing of the motor is attached to the mounting platform and the screw of the motor moves the pad attached to the ends supporter. Three assemblies of a prismatic joint were tested with the motor in order to determine the most suitable manufacturing technique and material. The third assembly manufactured with precision CNC machining in Delrin<sup>®</sup> proved to give the best performance.

The force of the Delrin<sup>®</sup> assembly was tested and the assembly proved to produce sufficient force to move the adhesive pads. Manufacturing of the whole robot using precision CNC machining was too expensive for the budget of the project so rapid prototyping was used instead in order to manufacture the locomotion mechanism. An assembly of one horizontal prismatic joint and one vertical prismatic joint was tested attaching and detaching the adhesive pad on tissue. The ability of the vertical prismatic joint to control the attachment and detachment of the pad was proved by applying different values of preload and obtaining different values of adhesion force accordingly. An assembly of one vertical joint and one horizontal joint was also tested showing the effect of using a horizontal force in order to control the detachment of the pad. Using four assemblies of one vertical prismatic joint and one horizontal prismatic joint, two prototypes of the robot were implemented and tested.

The first prototype of the robot was tested walking on a steel surface with magnetic pads of an attachment force similar to the adhesive pads. The locomotion sequence was programmed open-loop and the robot was tested walking several steps. A control system architecture was developed in order to make the locomotion sequence closed-loop. Following this control system architecture, a closed-loop controller was implemented in LabVIEW using linear encoders to control the position of the motors. The closed-loop controller was used in order to test the first prototype of the robot using magnetic pads and walking several steps on a steel surface. Force sensors are required in order to fully benefit from the closed-loop controller but no suitable force sensing technology was found for the application and budget of the robot.

A second prototype of the robot was built in order to tackle some issues experienced with the locomotion mechanism and improve the open-loop walking performance of the robot. The second prototype of the robot was tested walking with magnetic pads on a steel surface and also walking with the adhesive pads on tissue. Several issues were experienced with the locomotion mechanism due to the imprecision of rapid prototyping and manual assembly for the miniature size of the robot. In order to enhance the walking performance of the robot, several modifications were made to the hardware and an improved second prototype was implemented and tested. The improved second prototype walked consistently with magnetic pads on a steel surface and was able to detach and move the adhesive pad on tissue.

## **Chapter 6**

### **Peeling model of the adhesive pad**

#### **6.1 Introduction**

The previous chapter presented the development of the robot and showed the robot detaching and moving the magnetic pads on a steel surface and the bio-mimetic adhesive pads on tissue. While testing the prototype of the robot, the pad was observed to bend and peel off under the vertical and horizontal forces applied to the pads during the locomotion sequence and the question on how to control this process arose. Based on the experience gained with the implementation and testing of the robot, this chapter studies the process of detaching the pads, defining a peeling model of the adhesive pad. This peeling model determines the force and moment required to detach the pad depending on the geometry, material and adhesion of the pad. In Chapters 7 and 8, this peeling model enables the definition of the parameters of stability of the robot and to determine locomotion strategies in order to control the motion of the robot.

This chapter starts by explaining the premises of the peeling model and then presents the formulation of the model, considering the force and moment applied by the locomotion mechanism. The chapter presents the calculations of force and moment for the bio-mimetic adhesive pad using the peeling model and, after that, the last section summarises the contents of the chapter.

#### **6.2 Premises of the peeling model**

Prior to the formulation of the peeling model, this section explains:

- the materials of the pad and the Young's modulus considered for the peeling model,
- the features in the application of the robot that make the pad peel off, and
- how the pad bends during the detachment process.

### 6.2.1 Young's modulus of the adhesive pad attached to tissue

In the locomotion mechanism of the robot, the adhesive pad is composed of:

- a layer of plastic material, less than 1mm-thick, with the bio-mimetic adhesive pattern printed on its surface, and
- a layer of soft foam, 3 to 5 mm thick, backing the material with the adhesive surface.

Figure 110a shows the prototype of the robot and Figure 110b shows the adhesive pad and the layer of soft foam moved by a linear motor within a vertical prismatic joint.

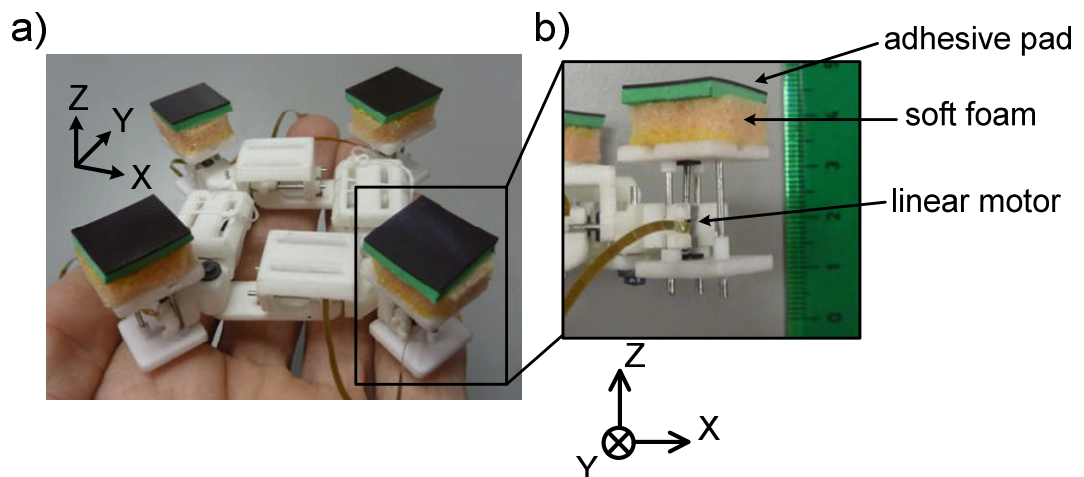


**Figure 110. (a) Prototype of the robot and (b) adhesive pad and soft foam moved by a linear motor within a vertical prismatic joint.**

A layer of soft foam backing the adhesive surface is beneficial for the application of the robot because:

- it favours contact between the adhesive pad and the tissue, and
- it help absorb any unwanted shearing force, pull (normal) force or moment applied to the pads.

The tissue is also soft and when the pad is attached to the tissue, the adhesive surface, the soft foam and the tissue form one block. In order to determine the stiffness of this block, the greatest Young's modulus of the adhesive surface, foam and tissue is considered dominant. When force or moment is applied to the pad, the dominant material determines how the adhesive surface bends and the other materials mould to this bending.

In the robot, the adhesive surface is printed on MacDermid Autotex<sup>®</sup> polymer which has a Young's modulus of 187.5 MPa [164]. The soft foam backing

the adhesive surface is made of Tempur<sup>®</sup> memory foam with a density of 0.085 g/cm<sup>3</sup>. Memory foam is made of polyurethane foam and the Young's modulus of polyurethane foam with a density of 0.09 g/cm<sup>3</sup> is 0.08-0.93 MPa [165]. The Young's modulus of the abdominal wall varies between 19.9 and 51.5 kPa depending on the plane of measurement [166]. The dominant Young's modulus is therefore that of the adhesive surface because it is two orders of magnitude greater than that of the soft foam and four orders of magnitude greater than that of the tissue.

### **6.2.2 Peeling-off of the adhesive pad**

When the locomotion mechanism of the robot applies force on the pad attached to the tissue, the pad peels off the surface of the tissue because:

- the attachment between the pad and the tissue is not perfectly uniform,
- the force applied by the locomotion mechanism to the pad is not perfectly perpendicular to the surface of the tissue, and
- the locomotion mechanism can apply force close to the edge of the pad and moment that cause peeling-off if the prismatic joint is connected closer to one edge of the pad than to the opposite edge.

The attachment between the pad and the tissue is not perfectly uniform. Thus, the adhesive pad is more strongly attached to the tissue in some areas of the pad depending on the contact and adhesive properties of those areas. In that case, when a pull force is applied to the pad, detachment starts from the area of the pad where attachment is weakest and then spreads to the rest of the pad.

The force applied by the locomotion mechanism to the adhesive pad is not perfectly perpendicular to the surface of the tissue. This is due to the inclination and curvature of the tissue and the fact that in the locomotion mechanism the screw of the motor moving the pad is not perfectly perpendicular to the adhesive surface. This causes detachment to start from one edge of the pad and progress along the adhesive surface until the whole pad is detached. In the peeling model, the angle between the force applied by the vertical motors and the surface of the tissue is the angle  $\alpha$ .

In the locomotion mechanism, if the centre of the pad is not aligned with the screw of the motor, the motor applies a force close to the edge of the pad. The locomotion mechanism can also apply a moment on the pad by actuating the horizontal prismatic joints when the pad is attached to the tissue. A pull force close to the edge of the pad and a moment applied on the pad cause peeling-off of the pad.

Figure 111 shows the vertical prismatic joint of the locomotion mechanism pulling the pad and peeling it off. Figure 111a shows the vertical prismatic joint ready to pull the pad and Figure 111b shows a close up of the pad. In Figure 111c the vertical motor is pulling the pad and Figure 111d shows one edge of the pad detached while the other edge is in contact with the surface. Figure 111e and Figure 111f show the vertical prismatic joint and the pad at the moment when the whole surface of the pad comes off.

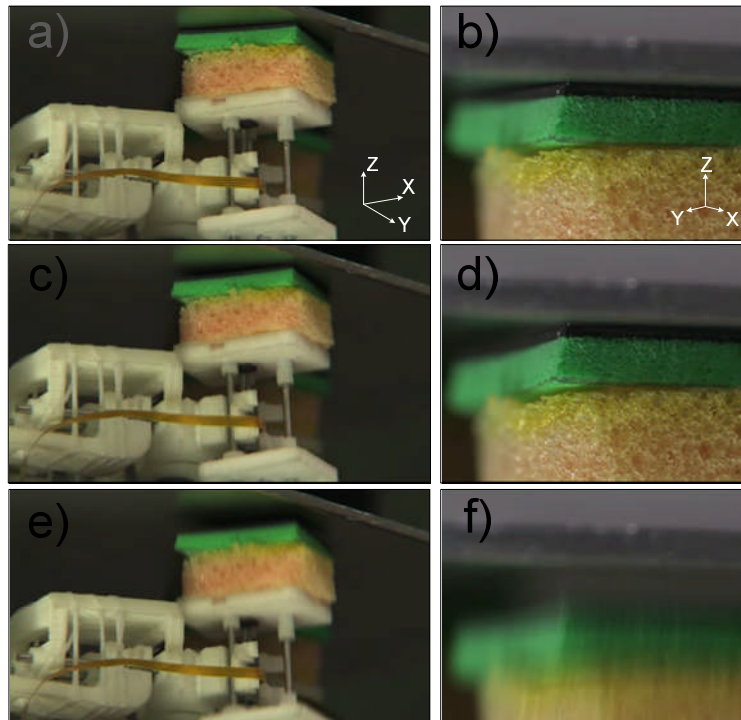


**Figure 111. (a-f) Locomotion mechanism of the robot peeling off the pad.**

For the sake of simplicity, shearing forces applied to the pad are considered to be fully absorbed by the soft foam and therefore have no effect on the adhesion and peeling-off of the pads.

### **6.2.3 Bending of the adhesive pad**

When a force or moment is applied to the adhesive pad, the pad is assumed to bend following the laws of Euler-Bernoulli's beam theory. The deformation considered for the material of the pad is up to 10% of its length, so it is a linear elastic material and follows Hooke's law.

The pad is considered to bend like a cantilever when force or moment is applied to the pad. Peeling starts at one edge of the pad and the detached surface is supported by the area of the pad still in contact with the tissue. The detached area of the pad is supported at the end where the pad is still attached to the tissue. The deformation of the detached area of the pad is determined by the force applied to the pad. The instant before detachment,

the whole surface of the pad will be bent by the force applied to the pad. Figure 112a shows the pad peeling off the surface. Figure 112b illustrates the situation in the peeling process when the pad is supported by the edge of the pad in contact with the tissue and the pad is bending like a cantilever.

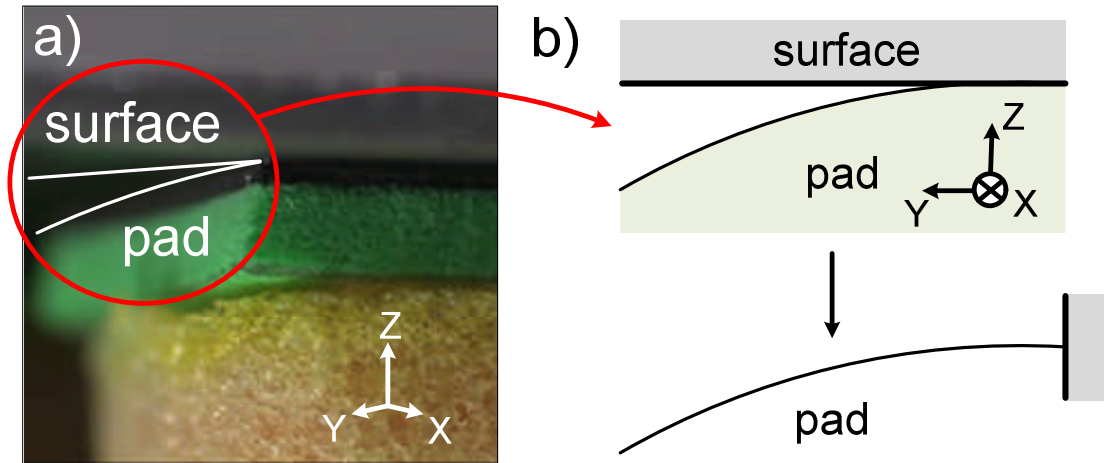


**Figure 112. (a) Pad detaching from the surface and (b) sketch of the pad peeling off the surface and bending like a cantilever.**

The instant before the adhesive surface comes off the tissue (see Figure 112), the force or moment causing the bending of the pad has worked against the adhesion of the whole adhesive surface. This final situation at the end of the peeling process is considered in the peeling model in order to calculate the force or moment that causes the pad to peel off.

### 6.3 Formulation of the peeling model

The peeling model calculates the force and moment required from the locomotion mechanism of the robot to peel off the pad. In order to find the expression of peeling force and peeling moment, this model uses:

- Kendall's peeling theory to calculate the energy of the pad and tissue when the pad peels off [167],
- Euler-Bernoulli's beam theory to calculate the bending of the pad causing detachment [168].

Considering the energy of the pad and the tissue, Kendall's equilibrium theory of adhesion gives the condition of energy when the pad peels off. This condition of energy depends on the peeling force and moment applied to the pad by the locomotion mechanism and it also depends on the bending moment present in the pad. The bending equations obtained with Euler-Bernoulli's beam theory determine the bending moment and thus enable to

calculate the peeling force and moment from the energy condition of Kendall's theory.

### 6.3.1 Kendall's peeling theory

Kendall's theory considers the peeling of a thin film shown in Figure 113.

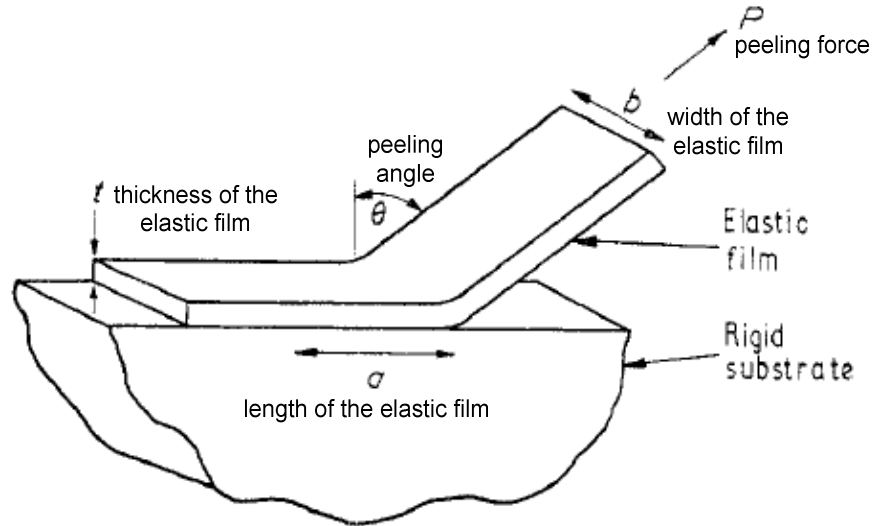


Figure 113. Kendall's peeling test [167].

According to Kendall's peeling theory, equilibrium fracture on an adhesive interface occurs when the variation of total potential energy with respect to the length of the adhesive interface is minimal [167]. The mathematical expression for Kendall's condition of fracture on an adhesive interface is:

$$U_T = U_S + U_E + U_P \quad (29)$$

$$\frac{\partial U_T}{\partial a} = 0 \quad (30)$$

For Equation ( 29 ):

- $U_T$  is the total energy of the system,
- $U_S$  is the surface energy, or the energy of adhesion,
- $U_E$  is the elastic energy, and
- $U_P$  is the potential energy of the applied force.

For Equation ( 30 ):

- $U_T$  is the total energy of the system given by Equation ( 29 ), and
- $a$  is the length of the film.

When Equation ( 30 ) is true: "the work done in breaking the adhesive joint is exactly compensated by the gain in surface energy of the system" [167]. Fracture must proceed at a low rate under this condition of equilibrium, so that no energy is lost in viscous processes [167].

In Kendall's peeling of thin films, a constant force is applied to the surface at a certain angle (force  $P$  in Figure 113). In Kendall's model, the elastic energy of the system ( $U_E$ ) is composed of two terms:

- the energy stored in the sharp bend of the film and
- the energy required to stretch the film.

The energy of the bend does not depend on the length of the film ( $a$ ). The elastic term is negligible when compared to the work of adhesion and the work of the force applied to peel the film ( $P$ ) [167].

### 6.3.2 Peeling theory applied to the adhesive pad

In the peeling model of the adhesive pad, a force and a moment are applied to the pad. The force and moment cause bending of the material, working against adhesion and peeling off the pad. In the adhesive pad peeling off the tissue, the total energy of the system is:

$$U_T = U_S + U_B + U_P \quad (31)$$

Where:

- $U_T$  is the total energy of the system,
- $U_S$  is the work of the adhesion force,
- $U_B$  is the work of the bending moment along the angle of deformation caused on the pad, and
- $U_P$  is the work of the force or moment causing the bending of the pad.

The first term in Equation ( 31 ):  $U_S$  is the work of adhesion along the surface of the pad. The expression of  $U_S$  is the same as in Kendall's model [167]:

$$U_S = -b \cdot x \cdot W_{adh} \quad (32)$$

Where  $b$  is the width of the pad,  $x$  is the length of the pad and  $W_{adh}$  is the work of adhesion of the pad per unit area.

The second term in Equation ( 31 ):  $U_B$  is the work of the bending moment of the pad, causing the pad to bend an angle  $\theta$ . The expression of  $U_B$  is:

$$U_B = \int M_z(x) \cdot d\theta \quad (33)$$

Where  $M_z(x)$  is the bending moment caused by the force or moment applied to the pad, and  $\theta$  is the angle or slope along the length of the pad.

The third term in Equation ( 31 ):  $U_P$  is the work of the force or moment applied to the pad along the separation between the pad and the tissue. In the locomotion mechanism of the robot, the force or moment applied on the pad can be:

- a force applied to the edge of the pad,
- a uniform load applied along the surface of the pad, and
- a moment applied to the pad.

A force can be applied to the edge of the pad, for instance, by attaching a linear motor or a Shape Memory Alloy wire to one of the edges of the pad; this actuator would peel off the pad by pulling from the edge of the pad the actuator is attached to. In the locomotion mechanism of the robot, this can be implemented by connecting the linear motor to the edge of the pad. Figure 114 shows a vertical motor of the robot connected to the edge of the pad and applying a force in order to peel off the pad.

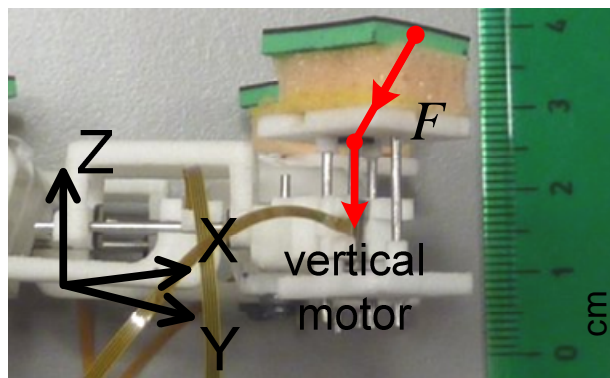


**Figure 114. Vertical motor of the robot applying a force to the edge of the adhesive pad.**

When a force is applied to the edge of the pad,  $U_p$  in Equation ( 31 ) is:

$$U_p^F = \int F \cdot dy \quad ( 34 )$$

Where  $F$  is the force applied to the pad and  $y$  is the distance between the pad and the tissue, in the direction perpendicular to the surface of the tissue.

A uniform load can be applied along the surface of the pad by pulling the whole surface of the pad with a linear motor. In the robot, this is the case when the vertical linear motor applies a force on the whole surface of the pad. In the robot, this is also the case when the pad is holding the weight of the locomotion mechanism connected to the pad. Figure 115 shows a vertical motor of the robot applying a uniform load along the surface of the pad in order to peel off the pad.

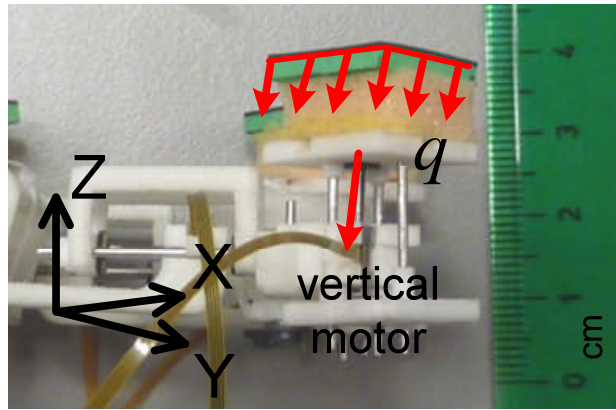


**Figure 115. Vertical motor of the robot applying a uniform load to the adhesive pad.**

When a uniform load is applied to the pad,  $U_p$  in Equation ( 31 ) is:

$$U_p^q = \int q(x) \cdot dy \quad (35)$$

Where  $q(x)$  is the load distributed along the length of the pad, and  $y$  is the distance between the pad and the tissue, in the direction perpendicular to the surface of the tissue.

A moment can be applied to the pad, for example, with a rotary motor directly connected to the edge of the pad. This peels off the pad by directly bending the pad and thus bending the adhesive surface. In the robot, this is the case of the horizontal linear motor pushing or pulling the pad at a distance from the pad. Figure 116 shows a horizontal motor of the robot applying a moment to the pad in order to peel it off.

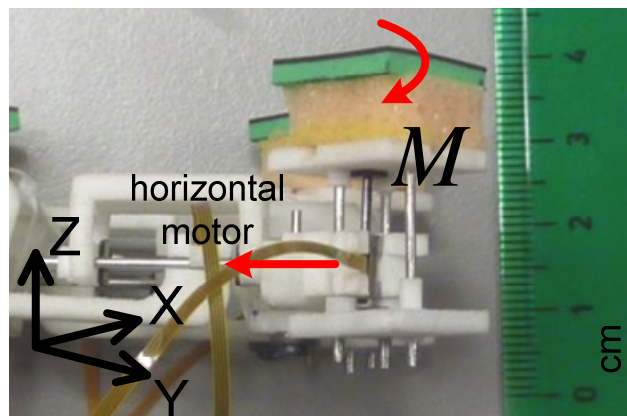


**Figure 116. Horizontal motor of the robot applying a moment to the adhesive pad.**

When a moment is applied to the pad,  $U_p$  in Equation ( 31 ) is:

$$U_p^M = \int M \cdot d\theta \quad (36)$$

Where  $M$  is the moment applied to the pad, and  $\theta$  is the angle or slope along the length of the pad.

A combination of force and moment can be applied to the adhesive pad in order to peel it off. Figure 117 shows the vertical motor applying a uniform load and the horizontal motor applying a moment to the pad.

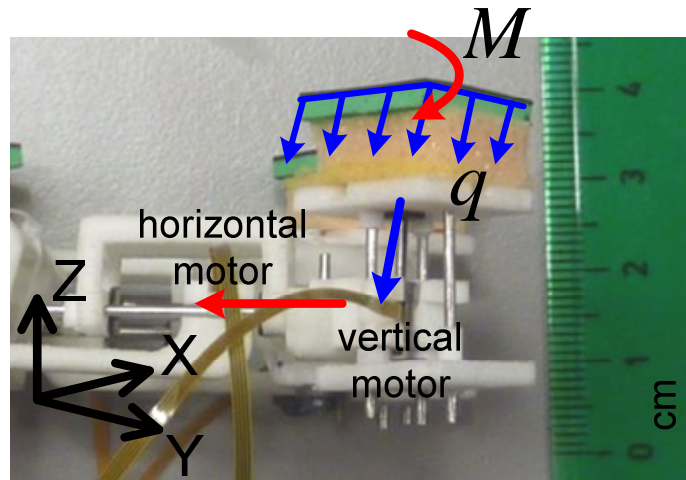


**Figure 117. Combination of a uniform load applied by the vertical motor and a moment applied by the horizontal motor to the adhesive pad.**

When a uniform load and a moment are applied to the pad, the total potential energy  $U_p$  in Equation ( 31 ) is:

$$U_p = U_p^q + U_p^M \quad (37)$$

Where  $U_p^q$  is the potential energy of the uniform load applied to the pad defined by Equation ( 35 ) and  $U_p^M$  is the potential energy of the moment applied to the pad defined by Equation ( 36 ).

In Kendall's peeling model for thin films: "peeling force is largely independent of the elastic properties of both the adherent film and the substrate" [167]. However, in the peeling model of the pad, the peeling force and peeling moment depend on the elastic properties of the material. This is the case in the adhesive pad because the pad detaches due to the bending of the material along with the force and moment applied to the pad.

### **6.3.3 Euler-Bernoulli's bending equations for a cantilever**

According to Euler-Bernoulli's beam theory, the deformation, slope and bending moment undergone by a beam depends on how the beam is supported and the force and moment applied to the beam. For this peeling model, the pad is considered to be supported as a cantilever and the force and moment the locomotion mechanism can apply to the pad are:

- force at one edge of the adhesive pad,
- uniform load applied along the length of the adhesive pad, and
- moment on the adhesive pad.

The sketch of a cantilever with a force applied at the free end of the cantilever is shown in Figure 118.

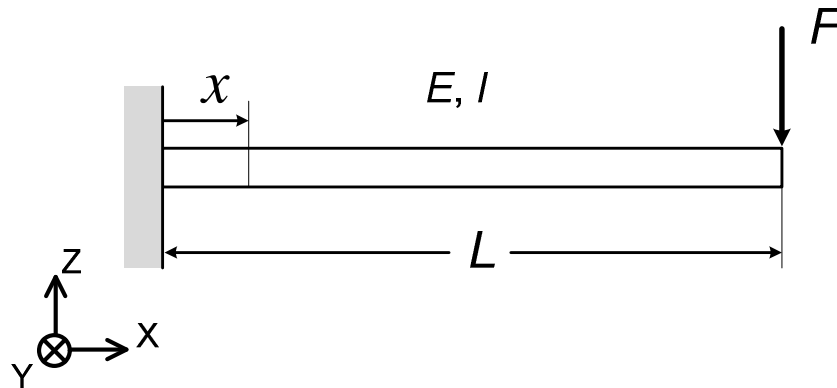


Figure 118. Force applied at the free end of a cantilever.

According to Euler-Bernoulli's beam theory, when a force is applied to the free end of a cantilever, the cantilever undergoes this deformation  $z_F(x)$ , slope  $\theta_F(x)$ , and bending moment  $M_F(x)$  [168]:

$$z_F(x) = -\frac{F \cdot x^2 \cdot (3 \cdot L - x)}{6 \cdot E \cdot I} \quad (38)$$

$$\theta_F(x) = -\frac{F \cdot (2 \cdot L - x) \cdot x}{2 \cdot E \cdot I} \quad (39)$$

$$M_F(x) = F \cdot (L - x) \quad (40)$$

In Figure 118 and Equations ( 38 ), ( 39 ) and ( 40 ):

- $F$  is the force applied at the free end of the cantilever,
- $L$  is the total length of the cantilever,
- $x$  is the distance from the fixed end of the cantilever,
- $E$  is Young's modulus of the material of the cantilever, and
- $I$  is the area moment of inertia of the cantilever.

The sketch of a cantilever with a uniform load applied along the length of the cantilever is shown in Figure 119.

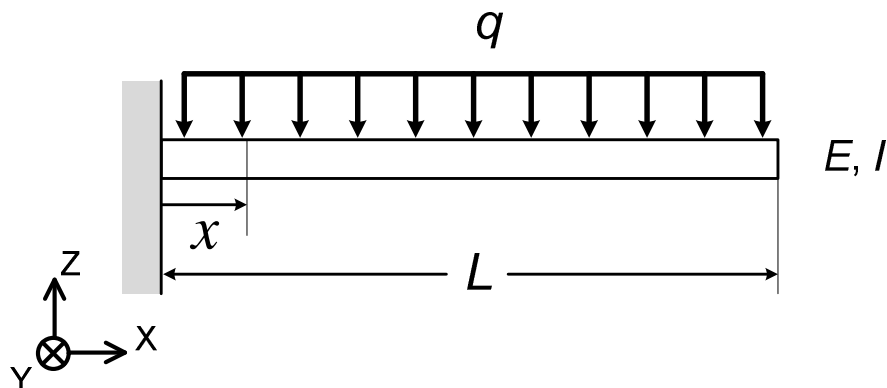


Figure 119. Uniform load applied along the length of a cantilever.

According to Euler-Bernoulli's beam theory, when a uniform load is applied along the length of a cantilever, the cantilever undergoes this deformation  $z_q(x)$ , slope  $\theta_q(x)$ , and bending moment  $M_q(x)$  [168]:

$$z_q(x) = -\frac{q \cdot x^2 \cdot (6 \cdot L^2 - 4 \cdot x \cdot L + x^2)}{24 \cdot E \cdot I} \quad (41)$$

$$\theta_q(x) = -\frac{q \cdot x \cdot (3 \cdot L^2 - 3 \cdot x \cdot L + x^2)}{6 \cdot E \cdot I} \quad (42)$$

$$M_q(x) = \frac{q \cdot (L - x)^2}{2} \quad (43)$$

In Figure 119 and Equations ( 41 ), ( 42 ) and ( 43 ):

- $q$  is the uniform load applied along the length of the cantilever,
- $L$  is the total length of the cantilever,
- $x$  is the distance from the fixed end of the cantilever,
- $E$  is Young's modulus of the material of the cantilever, and
- $I$  is the area moment of inertia of the cantilever.

The sketch of a cantilever with a moment applied at the free end of the cantilever is shown in Figure 120.

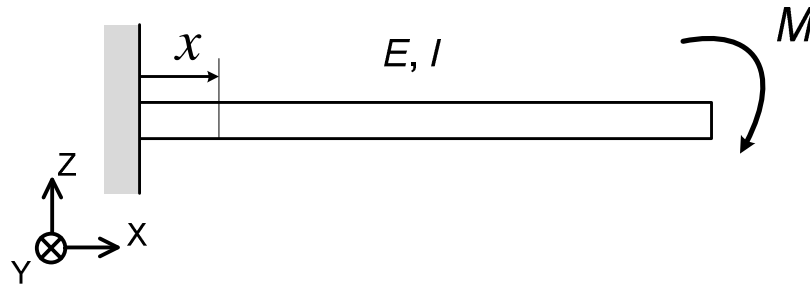


**Figure 120. Moment applied at the free end of a cantilever.**

According to Euler-Bernoulli's beam theory, when a moment is applied to the free end of a cantilever, the cantilever undergoes this deformation  $z_M(x)$ , slope  $\theta_M(x)$ , and bending moment  $M_M(x)$  [168]:

$$z_M(x) = -\frac{M \cdot x^2}{2 \cdot E \cdot I} \quad (44)$$

$$\theta_M(x) = -\frac{M \cdot x}{E \cdot I} \quad (45)$$

$$M_M(x) = M \quad (46)$$

In Figure 120 and Equations ( 44 ), ( 45 ) and ( 46 ):

- $M$  is the moment applied at the free end of the cantilever,
- $x$  is the distance from the fixed end of the cantilever,
- $E$  is Young's modulus of the material of the cantilever, and
- $I$  is the area moment of inertia of the cantilever.

### 6.3.4 Force to peel off the adhesive pad

Following Kendall's peeling theory, in order to find the force to peel off the pad, the total energy of the system ( $U_T^F$ ) is minimised with respect to the distance from the supported end of the pad ( $x$ ):

$$\frac{\partial U_T^F}{\partial x} = 0 \quad (47)$$

The total energy of the system when a force is applied to the edge of the pad is:

$$U_T^F = U_S^F + U_B^F + U_P^F \quad (48)$$

The terms of the total energy in Equation ( 48 ) are:

- $U_S^F$  is the work of adhesion along the surface of the pad:

$$U_S^F = -b \cdot x \cdot W_{adh} \quad (49)$$

where  $b$  is the width of the pad,  $x$  is the distance from the supported end of the pad and  $W_{adh}$  is the work of adhesion of the pad per unit area.

- $U_B^F$  is the work of the bending moment of the pad, causing the pad to bend an angle  $\theta_F(x)$ :

$$U_B^F = \int M_Z^F(x) \cdot d\theta_F(x) \quad (50)$$

where  $M_Z^F(x)$  is the bending moment defined by Euler-Bernoulli's beam theory in Equation ( 40 ) and  $\theta_F(x)$  is the slope defined in Equation ( 39 ).

- $U_P^F$  is the work of the force applied to the pad along the distance between the pad and the tissue:

$$U_P^F = \int F \cdot dz_F(x) \quad (51)$$

where  $F$  is the peeling force and  $z_F(x)$  is the distance between the pad and the tissue defined by Equation ( 38 ).

Figure 121a shows the vertical motor of the robot applying a force to the edge of the pad. Figure 121b shows a sketch of the pad peeling off the surface when a force is applied to the edge of the pad. Figure 121a and Figure 121b also show the parameters considered in order to obtain the force that causes the pad to peel off.

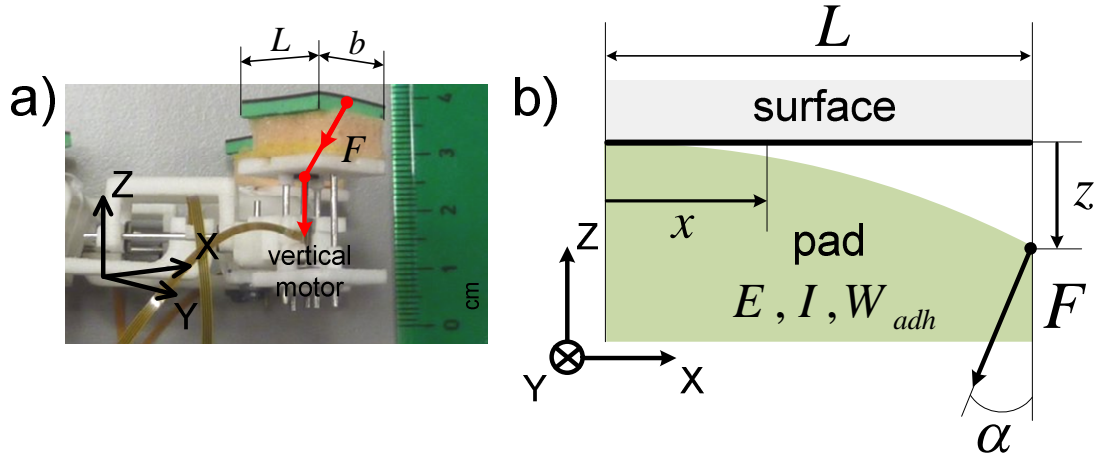


**Figure 121. (a) Vertical motor of the robot applying a force to the edge of the pad and (b) sketch of the pad peeling when a force is applied to the edge of the pad.**

The force is applied at an angle  $\alpha$  from the vertical as shown in Figure 121. Solving Equation ( 47 ), the resulting peeling force depends on the distance from the supported end of the pad ( $x$ ). The expression of the peeling force is:

$$F(x) = \frac{\sqrt{\frac{2 \cdot \rho}{l^F(x, L)}}}{\cos(\alpha)} \quad (52)$$

In Equation ( 52 ),  $\rho$  is a constant that depends on:

- the geometry of the pad: specifically the area moment of inertia  $I$  and the width  $b$  of the pad,
- the elastic properties or Young's modulus of the pad  $E$ , and
- the work of adhesion of the pad  $W_{adh}$ .

The constant  $\rho$  is defined as:

$$\rho = E \cdot I \cdot W_{adh} \cdot b \quad (53)$$

In Equation ( 52 ), the polynomial  $l^F(x, L)$  determines the way the peeling force changes along the length of the pad. The expression of the polynomial  $l^F(x, L)$  is:

$$l^F(x, L) = 3 \cdot L^2 - 4 \cdot L \cdot x + x^2 \quad (54)$$

Figure 122a shows a sketch of the pad supported at one end. For the length of the pad of  $L = 1 \text{ cm}$ , the value of the polynomial  $l^F(x)$  is shown in Figure 122b with respect to the distance from the supported end of the pad ( $x$ ).

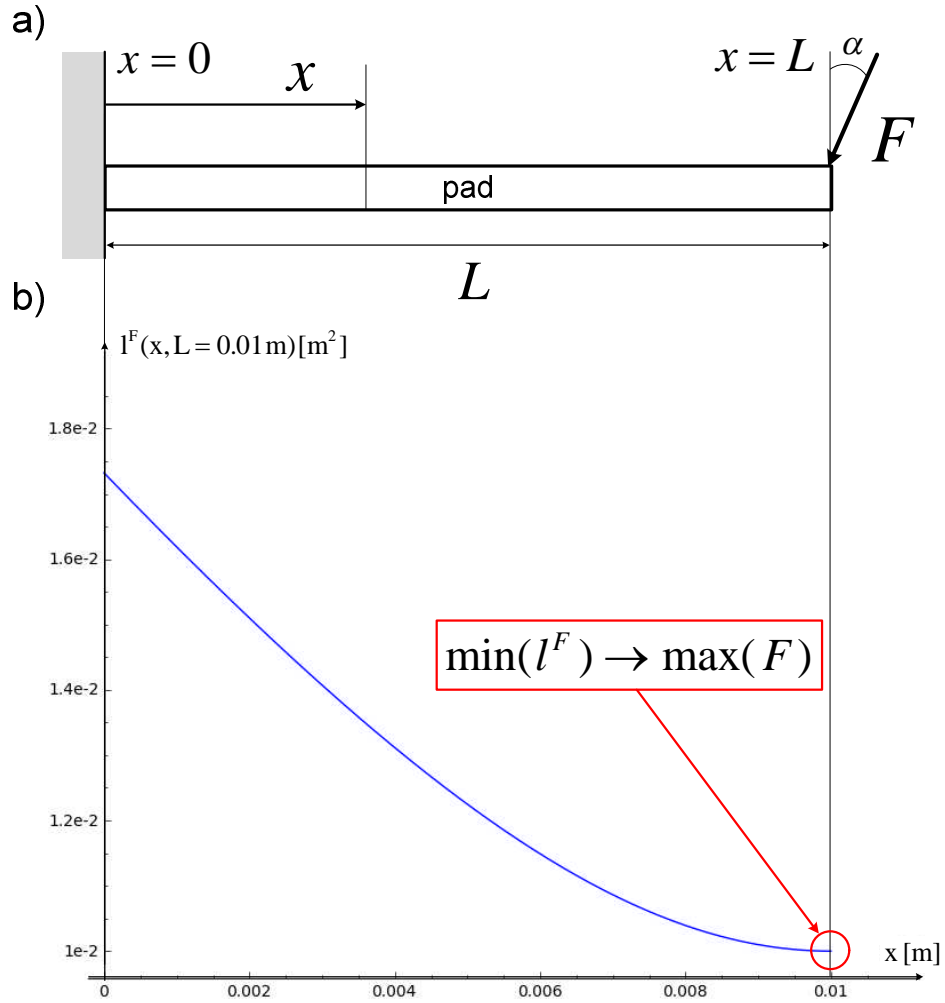


**Figure 122. Variation of the polynomial  $l^F(x, L)$  along the length of the adhesive pad for a total length of the pad of  $L = 1 \text{ cm}$ .**

According to Equation ( 52 ), the value of peeling force is inversely proportional to the value of  $l^F(x, L)$ , thus the maximum value of peeling force corresponds to the minimum value of  $l^F(x, L)$ . Figure 122b shows that the maximum force to peel the pad corresponds to the point of application of the force, at  $x = L$ . Therefore, the value of force required to peel off the pad is:

$$F = \frac{\sqrt{\frac{2 \cdot \rho}{l^F(x=L)}}}{\cos(\alpha)} = \frac{\sqrt{2 \cdot \rho}}{L \cdot \cos(\alpha)} \quad (55)$$

Where  $\rho$  is the constant defined in Equation ( 2 ),  $L$  is the total length of the pad and  $\alpha$  is the angle of inclination of the force.

The value of peeling force in Equation ( 55 ) increases with a greater angle of inclination of the force ( $\alpha$ ) and decreases as the total length of the pad ( $L$ ) increases. This is consistent with observation of the peeling process and the tests carried out with the pads during the implementation of the robot.

The peeling force in Equation ( 55 ) depends on the cross section of the pad and the elastic properties of the pad through the constant  $\rho$ , see Equation ( 2 ). As expected, the peeling force in Equation ( 55 ) increases with greater adhesion force from the pad.

The peeling force in Equation ( 55 ) is more sensitive to variation in the length of the pad and inclination angle:  $F \propto \frac{1}{L \cdot \cos(\alpha)}$ , than to variation in work of adhesion:  $F \propto \sqrt{\rho}$ .

### 6.3.5 Uniform load to peel off the adhesive pad

Following Kendall's peeling theory, in order to find the uniform load to peel off the pad, the total energy of the system ( $U_T^q$ ) is minimised with respect to the distance from the supported end of the pad ( $x$ ):

$$\frac{\partial U_T^q}{\partial x} = 0 \quad (56)$$

The total energy of the system when a uniform load is applied to the pad is:

$$U_T^q = U_S^q + U_B^q + U_P^q \quad (57)$$

The terms of the total energy in Equation ( 57 ) are:

- $U_S^q$  is the work of adhesion along the surface of the pad:

$$U_S^q = -b \cdot x \cdot W_{adh} \quad (58)$$

where  $b$  is the width of the pad,  $x$  is the distance from the supported end of the pad and  $W_{adh}$  is the work of adhesion of the pad per unit area.

- $U_B^q$  is the work of the bending moment of the pad, causing the pad to bend an angle  $\theta_q(x)$ :

$$U_B^q = \int M_z^q(x) \cdot d\theta_q(x) \quad (59)$$

where  $M_z^q(x)$  is the bending moment defined by Euler-Bernoulli's beam theory in Equation ( 43 ) and  $\theta_q(x)$  is the slope defined in Equation ( 42 ).

- $U_P^q$  is the work of the uniform load applied to the pad along the distance between the pad and the tissue:

$$U_P^q = \int q(x) \cdot dz_q(x) \quad (60)$$

where  $q(x)$  is the peeling uniform load and  $z_q(x)$  is the distance between the pad and the tissue defined by Equation ( 41 ).

Figure 123a shows the vertical motor of the robot applying a uniform load to the pad. Figure 123b shows a sketch of the pad peeling off the surface when

a uniform load is applied to the pad. Figure 123a and Figure 123b also show the parameters considered in order to obtain the uniform load that causes the pad to peel off.

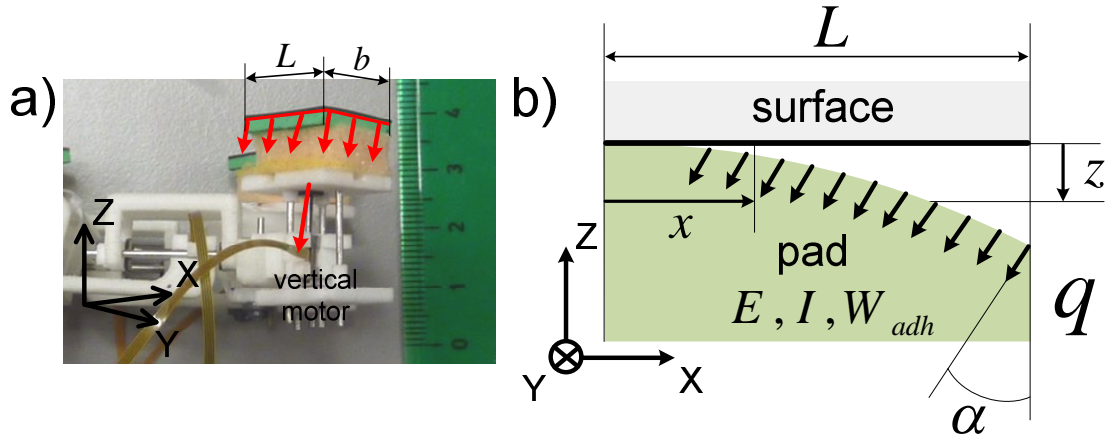


**Figure 123. (a) Vertical motor of the robot applying a uniform load to the pad and (b) sketch of the pad peeling when a uniform load is applied to the pad.**

The uniform load is considered constant along the length of the pad and it is applied at an angle  $\alpha$  from the vertical as shown in Figure 123. Solving Equation ( 56 ), the resulting peeling uniform load depends on the distance from the supported end of the pad ( $x$ ). The expression of the peeling uniform load per unit length is:

$$q(x) = \frac{2 \cdot \sqrt{3}}{\cos(\alpha)} \cdot \sqrt{\frac{\rho}{l^q(x, L)}} \quad (61)$$

Where  $\rho$  is the constant defined in Equation ( 2 ) and the polynomial  $l^q(x, L)$  determines the way the peeling uniform load changes along the length of the pad. The expression of the polynomial  $l^q(x, L)$  is:

$$l^q(x, L) = 3 \cdot L^4 - 12 \cdot L^3 \cdot x + 24 \cdot L^2 \cdot x^2 - 18 \cdot L \cdot x^3 + 5 \cdot x^4 \quad (62)$$

Figure 124a shows a sketch of the pad supported at one end. For the length of the pad of  $L = 1 \text{ cm}$ , the value of the polynomial  $l^q(x)$  is shown in Figure 124b with respect to the distance from the supported end of the pad ( $x$ ).

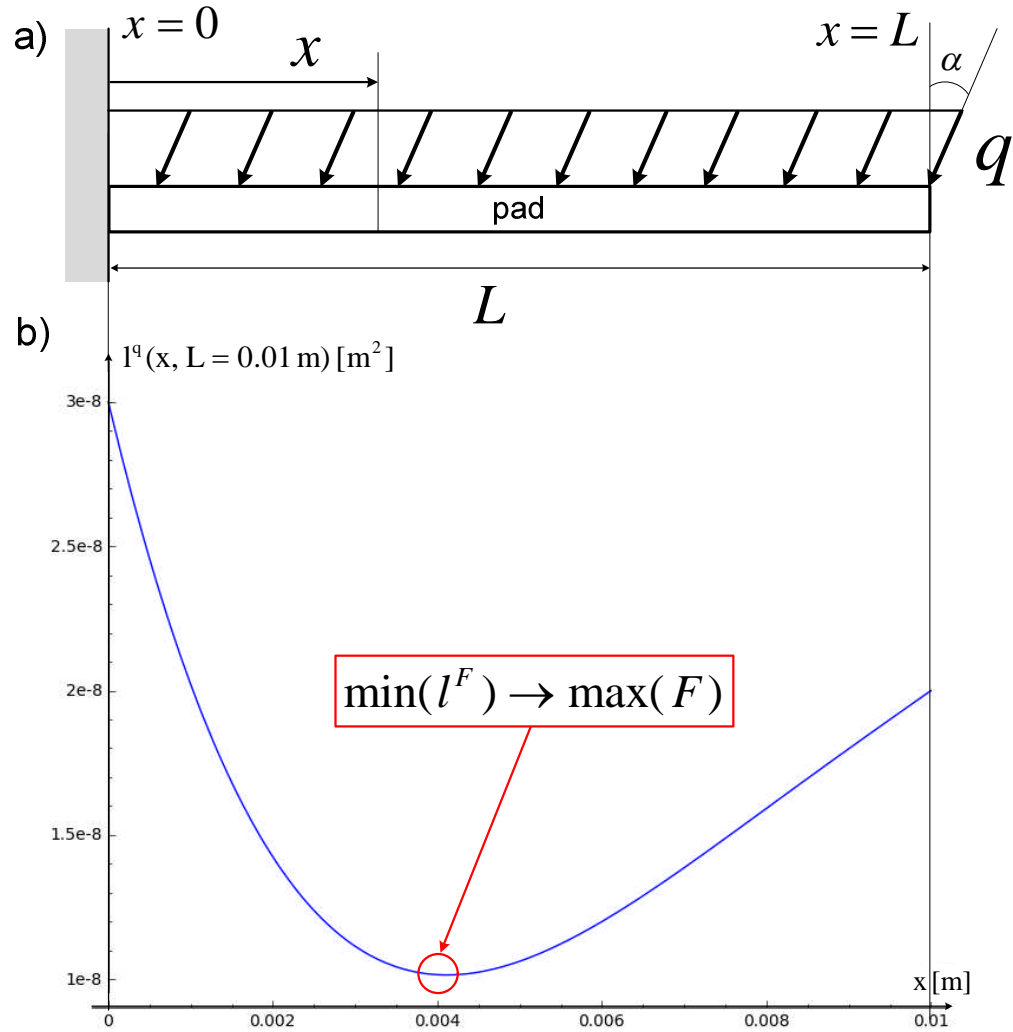


**Figure 124.** Variation of  $l^q(x, L)$  along the length of the pad for  $L = 1 \text{ cm}$ .

According to Equation ( 61 ), the value of peeling uniform load is inversely proportional to the value of  $l^q(x, L)$ , thus the maximum value of peeling force corresponds to the minimum value of  $l^q(x, L)$ . Figure 124b shows that the maximum force to peel the pad corresponds to the point  $x = \frac{2}{5}L$ . Therefore, the value of uniform load required to peel off the pad is:

$$q = \frac{2 \cdot \sqrt{3}}{\cos(\alpha)} \cdot \sqrt{\frac{\rho}{l^q(x = \frac{2}{5}L)}} = \frac{3.4}{L^2 \cdot \cos(\alpha)} \cdot \sqrt{\rho} \quad (63)$$

Where  $\rho$  is the constant defined in Equation ( 2 ),  $L$  is the total length of the pad and  $\alpha$  is the angle of inclination of the uniform load.

The peeling uniform load in Equation ( 63 ) decreases with the square of the total length of the pad ( $L^2$ ) because the uniform load is distributed along the length of the pad.

The peeling uniform load in Equation ( 63 ) increases with a greater angle of inclination of the uniform load ( $\alpha$ ). Thus, the less perpendicular the load is to

the tissue, the more load is required to peel off the pad. This was also the case with the force applied to the edge of the pad and is consistent with observation of the peeling process in the robot.

The peeling uniform load in Equation ( 63 ) depends on the cross section and elastic properties of the pad through the constant  $\rho$ , see Equation ( 2 ). The peeling uniform load increases with greater adhesion force from the pad.

### 6.3.6 Moment to peel off the adhesive pad

Following Kendall's peeling theory, in order to find the moment to peel off the pad, the total energy of the system ( $U_T^M$ ) is minimised with respect to the distance from the supported end of the pad ( $x$ ):

$$\frac{\partial U_T^M}{\partial x} = 0 \quad ( 64 )$$

The total energy of the system when a moment is applied to the pad is:

$$U_T^M = U_S^M + U^M \quad ( 65 )$$

The terms of the total energy in Equation ( 65 ) are:

- $U_S^M$  is the work of adhesion along the surface of the pad:

$$U_S^M = -b \cdot x \cdot W_{adh} \quad ( 66 )$$

where  $b$  is the width of the pad,  $x$  is the distance from the supported end of the pad and  $W_{adh}$  is the work of adhesion of the pad per unit area.

- $U^M$  is the work of the moment applied to the pad, causing the pad to bend an angle  $\theta_M(x)$ :

$$U_B^M = \int M \cdot d\theta_M(x) \quad ( 67 )$$

where  $M$  is the moment applied to the pad, which is also the bending moment defined by Euler-Bernoulli's beam theory in Equation ( 46 ), and  $\theta_M(x)$  is the slope defined in Equation ( 45 ).

Figure 125a shows the horizontal motor of the robot applying a moment to the pad. Figure 125b shows a sketch of the pad peeling off the surface when a moment is applied to the pad. Figure 125a and Figure 125b also show the parameters considered in order to obtain the moment that causes the pad to peel off.

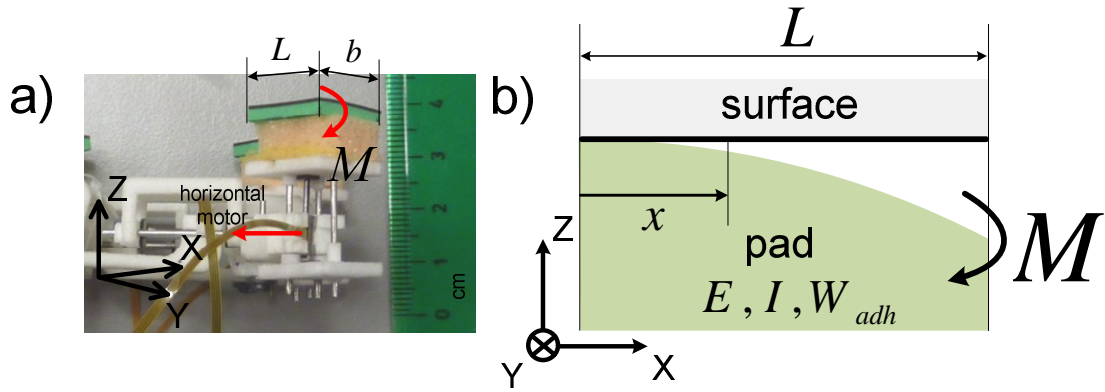


Figure 125. (a) Horizontal motor of the robot applying a moment to the pad and (b) sketch of the pad peeling when a moment is applied to the pad.

Solving Equation ( 64 ), the expression of the peeling moment is:

$$M = \sqrt{E \cdot I \cdot W_{adh} \cdot b} = \sqrt{\rho} \quad (68)$$

Where  $\rho$  is the constant defined in Equation ( 2 ).

The peeling moment in Equation ( 68 ) is constant along the length of the pad. The peeling moment depends on the cross section and the elastic properties of the pad through the constant  $\rho$  and increases with greater adhesion force.

### 6.3.7 Combination of uniform load and moment to peel off the adhesive pad

The locomotion of the robot detaches the pad by applying force with the vertical motor and can also apply force with the horizontal motor. When the vertical motor is actuated, the force from the motor is applied along the area of the pad and thus a uniform load is applied to the pad. The weight of the robot is also a uniform load applied to the pad. When the horizontal motor is actuated, the force from the motor is applied at a distance from the pad and thus a moment is applied to the pad.

Following Kendall's peeling theory, in order to find the combination of uniform load and moment to peel off the pad, the total energy of the system ( $U_T^{q,M}$ ) is minimised with respect to the distance from the supported end of the pad ( $x$ ):

$$\frac{\partial U_T^{q,M}}{\partial x} = 0 \quad (69)$$

The total energy of the system when a combination of uniform load and moment is applied to the pad is:

$$U_T^{q,M} = U_S^{q,M} + U_B^{q,M} + U_P^{q,M} \quad (70)$$

The terms of the total energy in Equation ( 70 ) are:

- $U_S^{q,M}$  is the work of adhesion along the surface of the pad:

$$U_S^{q,M} = -b \cdot x \cdot W_{adh} \quad (71)$$

where  $b$  is the width of the pad,  $x$  is the distance from the supported end of the pad and  $W_{adh}$  is the work of adhesion of the pad per unit area.

- $U_B^q$  is the work of the bending moment of the pad, causing the pad to bend an angle  $\theta_q(x)$ :

$$U_B^q = \int M_z^q(x) \cdot d\theta_q(x) + \int M \cdot d\theta_M(x) \quad (72)$$

where  $M_z^q(x)$  is the bending moment defined by Euler-Bernoulli's beam theory in Equation ( 43 ),  $\theta_q(x)$  is the slope defined in Equation ( 42 ),  $M$  is the moment applied to the pad, which is also the bending moment defined by Euler-Bernoulli's beam theory in Equation ( 46 ), and  $\theta_M(x)$  is the slope defined in Equation ( 45 ).

- $U_P^{q,M}$  is the work done by the uniform load applied to the pad along the distance between the pad and the tissue:

$$U_P^{q,M} = \int q(x) \cdot dz_q(x) \quad (73)$$

where  $q(x)$  is the peeling uniform load and  $z_q(x)$  is the distance between the pad and the tissue defined by Equation ( 41 ).

Figure 126a shows the vertical motor and the horizontal motor of the robot applying a combination of uniform load and moment to the pad. Figure 126b shows a sketch of the pad peeling off the surface when a uniform load and a moment are applied to the pad. Figure 126a and Figure 126b also show the parameters considered in order to obtain the combination of uniform load and moment that causes the pad to peel off.

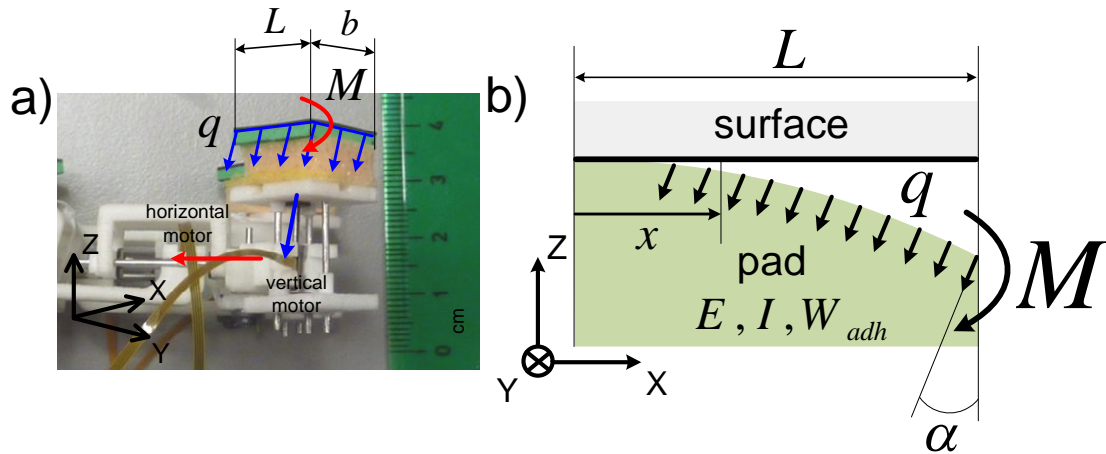


**Figure 126. (a) Combination of uniform load and moment applied to the adhesive pad and (b) sketch of the pad peeling when uniform load and moment are applied to the pad.**

The uniform load and moment are considered constant along the length of the pad and the uniform load is applied at an angle  $\alpha$  from the vertical as shown in Figure 126. Solving Equation ( 69 ), the expression of the peeling uniform load and moment is:

$$M(x) = \sqrt{\rho - \left(\frac{q \cdot \cos(\alpha)}{2 \cdot \sqrt{3}}\right)^2 \cdot l^q(x, L)} \quad (74)$$

$$q(x) = \frac{2 \cdot \sqrt{3}}{\cos(\alpha)} \cdot \sqrt{\frac{\rho - M^2}{l^q(x, L)}} \quad (75)$$

Where  $\rho$  is the constant defined in Equation ( 2 ),  $\alpha$  is the angle of inclination of the uniform load and  $L$  is the total length of the pad;  $x$  is the distance from the supported end of the pad and  $l^q(x, L)$  is the polynomial defined in Equation ( 62 ).

The maximum moment in order to keep the solution of Equation ( 75 ) a real number is:

$$M = \sqrt{\rho} \quad (76)$$

The moment in Equation ( 76 ) is the peeling moment when only a moment is applied to the pad, see Equation ( 68 ).

The maximum uniform load in order to keep the solution of Equation ( 74 ) a real number is:

$$q(x) = \frac{2 \cdot \sqrt{3}}{\cos(\alpha)} \cdot \sqrt{\frac{\rho}{l^q(x, L)}} \quad (77)$$

The moment in Equation ( 77 ) is the peeling uniform load when only a uniform load is applied to the pad.

The value of  $l^q(x, L)$  to calculate the peeling uniform load of the pad was shown in Figure 124 and corresponds to the point  $x = \frac{2}{5}L$ .

Thus, the peeling moment is calculated using Equation ( 74 ) for a value of uniform load between zero and the maximum load:  $q \in [0, \frac{2 \cdot \sqrt{3}}{\cos(\alpha)} \cdot \sqrt{\frac{\rho}{l_{MIN}^q}}]$ .

Likewise, the peeling uniform load is calculated using Equation ( 75 ) for a moment between zero and the maximum moment:  $M \in [0, \sqrt{\rho}]$ .

## 6.4 Calculations of peeling force, uniform load and moment for the bio-mimetic adhesive pad

This section applies the equations of peeling force, peeling uniform load and peeling moment to the bio-mimetic adhesive pad used for the robot to move on tissue. The bio-mimetic pad is made of a bio-compatible soft elastomer: MacDermid Autotex<sup>®</sup>, with Young's modulus  $E = 187.5 \text{ MPa}$  [164]. The dimensions of the bio-mimetic pad are:  $L \cdot b \cdot t = 1 \text{ cm} \cdot 1 \text{ cm} \cdot 0.1 \text{ cm}$  (length x width x thickness) and thus, the area moment of inertia of the pad is  $I = \frac{L \cdot t^3}{12} = 8.3 \cdot 10^{-13} \text{ m}^4$ .

In order to calculate the value of the constant  $\rho$ :  $\rho = E \cdot I \cdot W_{adh} \cdot b$ , the work of adhesion of the bio-mimetic pad on peritoneum is required. The work of adhesion of the pad is calculated with an indentation test on a sample of rat peritoneum.

### 6.4.1 Indentation test to calculate the work of adhesion of the pad

An indentation test of the pad provides a force-distance graph of the pad attaching and detaching from tissue. The work of adhesion is calculated from this force-distance graph as the area between the force and the horizontal axis of the graph representing the distance travelled by the pad during detachment. Figure 127 shows the force-distance graph obtained with an indentation test and the area of the plot corresponding to the work of adhesion of the pad.

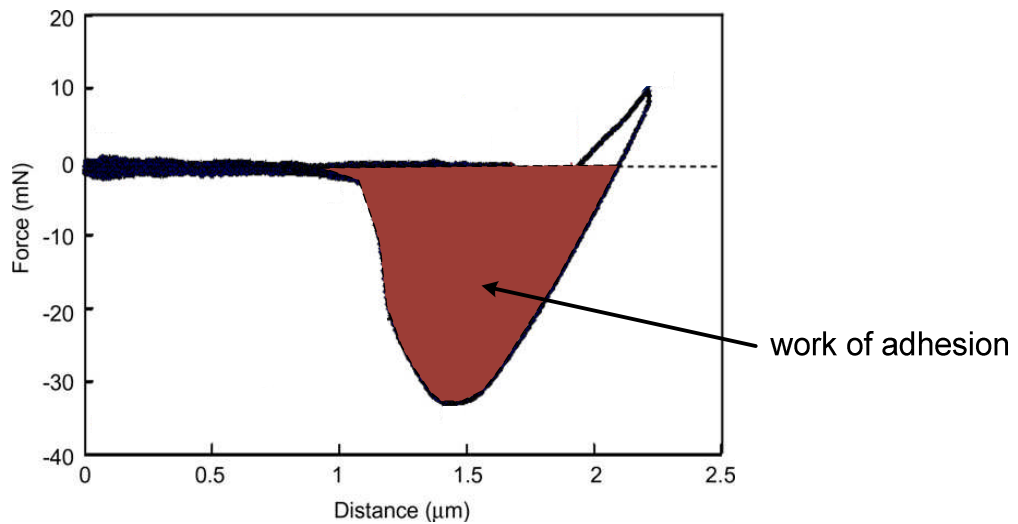


**Figure 127. Work of adhesion of the pad from the force-distance graph of an indentation test taken from [8].**

The indentation test is carried out with a Modular Universal Surface Tester (MUST). The MUST rig drives two pieces of material into contact with a predetermined value of preload and then separates them, measuring the attachment force.

For the indentation test of the bio-mimetic pad on peritoneum in the MUST rig, the pad is fixed to a plate that moves towards a force sensor. A piece of tissue is fixed to the cantilever of the force sensor in order to measure the force applied to the tissue. Figure 128 explains the indentation test showing the events of the test on a force-displacement graph obtained for the adhesive pad on peritoneum.

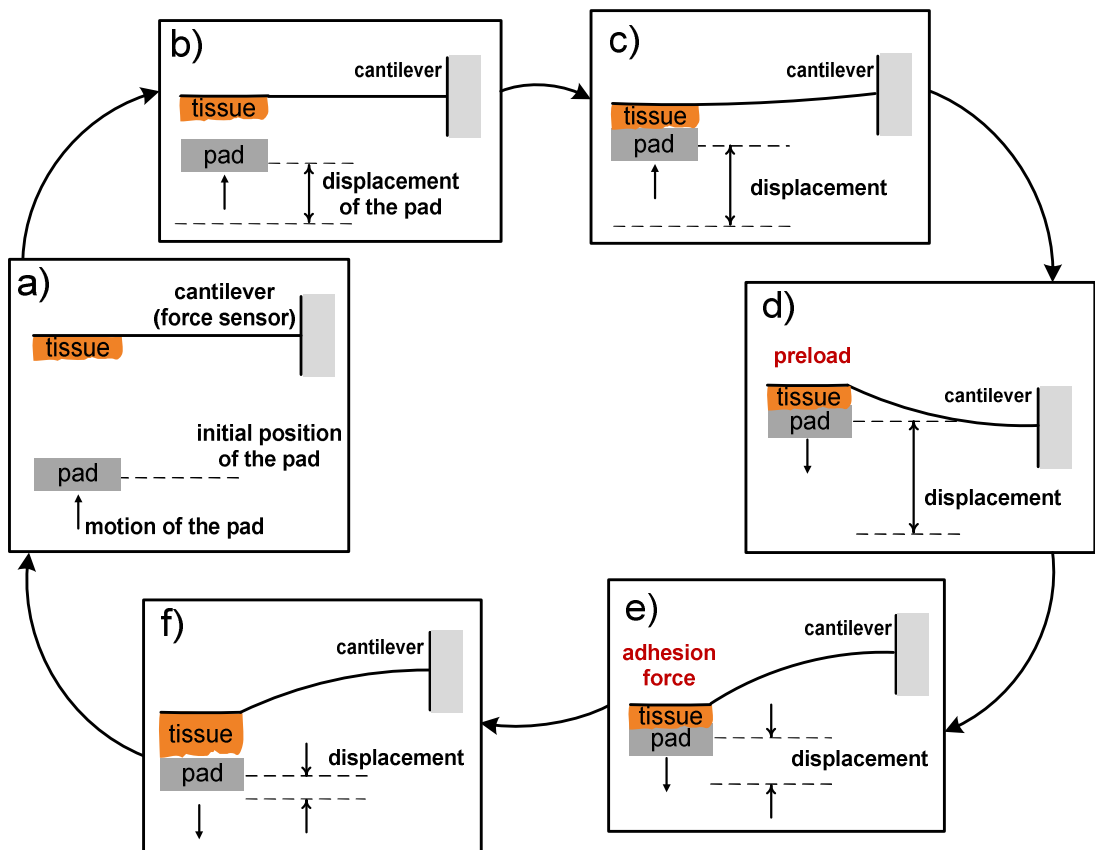
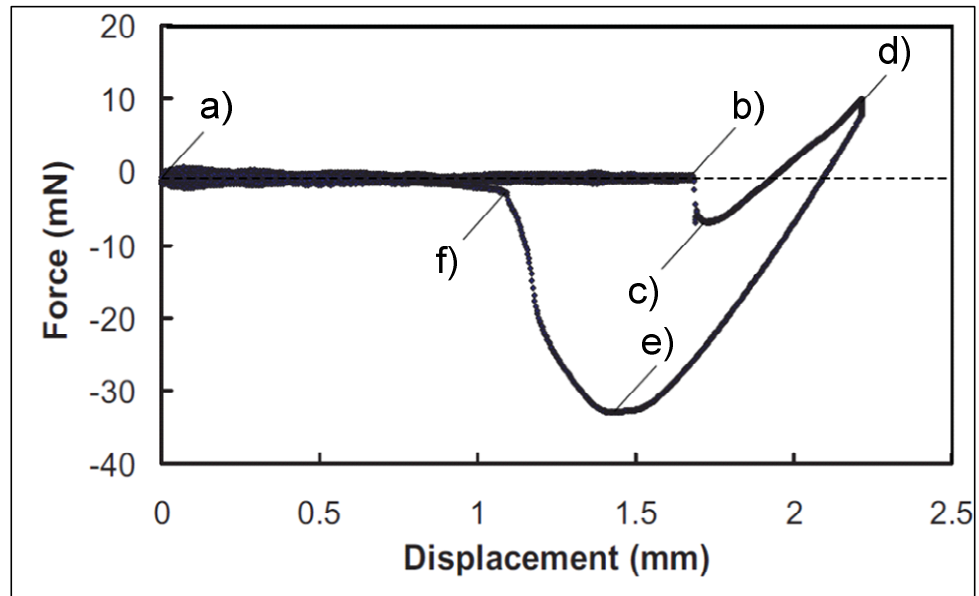


Figure 128. (a-f) Events of an indentation test for the adhesive pad shown below a force-displacement graph from [8].

In Figure 128, the events of an indentation test for the adhesive pad on tissue are:

- a) Initial position of the pad and the cantilever: the displacement of the pad is zero and there is no force applied to the tissue.

- b) An attraction force appears between the pad and the tissue when the pad is close to the tissue, this is registered by the force sensor as a negative value of force. This attraction force is due to interfacial forces between the surface of the pad and the surface of the tissue.
- c) Contact happens between the pad and the tissue, the pad pushes into the tissue in order to reach the preload.
- d) Preload: the value of preload force is reached. The preload is set to the programme of the MUST rig before the experiment starts and is registered by the force sensor as a positive value of force. Once the preload is reached, the motor moving the pad changes direction of motion and starts retracting the pad from the tissue.
- e) Adhesion force: the adhesion force is the maximum force registered by the cantilever when the pad is retracting from the tissue. This is registered by the force sensor as a negative value of force. After this point, the pad and the tissue start separating.
- f) Contact is lost between the pad and the tissue and the value of force registered by the sensor returns to zero.

In this way, for a given value of preload (see Figure 128d), the value of adhesion force (see Figure 128e) is obtained with an indentation experiment. When tested on peritoneum, a bio-mimetic adhesive pad with an area of  $113 \text{ mm}^2$  provides a maximum adhesion force between 105 and 140 mN [10]. The work of adhesion of the bio-mimetic adhesive pad on peritoneum is  $W_{adh} = 94 \text{ mJ/m}^2$  and thus, the value of the constant  $\rho$  for the pad is  $\rho = 1,444 \text{ mN}^2 \text{ cm}^2$ .

#### **6.4.2 Force, uniform load and moment to peel the pad**

The peeling force is considered constant and applied to the edge of the pad in a direction perpendicular to the surface of the pad:  $\alpha \cong 0^\circ$ . Applying Equation ( 55 ) of the peeling model to the bio-mimetic adhesive pad, the resulting peeling force is  $F = 54 \text{ mN}$ . This means that hanging 5.4 *grammes* of weight from the edge of the pad is sufficient to peel off the pad. The density of the material of the pad (MacDermid Autotex<sup>®</sup>) is  $1.4 \text{ g/cm}^3$  [164] and thus the weight of the pad is  $1.4 \text{ mN}$ , so the peeling force is approximately 38 times the weight of the pad.

The peeling moment is considered constant and applied to the edge of the pad. Applying Equation ( 63 ) of the peeling model to the bio-mimetic adhesive pad, the resulting peeling moment is  $M = 38 \text{ mNcm}$ . In the locomotion mechanism of the robot, the moment on the pad is applied by actuating the horizontal motor at a distance of  $2.5 - 2 \text{ cm}$  from the pad. Thus, applying a horizontal force of  $15 - 19 \text{ mN}$  at  $2.5 - 2 \text{ cm}$  of distance from the pad is sufficient to peel off the pad. Applying a peeling moment

instead of a peeling force reduces the force required from the motor to peel off the pad. The force required for the peeling moment is between 11 and 14 times the weight of the pad and approximately a third of the force required when applying a peeling force from the edge of the pad.

The peeling uniform load is considered constant and applied along the length of the pad in a direction perpendicular to the surface of the pad:  $\alpha \cong 0^\circ$ . Applying Equation ( 68 ) of the peeling model to the bio-mimetic adhesive pad, the resulting peeling uniform load along the length of the pad is  $q \cdot L = 130 \text{ mN}$ . This means that a force of 130 mN applied to the pad, or a mass of 13 grammes hanging from the pad, is sufficient to peel off the pad. Therefore, the peeling uniform load is 93 times the weight of the pad and more than twice the force required when applying a peeling force from the edge of the pad.

Figure 129 summarises and compares the force required from the motors of the locomotion mechanism in order to peel off the pad applying a force, a moment and a uniform load.

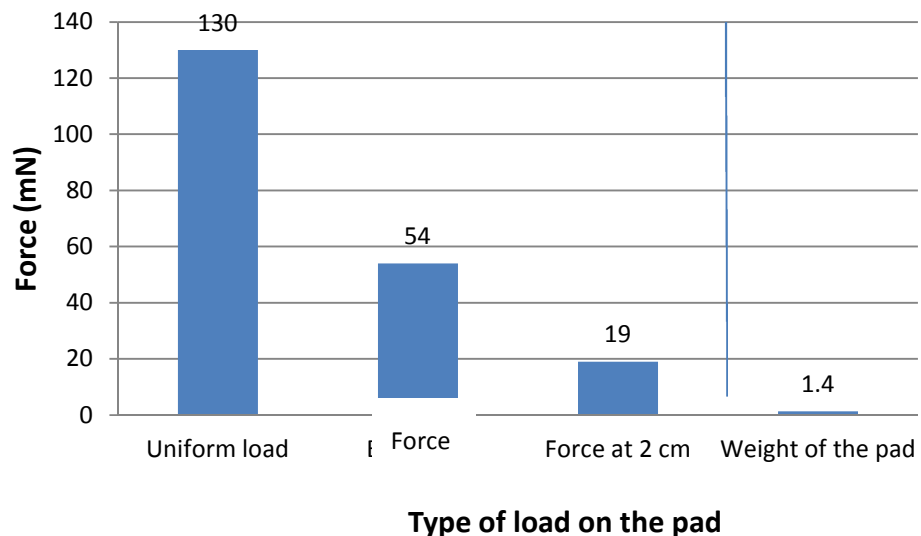


**Figure 129. Comparison of the force required in order to peel off the pad with a uniform load (see configuration in Figure 123), a force at the edge of the pad (see configuration in Figure 121) and a moment: force at 2cm from the pad (see configuration in Figure 125). The weight of the pad is shown as a reference value, as it is the minimum force the adhesive pad must support.**

For these calculations, the material of the adhesive surface (MacDermid Autotex<sup>®</sup>) is the only material considered for the bending of the pad. The value of the peeling force, moment and uniform load is proportional to the constant  $\rho$ , which depends on the material because  $\rho$  is proportional to the square root of the Young's modulus of the pad:  $\rho \propto \sqrt{E}$ . The constant  $\rho$  is sensitive to the thickness of the pad because  $\rho$  is proportional to the square

root of the area moment of inertia:  $\rho \propto \sqrt{I}$ , and the area moment of inertia is proportional to the cube of the thickness of the pad:  $I \propto t^3$ .

Considering the material of the adhesive surface the only material bending in the pad is a simplification of the peeling model because the pad is composed of several layers of different materials. Thus, the thickness of the pad affecting the area moment of inertia can be greater than the thickness of the adhesive surface. Figure 130 shows the value of peeling uniform load for several values of thickness considered for the pad. The calculations of uniform load for Figure 130 only consider the Young's modulus of the adhesive surface for the whole thickness of the pad.

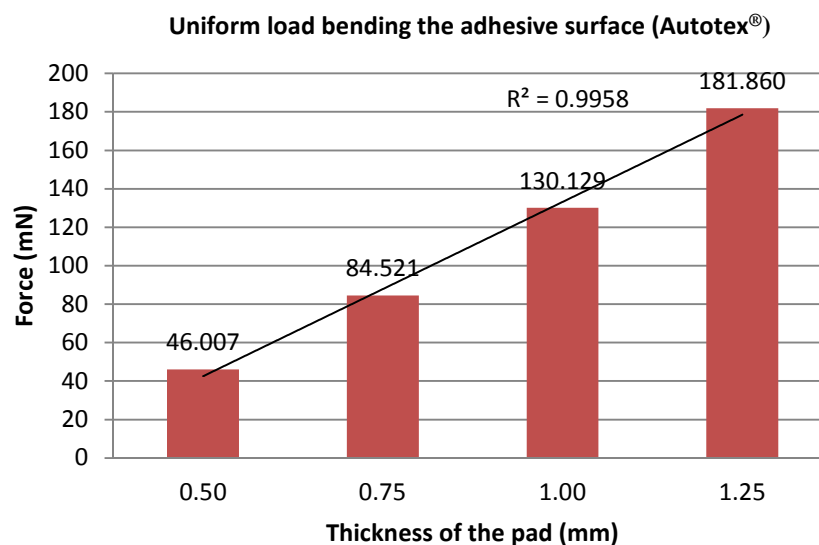


**Figure 130. Uniform load to peel off the pad when only the adhesive surface is bending for several values of thickness of the pad.**

If the tissue is softer than the pad, the motors bend the tissue in order to peel off the pad. In this case, the bending caused on the surface of the tissue determines the peeling force, moment and uniform load. In order to apply the peeling model to the locomotion of the robot on tissue, the peeling model should consider both the properties of the materials of the pad and the properties of the tissue. Figure 131 shows the value of peeling uniform load when only the tissue is bending, considering several values of thickness of the tissue.

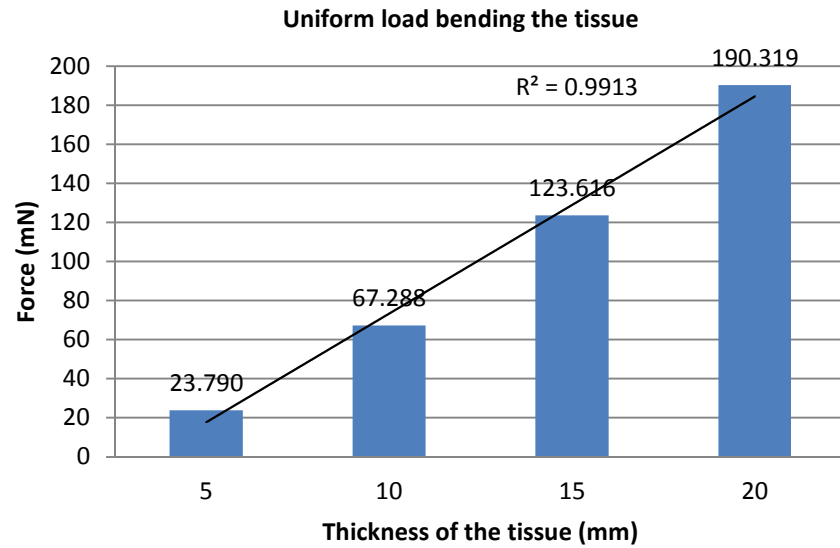


Figure 131. Uniform load to peel off the pad when only the tissue is bending for several values of thickness of the tissue.

### 6.4.3 Combination of uniform load and moment to peel the pad

In the locomotion mechanism of the robot, the vertical motor and the horizontal motor can be actuated simultaneously applying a combination of uniform load and moment to the bio-mimetic adhesive pad. This combination of uniform load and moment is calculated with Equations ( 74 ) and ( 75 ) of the peeling model. For a uniform load between 0 and 130 mN applied by the vertical motor to the pad, a force between 0 and 19 mN can be applied from the horizontal motor. In the locomotion mechanism of the robot, the horizontal motor applies force at approximately 2 cm from the pad, causing a peeling moment on the pad. Figure 132 illustrates the combination of force from a vertical motor and a horizontal motor in order to peel off the pad by applying a uniform load and a moment.

The graph in Figure 132 shows that for each increment of force from the vertical motor, the force required from the horizontal motor in order to peel off the pad decreases at a much slower rate. For a linear increment of vertical force, the horizontal force follows a polynomial line. The value of horizontal force is practically constant up to a vertical force of 50 mN as shown in Figure 132 (combined actuation point number 5). Thus, for low values of vertical force, practically the same horizontal force is required to peel off the pad; for high values of vertical force, the horizontal force required to peel off the pad diminishes accordingly.

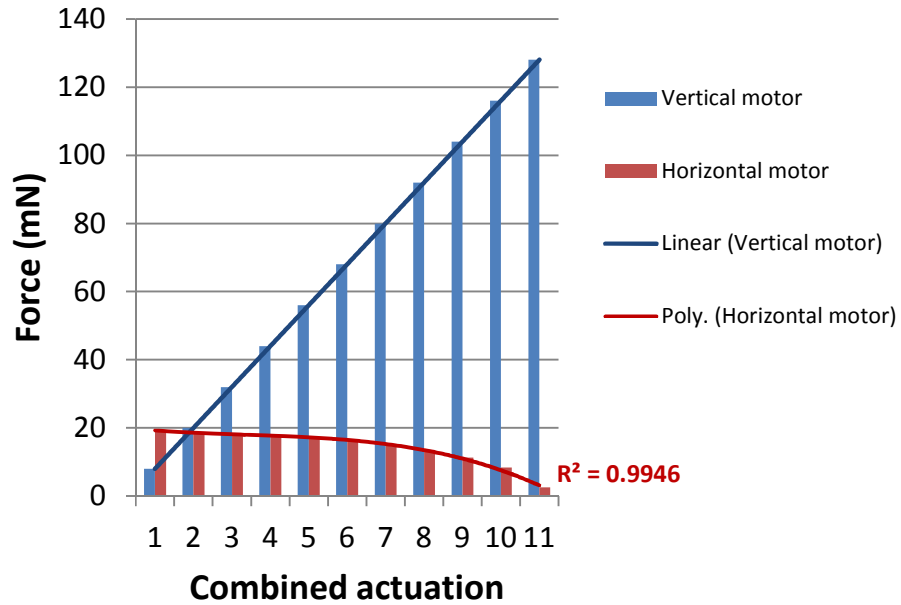


Figure 132. Combination of peeling uniform load and moment applied to the pad.

#### 6.4.4 Comparison between the peeling model and experimental results

When the pad is tested on rat peritoneum without a soft backing layer for the pad, the force required from a linear actuator to detach the pad is between 105 and 140 mN [10]. If there is no soft backing layer for the pad, the pad force from the actuator bends the tissue and the bending of the tissue determines the peeling force.

According to the peeling model, a peeling uniform load between 105 and 140 is obtained for a thickness of the tissue between 10 and 20 mm (see Figure 131). For a pad with a soft backing layer, a peeling uniform load between 105 and 140 is obtained for a thickness of the adhesive surface between 0.75 and 1.25 mm (see Figure 130).

As part of a project associated to the research of this thesis, experiments were carried out in order to compare peeling-off of with a uniform load and peeling-off with a force applied to the edge of the pad [169]. The experiments of this associated project also investigated the effect of peeling angle when a force is applied to the edge of the pad [169]. Figure 133a and Figure 133b are taken from the work carried out in this associated project. Figure 133a shows the force-displacement graph of an indentation test comparing the uniform load required to peel off the pad and the peeling force when a force is applied to the edge of the pad. Figure 133b shows the force-displacement graph of an indentation test comparing the peeling force required when the peeling angle is 0° and when the peeling angle is 45°.

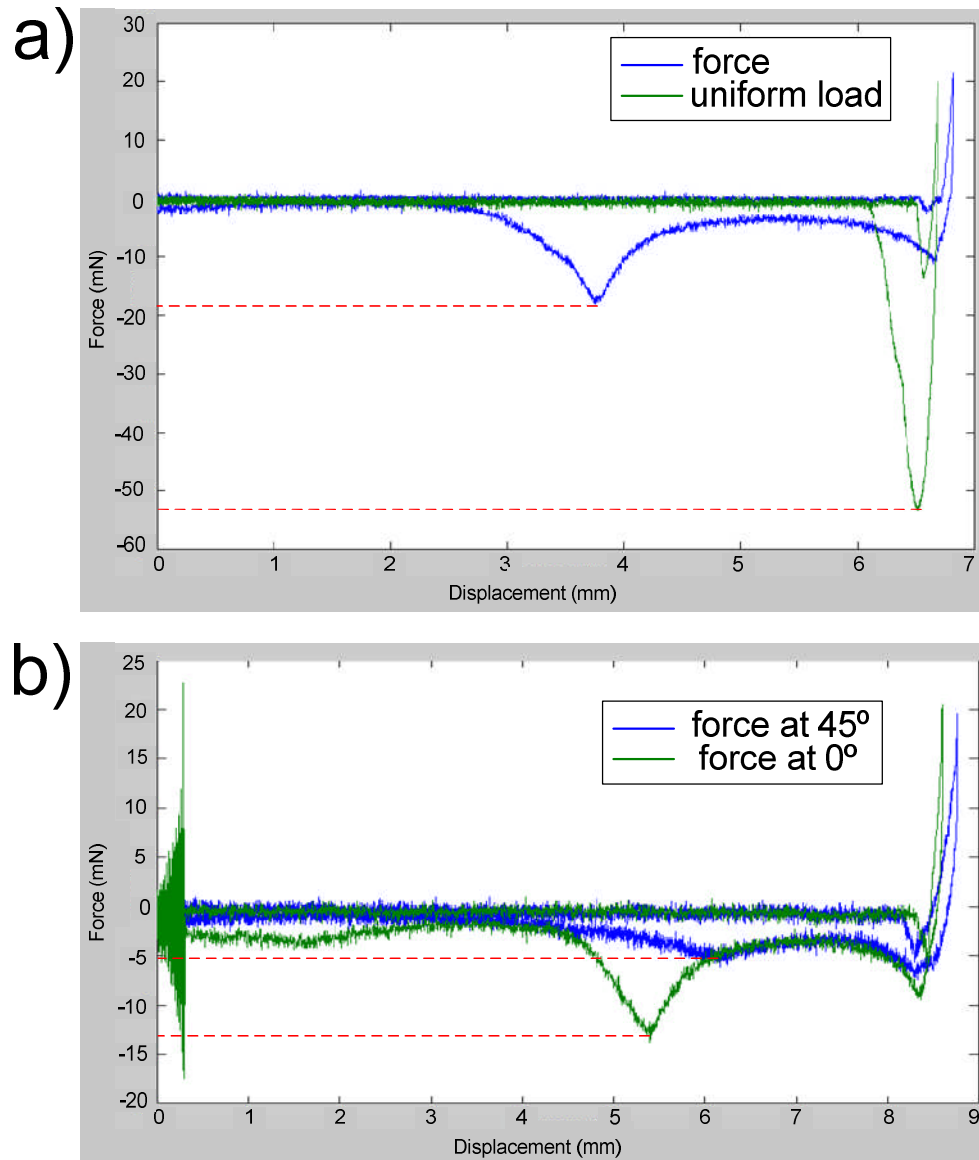


**Figure 133. (a) Force-displacement graph comparing the peeling force and peeling uniform load of the bio-mimetic adhesive pad, and (b) force-displacement graph comparing the peeling force at 0° and 45°, adapted from [169].**

In Figure 133a, the force required to detach the pad is reduced from 53 mN to 18 mN when a peeling force is applied to the edge of the pad compared to a peeling uniform load. Thus, the force required to detach the pad is reduced by 3 when the force is applied to the edge of the pad according to experimental data [169]. The peeling model predicts that the force to detach the pad is reduced by 2.4 when the force is applied to the edge of the pad (see Figure 129). The difference in value obtained between the experimental data and the peeling model can be due to these sources of error:

- in the experimental set-up, the mechanism used in the MUST rig in order to apply a force to the edge of the pad diminishes the force required to detach the pad,

- in the experimental set-up, when the pad and the tissue are in contact, the weight of the pad causes a moment, reducing the value of force required to detach the pad.
- in the peeling model, it is difficult to choose which material bends when a force is applied to the pad and what thickness of the pad should be considered.

In Figure 133b, when the peeling angle increases from  $0^\circ$  to  $45^\circ$ , the force to detach the pad diminishes from 13.2 mN to 5.3 mN. However, the peeling model predicts that the peeling force increases with the peeling angle, see Equation ( 52 ). This discrepancy between experimental data and the peeling model is because, for the sake of simplicity, the peeling model does not consider the effect of shear force on the adhesive. Shear force can indeed have a great effect on the adhesion of the pad as shown in Figure 133b and in previous experimental work [10], and a future development of the peeling model should include this effect in its formulation.

## 6.5 Discussion and conclusion

The peeling model presented in this chapter enables calculation of the force and moment required to peel off an adhesive pad and therefore sets the base for controlling the attachment of the robot to the tissue. The premise of the model, that the pads peel off when bent by the vertical and horizontal forces applied to them, is based on the testing and observation of the locomotion sequence of the robot. For the formulation of the model, it was postulated that the peeling off of the pad could be explained with Kendall's theory and that the bending of the pad followed Euler-Bernoulli's equations.

The value of peeling-off uniform load calculated with the model: 130 mN, is consistent with the value of detachment force found out experimentally for the pad: 105-140 mN. The model also predicts a ratio between the peeling uniform load and the peeling force of 2.4 times, consistent with experimental measurements: 3 times. This comparison between the predictions of the model and the result of experimental work prove the suitability of the model in postulating that Kendall's and Euler-Bernoulli's theories were applicable to the observed peeling off and bending of the pad. Nonetheless, for the sake of simplicity and in order to make the model easy to manage mathematically, the effect of some variables present in the system have not been factored in. These variables include the effect of a shearing force applied to the adhesive surface and the thickness of the pad and tissue that is considered to bend under the action of a force or moment. Notably, the effect of a shearing force, the component of the force or uniform load parallel to the

tissue, can be very effective in detaching the pad. Currently, this effect and others are not considered in the peeling model and will need to be included in further developments in order for the model to represent the variables taking effect in the detachment process more accurately.

In any case, the comparison of the predictions of the model with experimental results proves that an accurate enough description of the detachment process is obtained with the model.

## **6.6 Summary**

In this chapter, detachment of the pad in the locomotion mechanism of the robot is mathematically modelled in order to calculate the force and moment that causes the adhesive pad to detach. This model considers that the pad bends causing the adhesive surface to peel off the tissue when a force or moment is applied to the adhesive surface backed with a soft layer.

In order to calculate the peeling force and moment, the model applies Kendall's peeling theory to the adhesive pad attached to the tissue. The force and moment that cause the pad to peel off are calculated applying Kendall's condition of minimal energy along the length of the pad when the adhesive interface is broken.

In order to calculate the energy of the system, the moment causing the pad to bend is required along with the work of the force and moment applied to the pad. Considering that the pad bends like a cantilever, Euler-Bernoulli's beam theory is used in order to calculate the bending moment on the pad and the work of the force and moment applied to the pad.

Using Kendall's peeling theory and Euler-Bernoulli's bending equations, the expression of the force, uniform load and moment required to peel off the adhesive pad are calculated. This expression of peeling force, peeling uniform load and peeling moment depend on the geometry, material and adhesion of the pad, and the angle of inclination of the force. The combination of uniform load and moment required to peel off the pad is also calculated with the peeling model. In the locomotion mechanism a combination of uniform load and moment is applied to the pad when the vertical motor and the horizontal motor are actuated.

The force, uniform load and moment to peel off the bio-mimetic adhesive pad used for the robot were calculated using the equations of the peeling model. The results of force, uniform load and moment obtained with the peeling model were compared to experimental data obtained prior to the

model. The results of the model are consistent with experimental data when calculating the peeling force applied to the edge of the pad and the peeling uniform load. The predictions of the peeling model can improve by considering the bending of the tissue and the different materials composing the pad as well as by including the effect of a shear force in the model.

## **Chapter 7**

### **Stability criterion for adhesion-reliant robots**

#### **7.1 Introduction**

In the previous chapter, a peeling model of the adhesive pad was presented, enabling to calculate the force and moment that cause the pads of the robot to detach. This peeling model defined the maximum force and moment that can be applied to the pads of the robot before detachment. Using this limit of force and moment, this chapter defines a stability criterion for upside-down locomotion of adhesion-reliant robots.

This chapter starts with a brief review of the stability criteria for walking robots available in the literature. Then, the chapter defines a new stability criterion for the locomotion of adhesion-reliant robots walking upside-down. After that, the chapter analyses the design parameters of a two-padded robot using the stability criterion. The stability criterion is also applied to the stability analysis of a four-padded robot taking one step. The last section summarises the contents of the chapter.

#### **7.2 Stability criteria for walking robots**

Stability for walking robots, especially hexapods, quadrupeds and bipeds, has been extensively researched. Assessing the stability of a robot enables the controller of the robot to avoid an unstable state that makes the robot fall over. For walking robots, several stability criteria have been proposed [67, 170]; these criteria measure stability using a stability margin, which calculates how close to an unstable state the robot is. Depending on how fast the robot moves, stability criteria are divided into:

- static stability criteria: when the robot is walking slow enough to consider its gait a sequence of static positions, and
- dynamic stability criteria: when dynamic effects are important for the stability of the robot.

##### **7.2.1 Static stability criteria for walking robots**

Static stability criteria use the polygon of support of the walking robot in order to define stability. The polygon of support of the robot is the polygon formed by joining the position of the feet of the robot on the ground. For static stability, an unstable state is: “[a state] in which the resultant vector of

the gravitational and inertial forces meets the ground outside the base of support” [70]. This definition was first proposed for a static situation on flat terrain [171] and then extended to uneven terrain [172]. The static stability margin is “the smallest of the distances from the centre of gravity (COG) projection on the ground to the edges of the support polygon” [70]. Figure 134 shows a sketch of the support polygon and the stability margin of a walking robot.

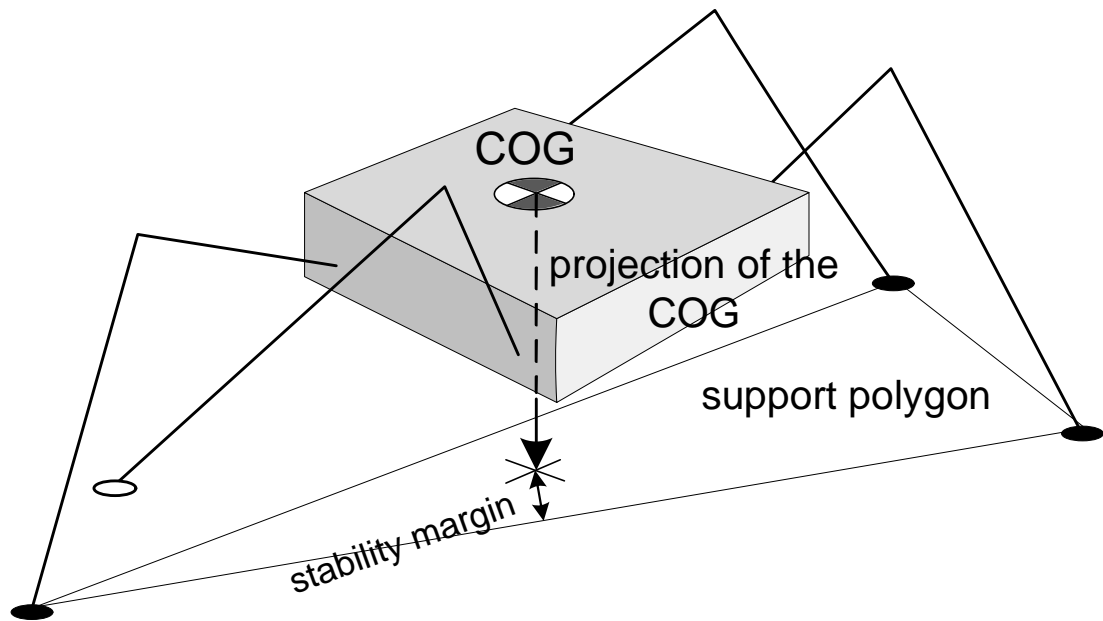


**Figure 134. Sketch of the support polygon and stability margin of a walking robot with one leg in the air.**

Modifications to this static stability criterion have been proposed in order to simplify the computation of the stability margin [173, 174] and guarantee stability of the system in the event of leg failure [175].

Considering the energy of the robot, the energy stability margin is defined as the minimum potential energy required to tip the robot over [176, 177]. Modifications to the energy static stability criterion consider compliant terrain and the stabilizing effect of a leg in the air [178], as well as the power consumption and joint torques of the actuators [179].

For wall climbing robots using magnetic feet, the stability margin has been defined considering the slipping force of the leg [180, 181].

### **7.2.2 Dynamic stability criteria for walking robots**

Considering the dynamic effects on the robot during locomotion, “a robot is dynamically stable if the projection of the COG along the direction of the resultant force acting on the COG lies inside the support polygon” [182]. The

effective mass centre (EMC) is used in dynamic stability and is defined as “the point on the support plane where the resultant moment due to terrain-reaction forces and moments cancel one another” [183].

Considering the moment applied to the robot, the dynamic stability margin is defined as “the smallest of all moments for every rotation axis in the support polygon” [184]. In a scenario where the robot is falling with one leg in the air, the robot is dynamically stable if there is a foot in the direction of rotation of the robot that prevents the fall [185, 186].

Other dynamic stability criteria define stability in terms of the angle of the resultant force on the robot [187] and also in terms of the potential energy and the external disturbances on the robot [188]. Performance criteria of the walking robot have been defined in order to optimise either the energy of the robot or the stability depending on the application of the walking robot [189]. A unified way to assess stability has been proposed with the concept of m-stability [190].

The Zero Moment Point (ZMP) has been used extensively in order to define the stability of bipeds [191, 192]. The ZMP is equivalent to the EMC and corresponds to the point on the ground where the robot can step in order to cancel the horizontal moment acting on the robot and avoid a fall. Based on the ZMP some stability criteria have been defined for humanoids considering the contact and friction of the feet and hands of the robot [193, 194] and also considering the rotation of the foot [195].

### **7.3 Stability criterion for adhesion-reliant robots walking upside-down**

A climbing robot relies on the attachment between the feet of the robot and the surface in order to prevent a fall. If the robot uses adhesive pads, the force of adhesion prevents the robot from falling down and thus, the stability analysis of an adhesion-reliant robot focuses on the adhesion force of the pads. The force and moment affecting adhesion on the pads of the robot are considered in order to measure the stability of an adhesion-reliant robot. The force and moment applied to the pads of the robot determine how close to detachment each pad is, enabling to measure how close to a fall the whole robot is.

This section defines a stability criterion for adhesion-reliant robots walking upside-down considering:

- the role of the adhesive pads during the locomotion sequence, and

- the force and moment that cause the adhesive pad to peel off.

The role of the adhesive pads changes during the locomotion sequence of the robot. Within the locomotion sequence of the robot, the pads can be attached to the surface and therefore supporting the robot, or the pads can be detached and moving to a new position.

The force and moment that cause the adhesive pad to peel off were defined in the peeling model of the previous chapter. According to the peeling model, the value of peeling force and moment depend on the geometry, material and adhesion of the pad.

### 7.3.1 Supporting, moving and critical pads

When the intra-abdominal robot walks upside-down, three pads of the robot resist the pull of gravity while one pad reaches a new position. When this one pad reaches the new position, another pad detaches and starts moving to a new position. In this way, the pads of the robot can be supporting the motion of another pad or moving to a new position, supported by the other pads. Figure 135 shows the supporting pads and the moving pad during the motion of a pad within the locomotion sequence of the intra-abdominal robot.

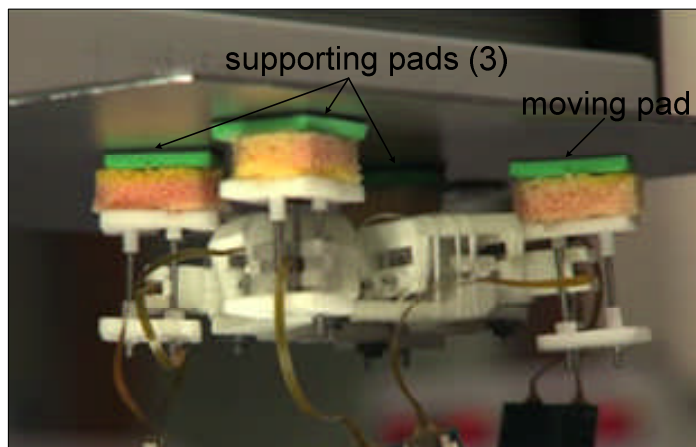


Figure 135. Supporting pads and moving pad of the robot.

In theory, one pad with strong adhesion would be sufficient to keep the robot attached to the surface. However, the robot has been experimentally proved to require a minimum of three supporting pads in order to stay attached to the surface and complete the locomotion sequence. The minimum number of supporting pads required to hold the robot at any one time during the locomotion sequence are the critical pads. If the critical pads detach, the robot is unable to follow the locomotion sequence and reach a new position. The robot is unable to follow the locomotion sequence when the robot falls or when the locomotion mechanism cannot move the pads to the required position. For instance, the weight of the moving pad can bend the supporting

pads in such a way that it is not possible for the robot to re-attach the pad to the surface.

The stability of an adhesion-reliant robot is determined by how close to detachment the critical pads are depending on the force and moment applied to the pads. At any one time during the locomotion sequence, the stability margin of an adhesion-reliant robot can be measured by determining which of the supporting pads are critical and calculating the forces and moments applied to the critical pads.

### 7.3.2 Definition of the detachment margin of an adhesive pad

The force and moment applied to the pad can either detach or preload the pad favouring adhesion, depending on the direction of the force and moment applied by the motors of the robot. Therefore, the total force or moment applied to the pad is:

$$\sigma = \sigma_d - \sigma_a \quad (78)$$

Where  $\sigma$  is the force or moment applied to the pad,  $\sigma_d$  is the total force or moment that causes detachment and  $\sigma_a$  is the total force or moment that preloads the pad.

Considering that the adhesive pad detaches when sufficient force or moment are applied to the pad, the detachment margin of an individual pad of the robot is:

$$\Delta D_p = \frac{\sigma_{det} - \sigma}{\sigma_0} \quad (79)$$

Where:

- $\Delta D_p$  is the detachment margin of the adhesive pad,
- $\sigma$  is the force, moment or combination of force and moment applied to the pad,
- $\sigma_{det}$  is the value of  $\sigma$  that causes detachment of the pad, and
- $\sigma_0$  is the default value of  $\sigma$  present in the system throughout the detachment process, for instance the weight of the pad.

The detachment margin of the adhesive pad:  $\Delta D_p$  considers the force and moment applied to the pad:  $\sigma$ , and compares it to the value of force and moment that peels off the pad:  $\sigma_{det}$ .

The stability margin of the adhesive pad is normalised with respect to the default value of force or moment applied to the pad:  $\sigma_0$ . Normalising the stability margin of the adhesive pad enables comparison of the stability

margin amongst different pads. If there is no default value of  $\sigma$  in the system, the stability margin of an individual pad of the robot is:

$$\Delta D_p = \sigma_{det} - \sigma \quad (80)$$

Where  $\Delta D_p$  is the detachment margin of the adhesive pad,  $\sigma$  is the force, moment or combination of force and moment applied to the pad and  $\sigma_{det}$  is the value of  $\sigma$  that detaches the pad.

Thus, a pad detaches when:

$$\Delta D_p = 0 \quad (81)$$

Where  $\Delta D_p$  is the detachment margin of the adhesive pad defined in Equations ( 79 ) and ( 80 ).

The variables causing detachment of the pad can be dependent on each other. In this case, one of the variables can be used for the calculation of the detachment margin, considering the relation between  $\sigma_{det}$  and the other variables causing detachment of the pad. For this case, the pad detaches when:

$$\Delta D_p(\sigma_{det} = f(\delta_1, \delta_2 \dots \delta_m)) = 0 \quad (82)$$

Where  $\Delta D_p$  is the detachment margin for the selected variable used for the calculation of the detachment margin of the pad. The detachment value of the selected variable:  $\sigma_{det} = f(\delta_1, \delta_2 \dots \delta_m)$  is a function of the other variables that cause detachment of the pad. In Equation ( 82 ), there are  $m$  variables causing detachment of the pad:  $\delta_1, \delta_2 \dots \delta_m$ .

If several variables cause detachment of the pads and these variables are not related, one detachment margin can be calculated for each variable. In this case, the pad detaches when:

$$\prod_{i=1}^n \Delta D_{p_i} = 0 \quad (83)$$

Where  $\Delta D_{p_i}$  is the detachment margin of the pad for the variable  $i$ , and  $n$  is the total number of variables causing detachment of the pads. The detachment margin of the pad is defined as a product of the detachment margin for each variable because the pad detaches as soon as any of those variables reaches its detachment value.

The condition of detachment of the pad, Equation ( 81 ), is applied to the critical pads of the robot in order to detect when the robot is in an unstable state.

### 7.3.3 Definition of the stability criterion for an adhesion-reliant robot

The stability of an adhesion-reliant robot depends on how close to detachment the critical pads of the robot are. The adhesion-reliant robot is in an unstable state if one the critical pads detaches. Considering the detachment margin of the critical pads of the robot, the stability margin of the adhesion-reliant robot is:

$$\Delta S_A = \prod_{i=1}^q \Delta D_{p_i} \quad (84)$$

Where  $\Delta S_A$  is the stability margin of the adhesion-reliant robot,  $\Delta D_{p_i}$  is the detachment margin of the critical pad number  $i$ , and  $q$  is the total number of critical pads of the robot. The stability margin of the robot is defined as a product of the detachment margin of the critical pads because the locomotion of the robot becomes unstable as soon as one critical pad detaches.

The locomotion of an adhesion-reliant robot is stable if all the critical pads are attached at any one time during the locomotion sequence. An adhesion-reliant robot is in an unstable state if one or more of the critical pads lose contact with the surface. Thus, the adhesion-reliant robot is in an unstable state when:

$$\Delta S_A = 0 \quad (85)$$

Where  $\Delta S_A$  is the stability margin of the adhesion-reliant robot defined in Equation ( 84 ).

For the intra-abdominal robot, the variable that determines detachment of the pads:  $\sigma$  is a force, a moment or a combination of force and moment under static or dynamic conditions. The stability criterion defined in Equation ( 85 ) can be applied to other variables, like energy, if those variables also determine the detachment of the pad.

## 7.4 Stability analysis of a two-padded robot

This section considers a robot with two adhesive pads in order to illustrate the stability analysis of an adhesion-reliant robot using the stability criterion defined in Equation ( 85 ). Figure 136 shows the sketch of the two-padded robot considered for this stability analysis.

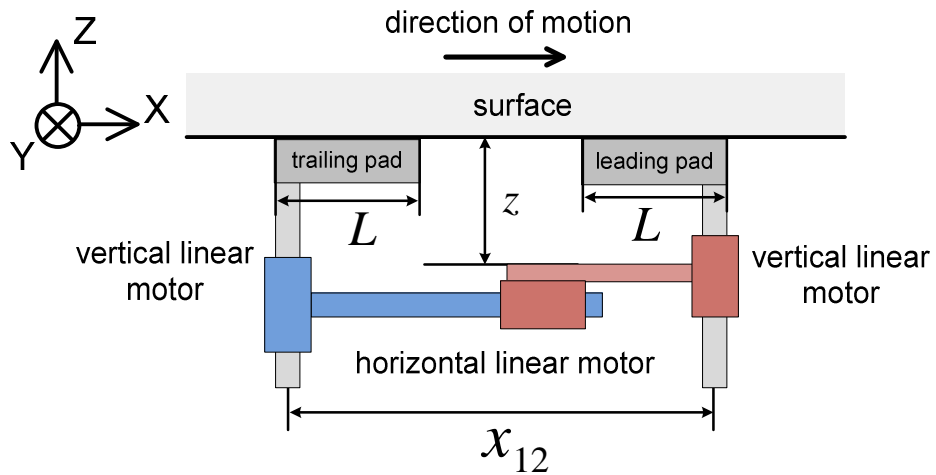


Figure 136. Sketch of a robot with two adhesive pads.

As shown in Figure 136, the parameters considered for the stability analysis of the two-padded robot are:

- the length of the pads:  $L$ ,
- the distance between the surface of attachment and the horizontal linear motor between the two pads:  $z$ , and
- the distance between pads:  $x_{12}$ .

The vertical linear motors are attached to the edge of the adhesive pads and peel off the pads by pulling the adhesive surface from the edge of the pads.

The two-padded robot walks in inverted locomotion on a flat surface using an inchworm locomotion sequence. Figure 137 shows the locomotion sequence of the two-padded robot.

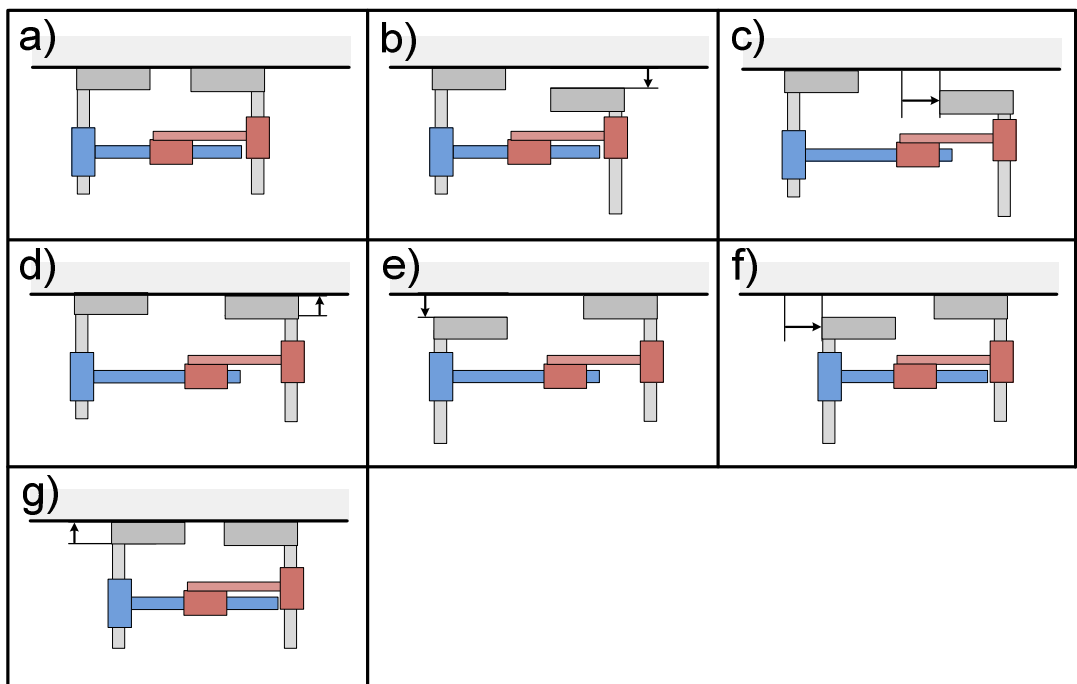


Figure 137. (a-g) Locomotion sequence of the two-padded robot.

In Figure 137, the locomotion sequence of the two-padded robot is:

- a) initial position with the two pads attached to the surface,
- b) the vertical motor of the leading pad pulls the pad, peeling it off the surface,
- c) the horizontal motor moves the leading pad across the surface to a new position,
- d) the vertical motor of the leading pad pushes the pad and re-attaches it to the surface,
- e) the vertical motor of the trailing pad pulls the pad, peeling it off the surface,
- f) the horizontal motor moves the trailing pad across the surface to the new position,
- g) the vertical motor of the trailing pad pushes the pad and re-attaches it to the surface, completing one step of the robot.

In the locomotion sequence of the two-padded robot, each pad of the robot can be:

- detaching, because a vertical motor is peeling off the pad from the surface,
- detached and hanging freely without contact with the surface,
- moving across the surface, because the horizontal motor is moving the pad toward a new position,
- moving towards or away from the surface, following the motion of a vertical motor, and
- attaching to the surface, because a vertical motor is preloading the pad against the surface.

#### **7.4.1 Stability when the pad is detaching from the surface**

In this scenario, the pad is initially attached to the surface and the vertical motor applies a force to the edge of the pad in order to detach it. Figure 138 shows this scenario in the locomotion sequence of the two-padded robot.

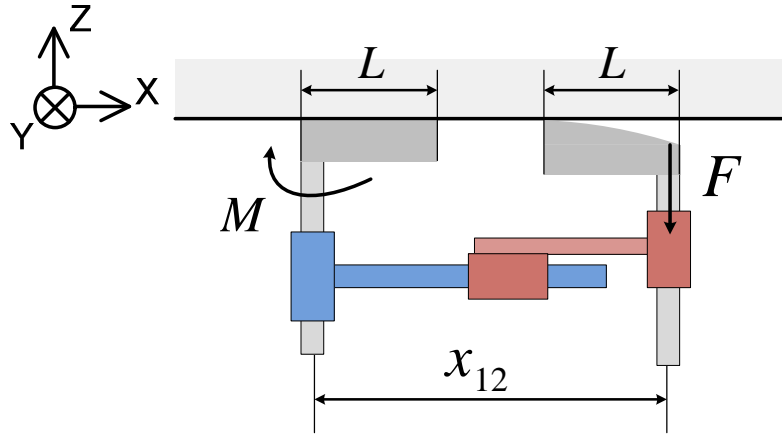


**Figure 138. Force and moment on the pads of the robot when one pad is detaching from the surface. The force shown on the sketch is the force applied at the bottom of the detaching pad by the right vertical motor. The moment shown on the sketch is the moment felt at the top of the supporting pad.**

Figure 138 shows the force applied by the vertical motor to the edge of the moving pad and the resulting moment on the supporting pad. The supporting pad of the robot is the only critical pad and it is considered that there is no default moment applied to the supporting pad. In order to keep the supporting pad attached to the surface, the stability margin of the robot is:

$$\Delta S_A = M_{det} - M > 0 \quad (86)$$

Where  $M$  is the moment applied to the supporting pad and  $M_{det}$  is the peeling moment of the supporting pad.

The peeling moment of the supporting pad, obtained with the peeling model of the pad (see Chapter 6 Equation ( 68 )), is:

$$M_{det} = \sqrt{\rho} \quad (87)$$

The moment on the supporting pad caused by the force on the moving pad is:

$$M = F \cdot x_{12} \quad (88)$$

Where  $M$  is the moment on the supporting pad,  $F$  is the force from the vertical motor, and  $x_{12}$  is the separation between the pads of the robot.

The force from the vertical motor:  $F$  is the force to peel off the pad and is defined by the peeling model (see Chapter 6 Equation ( 55 )) as:

$$F = \frac{\sqrt{2 \cdot \rho}}{L} \quad (89)$$

Where  $L$  is the length of the pad and  $\rho$  is defined by the peeling model as:  $\rho = E \cdot I \cdot W_{adh} \cdot b$  (see Chapter 6 Equation ( 53 )). The constant  $\rho$  depends

on the Young's modulus of the pad:  $E$ , the area moment of inertia of the pad:  $I$ , the work of adhesion:  $W_{adh}$  and the cross section of the pad:  $b$ .

Thus, in order to keep the supporting pad attached to the surface, this condition is obtained:

$$x_{12} < \frac{L}{\sqrt{2}} \quad (90)$$

Where  $x_{12}$  is the distance between the two pads of the robot and  $L$  is the length of the pad.

### 7.4.2 Stability when the pad is detached

In this scenario, the pad is fully detached from the surface and the supporting pad withstands the moment caused by the weight of the detached pad. Figure 139 shows this scenario in the locomotion sequence of the two-padded robot.

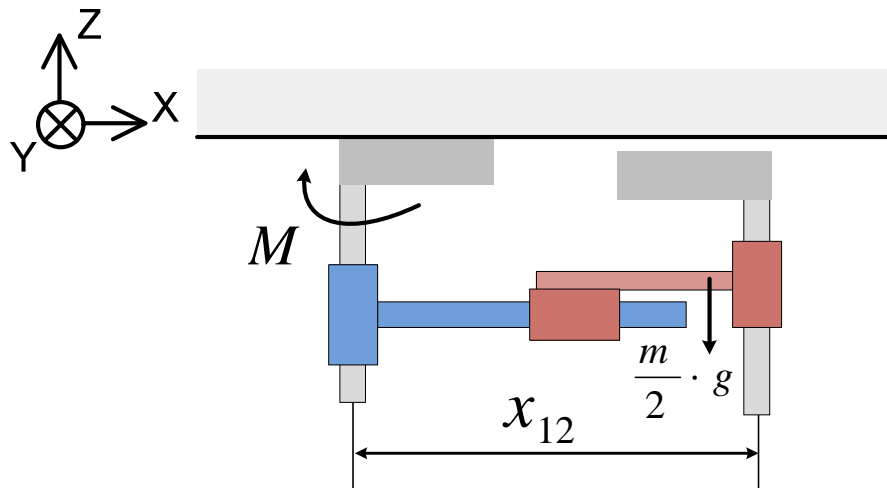


**Figure 139.** Force and moment on the pads of the robot when one pad is detached from the surface.

In order to keep the supporting pad attached to the surface, the stability margin of the robot is:

$$\Delta S_A = M_{det} - M > 0 \quad (91)$$

Where  $M$  is the moment applied to the supporting pad and  $M_{det}$  is the peeling moment of the supporting pad.

The peeling moment of the supporting pad, obtained with the peeling model of the pad, is:

$$M_{det} = \sqrt{\rho} \quad (92)$$

The moment on the supporting pad caused by the weight of the detached pad is:

$$M = \frac{m}{2} \cdot g \cdot x_{12} \quad (93)$$

Where  $m$  is the total mass of the robot,  $\frac{m}{2} \cdot g$  is the weight of the detached pad, assuming even mass distribution, and  $x_{12}$  is the distance between the pads.

Thus, in order to keep the supporting pad attached to the surface, this condition is obtained:

$$m < \frac{2 \cdot \sqrt{\rho}}{g \cdot x_{12}} \quad (94)$$

Where  $m$  is the total mass of the robot and  $x_{12}$  is the distance between the pads of the robot.

### 7.4.3 Stability when the pad moves across the surface

In this scenario, the pad is detached and the horizontal motor is moving the pad to a new position across the surface. The weight of the detached pad and the motion of the pad across the surface cause a moment on the supporting pad. Figure 140 shows this scenario in the locomotion sequence of the two-padded robot.

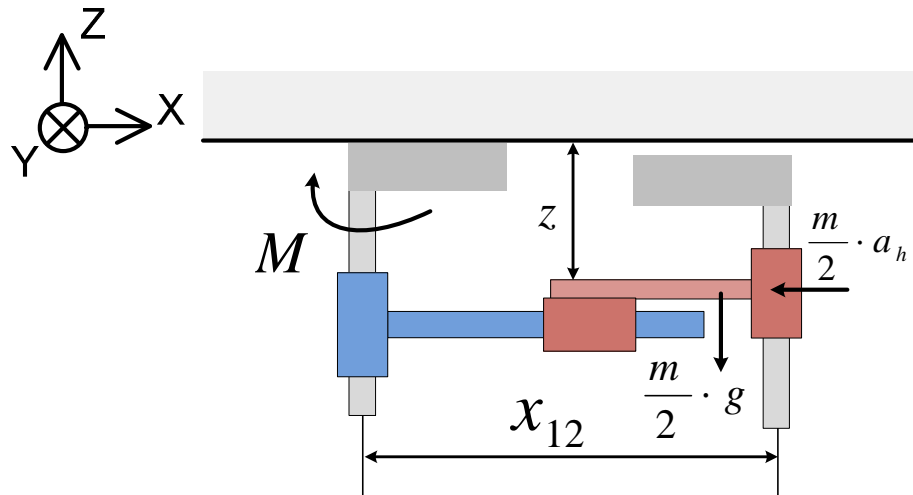


Figure 140. Force and moment on the pads of the robot when the horizontal motor is moving the pad across the surface.

In order to keep the supporting pad attached to the surface, the stability margin of the robot is:

$$\Delta S_A = M_{det} - M > 0 \quad (95)$$

Where  $M$  is the moment applied to the supporting pad and  $M_{det}$  is the peeling moment of the supporting pad.

The peeling moment of the supporting pad, obtained with the peeling model of the pad, is:

$$M_{det} = \sqrt{\rho} \quad (96)$$

In Figure 140, the moment on the supporting pad caused by the weight of the pad and the horizontal motion of the pad is:

$$M = \frac{m}{2} \cdot (g \cdot x_{12} + a_h \cdot z) \quad (97)$$

Where  $m$  is the total mass of the robot,  $\frac{m}{2} \cdot g$  is the weight of the detached pad and  $x_{12}$  is the distance between the pads. The horizontal acceleration of the pad caused by the horizontal motor is  $a_h$ , and  $z$  is the distance between the surface and the horizontal motor.

The direction of the horizontal acceleration on the pad:  $a_h$  and the corresponding moment on the supporting pad:  $M$  are determined by the direction of motion of the horizontal motor. The horizontal motor can move forward causing an acceleration:  $a_h > 0$  or backward, causing an acceleration:  $a_h < 0$ .

For forward motion of the pad:  $a_h > 0$ , in order to keep the supporting pad attached to the surface, this condition is obtained:

$$a_h < \frac{1}{z} \cdot \left( \frac{2 \cdot \sqrt{\rho}}{m} - g \cdot x_{12} \right) \quad (98)$$

For backward motion of the pad:  $a_h < 0$ , in order to keep the supporting pad attached to the surface, this condition is obtained:

$$a_h > \frac{1}{z} \cdot \left( g \cdot x_{12} - \frac{2 \cdot \sqrt{\rho}}{m} \right) \quad (99)$$

In Equations ( 98 ) and ( 99 ):  $a_h$  is the horizontal acceleration of the pad,  $z$  is the distance between the surface and the horizontal motor,  $m$  is the total mass of the robot and  $x_{12}$  is the distance between the pads.

If the pad moves at a constant velocity:  $a_h = 0$ , Equations ( 98 ) and ( 99 ) are equivalent to Equation ( 94 ), when the pad is detached from the surface without moving.

### 7.4.4 Stability when the pad moves toward or away from the surface

In this scenario, the pad is detached and the vertical motor is moving the pad toward or away from the surface. The weight of the detached pad and the vertical motion of the pad cause a moment on the supporting pad. The vertical motor of the pad is either separating the pad from the surface after detachment or moving the pad back to the surface when the pad has reached the new position across the surface. Figure 141 shows this scenario in the locomotion sequence when the pad moves toward or away from the surface.

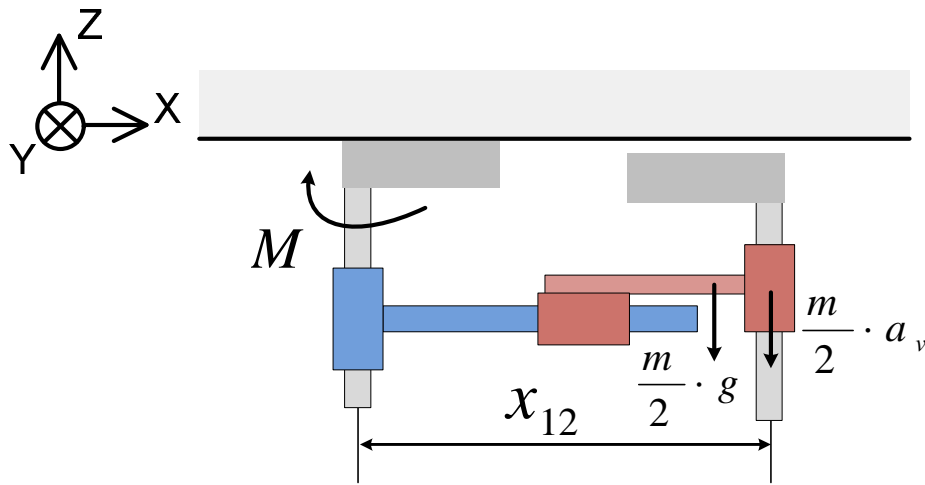


**Figure 141. Force and moment on the pads of the robot when the vertical motor is moving the pad toward or away from the surface.**

In order to keep the supporting pad attached to the surface, the stability margin of the robot is:

$$\Delta S_A = M_{det} - M > 0 \quad (100)$$

Where  $M$  is the moment applied to the supporting pad and  $M_{det}$  is the peeling moment of the supporting pad.

The peeling moment of the supporting pad, obtained with the peeling model of the pad, is:

$$M_{det} = \sqrt{\rho} \quad (101)$$

In Figure 140, the moment on the supporting pad caused by the weight of the pad and the vertical motion of the pad is:

$$M = \frac{m}{2} \cdot (g + a_v) \cdot x_{12} \quad (102)$$

Where  $m$  is the total mass of the robot,  $\frac{m}{2} \cdot g$  is the weight of the detached pad,  $x_{12}$  is the distance between the pads and the vertical acceleration of the pad caused by the horizontal motor is  $a_v$ .

The direction of the vertical acceleration on the pad:  $a_v$  and the corresponding moment on the supporting pad:  $M$  are determined by the direction of motion of the vertical motor. The vertical motor can move upward, causing a vertical acceleration:  $a_v > 0$  or downward, causing a vertical acceleration:  $a_v < 0$ .

For upward motion of the pad:  $a_v > 0$ , in order to keep the supporting pad attached to the surface, this condition is obtained:

$$a_v < \frac{2 \cdot \sqrt{\rho}}{m \cdot x_{12}} - g \quad (103)$$

For downward motion of the pad:  $a_v < 0$ , in order to keep the supporting pad attached to the surface, this condition is obtained:

$$a_v > g - \frac{2 \cdot \sqrt{\rho}}{m \cdot x_{12}} \quad (104)$$

In Equations ( 103 ) and ( 104 ):  $a_v$  is the vertical acceleration of the pad,  $m$  is the total mass of the robot and  $x_{12}$  is the distance between the pads.

If the pad moves at a constant velocity:  $a_v = 0$ , Equations ( 103 ) and ( 104 ) are equivalent to Equation ( 94 ), when the pad is detached from the surface without moving.

#### **7.4.5 Stability when the pad is attaching to the surface**

In this scenario, there is contact between the pad and the surface, and the vertical motor is preloading the pad in order to re-attach it to the surface. There is still no adhesion between the pad and the surface so the weight of the pad causes a moment on the supporting pad. The preload applied by the vertical motor, pushing the pad into the surface, also causes a moment on the supporting pad. Figure 142 shows this scenario in the locomotion sequence of the two-padded robot when the pad is attaching to the surface.

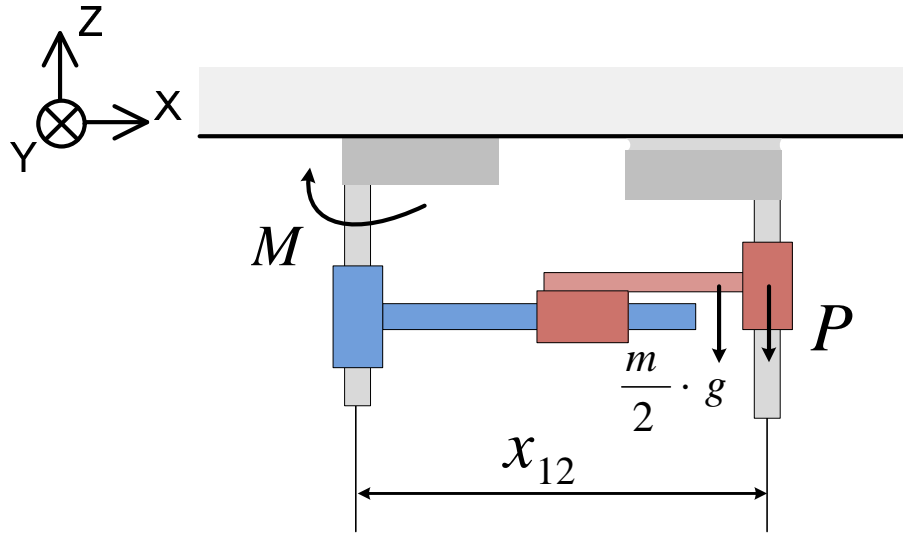


**Figure 142. Force and moment on the pads of the robot when the vertical motor is preloading the pad in order to re-attach it to the surface.**

In order to keep the supporting pad attached to the surface, the stability margin of the robot is:

$$\Delta S_A = M_{det} - M > 0 \quad (105)$$

Where  $M$  is the moment applied to the supporting pad and  $M_{det}$  is the peeling moment of the supporting pad.

The peeling moment of the supporting pad, obtained with the peeling model of the pad, is:

$$M_{det} = \sqrt{\rho} \quad (106)$$

In Figure 140, the moment on the supporting pad caused by the weight of the pad and the preload is:

$$M = (P + \frac{m}{2} \cdot g) \cdot x_{12} \quad (107)$$

Where  $m$  is the total mass of the robot,  $\frac{m}{2} \cdot g$  is the weight of the pad,  $x_{12}$  is the distance between the pads and  $P$  is the preload.

Thus, in order to keep the supporting pad attached to the surface, this condition is obtained:

$$m < \frac{2}{g} \cdot (\frac{\sqrt{\rho}}{x_{12}} - P) \quad (108)$$

If there is no preload:  $P = 0$ , Equation ( 108 ) is equivalent to Equation ( 94 ) when the pad is detached. The upper limit of mass obtained with Equation ( 108 ) is more restrictive than the upper limit of mass obtained with Equation ( 94 ) when the pad is detached.

Equation ( 108 ) also enables to determine the maximum preload that the vertical motor can apply to the pad without detaching the supporting pad. In order not to detach the supporting pad, the preload is:

$$P < \frac{\sqrt{\rho}}{x_{12}} \quad (109)$$

Where  $P$  is the preload applied to the pad and  $x_{12}$  is the distance between the pads.

#### 7.4.6 Design parameters for stable locomotion of the two-padded robot

The application of the stability criterion to the five scenarios in the locomotion sequence of the two-padded robot results in this system of inequalities:

$$x_{12} < \frac{L}{\sqrt{2}} \quad (110)$$

$$m < \frac{2}{g} \cdot \left( \frac{\sqrt{\rho}}{x_{12}} - P \right) \quad (111)$$

$$P < \frac{\sqrt{\rho}}{x_{12}} \quad (112)$$

$$a_h < \frac{1}{z} \cdot \left( \frac{2 \cdot \sqrt{\rho}}{m} - g \cdot x_{12} \right) \quad (113)$$

$$a_h > \frac{1}{z} \cdot \left( g \cdot x_{12} - \frac{2 \cdot \sqrt{\rho}}{m} \right) \quad (114)$$

$$a_v < \frac{2 \cdot \sqrt{\rho}}{m \cdot x_{12}} - g \quad (115)$$

$$a_v > g - \frac{2 \cdot \sqrt{\rho}}{m \cdot x_{12}} \quad (116)$$

This system of inequalities defines the limits of the design parameters of the robot:

- the length of the pad:  $L$ , the distance between the pads of the robot:  $x_{12}$  and the distance between the surface and the horizontal motor:  $z$ ,
- the mass of the robot:  $m$ ,
- the horizontal acceleration that the motors can apply to the pad:  $a_h$ ,
- the vertical acceleration that the motors can apply to the pad:  $a_v$ , and
- the preload that the vertical motors can apply to the pad:  $P$ .

The method to calculate the limits of the design parameters of a two-padded robot is schematically shown in Figure 143.

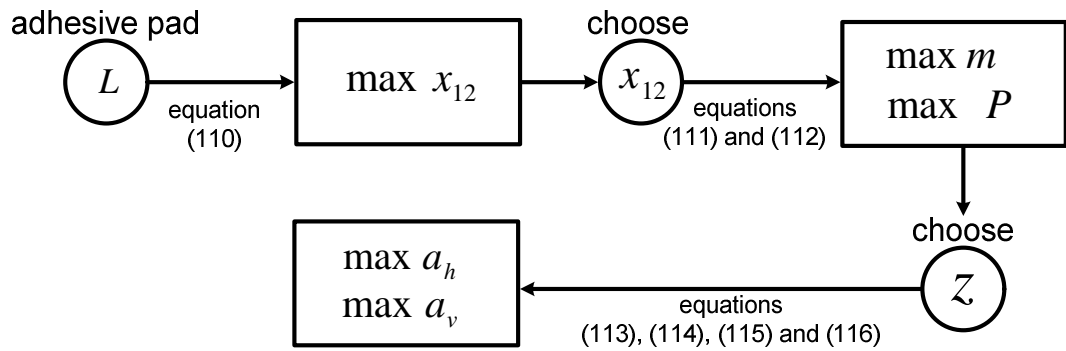


**Figure 143. Calculation of the design parameters for a two-padded robot.**

The calculation of the design parameters of the two-padded robot shown in Figure 143 starts with the length of the pad:  $L$ . The length of the pad:  $L$  is given by the size of the adhesive pad required to support the weight of the robot. For a specific value of  $L$ , a value of the distance between the pads of the robot:  $x_{12}$  is chosen, within the limit given by Equation ( 110 ).

The value of distance between the pads determines the maximum mass of the robot:  $m$ , given by Equation ( 111 ). The value of preload:  $P$  in Equation ( 111 ) is known for a specific adhesive pad and should not exceed the maximum given by Equation ( 112 ).

The distance between the surface and the horizontal link:  $z$  is also chosen for the specific design of the robot. Knowing the distance between the surface and the horizontal link:  $z$ , the limits of the acceleration applied to the pad by the motors can be calculated. Depending on the direction of motion, the limits of horizontal and vertical acceleration:  $a_h$  and  $a_v$ , are calculated with Equations ( 113 )-( 116 ).

Most design parameters are fixed by the design and components of the robot; these parameters are: the length of the pad:  $L$ , the mass of the robot:  $m$ , the maximum acceleration of the motors:  $a_h$  and  $a_v$ , and the preload of the pad:  $P$ .

However, some other design parameters can change within a range during the motion of the robot; these parameters are the distance between the pads of the robot:  $x_{12}$  and the distance between the surface and the horizontal motor:  $z$ . The distance between the pads of the robot is controlled by the horizontal motor, so Equation ( 110 ) determines the maximum separation of the pads within the range of motion of the horizontal motor. The distance between the surface and the horizontal motor is controlled by the vertical motors. Thus, the value of  $z$  chosen for Equation ( 113 ) is the maximum vertical distance within the range of motion of the vertical motor. The value

of  $z$  chosen for Equation ( 114 ) is the minimum vertical distance within the range of motion of the vertical motor.

During the locomotion sequence of the robot, perturbations can occur applying unexpected force and moment to the pads. If the value of the perturbations is measured, the previous equations can calculate the stability margin of the robot considering the perturbations. If an unstable state is detected, the controller of the robot can react against the perturbation bringing the robot back to a stable state.

#### **7.4.7 Design parameters of a two-padded robot using the bio-mimetic adhesive pads**

In this section, the previous method to calculate the design parameters of a two-padded robot is applied to a robot using the bio-mimetic adhesive pads. The calculations in this section give a sense of the order of magnitude of the design parameters for a robot using the bio-mimetic adhesive pads.

The dimensions of the bio-mimetic pad are:  $L \cdot b \cdot t = 1 \text{ cm} \cdot 1 \text{ cm} \cdot 0.1 \text{ cm}$  (Length x width x thickness) and the value of the constant  $\rho$  is  $\rho = 1,444 \text{ mN}^2\text{cm}^2$ .

If the length of the bio-mimetic adhesive pad is  $L = 1 \text{ cm}$ , the distance between the pads is  $x_{12} < 0.71 \text{ cm}$ . Choosing a distance between the vertical motors of  $x_{12} = 0.7 \text{ cm}$ , the preload of the pad is  $P < 55 \text{ mN}$ .

Considering that a preload of  $P = 10 \text{ mN}$  provides the maximum adhesion force available from the pad [10], the total mass of the robot is  $m < 9.2 \text{ grammes}$ . If no preload was required to attach the pad, the maximum mass of the robot would increase 20%, up to  $m < 11.1 \text{ grammes}$ . For a mass of the robot of  $m = 9 \text{ grammes}$ , the weight of the robot is  $w_{robot} = 90 \text{ mN}$  which is around 64 times the weight of the pad.

A distance between the surface and the horizontal motor of  $z = 2 \text{ cm}$  is chosen. Thus, the acceleration from the motors must be  $-0.8 \frac{\text{m}}{\text{s}^2} < a_h < 0.8 \frac{\text{m}}{\text{s}^2}$  in the horizontal direction and  $-2 \frac{\text{m}}{\text{s}^2} < a_v < 2 \frac{\text{m}}{\text{s}^2}$  in the vertical direction.

In order to follow the locomotion sequence of the robot, the motors need to exert a force of:

- $F = \frac{\sqrt{2 \cdot \rho}}{L}$  in order to detach the pad,
- $F = m \cdot a_h$  to move the pad horizontally,
- $F = m \cdot a_v$  to move the pad vertically, and
- $P$  to preload the pad and re-attach it to the surface.

Therefore, the maximum of the previous forces determines the maximum force required from the motors:

$$F_{max} = \max\left(\frac{\sqrt{2 \cdot \rho}}{L}, \frac{m}{2} \cdot \max(|a_h|), \frac{m}{2} \cdot \max(|a_v|), P\right) \quad (117)$$

For the bio-mimetic adhesive pads, the value of maximum force required from the motors is:  $F_{max} = 54 \text{ mN}$ .

## 7.5 Stability analysis of a four-padded robot taking one step

This section considers a robot with four adhesive pads in order to illustrate the stability analysis during the locomotion sequence of the robot using the stability criterion defined in Equation ( 85 ). Figure 144 shows the locomotion sequence for one step of the four-padded robot considered for this stability analysis.

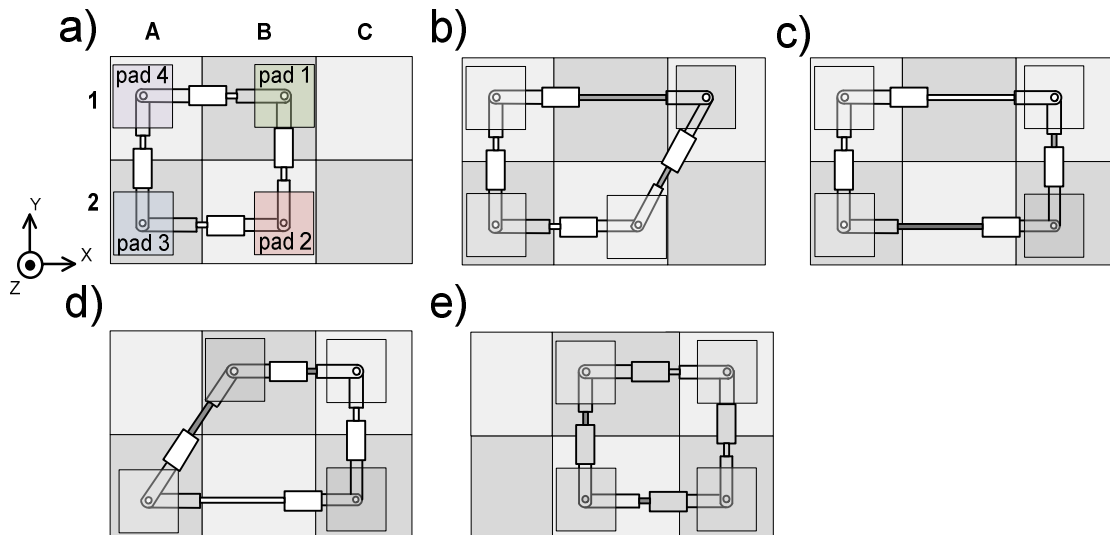


Figure 144. (a-e) Locomotion sequence of a four-padded robot.

For the locomotion sequence in Figure 144, six regions of the surface are considered: A1, A2, B1, B2, C1 and C2, each of these regions provide a

different value of adhesion. In Figure 144, the steps of the locomotion sequence are:

- a) the four pads are initially attached to the surface: pad 1 is attached to region B1, pad 2 is attached to region B2, pad 3 is attached to region A2 and pad 4 is attached to region A1;
- b) pad 1 moves to region C1;
- c) pad 2 moves to region C2;
- d) pad 3 moves to region B1;
- e) pad 4 moves to region B2.

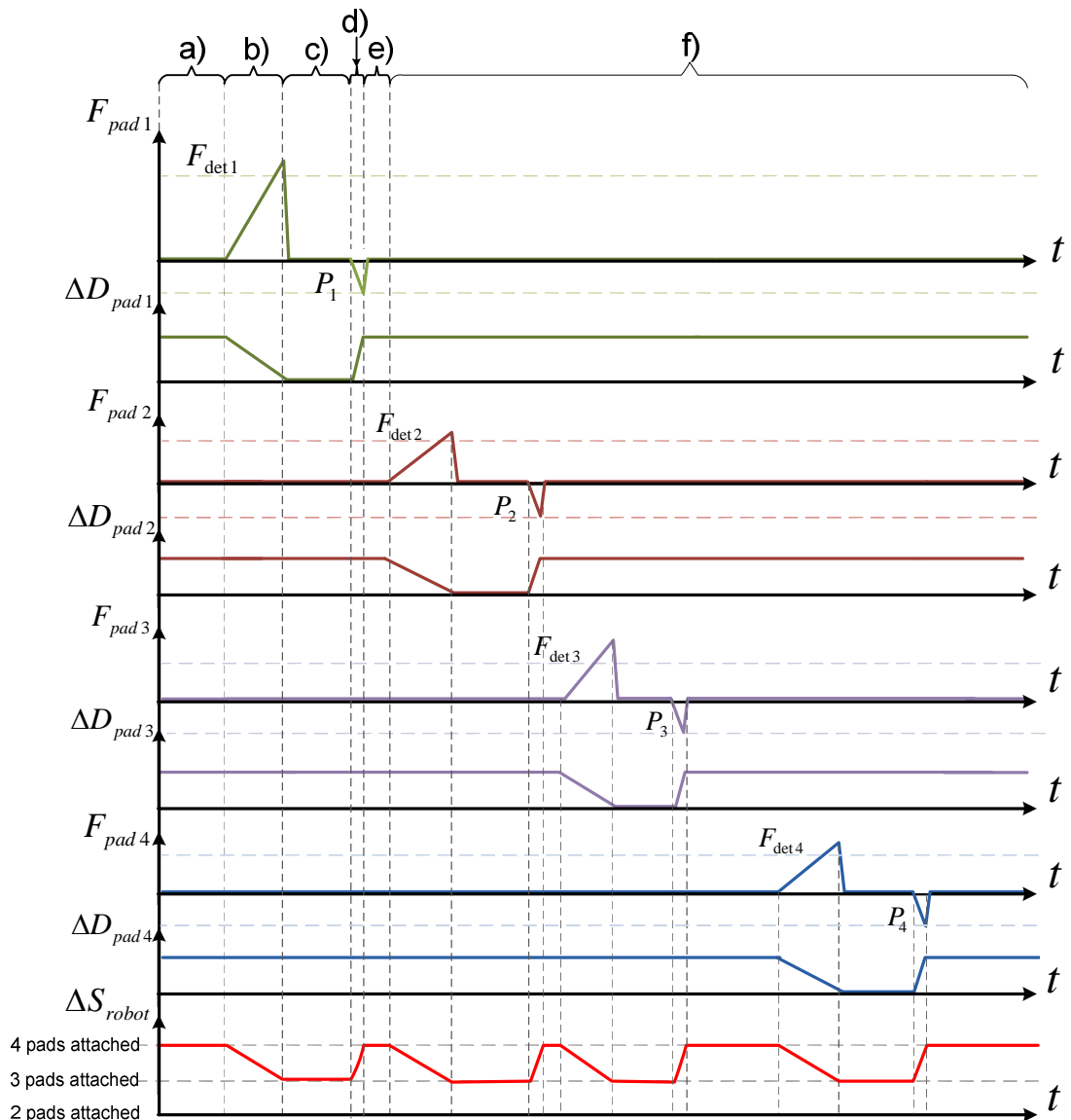
The motion of each pad in Figure 144 requires detaching the pad, moving the pad across to the new region and re-attaching the pad to the new region. The pads are detached by applying a force to the edge of the pad and it is assumed that the force required to peel off the pads is known for each region of the surface. For the sake of simplicity, it is also assumed that the motion of one pad has no effect on the adhesion of the other pads. As proved experimentally, the number of critical pads for this four-padded robot is three, so the locomotion of the robot is unstable if more than one pad are detached.

Figure 145 shows a time diagram of a theoretical simulation of the force applied to the pads of the robot in order to follow the locomotion sequence. Figure 145 also shows how the detachment margin of each pad and the stability margin of the robot change during the locomotion sequence.

In Figure 145, the steps for moving one pad of the robot within the locomotion sequence are:

- a) initially the four pads are attached to the surface, there is no force applied by the motors to the pads and the stability margin of the robot ( $\Delta S_{robot}$ ) is at the "4 pads attached" level at the bottom diagram of Figure 145;
- b) the motor applies force to the pad in order to detach it, the force on pad 1 increases from zero to above the detachment force:  $F_{det1}$ , the detachment margin of the pad ( $\Delta D_{pad1}$ ) decreases accordingly and the stability margin of the robot drops from the "four pads attached" level to the "3 pads attached" level;
- c) the pad moves to the new position: when the pad detaches the force applied on the pad drops to zero and stays at zero during the motion of the pad, the stability margin of the robot stays at the "3 pads attached level";
- d) the motor preloads the pad in order to re-attach it: the force applied to the pad increases from zero to the value of preload:  $P_1$ , the detachment margin of the pad increases accordingly and the stability margin of the robot returns to the "4 pads attached" level;

- e) waiting for the next pad: the controller of the robot waits for the next pad in the locomotion sequence to be ready;  
 the previous sequence is repeated for the rest of the pads of the robot.



**Figure 145. Theoretical simulation of the force applied to the pads, detachment margin of the pads and the stability margin of the robot during the locomotion sequence of the four-padded robot.**

In the theoretical simulation of Figure 145, the stability margin of the robot does not drop to the “2 pads attached” level and thus, the locomotion sequence of the robot is stable. The stability margin of the robot follows the detachment margin of the pads because, for the sake of simplicity, detachment of each pad is considered to have no effect on the supporting pads.

However, in the locomotion mechanism of the robot, the motors apply force and moment to the supporting pads when detaching, moving or re-attaching one pad. Therefore, the stability margin of the robot changes during the locomotion sequence depending on the force and moment applied to the moving pad and the supporting pads. The motors of the supporting pads can be actuated in order to cancel the force and moment on the supporting pads and thus, increase the stability margin of the robot. The way the motors can be actuated in order to control and enhance the stability of the robot is the subject of study in Chapter 8.

## **7.6 Discussion and conclusion**

After reviewing the stability criteria traditionally used for walking robots, this chapter proposed a new approach to measuring the stability of a robot in inverted adhesion-reliant locomotion based on observation of the locomotion sequence of the prototype. The stability criterion proposes that for a robot relying on a number of adhesive pads in order to stay attached to the support surface, stability is determined by how close to detachment the adhesive pads are.

The formulation of the model assumes that the value of force or moment that causes detachment of the pad is known; this value of detachment force or moment can be predicted using the peeling model proposed in Chapter 6. The stability criterion compares this detachment value to the force or moment applied to the pad by the robot in order to calculate the stability margin of the individual pads and of the whole locomotion mechanism. The usefulness of the proposed stability criterion is proved by observation of the locomotion sequence of the robot, whose performance is determined by whether a sufficient number of pads is attached to the surface and by the strength of the adhesive force.

## **7.7 Summary**

In this chapter, the stability criteria currently available for walking robots was briefly reviewed showing the gap of knowledge in defining stability for adhesion-reliant robots walking upside-down. Considering the context of the intra-abdominal robot, this chapter proposes a new stability criterion for adhesion-reliant robots walking upside-down. This new stability criterion is based on the role of the adhesive pads within the locomotion sequence and on how close to detachment the pads are. The peeling model presented in

the previous chapter is used in order to determine how close to detachment the pads are.

The pads of the robot can be either moving or supporting the motion of the robot. The supporting pads of the robot are critical if the robot cannot carry on walking when these pads detach. The detachment margin of the pad measures the difference between the force and moment applied to the pad and the force and moment required to peel off the pad. The stability margin of the robot is defined as the product of the detachment margin of the critical supporting pads. When one of the critical pads detaches, the detachment margin of the pad becomes zero and the robot stops walking.

In order to illustrate the application of the stability criterion, the design parameters of a two-padded robot are analysed by applying the stability criterion to each scenario of the locomotion sequence of the robot. In this way, the stability criterion enables to calculate: the limit of the size and mass of the two-padded robot, the maximum preload of the pad and the limit of acceleration from the motors. The equations of these design parameters are applied to the bio-mimetic adhesive pad.

In order to illustrate the application of the stability criterion during locomotion, the stability of a four-padded robot taking one step is analysed using the stability criterion. This stability analysis shows how the detachment margin of the pads and the stability margin of the robot changes when the pads are detached and re-attached during the locomotion sequence of the robot.

## **Chapter 8**

### **Control strategies for adhesion-reliant robots**

#### **8.1 Introduction**

In the previous chapter, a stability criterion for adhesion-reliant robots was presented enabling the prediction and detection of an unstable state of the robot during the locomotion sequence. This stability criterion was defined in terms of how many pads the robot requires to follow the locomotion sequence and how close to detachment those pads are. In the definition of the stability margin of the robot, the peeling model presented in Chapter 6 is used in order to determine how close to detachment the pads are.

This chapter defines control strategies for adhesion-reliant robots in order to increase the stability margin of the robot by controlling the force and moment that cause detachment of the pads. The chapter begins by defining a stiffness model of the soft pad backing the adhesive surface of the robot. Then, the forces and moments on the locomotion mechanism are analysed when the vertical and horizontal motors of the robot are actuated in a configuration with two and three pads. The chapter explains how the analysis of a robot with three pads can be used in order to analyse the force and moment in a robot with four pads. After that, the chapter suggests some configurations of the robot with more than four pads and summarises the contents of the chapter in the last section.

#### **8.2 Stiffness model of the soft adhesive pad and the tissue**

This section presents a model of the soft pad used for the attachment of the robot. The soft pad is composed of the adhesive surface, making contact with the attachment surface, and a layer of soft material, backing the adhesive surface.

##### **8.2.1 Advantages of using a soft pad to attach to tissue**

The use of a soft backing layer for the adhesive pad has proved to be beneficial for the locomotion of the robot. The soft backing layer helps the adhesive surface make full contact with the attachment surface and makes detachment and re-attachment of the pads smoother.

In the application of the intra-abdominal robot a soft pad causes less tissue damage than a hard pad by moulding to the surface of the tissue. A hard pad causes a deeper indentation on the tissue in order to make full contact with the surface of the tissue. Figure 146a shows a sketch of the soft pad making contact with tissue and Figure 146b shows a hard pad making contact with tissue.

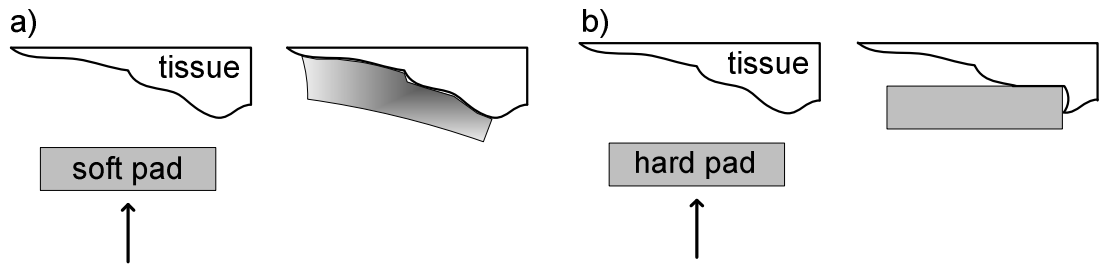


**Figure 146. (a) Soft pad making contact with tissue and (b) hard pad making contact with tissue.**

The tissue is also soft and the force and moment applied by the motors stretch and compress the pads in contact with tissue in order to detach or re-attach the pads. The stiffness of the pads in contact with tissue determines how the locomotion mechanism shifts with respect to the attachment surface.

### **8.2.2 Reference surface for the stretch and compression of the pad and tissue**

In order to measure the shift caused by stretching and compressing the pad and the tissue, the reference surface is the surface of the abdominal wall at rest. This reference is equivalent to the surface of the cantilever used in order to measure the adhesion force in an indentation experiment with a MUST rig (see Chapter 6 Section 6.4.1). Figure 147 shows how the force applied to the pad and tissue relates to the bending of the cantilever in an indentation test and the stretching of the abdominal wall. Figure 147a shows the force-displacement graph obtained in an indentation test of the adhesive pad. Figure 147b shows the pad and tissue in the set-up for an indentation test and Figure 147c shows the pad and tissue inside the abdominal cavity.

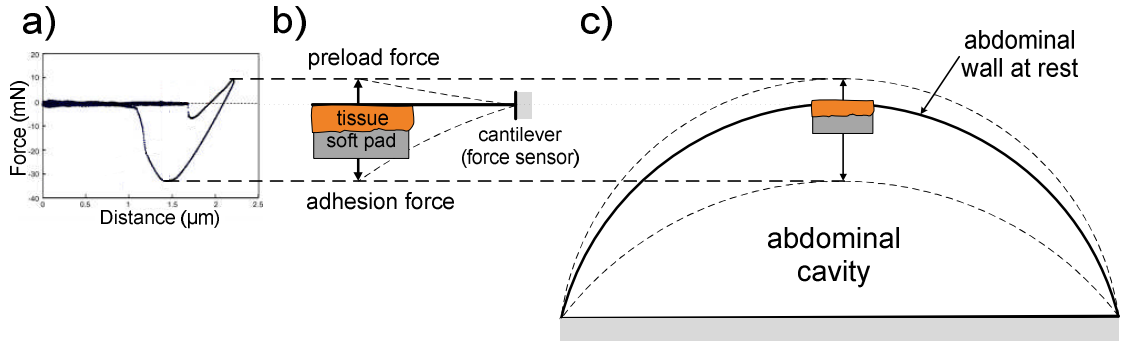


Figure 147. (a) Force-displacement graph from an indentation test of the adhesive pad, (b) pad and tissue on the force sensor for the indentation test, and (c) pad and tissue on the abdominal wall.

### 8.2.3 Stiffness model of the pad attached to tissue in the vertical direction and the horizontal plane

The pad attached to the tissue is modelled as a link element between the robot and the reference surface at the abdominal wall. The model for this link element is composed of:

- a linear spring, stretching or compressing along the vertical direction, perpendicular to the surface of the tissue, and
- a torsion spring, bending along the two directions of the horizontal plane, parallel to the surface of the tissue.

More complex models can be used in order to describe tissue mechanics [11] and the mechanics of soft materials like the foam used for the pads. The springs model presented here simplifies calculations whilst still allowing relevant conclusions to be drawn. Figure 148 shows the model of the pad and tissue together with the force and moment that the motors of the robot apply to the pad. Figure 148a shows the linear spring modelling the stiffness of the pad and tissue in the vertical direction. Figure 148b shows the torsion springs modelling the stiffness of the pad in the horizontal plane.

The model of the soft pad and tissue assumes that there is no shearing force applied on the pad (force in the X and Y direction in Figure 148a) and there is no twisting moment applied to the pad (moment around the Z direction in Figure 148b). The softness of the pad and tissue allows stretching along the vertical direction and bending in the horizontal plane. As shown in Figure 148, the force and moment applied to the pad attached to tissue are:

$$F_z = K_{tp} \cdot \Delta z \quad (118)$$

$$M_x = K_{Ttp}^x \cdot \Delta \theta_x \quad (119)$$

$$M_y = K_{Ttp}^y \cdot \Delta \theta_y \quad (120)$$

In Equation ( 118 ),  $F_z$  is the vertical force applied to the pad,  $K_{tp}$  is the stiffness of the pad attached to tissue in the vertical direction ( $Z$  direction), and  $\Delta z$  is the stretch (extension) of the pad. The stiffness of the pad and tissue  $K_{tp}$  can be tension or compression stiffness depending on the direction of the force  $F_z$ , thus  $\Delta z$  can be a stretch or a compression of the pad attached to tissue.

In Equation ( 119 ),  $M_x$  is the moment applied to the pad along the  $X$  direction of the horizontal plane ,  $K_{Ttp}^x$  is the torsional stiffness of the pad attached to tissue, and  $\Delta\theta_x$  is the bending angle.

In Equation ( 120 ):  $M_y$  is the moment applied to the pad along the  $Y$  direction of the horizontal plane,  $K_{Ttp}^y$  is the torsional stiffness of the pad and tissue, and  $\Delta\theta_y$  the bending angle.

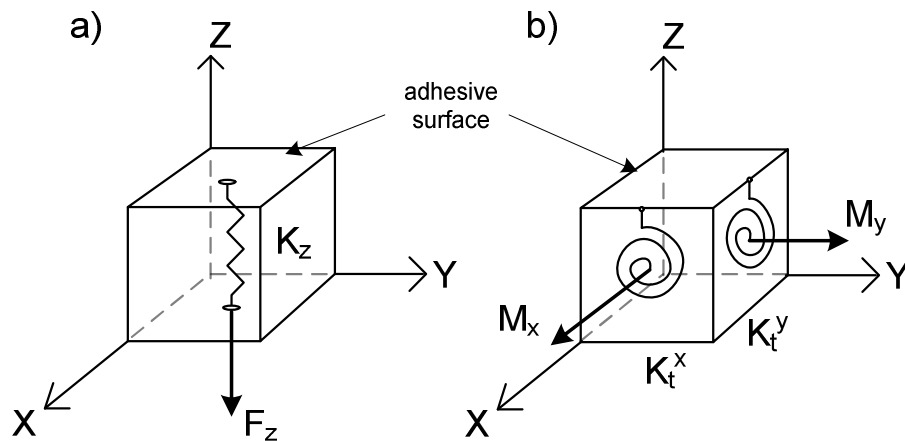


**Figure 148. (a) Model of the soft pad and tissue as a linear spring in the vertical direction;  $F_z$  is the vertical force applied to the pad. (b) Model of the soft pad and tissue as two torsion springs in the horizontal plane;  $M_x$  and  $M_y$  are the moments applied around the two directions of the horizontal plane.**

In Equations ( 118 ), ( 119 ) and ( 120 ), the stiffness of the soft pad attached to tissue:  $K_{tp}$ ,  $K_{Ttp}^x$  and  $K_{Ttp}^y$ , are a combination of the stiffness of the pad and the stiffness of the tissue. The stiffness of the soft pad is in series with the stiffness of the tissue because they both feel the same force and the same moment from the motors. Figure 149a shows the soft pad attached to the tissue as well as the reference surface. Figure 149b shows two springs in series modelling the stiffness of the soft pad in series with the stiffness of the tissue along the vertical direction. Figure 149c shows two torsion springs in series modelling the torsional stiffness of the soft pad in series with the torsional stiffness of the tissue in the horizontal plane.

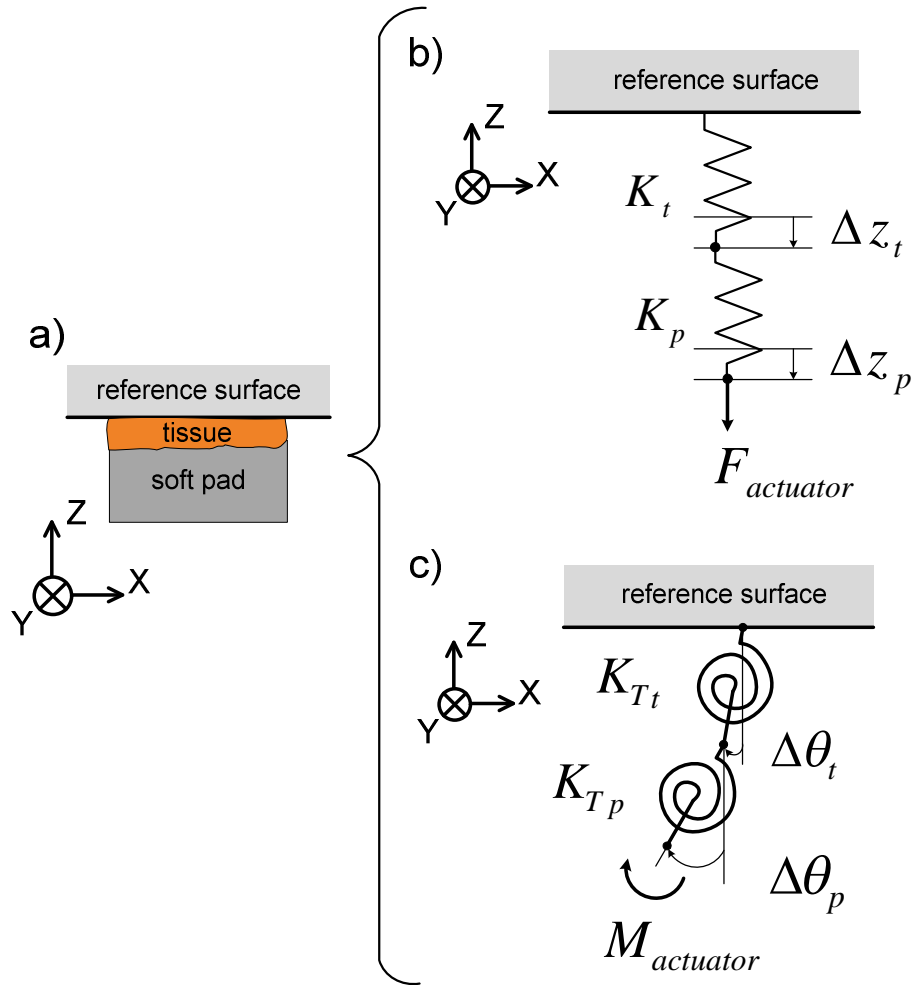


**Figure 149. (a) Soft pad attached to the tissue, (b) linear springs modelling the stiffness of the pad and the tissue in the vertical direction, (c) torsion springs modelling the stiffness of the pad and the tissue in the horizontal plane.**

In the vertical direction, shown in Figure 149b, the equivalent stiffness of the pad attached to the tissue is:

$$K_{tp} = \frac{K_t \cdot K_p}{K_t + K_p} \quad (121)$$

Where  $K_{tp}$  is the stiffness of the pad attached to tissue,  $K_t$  is the stiffness of the tissue and  $K_p$  is the stiffness of the pad. If the elastic properties of the material of the pad and the tissue are known, the stiffness of the pad or the tissue is:

$$K_z = \frac{E \cdot A}{h_0} \quad (122)$$

Where  $K_z$  is the stiffness of the material (pad or tissue) along the vertical direction (Z direction),  $E$  is Young's modulus of the material,  $A$  is the cross section and  $h_0$  is the thickness.

In the horizontal plane shown in Figure 149c, the equivalent torsional stiffness of the pad attached to the tissue is:

$$K_{T_{tp}} = \frac{K_{T_t} \cdot K_{T_p}}{K_{T_t} + K_{T_p}} \quad (123)$$

Where  $K_{T_{tp}}$  is the torsional stiffness of the pad attached to the tissue,  $K_{T_t}$  is the torsional stiffness of the tissue and  $K_{T_p}$  is the torsional stiffness of the pad. In Figure 149c, only the torsional stiffness along the Y direction in the horizontal plane is shown; the torsional stiffness model along the X direction is the same as along the Y direction.

### 8.3 Force and moment in the locomotion mechanism of a two-padded robot

A robot with two pads is the simplest design for an adhesion-reliant walking robot, using one pad to support the motion of the other pad and alternating the motion of the two pads. Using the previous model of the soft pad attached to tissue, this section analyses the force and moment in a two-padded robot when the motors of the robot detach one pad.

#### 8.3.1 Locomotion mechanism of a two-padded robot

The locomotion mechanism of a two-padded robot is composed of two pads and three motors:

- one linear motor to move the first adhesive pad in the vertical direction, controlling the distance between the first pad and the reference surface;
- one linear motor to move the second adhesive pad in the vertical direction, controlling the distance between the second pad and the reference surface;
- one linear motor between the two pads, controlling the separation between the pads.

Figure 150a shows a sketch of the locomotion mechanism of a two-padded robot and the distance controlled by each motor. In Figure 150a:  $z_1$  is the distance controlled by the first vertical motor,  $z_2$  is the distance controlled by the second vertical motor and  $x_{12}$  is the distance controlled by the horizontal motor. Figure 150b shows the model of the soft pad attached to tissue in the vertical direction and Figure 150c shows the model of the soft pad attached to tissue in the horizontal plane.

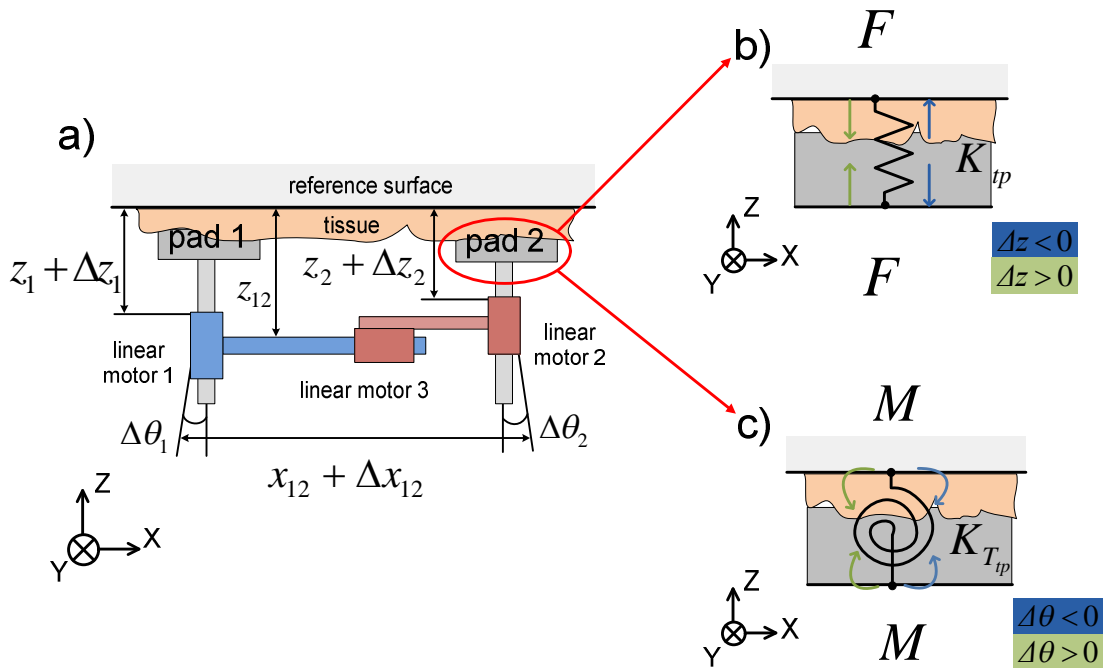


**Figure 150. (a) Sketch of a two-padded robot, (b) model of the soft pad attached to tissue in the vertical direction and (c) model of the soft pad attached to tissue in the horizontal plane.**

In Figure 150a and Figure 150b, the vertical motor causes an increment of the distance between the pads and the reference surface:  $\Delta z_1$  and  $\Delta z_2$ . This increment of distance:  $\Delta z_1$  and  $\Delta z_2$  is negative ( $\Delta z < 0$ ) when the motor is stretching the pad, and positive ( $\Delta z > 0$ ) when the motor is pressing the pad against the tissue. The direction of force applied to the pad corresponding to the sign of  $\Delta z_1$  and  $\Delta z_2$  is also shown in Figure 150b.

In Figure 150a and Figure 150c, the horizontal motor causes an increment of the angle between the vertical motors and the vertical:  $\Delta \theta_1$  and  $\Delta \theta_2$ . This increment of angle with respect to the vertical:  $\Delta \theta$  is considered negative ( $\Delta \theta < 0$ ) when the motor is separating the pads, and positive ( $\Delta \theta > 0$ ) when the motor is pulling the pads together. The direction of moment applied to the pad corresponding to the sign of  $\Delta \theta_1$  and  $\Delta \theta_2$  is also shown in Figure 150c.

### 8.3.2 Vertical force on the moving pad

When the vertical motor stretches the pad:  $\Delta z < 0$ , the distance between the pad attached to the tissue and the reference is shortened and the supporting pad feels this stretch as a compression force. When the vertical motor compresses the pad:  $\Delta z > 0$ , the distance between the pad attached to the tissue and the reference surface is lengthened and the supporting pad feels

this compression as a pull force. The vertical force applied to the moving pad causes force and moment on the supporting pad.

Figure 151a shows the force on the free body diagram of the moving pad and the supporting pad when a detach force and a preload are applied to the moving pad. Figure 151b shows the moment on the free body diagram of the moving pad and the supporting pad when a detach force and a preload are applied to the moving pad.

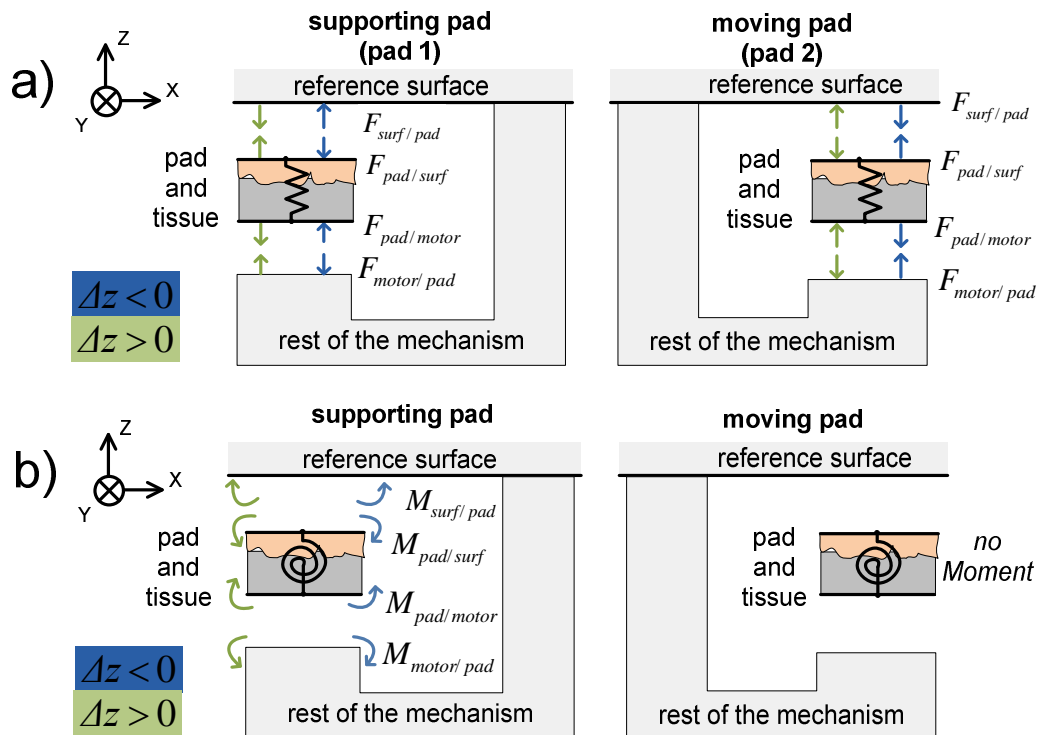


**Figure 151. (a) Free body diagram of the force on the supporting pad and the detaching pad when vertical force is applied to the moving pad, and (b) free body diagram of the moment on the supporting pad and the detaching pad when vertical force is applied to the moving pad.**

All the forces in Figure 151a are the same value, which is the force applied by the motor on the pad:

$$F_2 = K_{tp} \cdot \Delta z_2 \quad (124)$$

Where  $K_{tp}$  is the stiffness of the moving pad attached to the tissue and  $\Delta z_2$  is the stretch of the moving pad caused by the motor. The stiffness of the pad attached to the tissue:  $K_{tp}$  can be tension or compression stiffness depending on the sign of  $\Delta z_2$ .

All the moments in Figure 151b are the same value:

$$M_2 = F_2 \cdot x_{12} \quad (125)$$

Where  $F_2$  is the force applied by the motor and  $x_{12}$  is the distance between the pads.

If the torsional stiffness of the pad is known, the moment can also be calculated as:

$$M_2 = K_{T_{tp}} \cdot \Delta\theta_2 \quad (126)$$

Where  $K_{T_{tp}}$  is the torsional stiffness of the pad attached to the tissue and  $\Delta\theta_2$  is the bending angle of the supporting pad caused by the force applied to the moving pad.

The angle  $\Delta\theta_2$  is small because the stretch  $\Delta z_2$  is small and therefore:

$$\Delta\theta_2 \approx \frac{\Delta z_2}{R} \quad (127)$$

Where  $\Delta\theta_2$  is the bending angle of the supporting pad,  $\Delta z_2$  is the stretch of the moving pad and  $R$  is the distance between the supporting pad and the vertical motor of the moving pad.

The distance  $R$  is:

$$R = \sqrt{z_2^2 + x_{12}^2} \quad (128)$$

Where  $z_2$  is the distance from the reference surface to the vertical motor of the supporting pad and  $x_{12}$  the separation between the pads (see Figure 150).

### 8.3.3 Vertical force on the supporting pad

When the vertical motor of the supporting pad is actuated in the same direction as the motor of the moving pad, peeling of the moving pad is cancelled. In that case, the two vertical motors move simultaneously, moving the horizontal motor between the pads upward or downward depending on the direction of motion.

However, when the vertical motor of the supporting pad is actuated in the direction opposite to the motor of the moving pad, the peeling or preloading of the moving pad intensifies. Figure 152a shows the force on the free body diagram of the moving pad and the supporting pad when the vertical motor of the supporting pad is actuated. Figure 152b shows the moment on the free body diagram of the moving pad and the supporting pad when the vertical motor of the supporting pad is actuated.

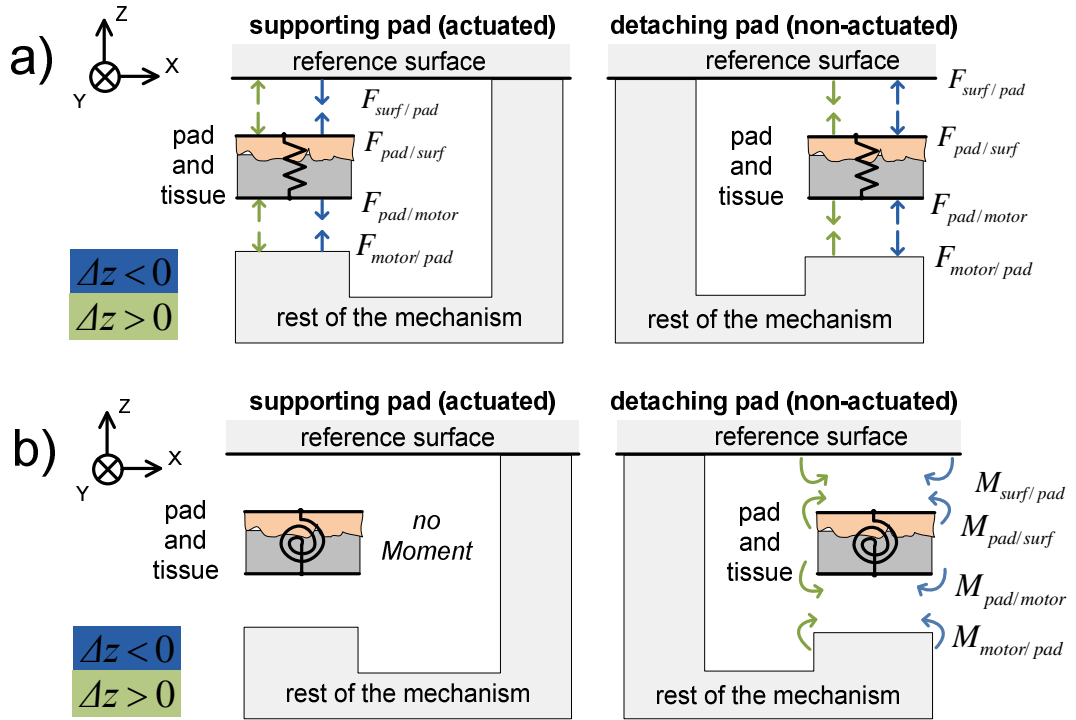


**Figure 152. Free body diagram of the forces (a) and moments (b) in a two-padded robot when the vertical motor of the supporting pad is actuated.**

All the forces in Figure 152a are the same value, which is the force applied by the vertical motor:

$$F_1 = K_{tp} \cdot \Delta z_1 \quad (129)$$

Where  $K_{tp}$  is the stiffness of the supporting pad attached to the tissue and  $\Delta z_1$  is the stretch of the supporting pad caused by the motor. The stiffness of the pad attached to the tissue:  $K_{tp}$  can be tension or compression stiffness depending on the sign of  $\Delta z_1$ .

All the moments in Figure 151b are the same value:

$$M_1 = F_1 \cdot x_{12} \quad (130)$$

Where  $F$  is the force applied by the motor and  $x_{12}$  is the distance between the pads.

### 8.3.4 Horizontal force between the pads

When the horizontal motor is actuated, the distance between the pads increases or decreases, depending on the direction of actuation of the motor, causing the pads to bend. This bend on the supporting and the moving pad causes a moment on the pad which can help preloading or detaching the adhesive surface of the pads.

Figure 153a shows the two torsion springs modelling the supporting and the moving pad in the horizontal plane. Figure 153a also shows the angle on the torsion springs caused by the increment and decrement of distance between the pads when the horizontal motor is actuated. Figure 153b shows the moment on the free body diagram of the moving pad and the supporting pad when the horizontal motor is actuated.

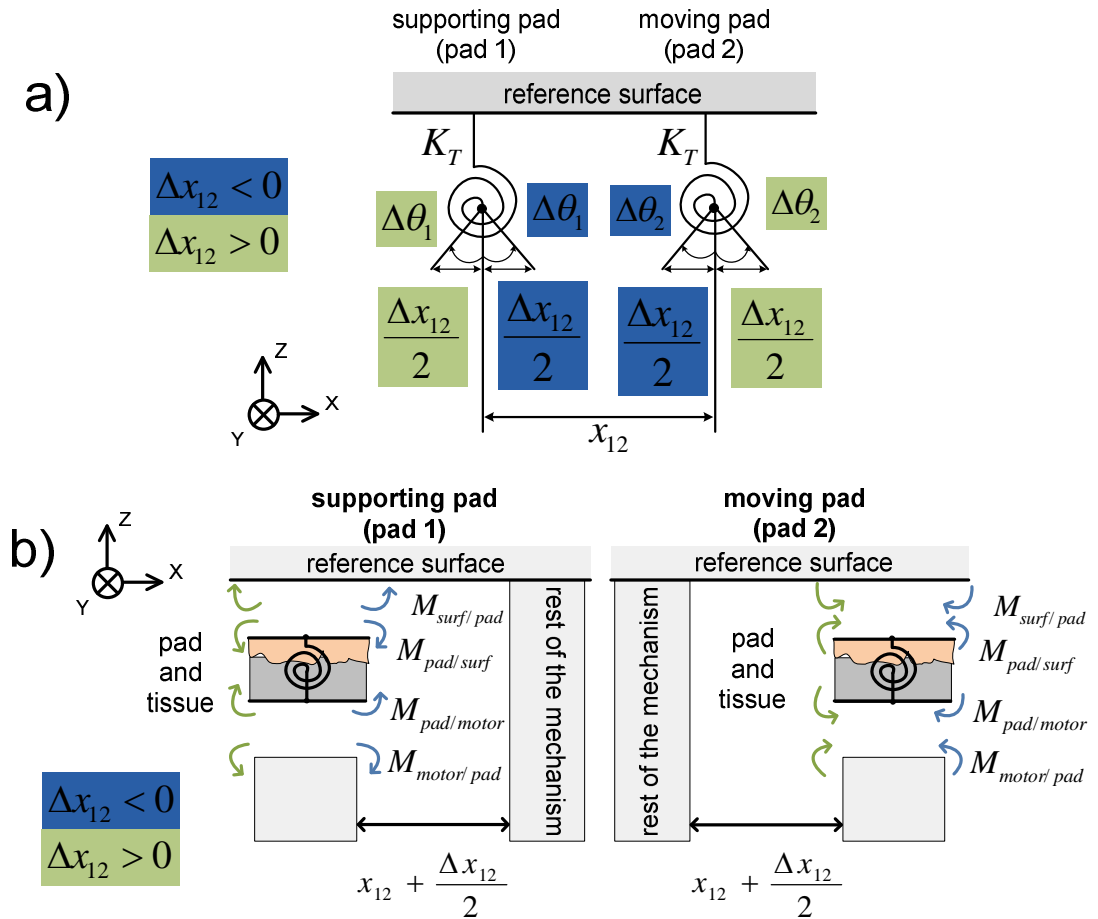


**Figure 153. (a) Torsion springs modelling the moving pad and the supporting pad and (b) free body diagram of the moment on the supporting pad and the detaching pad when the horizontal motor is actuated.**

In Figure 153a, when the horizontal motor shortens the distance between the pads:  $\Delta x_{12} < 0$ , the pads are pulled together; when the horizontal motor lengthens the distance between the pads:  $\Delta x_{12} > 0$ , the pads are pushed apart. The increment of distance between the pads is small and therefore the bending angle of the pads is:

$$\Delta\theta_1 = \Delta\theta_2 = \frac{\Delta x_{12}}{2 \cdot x_{12}} \quad (131)$$

Where  $\Delta x_{12}$  is the increment of distance between the pads caused by the horizontal motor and  $x_{12}$  is the initial separation between the pads.

The moment caused by actuating the horizontal motor between the pads is:

$$M_{12} = F_{12} \cdot z_{12} \quad (132)$$

Where  $F_{12}$  is the force from the horizontal motor and  $z_{12}$  is the vertical distance from the reference surface to the horizontal motor.

### 8.3.5 Control strategies for a two-padded robot

Considering the previous analysis of force and moment in the two-padded robot, when the vertical motor pulls the moving pad, a preload force and a moment are applied to the supporting pad. When the vertical motor preloads the moving pad, pushing the pad into the tissue, a peeling force and a moment are applied to the supporting pad. Stability of the robot enhances when the force and moment applied to the supporting pad are cancelled.

When detaching the moving pad, in order to cancel the force and moment on the supporting pad and intensify detachment on the moving pad:

- the horizontal motor can increase the separation between the pads, counteracting the peeling moment on the supporting pad and applying a peeling moment on the moving pad;
- the vertical motor on the supporting pad can push the supporting pad into the tissue, applying a peeling force and moment on the moving pad.

When preloading the moving pad, in order to cancel the force and moment on the supporting pad, and intensify the preload on the moving pad:

- the horizontal motor can decrease the separation between the pads, counteracting the peeling moment on the supporting pad;
- the vertical motor on the supporting pad can pull the supporting pad, applying a preload on the moving pad.

## 8.4 Links and joints for a third pad

Adding a third pad to the locomotion mechanism of the robot enables the robot to carry a higher payload without changing the geometry or adhesion of the pads. The third pad carries a proportion of the vertical force applied to the moving pad, reducing the force and moment on the supporting pads. The position of the third pad with respect to the other two and the connections between the three pads determine the force and moment in the mechanism of the three-padded robot.

The third pad can be positioned in line with the other two pads or forming a triangle with the other two pads. Considering the moving pad in a two-

padding configuration, in order to form a triangle, the third pad links to the robot with these connections:

- a link between the third pad and the moving pad, called radial link; the length of this link is controlled by a linear motor,
- a link between the third pad and the supporting pad, called perimetric link, the length of this link is controlled by a linear motor, and
- a passive revolute joint at the connection between the link of the third pad with the moving pad and the supporting pad.

Figure 154a shows the radial link, Figure 154b shows the perimetric link and Figure 154c shows the revolute joints between the third pad and the moving and supporting pad in a two-padded robot.

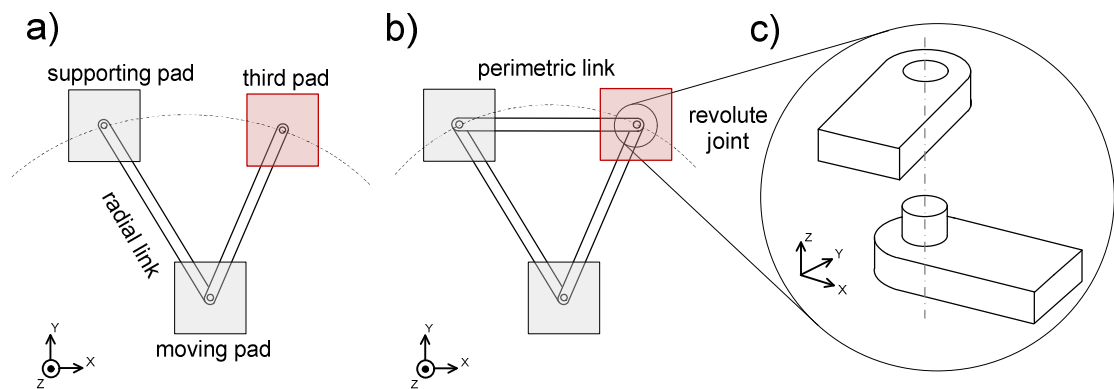


**Figure 154. (a) Radial link between the third pad and the moving pad, (b) perimetric link between the third pad and the supporting pad, and (c) revolute joint connecting the links between the third pad and the moving and supporting pad.**

## 8.5 Force and moment in the locomotion mechanism of a robot with three pads in a line

A robot with three pads in a line uses two pads to support the motion of one pad, reducing the force and moment applied on the supporting pads and thus enhancing stability of the robot. A robot with three pads in a line can move in a straight line alternating the motion of the three pads. Using the previous model of the soft pad attached to tissue, this section analyses the force and moment in a robot with three pads in a line.

### 8.5.1 Locomotion mechanism of a robot with three pads in a line

The locomotion mechanism of a robot with three pads in a line is composed of five linear motors: one vertical motor for each pad and two horizontal motors to separate the pads. Figure 155a shows a sketch of the robot with three pads in a line: pad 1 is the moving pad and pads 2 and 3 are the

supporting pads. Figure 155a also shows the parameters considered for the analysis of force and moment in the locomotion mechanism when pad 1 is moving:

- the distance from the reference surface to each pad:  $z_1$ ,  $z_2$  and  $z_3$ , and
- the horizontal distance between the three pads:  $x_{12}$ ,  $x_{13}$  and  $x_{23}$ .

Figure 155b shows the three springs in parallel modelling the stiffness of the three pads of the robot in the vertical direction. Figure 155c shows the three torsion springs modelling the bending of the three pads of the robot in the horizontal plane.

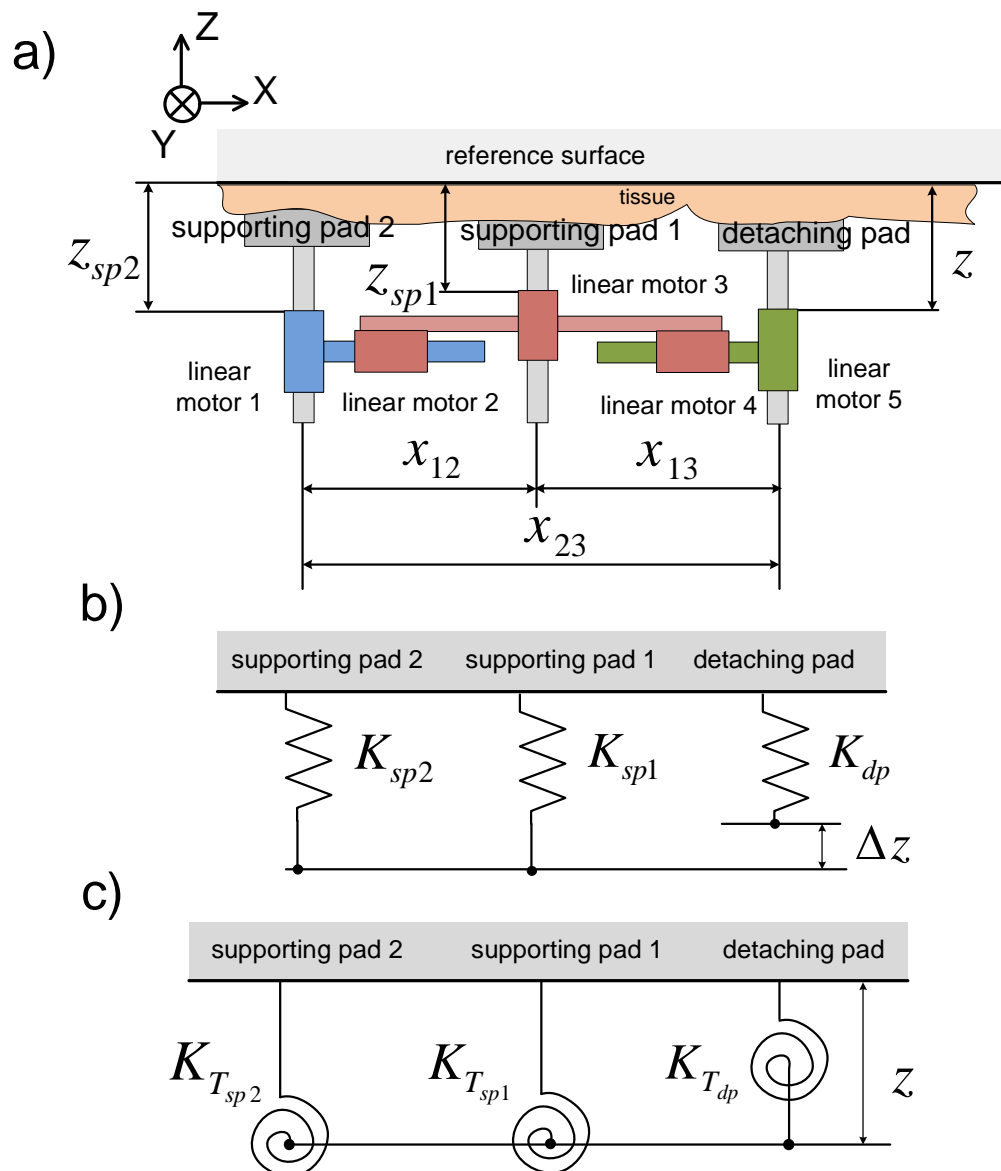


Figure 155. (a) Sketch of the robot with three pads in a line, (b) three springs in parallel modelling the three pads in the vertical direction, and (c) three torsion springs modelling the bending of the pads in the horizontal plane.

In Figure 155b, when the vertical motor on the detaching pad is actuated, the stretch of the detaching pad and the supporting pads is the same:  $\Delta z$ . The springs modelling the stiffness of the supporting pads are in parallel and the force applied by the vertical motor of the detaching pad splits between the supporting pads. In general, if the detaching pad is connected to  $n$  supporting pads, the force applied by the vertical motor of the detaching pad to each supporting pad is:

$$F_{sup_i} = \frac{F}{n} \quad (133)$$

Where  $F$  is the force from the vertical motor of the detaching pad (see Equation (124)),  $i = 1, 2 \dots n$  is the number of supporting pad and  $n$  is the total number of supporting pads. In a three-padded robot, the force on each supporting pad is half the force applied to the detaching pad.

Figure 155c showed the torsion springs modelling the bending of the pads when there is no stretch on the pads caused by the vertical motors. When the vertical motor on the detaching pad is actuated, the detaching pad and the supporting pads stretch  $\Delta z$  with respect to the reference surface. The detaching pad does not bend when the vertical motor is actuated, but the two supporting pads bend and further stretch. Figure 156a shows the stretch caused on supporting pad 2 by the bend on supporting pad 1 when the vertical motor of the detaching pad is actuated. Figure 156b shows the stretch caused on supporting pad 1 by the bend on supporting pad 2 when the vertical motor of the detaching pad is actuated.

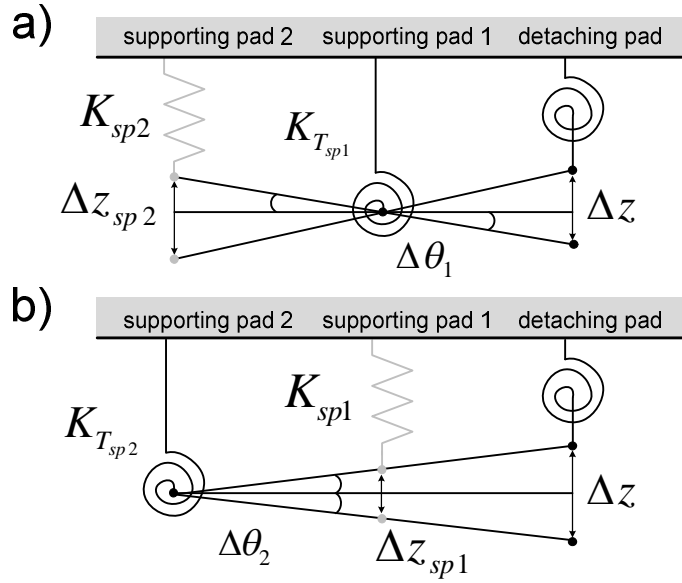


**Figure 156. (a) Stretch caused on supporting pad 2 by the bend on supporting pad 1 when the vertical motor of the detaching pad is actuated and (b) stretch caused on supporting pad 1 by the bend on supporting pad 2 when the vertical motor of the detaching pad is actuated.**

In Figure 156a, the bending angle of supporting pad 1:  $\Delta\theta_1$  causes a stretch of supporting pad 2:  $\Delta z_{sp2}$  and therefore applies a force to supporting pad 2. Considering that the bending angle is small, the stretch on supporting pad 2 caused by the bending angle of supporting pad 1 is:

$$\Delta z_{sp2} = \Delta\theta_1 \cdot x_{12} = \Delta z \cdot \frac{x_{12}}{x_{23}} \quad (134)$$

Where  $\Delta\theta_1$  is the bending angle of supporting pad 1,  $x_{12}$  is the distance between the two supporting pads,  $\Delta z$  is the stretch of the detaching pad and  $x_{23}$  is the distance between supporting pad 2 and the detaching pad.

In Figure 156b, the bending angle of supporting pad 2:  $\Delta\theta_2$  causes a stretch of supporting pad 1:  $\Delta z_{sp1}$  and therefore applies a force to supporting pad 1. The stretch on supporting pad 1 caused by the bending angle of supporting pad 2 is:

$$\Delta z_{sp1} = \Delta\theta_2 \cdot x_{13} = \Delta z \cdot \frac{x_{12}}{x_{23} + x_{12}} \quad (135)$$

Where  $\Delta\theta_2$  is the bending angle of supporting pad 2,  $x_{13}$  is the distance between supporting pad 1 and the detaching pad,  $\Delta z$  is the stretch of the detaching pad. The distance between the two supporting pads is  $x_{12}$  and  $x_{23}$  is the distance between supporting pad 2 and the detaching pad.

### 8.5.2 Vertical force on the detaching pad

When vertical force is applied to the moving pad, the stretch of the moving pad applies causes the supporting pads to stretch and bend, applying a

force and moment to the supporting pads. Figure 157a shows the force on the free body diagram of the moving pad and the supporting pads when a detach force and a preload are applied to the moving pad. Figure 157b shows the moment on the free body diagram of the moving pad and the supporting pad when a detach force and a preload are applied to the moving pad. For the sake of clarity, Figure 157 does not show the force caused by the supporting pads on each other.

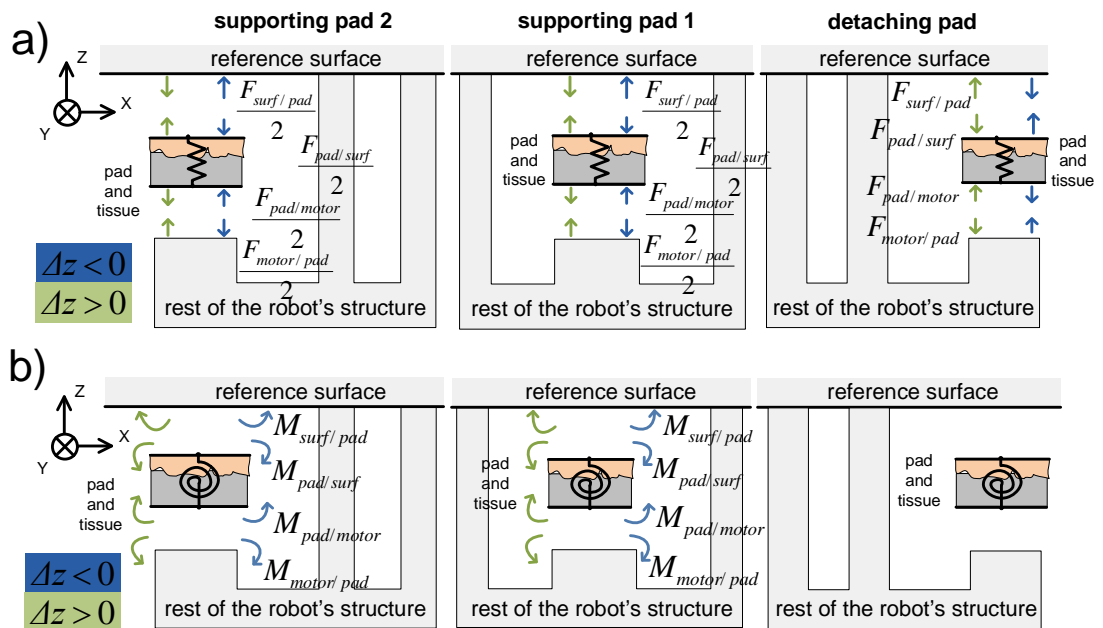


**Figure 157. (a) Free body diagram of the force on the supporting pads and the detaching pad when vertical force is applied to the moving pad, and (b) free body diagram of the moment on the supporting pads and the detaching pad when vertical force is applied to the moving pad.**

The force and moment applied to the detaching pad and the supporting pads by the vertical motor on the detaching pad are expressed in terms of:

- the stiffness of the pads in tension:  $K_t$ , and compression:  $K_c$ ,
- the stretch caused by the vertical motor of the detaching pad:  $\Delta z$ ,
- the distance between the pads:  $x_{12}$ ,  $x_{13}$  and  $x_{23}$ , and
- the total number of supporting pads:  $n$ , in a three pads:  $n = 2$ .

Table 14 shows the equations of the force and moment applied to the pads of the robot when force is applied to the detaching pad.

Table 14. Force and moment on the pads of a robot with three pads in a line when the vertical motor of the detaching pad is actuated.

		Supp. pad 2	Supp. pad 1	Det. pad
<b>Force</b> (Figure 158 a)	Detach: ( $\Delta z < 0$ )	$K_t \cdot \Delta z \cdot \left( \frac{x_{12}}{x_{23}} - \frac{1}{n} \right)$	$-(K_c \cdot \frac{x_{12}}{x_{23} + x_{12}} + K_t \cdot \frac{1}{n}) \cdot \Delta z$	$K_t \cdot \Delta z$
	Preload: ( $\Delta z > 0$ )	$K_c \cdot \Delta z \cdot \left( \frac{1}{n} - \frac{x_{12}}{x_{23}} \right)$	$(K_t \cdot \frac{x_{12}}{x_{23} + x_{12}} + K_c \cdot \frac{1}{n}) \cdot \Delta z$	$-K_c \cdot \Delta z$
<b>Moment</b> (Figure 158 b)	Detach: ( $\Delta z < 0$ )	$\left[ K_c \cdot \left( \frac{x_{12}}{x_{23} + x_{12}} \right)^2 - K_t \right] \cdot (x_{23} + x_{12}) \cdot \Delta z$	$K_t \cdot \left( \frac{x_{12}^2}{x_{23}^2} - 1 \right) \cdot x_{23} \cdot \Delta z$	<i>no <math>M_{det.}</math></i>
	Preload: ( $\Delta z > 0$ )	$\left[ K_c - K_t \cdot \left( \frac{x_{12}}{x_{23} + x_{12}} \right)^2 \right] \cdot (x_{23} + x_{12}) \cdot \Delta z$	$K_c \cdot \left( 1 - \frac{x_{12}^2}{x_{23}^2} \right) \cdot x_{23} \cdot \Delta z$	<i>no <math>M_{det.}</math></i>

Figure 158 shows the sketch of the force and moment summarised in Table 14 applied to the pads of the robot at the reference surface.

Figure 158a shows the force and Figure 158b shows moment caused by the stretch of the detaching pad on the supporting pads and also the force and moment caused by the bending of the supporting pads.

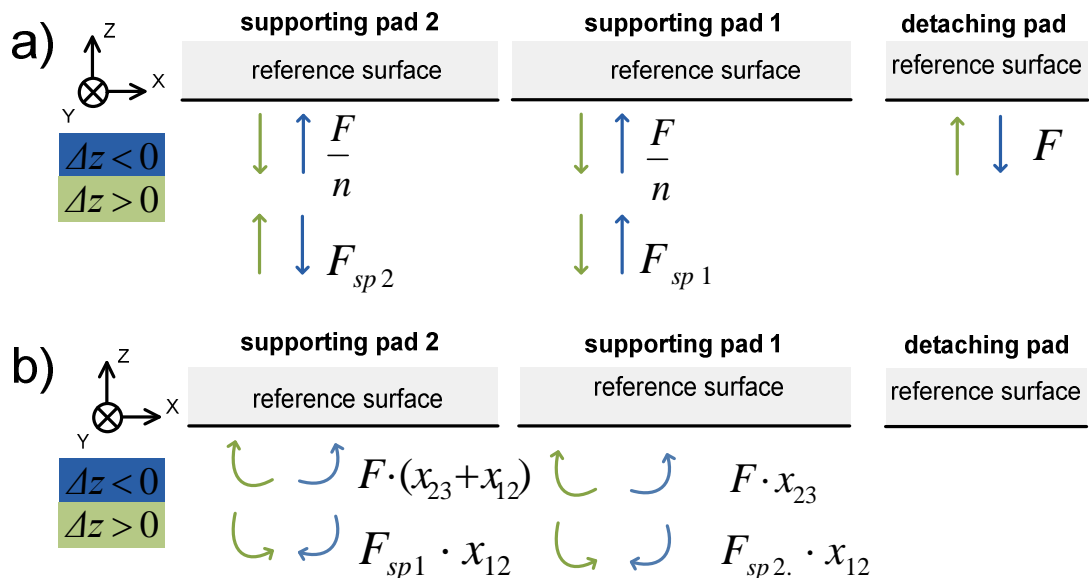


Figure 158. (a) Force applied to the detaching pad and supporting pads when the vertical motor of the detaching pad is actuated and (b) moment applied to the detaching pad and supporting pads when the vertical motor of the detaching pad is actuated.

In Figure 158a and Figure 158b, the first row of force and moment is the force and moment caused by the stretch of the detaching pad when the vertical motor of the detaching pad is actuated. The second row of force and moment in Figure 158a and Figure 158b is the force and moment caused by the bend of the supporting pads.

The force applied by the vertical motor of the detaching pad is:

$$F = K \cdot \Delta z \quad (136)$$

Where  $K = K_t$  is the stiffness of the pad in tension when  $\Delta z < 0$ ,  $K = K_c$  is the stiffness of the pad in compression when  $\Delta z > 0$ , and  $\Delta z$  is the stretch of the detaching pad.

The force caused on supporting pad 1 by the bend on supporting pad 2 is:

$$F_{sp1} = K \cdot \Delta z_{sp1} \quad (137)$$

Where  $\Delta z_{sp1}$  is the stretch of supporting pad 1 caused by the bending angle on supporting pad 2 (see Equation (134)).

The force caused on supporting pad 2 by the bend on supporting pad 1 is:

$$F_{sp2} = K \cdot \Delta z_{sp2} \quad (138)$$

Where  $\Delta z_{sp2}$  is the stretch of supporting pad 2 caused by the bending angle on supporting pad 1 (see Equation (135)).

### 8.5.3 Vertical force on the supporting pads

The analysis of force and moment when vertical force is applied to supporting pad 2, the supporting pad opposite to the detaching pad, is identical to the analysis for the detaching pad. When vertical force is applied to supporting pad 2, the force from the vertical motor is:

$$F_2 = K^{sp2} \cdot \Delta z_2 \quad (139)$$

Where  $K^{sp2}$  is the stiffness of supporting pad 2 and  $\Delta z_2$  is the stretch of supporting pad 2.

When the vertical motor on supporting pad 2 is actuated, the force caused on the detaching pad by the bend on supporting pad 1 is:

$$F_{det,2} = K^{sp2} \cdot \Delta z_{det} = K^{sp2} \cdot \frac{x_{23}}{x_{12}} \cdot \Delta z_2 \quad (140)$$

Where  $K^{sp2}$  is the stiffness of supporting pad 2,  $\Delta z_{det}$  is the stretch of the detaching pad caused by the bending angle on supporting pad 1,  $x_{23}$  is the distance between supporting pad 2 and the detaching pad,  $x_{12}$  is the

distance between the supporting pads and  $\Delta z_2$  is the stretch of supporting pad 2.

When the vertical motor on supporting pad 2 is actuated, the force caused on supporting pad 1 by the bend on the detaching pad is:

$$F_{sp1,2} = K^{sp2} \cdot \Delta z_{sp1} = K^{sp2} \cdot \frac{x_{23}}{x_{12} + x_{23}} \cdot \Delta z_2 \quad (141)$$

Where  $K^{sp2}$  is the stiffness of supporting pad 2,  $\Delta z_{sp1}$  is the stretch of supporting pad 1 caused by the bending angle on the detaching pad,  $x_{23}$  is the distance between supporting pad 2 and the detaching pad,  $x_{12}$  is the distance between the supporting pads and  $\Delta z_2$  is the stretch of supporting pad 2.

For the analysis of force and moment when vertical force is applied to supporting pad 1, the mechanism of the robot is considered the superposition of:

- a two-padded robot composed of supporting pad 1 and the detaching pad, and
- a two-padded robot composed of supporting pad 1 and supporting pad 2.

When vertical force is applied to supporting pad 1, the force from the vertical motor on supporting pad 1 is:

$$F_1 = K^{sp1} \cdot \Delta z_1 \quad (142)$$

Where  $K^{sp1}$  is the stiffness of supporting pad 1 and  $\Delta z_1$  is the stretch of supporting pad 1.

#### **8.5.4 Force from the horizontal motor between the pads**

When the horizontal motors between the pads are actuated, the force and moment on the pads are calculated considering the mechanism of the robot the superposition of:

- the actuation of the horizontal motor in a two-padded robot composed of supporting pad 1 and the detaching pad, and
- the actuation of the horizontal motor in a two-padded robot composed of supporting pad 2 and supporting pad 1.

The moment from the horizontal motor between supporting pad 1 and the detaching pad is:

$$M_{13} = F_{h13} \cdot z_{sp1} \quad (143)$$

Where  $F_{h13}$  is the force from the horizontal motor between supporting pad 1 and the detaching pad and  $z_{sp1}$  is the distance between the reference surface and the horizontal motor.

The moment from the horizontal motor between the supporting pads is:

$$M_{12} = F_{h12} \cdot z_{sp2} \quad (144)$$

Where  $F_{h12}$  is the force from the horizontal motor between the supporting pads and  $z_{sp2}$  is the distance between the reference surface and the horizontal motor.

### **8.5.5 Control strategies for a robot with three pads in a line**

In order to enhance the stability of the robot, the strategies considered in the first place are the strategies that can be implemented with only one vertical motor applying force to one pad. If the stability margin of the pads needs to increase further, the vertical motors of the supporting pads and the horizontal motors can also be actuated.

#### **8.5.5.1 Strategies to reduce the force and moment on the supporting pads when the vertical motor of the detaching pad is actuated**

Considering the previous analysis of force and moment in a robot with three pads in a line, when the vertical motor on the detaching pad is actuated, the force applied to supporting pad 2 is cancelled when:

$$x_{12} = \frac{x_{23}}{n} \quad (145)$$

Thus, for three pads:  $n = 2$ , the force on supporting pad 2 is cancelled when the distance between the two supporting pads is half the distance between supporting pad 1 and the detaching pad. The force applied to supporting pad 2 also diminishes with softer pads.

When the vertical motor on the detaching pad is actuated, the force applied to supporting pad 1 cannot be cancelled but can be reduced:

- increasing  $n$ , that is, adding more pads in line with the three pads of the robot,
- with softer pads (lower value of the stiffness constant),
- increasing  $x_{23}$ : the distance between supporting pad 2 and the detaching pad.

When the vertical motor on the detaching pad is applying a force to detach the pad, the moment on supporting pad 2 is cancelled when the relation between the compression and tension stiffness of the pad is:

$$K_c = K_t \cdot \left( \frac{x_{12}}{x_{23} + x_{12}} \right)^2 \quad (146)$$

When the vertical motor on the detaching pad is preloading the pad, in order to cancel the moment on supporting pad 2, the relation between the tension and the compression stiffness of the pad is:

$$K_t = K_c \cdot \left( \frac{x_{12}}{x_{23} + x_{12}} \right)^2 \quad (147)$$

For a given ratio of the compression and tension stiffness ( $r_K$ ), the relation between the two distances:  $x_{12}$  and  $x_{23}$  in Equation ( 147 ) is:

$$x_{12} = \frac{r_K \pm \sqrt{r_K}}{1 - r_K} \cdot x_{23} \quad (148)$$

Where the ratio of compression and tension stiffness is:  $r_K = \frac{K_t}{K_c}$  when the pad is detaching, and  $r_K = \frac{K_c}{K_t}$  when the pad is preloading. This ratio of stiffness:  $r_K$  is smaller than 1.

When the vertical motor on the detaching pad is actuated, the moment on supporting pad 1 is cancelled when:

$$x_{12} = x_{23} \quad (149)$$

Thus, according to ( 149 ), the moment on supporting pad 1 is cancelled by keeping the detaching pad and supporting pad 2 at the same distance from supporting pad 1. The moment on supporting pad 1 is also diminished by reducing the stiffness of the pad.

### 8.5.5.2 Force and moment on the supporting pads when the vertical and horizontal motors of the robot are actuated

The vertical motors on the supporting pads and the horizontal motors between the pads can also be actuated in order to cancel or diminish the force and moment on the supporting pads. When the vertical motors of the supporting pads and the horizontal motors are actuated, the total force on the detaching pad is:

$$\sum F_{DET} = -F + \frac{F_2}{2} - F_{det,2} + \frac{F_1}{2} \quad (150)$$

The total force on supporting pad 1 is:

$$\sum F_{SUP1} = \frac{F}{2} + F_{sp1} + \frac{F_2}{2} + F_{sp1,2} - F_1 \quad (151)$$

The total force on supporting pad 2 is:

$$\sum F_{SUP2} = \frac{F}{2} - F_{sp2} - F_2 + \frac{F_1}{2} \quad (152)$$

Actuating the vertical motors of the supporting pads and the horizontal motors, the resulting moment on the detaching pad is:

$$\sum M_{DET} = F_2 \cdot (x_{12} + x_{23}) - F_{sp1,2} \cdot x_{23} + F_1 \cdot x_{23} + M_{23} \quad (153)$$

The resulting moment on supporting pad 1 is:

$$\sum M_{SUP1} = -F \cdot x_{23} + F_{sp2} \cdot x_{12} - F_{det} \cdot x_{23} + M_{12} - M_{23} \quad (154)$$

The resulting moment on supporting pad 2 is:

$$\sum M_{SUP2} = -F \cdot (x_{23} + x_{12}) + F_{sp1} \cdot x_{12} - F_1 \cdot x_{12} - M_{12} \quad (155)$$

In the previous Equations ( 150 )-( 155 ), the sign of the force considers that the pad is detaching and thus the stretch of the pad is:  $\Delta z < 0$ . For preloading of the pad:  $\Delta z < 0$ , the sign of each force in Equations ( 150 )- ( 155 ) is the opposite.

Therefore, the force and moment on the supporting pads can be reduced and cancelled by combining the actuation of all the motors in a robot with three pads in a line. The stage in the locomotion sequence, the adhesion between the pads and the tissue and the perturbations applied to the robot determine when the actuation of the motors is required in order to enhance stability.

## 8.6 Force and moment in the locomotion mechanism of a robot with three pads in a triangle

A robot with three pads in a line can only follow a straight line but a robot with three pads forming a triangle can steer, obtaining two-dimensional motion in the horizontal plane. Using the previous model of the soft pad attached to tissue, this section analyses the force and moment in a robot with three pads forming a triangle.

### 8.6.1 Locomotion mechanism of a robot with three pads in a triangle

The locomotion mechanism of a robot with three pads in a triangle is composed of six linear motors: one vertical motor for each pad and three horizontal motors to separate the pads. Figure 159a shows the sketch of a robot with three pads in a triangle: pad 1 is the moving pad and pads 2 and 3 are the supporting pads. Figure 159a also shows the parameters considered for the analysis of force and moment in the locomotion mechanism when pad 1 is moving:

- the distance from the reference surface to each pad:  $z_1$ ,  $z_2$  and  $z_3$ , and
- the distance between the three pads:  $d_{12}$ ,  $d_{13}$  and  $d_{23}$ .

Figure 159b shows the two-padded mechanism formed by pads 1 and 3 of the robot with three pads in a triangle. Figure 159c shows the two-padded mechanism formed by pads 1 and 2. Figure 159d shows the two-padded mechanism formed by pads 2 and 3.

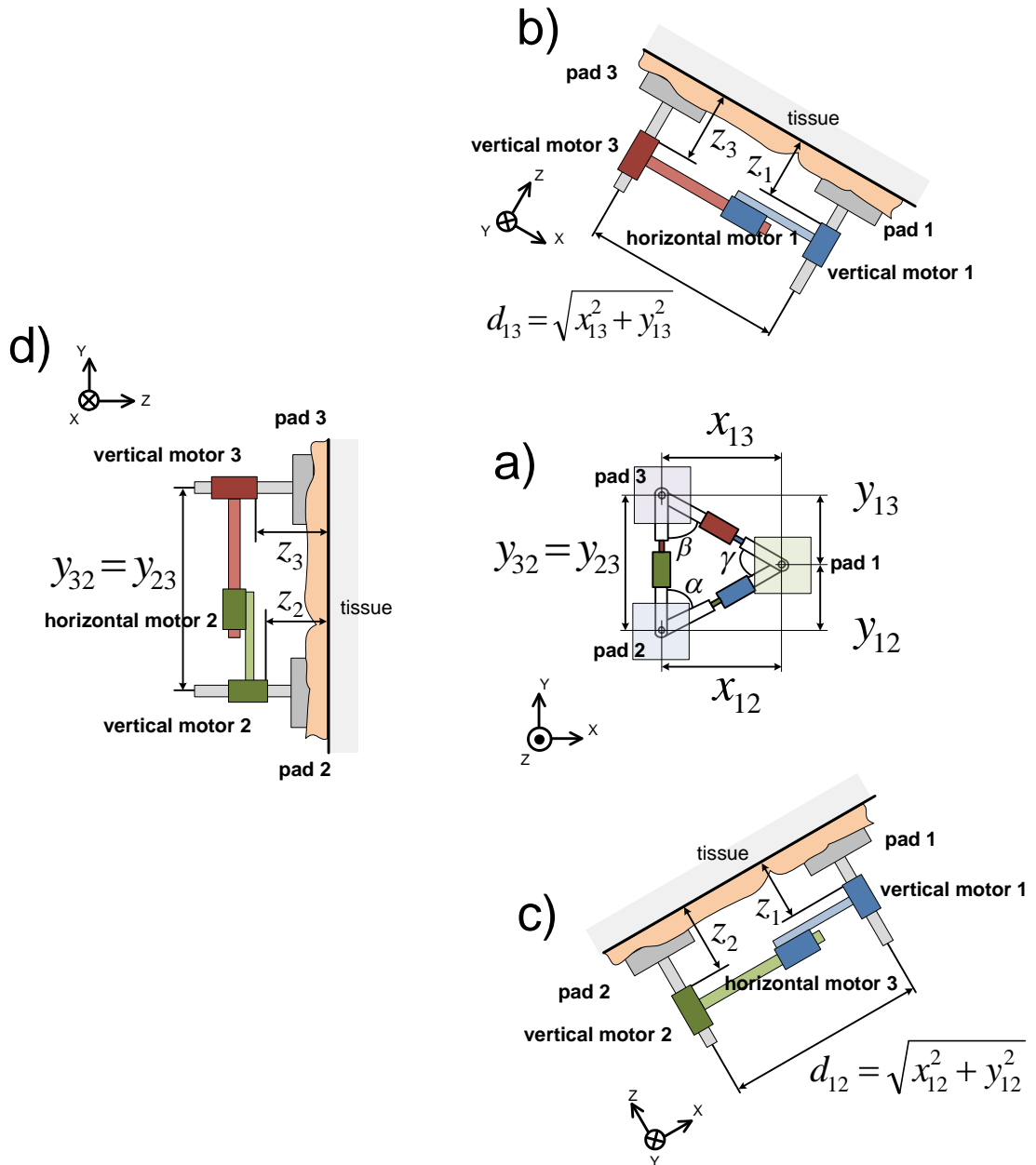


Figure 159. (a) Sketch of a robot with three pads in a triangle, (b) two-padded mechanism formed by pads 1 and 3, (c) two-padded mechanism formed by pads 1 and 2 and (d) two-padded mechanism formed by pads 2 and 3.

In Figure 159, the angles between the two horizontal links of the robot are:

$$\alpha = \text{atan}\left(\frac{x_{12}}{y_{12}}\right) \quad (156)$$

$$\beta = \text{atan}\left(\frac{x_{13}}{y_{13}}\right) \quad (157)$$

$$\gamma = 180^\circ - \alpha - \beta \quad (158)$$

Where  $x_{12}$  and  $y_{12}$  are the distance from pad 2 to the detaching pad along the X and Y axes respectively and,  $x_{13}$  and  $y_{13}$  are the distance from pad 3 to the detaching pad along the X and Y axes respectively.

Figure 160a shows the three springs in parallel modelling the stiffness of the three pads of the robot in the vertical direction. Figure 160b shows the two torsion springs modelling the bending of pad 1 and 3 in the horizontal plane. Figure 160c shows the two torsion springs modelling the bending of pad 1 and 2 in the horizontal plane.

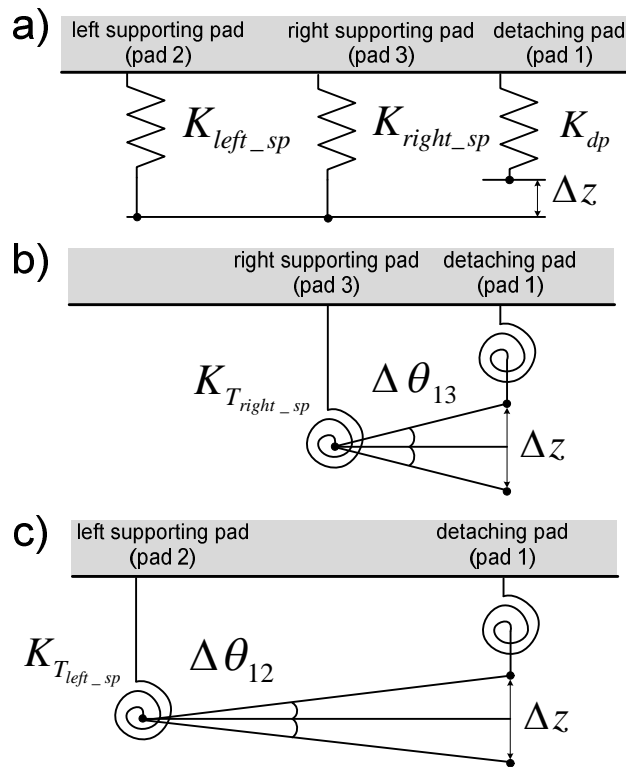


**Figure 160. (a) Linear springs modelling the stiffness of the pads in the vertical direction, (b) torsion spring modelling the bending of pad 3 and (c) torsion springs modelling the bending of pad 2.**

In Figure 160a, the two supporting pads of the robot feel the same stretch from the detaching pad:  $\Delta z$ . Two pads of the robot support the detachment of the pad and the force on each supporting pad is half the force applied to the detaching pad.

In Figure 160b, the bending angle of the right supporting pad (pad 3) is considered small and calculated as:

$$\Delta\theta_{13} = \frac{\Delta z}{d_{13}} \quad (159)$$

Where  $\Delta z$  is the stretch of the detaching pad and  $d_{13}$  is the distance between the detaching pad and the right supporting pad.

In Figure 160c, the bending angle of the left supporting pad (pad 2) is considered small and calculated as:

$$\Delta\theta_{12} = \frac{\Delta z}{d_{12}} \quad (160)$$

Where  $\Delta z$  is the stretch of the detaching pad and  $d_{12}$  is the distance between the detaching pad and the left supporting pad.

### **8.6.2 Vertical force on the detaching pad**

When vertical force is applied to the moving pad, the supporting pads stretch and bend, thus applying force and moment to the supporting pads. In a robot with three pads in a triangle, the bending of each supporting pad causes the other supporting pad to stretch and compress because of the link between the two supporting pads. Figure 161 shows the force and moment transmitted along the link between the two supporting pads of the robot. Figure 161a shows the force on the free body diagram of the left supporting pad and the right supporting pad when a detach force and a preload are applied to the moving pad. Figure 157b shows the moment on the free body diagram of the left supporting pad and the right supporting pad when a detach force and a preload are applied to the moving pad.

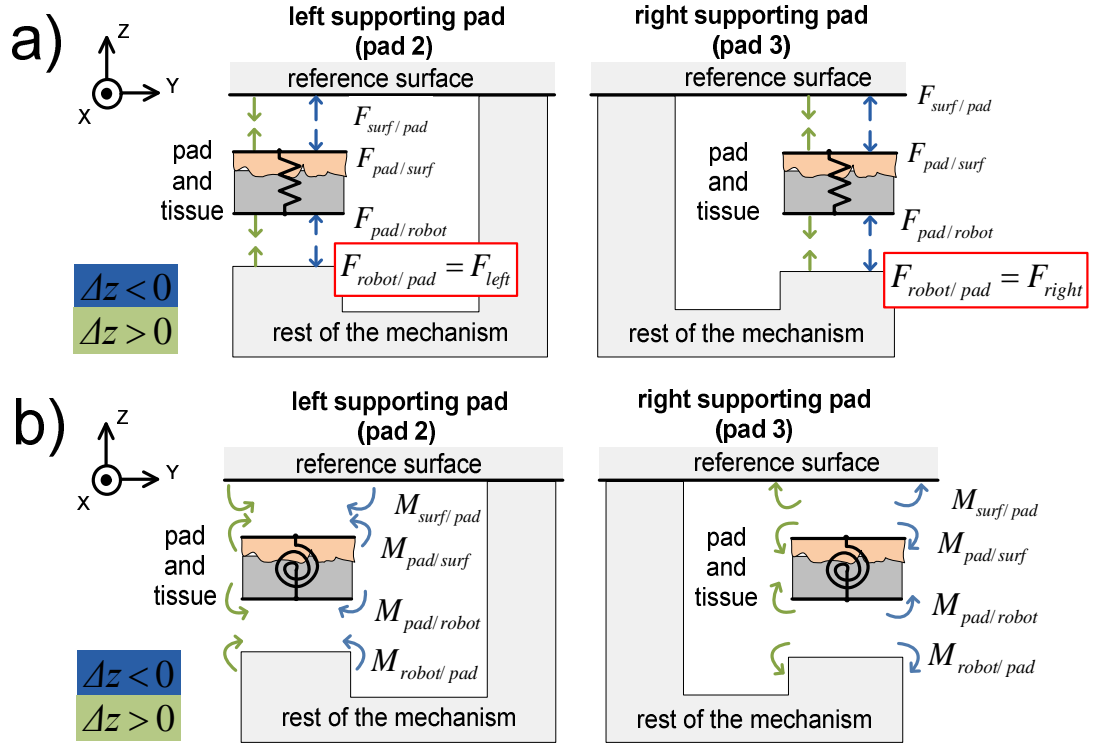


Figure 161. (a) Free body diagram of the force on the supporting pads when vertical force is applied to the moving pad, and (b) free body diagram of the moment on the supporting pads when vertical force is applied to the moving pad.

In Figure 161a, when vertical force is applied to the detaching pad, the link between the supporting pads causes stretch on each supporting pad. The stretch of the left supporting pad causes force on the right supporting pad:  $F_{right}$ . The stretch of the right supporting pad causes force on the left supporting pad:  $F_{left}$ . These forces:  $F_{right}$  and  $F_{left}$  cause the moment on the supporting pads shown in Figure 161b. The value of  $F_{right}$  and  $F_{left}$  is:

$$F_{right} = K \cdot \Delta z_{left} \quad (161)$$

$$F_{left} = K \cdot \Delta z_{right} \quad (162)$$

Where  $K = K_c$  is the compression stiffness of the pad and tissue when  $\Delta z < 0$  and  $K = K_t$  is the tension stiffness of the pad and tissue when  $\Delta z > 0$ . The value of  $\Delta z_{left}$  is the stretch of the left supporting pad that causes  $F_{right}$  and  $\Delta z_{right}$  is the stretch of the right supporting pad that causes  $F_{left}$ .

In terms of the stretch of the detaching pad, the distance between the pads and the angle between the horizontal links, the stretch of the left supporting pad is:

$$\Delta z_{left} = \frac{\Delta z}{d_{12}} \cdot \cos(\alpha) \cdot d_{23} \quad (163)$$

Where  $\Delta z$  is the stretch of the detaching pad,  $d_{12}$  is the distance between the detaching pad (pad 1) and the left supporting pad (pad 2),  $\alpha$  is the angle between horizontal motor 2 and horizontal motor 3 (see Figure 159) and  $d_{23}$  is the distance between the supporting pads.

The stretch of the right supporting pad is:

$$\Delta z_{right} = \frac{\Delta z}{d_{13}} \cdot \cos(\beta) \cdot d_{23} \quad (164)$$

Where  $\Delta z$  is the stretch of the detaching pad,  $d_{13}$  is the distance between the detaching pad (pad 1) and the right supporting pad (pad 3),  $\beta$  is the angle between horizontal motor 1 and horizontal motor 2 (see Figure 159) and  $d_{23}$  is the distance between the supporting pads.

The force and moment applied to the detaching pad and the supporting pads by the vertical motor on the detaching pad are expressed in terms of:

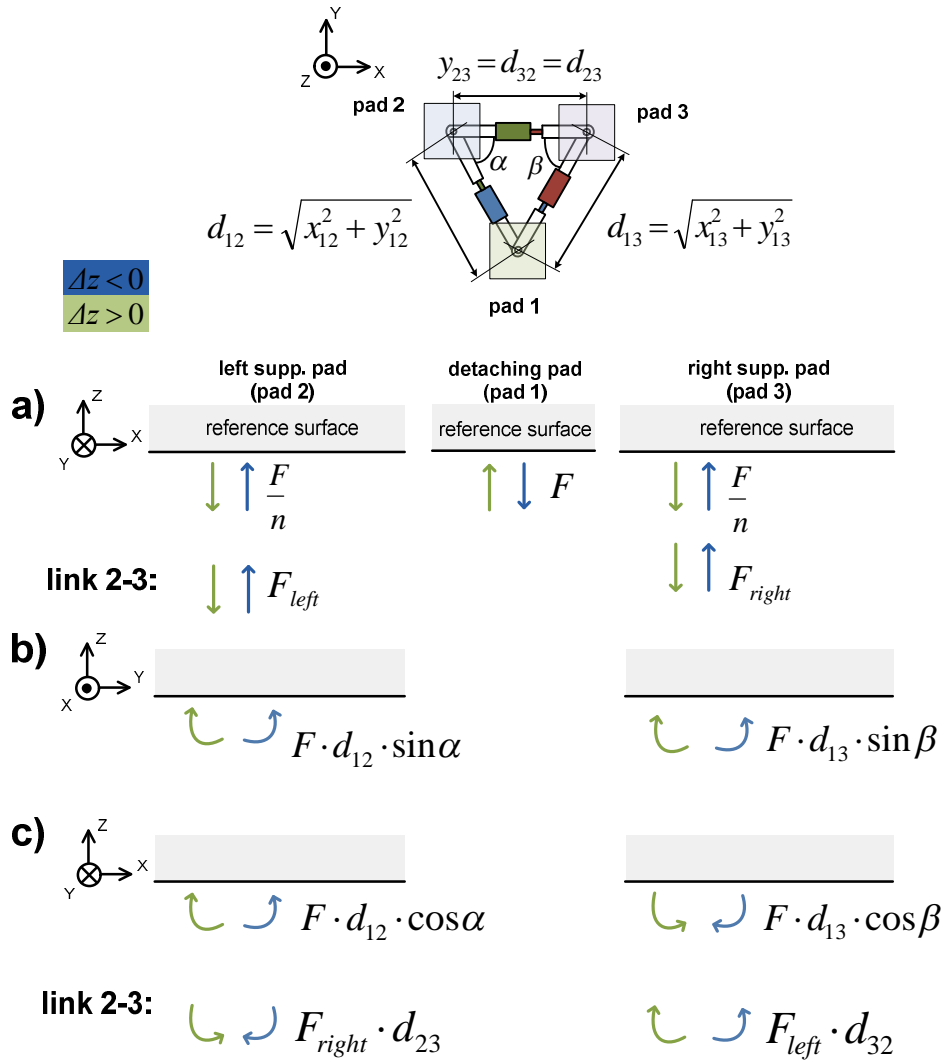
- the stiffness of the pads in tension:  $K_t$ , and compression:  $K_c$ ,
- the stretch caused by the vertical motor of the detaching pad:  $\Delta z$ ,
- the distance between the pads:  $d_{12}$ ,  $d_{13}$  and  $d_{23}$ ,
- the angle between the horizontal links of the robot:  $\alpha$  and  $\beta$ , and
- the total number of supporting pads:  $n$ , in a three pads:  $n = 2$ .

Table 15 shows the equations of the force and moment applied to the pads of the robot when the vertical motor of the detaching pad is actuated.

Table 15. Force and moment on the pads of a robot with three pads in a triangle when the vertical motor of the detaching pad is actuated.

		Left supp. pad	Det. Pad	Right supp. pad
<b>Force (Figure 162a)</b>	Detach: ( $\Delta z < 0$ )	$\left(\frac{K_t}{n} + K_c \cdot \cos \beta \cdot \frac{d_{32}}{d_{13}}\right) \cdot \Delta z$	$-K_t \cdot \Delta z$	$\left(\frac{K_t}{n} + K_c \cdot \cos \alpha \cdot \frac{d_{23}}{d_{12}}\right) \cdot \Delta z$
	Preload: ( $\Delta z > 0$ )	$-\left(\frac{K_c}{n} + K_t \cdot \cos \beta \cdot \frac{d_{32}}{d_{13}}\right) \cdot \Delta z$	$K_c \cdot \Delta z$	$-\left(\frac{K_c}{n} + K_t \cdot \cos \alpha \cdot \frac{d_{23}}{d_{12}}\right) \cdot \Delta z$
<b>Moment (X axis) (Figure 162b)</b>	Detach: ( $\Delta z < 0$ )	$-K_t \cdot d_{12} \cdot \sin \alpha \cdot \Delta z$	<i>no M</i>	$-K_t \cdot d_{13} \cdot \sin \beta \cdot \Delta z$
	Preload: ( $\Delta z > 0$ )	$K_c \cdot d_{12} \cdot \sin \alpha \cdot \Delta z$	<i>no M</i>	$K_c \cdot d_{13} \cdot \sin \beta \cdot \Delta z$
<b>Moment (Y axis) (Figure 162c)</b>	Detach: ( $\Delta z < 0$ )	$\left(K_c \cdot \frac{d_{23}^2}{d_{12}} - K_t \cdot d_{12}\right) \cdot \cos \alpha \cdot \Delta z$	<i>no M</i>	$\left(K_t \cdot d_{13} - K_c \cdot \frac{d_{32}^2}{d_{13}}\right) \cdot \cos \beta \cdot \Delta z$
	Preload: ( $\Delta z > 0$ )	$\left(K_c \cdot d_{12} - K_t \cdot \frac{d_{23}^2}{d_{12}}\right) \cdot \cos \alpha \cdot \Delta z$	<i>no M</i>	$\left(K_t \cdot \frac{d_{32}^2}{d_{13}} - K_c \cdot d_{13}\right) \cdot \cos \beta \cdot \Delta z$

Figure 162 shows the sketch of the force and moment summarised in Table 15 applied to the pads of the robot at the reference surface. Figure 162 shows the force and moment caused by the stretch of the detaching pad on the supporting pads. Figure 162 also shows the force and moment caused by the stretch of the supporting pads transmitted through the link connecting the supporting pads.



**Figure 162. (a) Force applied to the pads and when the vertical motor of the detaching pad is actuated, (b) moment applied to the supporting pads in the X direction and (c) moment applied to the supporting pads in the Y direction.**

In Figure 162a, Figure 162b and Figure 162c, the first row of force and moment is caused by the stretch of the detaching pad when the vertical motor of the detaching pad is actuated:  $F$ . In Figure 162a and Figure 162c, the second row of force and moment is caused by the stretch of the supporting pads through the link between the supporting pads:  $F_{right}$  and  $F_{left}$ .

### 8.6.3 Vertical force on the supporting pads

The analysis of force and moment when vertical force is applied to the left supporting pad (pad 2) and the right supporting pad (pad 3), is identical to the analysis for the detaching pad. When vertical force is applied to the left supporting pad (pad 2), the force from the vertical motor is:

$$F_2 = K^{sp2} \cdot \Delta z_2 \quad (165)$$

Where  $K^{sp2}$  is the stiffness of the left supporting pad and  $\Delta z_2$  is the stretch of the left supporting pad.

When the vertical motor of the left supporting pad is actuated, the forces that the other two pads cause on each other are:

$$F_{right,2} = K^{sp2} \cdot \frac{d_{13}}{d_{23}} \cdot \cos(\beta) \cdot \Delta z_2 \quad (166)$$

$$F_{left,2} = K^{sp2} \cdot \frac{d_{13}}{d_{12}} \cdot \cos(\gamma) \cdot \Delta z_2 \quad (167)$$

Where:

- $K^{sp2}$  is the stiffness of the left supporting pad,
- $d_{13}$  is the distance between the detaching pad and the right supporting pad,
- $d_{23}$  is the distance between the supporting pads,
- $d_{12}$  is the distance between the detaching pad and the left supporting pad,
- $\Delta z_2$  is the stretch of the left supporting pad,
- $\beta$  is the angle between horizontal motor 1 and horizontal motor 2 (see Figure 159), and
- $\gamma$  is the angle between horizontal motor 1 and horizontal motor 3 (see Figure 159).

When vertical force is applied to the right supporting pad (pad 3), the force from the vertical motor is:

$$F_3 = K^{sp3} \cdot \Delta z_3 \quad (168)$$

Where  $K^{sp3}$  is the stiffness of the right supporting pad and  $\Delta z_3$  is the stretch of the right supporting pad.

When the vertical motor of the right supporting pad is actuated, the forces that the other two pads cause on each other are:

$$F_{right,3} = K^{sp3} \cdot \frac{d_{12}}{d_{13}} \cdot \cos(\alpha) \cdot \Delta z_3 \quad (169)$$

$$F_{left,3} = K^{sp3} \cdot \frac{d_{12}}{d_{23}} \cdot \cos(\gamma) \cdot \Delta z_3 \quad (170)$$

Where:

- $K^{sp3}$  is the stiffness of the right supporting pad,
- $d_{13}$  is the distance between the detaching pad and the right supporting pad,
- $d_{23}$  is the distance between the supporting pads,
- $d_{12}$  is the distance between the detaching pad and the left supporting pad,

- $\Delta z_3$  is the stretch of the right supporting pad,
- $\alpha$  is the angle between horizontal motor 2 and horizontal motor 3 (see Figure 159), and
- $\gamma$  is the angle between horizontal motor 1 and horizontal motor 3 (see Figure 159).

#### 8.6.4 Force from the horizontal motor between the pads

When the horizontal motors between the pads are actuated, the force and moment on the pads are calculated considering the mechanism of the robot the superposition of:

- the actuation of the horizontal motor in a two-padded robot composed of the left supporting pad (pad 2) and the detaching pad,
- the actuation of the horizontal motor in a two-padded robot composed of the left supporting pad (pad 2) and the right supporting pad (pad 3), and
- the actuation of the horizontal motor in a two-padded robot composed of the detaching pad and the right supporting pad (pad 3).

The moment from the horizontal motor between the detaching pad (pad 1) and the left supporting pad (pad 2) is:

$$M_{12} = F_{h12} \cdot z_{12} \quad (171)$$

Where  $F_{h12}$  is the force from the horizontal motor 3 (see Figure 159) and  $z_{12}$  is the distance between the reference surface and the horizontal motor.

The moment from the horizontal motor between the left supporting pad (pad 2) and the right supporting pad (pad 3), is:

$$M_{23} = F_{h23} \cdot z_{23} \quad (172)$$

Where  $F_{h23}$  is the force from the horizontal motor 2 (see Figure 159) and  $z_{23}$  is the distance between the reference surface and the horizontal motor.

The moment from the horizontal motor between the detaching pad (pad 1) and the right supporting pad (pad 3) is:

$$M_{13} = F_{h13} \cdot z_{13} \quad (173)$$

Where  $F_{h13}$  is the force from the horizontal motor 1 (see Figure 159) and  $z_{13}$  is the distance between the reference surface and the horizontal motor.

#### 8.6.5 Control strategies for a robot with three pads in a triangle

In order to enhance the stability of the robot, the strategies considered in the first place are the strategies that can be implemented when only the vertical

motor of the detaching pad is actuated. If the stability margin of the pads needs to increase further, the vertical motors of the supporting pads and the horizontal motors in the locomotion mechanism can also be actuated.

#### **8.6.5.1 Strategies to reduce the force and moment on the supporting pads when the vertical motor of the detaching pad is actuated**

Considering the previous analysis of force and moment in a robot with three pads in a triangle, when the vertical motor on the detaching pad is actuated, the force on the supporting pads cannot be cancelled.

When the vertical motor on the detaching pad is actuated, the force on the supporting pads can be reduced by increasing the value of the angles  $\beta$  and  $\alpha$ . In order to increase  $\beta$ : the distance  $x_{13}$  can increase and the distance  $y_{13}$  can decrease; in order to increase  $\alpha$ : the distance  $x_{12}$  can increase and the distance  $y_{12}$  can decrease.

The force on the supporting pads can also be reduced by decreasing the distance  $y_{32}$ . The value of  $x_{13}$  and  $y_{13}$  can be increased in order to increase  $d_{13}$  and therefore decrease the force on the left supporting pad. The value of  $x_{12}$  and  $y_{12}$  can be increased in order to increase  $d_{12}$  and therefore decrease the force on the right supporting pad.

Increasing  $x_{13}$  and  $x_{12}$  is beneficial in order to increase the angles:  $\beta$  and  $\alpha$  and also the distances:  $d_{13}$  and  $d_{12}$ , thus reducing the force on the supporting pads. When  $y_{13}$  and  $y_{12}$  increase, the force on the supporting pads is reduced by increasing the distances:  $d_{13}$  and  $d_{12}$ . However, increasing  $y_{13}$  and  $y_{12}$  also decrease the angles:  $\beta$  and  $\alpha$ , increasing the force on the supporting pads.

When the vertical motor on the detaching pad is actuated, the moment along the X direction of the horizontal plane cannot be cancelled with three pads in a triangle. The moment along the X direction of the horizontal plane cancels with three pads in a line as previously shown. The moment along the X direction is not cancelled in a robot with three pads in a triangle because this configuration lacks a supporting pad directly opposite to the detaching pad.

The moment along the X direction of the horizontal plane can be reduced:

- with softer pads,
- decreasing  $d_{12}$  and  $d_{13}$ , by reducing  $x_{12}$  and  $y_{12}$  on the left supporting pad and reducing  $x_{13}$  and  $y_{13}$  on the right supporting pad,
- decreasing  $\sin(\alpha)$  and  $\sin(\beta)$  by reducing  $x_{12}$  and  $x_{13}$ , and also by increasing  $y_{12}$  and  $y_{13}$ .

When the vertical motor on the detaching pad is actuated, the moment along the Y axis on the left supporting pad is cancelled when:

$$d_{23} = d_{12} \cdot \sqrt{r_K} \quad (174)$$

The moment along the Y axis on the right supporting pad is cancelled when:

$$d_{23} = d_{13} \cdot \sqrt{r_K} \quad (175)$$

In Equations ( 174 ) and ( 175 ):  $r_K = \frac{K_t}{K_c}$  is the ratio of tension and compression stiffness of the pad when the pad is detaching:  $\Delta z < 0$ , and  $r_K = \frac{K_c}{K_t}$  is the ration of compression and tension stiffness of the pad when the motor is preloading the pad:  $\Delta z > 0$ .

If compression stiffness and the tension stiffness of the pad and tissue are the same ( $K_c = K_t$ ) the moment along the Y axis on both supporting pads is cancelled when the distance between the pads is the same:

$$d_{12} = d_{23} = d_{13} \quad (176)$$

The moment on the pads is also reduced if  $\cos(\alpha)$  and  $\cos(\beta)$  diminish by increasing  $x_{12}$  and  $x_{13}$ , and decreasing  $y_{12}$  and  $y_{13}$ .

### 8.6.5.2 Force and moment on the supporting pads when the vertical and horizontal motors of the robot are actuated

The vertical motors on the supporting pads and the horizontal motors between the pads can also be actuated in order to cancel or diminish the force and moment on the supporting pads. When the vertical motors of the supporting pads and the horizontal motors are actuated, the total force on the detaching pad is:

$$\sum F_{DET} = -F + \frac{F_2}{2} + F_{right,2} + \frac{F_3}{2} + F_{left,3} \quad (177)$$

The total force on the left supporting pad (pad 2) is:

$$\sum F_{LEFT} = \frac{F}{2} + F_{left} - F_2 + \frac{F_3}{2} + F_{right,3} \quad (178)$$

The total force on the right supporting pad (pad 3) is:

$$\sum F_{RIGHT} = \frac{F}{2} + F_{right} + \frac{F_2}{2} + F_{left,2} - F_3 \quad (179)$$

Actuating the vertical motors of the supporting pads and the horizontal motors, the resulting moment on the detaching pad along the X direction of the horizontal plane is:

$$\begin{aligned} \sum M_{DET}^X &= F_2 \cdot d_{12} \cdot c_1(\beta, \gamma) - F_{left,2} \cdot d_{13} \cdot \cos(\beta) + F_3 \cdot d_{13} \cdot c_2(\gamma) \\ &\quad + F_{right,3} \cdot d_{12} \cdot \sin\left(\frac{\gamma}{2}\right) - M_{12} \cdot \cos(\alpha) + M_{13} \cdot \cos(\beta) \end{aligned} \quad (180)$$

Where  $c_1(\beta, \gamma)$  and  $c_2(\gamma)$  are geometrical functions which depend on the angles  $\beta$  and  $\gamma$ :  $c_1(\beta, \gamma) = \cos(\gamma) \cdot \sin(\beta) - \sin(\gamma) \cdot \cos(\beta)$ ,  $c_2(\gamma) = \cos(\gamma) \cdot \cos\left(\frac{\gamma}{2}\right) - \sin(\gamma) \cdot \sin\left(\frac{\gamma}{2}\right)$ .

The resulting moment on the detaching pad along the Y direction of the horizontal plane is:

$$\begin{aligned} \sum M_{DET}^Y &= -F_2 \cdot d_{12} \cdot c_3(\beta, \gamma) - F_{left,2} \cdot d_{13} \cdot \sin(\beta) + F_3 \cdot d_{13} \cdot c_4(\gamma) \\ &\quad - F_{right,3} \cdot d_{12} \cdot \cos\left(\frac{\gamma}{2}\right) - M_{12} \cdot \sin(\alpha) - M_{13} \cdot \sin(\beta) \end{aligned} \quad (181)$$

Where  $c_3(\beta, \gamma)$  and  $c_4(\gamma)$  are geometrical functions which depend on the angles  $\beta$  and  $\gamma$ :  $c_3(\beta, \gamma) = \sin(\gamma) \cdot \sin(\beta) + \cos(\gamma) \cdot \cos(\beta)$ ,  $c_4(\gamma) = \cos(\gamma) \cdot \cos\left(\frac{\gamma}{2}\right) + \cos(\gamma) \cdot \sin\left(\frac{\gamma}{2}\right)$ .

Actuating the vertical motors of the supporting pads and the horizontal motors, the resulting moment on the left supporting pad (pad 2) along the X direction of the horizontal plane is:

$$\begin{aligned} \sum M_{LEFT}^X &= F \cdot d_{12} \cdot \sin(\alpha) - F_{right} \cdot d_{23} - F_3 \cdot d_{23} \cdot c_5(\alpha, \gamma) \\ &\quad - F_{left,3} \cdot d_{12} \cdot \sin\left(\frac{\gamma}{2}\right) + M_{23} + M_{12} \cdot \cos(\alpha) \end{aligned} \quad (182)$$

Where  $c_5(\alpha, \gamma)$  is a geometrical function which depends on the angles  $\alpha$  and  $\gamma$ :  $c_5(\alpha, \gamma) = \sin(\alpha) \cdot \sin\left(\frac{\gamma}{2}\right) + \cos(\alpha) \cdot \cos\left(\frac{\gamma}{2}\right)$ .

The resulting moment on the left supporting pad (pad 2) along the Y direction of the horizontal plane is:

$$\begin{aligned} \sum M_{LEFT}^Y &= -F \cdot d_{13} \cdot \cos(\alpha) + F_3 \cdot d_{23} \cdot c_6(\alpha, \gamma) + F_{left,3} \cdot d_{12} \\ &\quad \cdot \cos\left(\frac{\gamma}{2}\right) + M_{12} \cdot \sin(\alpha) \end{aligned} \quad (183)$$

Where  $c_6(\alpha, \gamma)$  is a geometrical function which depends on the angles  $\alpha$  and  $\gamma$ :  $c_6(\alpha, \gamma) = \sin(\alpha) \cdot \cos\left(\frac{\gamma}{2}\right) - \cos(\alpha) \cdot \sin\left(\frac{\gamma}{2}\right)$ .

Actuating the vertical motors of the supporting pads and the horizontal motors, the resulting moment on the right supporting pad (pad 3) along the X direction of the horizontal plane is:

$$\begin{aligned} \sum M_{RIGHT}^X &= F \cdot d_{13} \cdot \sin(\beta) + F_{left} \cdot d_{23} - F_2 \cdot d_{23} \cdot c_7(\beta) \\ &\quad + F_{right,2} \cdot d_{13} \cdot \cos(\beta) - M_{23} - M_{13} \cdot \cos(\beta) \end{aligned} \quad (184)$$

Where  $c_7(\beta)$  is a geometrical function which depends on the angle  $\beta$ :  $c_7(\beta) = 2 \cdot \sin(\beta) \cdot \cos(\beta)$ .

The resulting moment on the right supporting pad (pad 3) along the Y direction of the horizontal plane is:

$$\sum M_{RIGHT}^Y = F \cdot d_{13} \cdot \cos(\beta) - F_2 \cdot d_{23} \cdot c_8(\beta) + F_{right,2} \cdot d_{13} \cdot \sin(\beta) + M_{13} \cdot \sin(\beta) \quad (185)$$

Where  $c_8(\beta)$  is a geometrical function which depends on the angle  $\beta$ :  $c_8(\beta) = \sin^2(\beta) - \cos^2(\beta)$ .

The sign of the force in Equations ( 177 )-( 185 ) consider that the pad is detaching and thus the stretch of the pad is:  $\Delta z < 0$ . For preloading of the pad:  $\Delta z < 0$ , the sign of each force in Equations ( 177 )-( 185 ) is the opposite.

In Equations ( 177 )-( 185 ), the sign of the moment depends on the sign of the geometrical constants:  $c_1$  to  $c_8$ , which depend on the value of the angles between the horizontal links of the robot:  $\alpha$ ,  $\beta$  and  $\gamma$ . The value of the angles  $\alpha$ ,  $\beta$  and  $\gamma$  is considered between  $0^\circ$  and  $90^\circ$ .

Therefore, combining the actuation of all the motors in a robot with three pads in a triangle can reduce and cancel the force and moment on the supporting pads. The actuation of the motors required in order to enhance stability depends on the stage in the locomotion sequence, the adhesion between the pads and tissue and the perturbations on the robot.

## 8.7 An adhesion-reliant robot with four pads forming a quadrilateral

The benefit of having three pads in a line and having three pads in a triangle are combined by including a fourth pad in the locomotion mechanism of the robot. In a robot with three pads in a line, the moment in the X direction of the horizontal plane is cancelled for the supporting pad in the middle of the mechanism. With three pads in a triangle, the robot can move in both directions of the horizontal plane and the moment in the Y direction of the horizontal plane is cancelled for the supporting pads. The cancellation of moment on the supporting pads increases the stability margin of the robot by reducing the moment that causes the pads to peel off.

In this way, a robot with four adhesive pads can be considered the superposition of a locomotion mechanism with three pads in a line and a locomotion mechanism with three pads forming a triangle. Figure 163 shows

how the locomotion mechanism of a robot with four pads can be analysed as a robot with three pads in a line and a robot with three pads in a triangle.

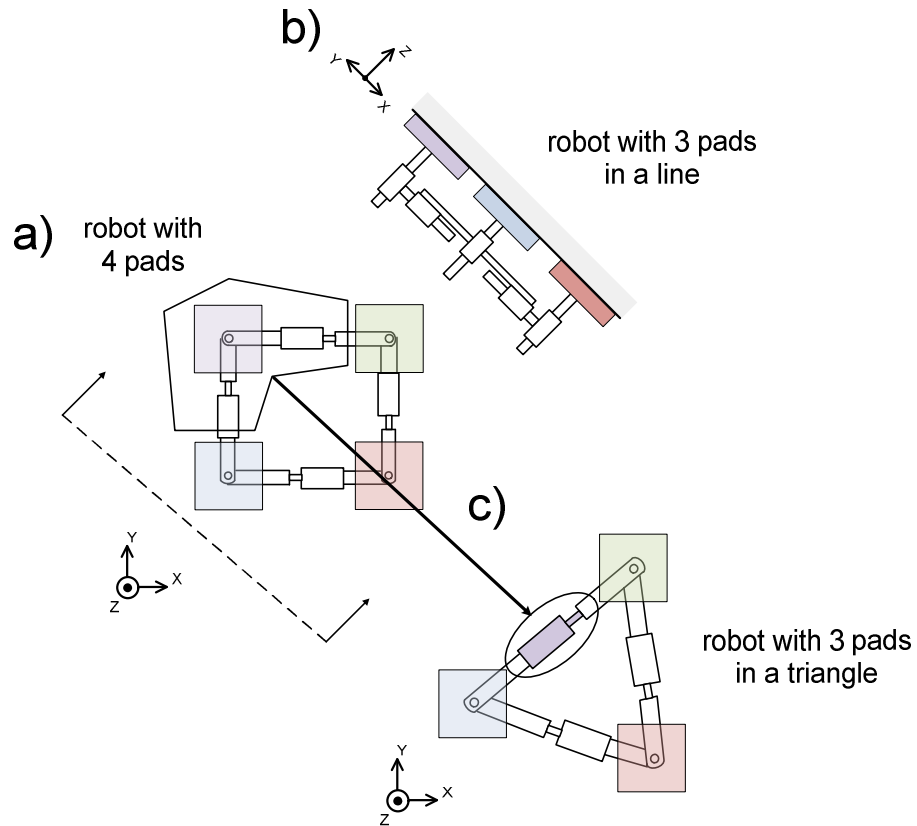


**Figure 163. (a) Sketch of a robot with four pads, (b) a robot with four pads can be analysed as a robot with three pads in a line and (c) a robot with four pads can be analysed as a robot with three pads in a triangle.**

Figure 163a shows the sketch of a robot with four pads arranged in a quadrilateral like the intra-abdominal robot. A robot with four pads arranged in a quadrilateral can be analysed as a robot with three pads in a line along the diagonal of the quadrilateral formed by the four pads as shown in Figure 163b. Considering the horizontal motors joined at the fourth pad as a horizontal link, a robot with four pads can be analysed as a robot with three pads in a triangle as shown in Figure 163c. Therefore, the control strategies for a robot with three pads can be combined in order to reduce and cancel the force and moment on the supporting pads of a robot with four pads.

In the implementation of the intra-abdominal robot, a robot with four pads proved to be a design able to obtain upside-down locomotion using adhesive pads. For the intra-abdominal robot, a locomotion mechanism with two pads and with three pads in a triangle were tested unsuccessfully. In these two-padded and three-padded robots, the detaching force and weight of the detached pad caused the supporting pads to peel off, making the robot to fall

off. Figure 164 shows the prototype of a robot with two magnetic pads and three motors. In Figure 164, the vertical motor of the detaching pad is actuated causing the detaching pad to peel off but also causing the supporting pad to peel off.

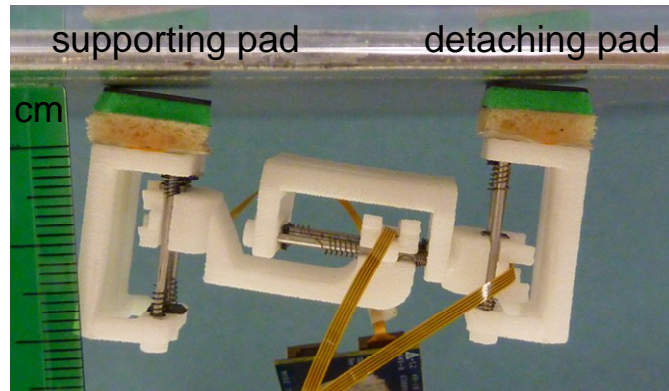


Figure 164. Prototype of a robot with two pads detaching one pad.

## 8.8 Alternative designs for an adhesion-reliant robot with four adhesive pads forming a quadrilateral

Alternative designs of a robot with four pads can be produced by linking the pads of the robot along the diagonals of the quadrilateral formed by the horizontal motors. These links are extensible in order to enable locomotion and the way these links are connected determines the transmission of moment between the pads:

- if the diagonal links are unconnected at the centre of the quadrilateral, the moment from the detaching pad is only transmitted to the supporting pad connected to the detaching pad,
- if the diagonal links are connected at the centre of the quadrilateral, the moment from the detaching pad is distributed amongst all the supporting pads.

Figure 165a shows the sketch of a four-padded robot with diagonal links unconnected at the centre of the quadrilateral. Figure 165b shows the sketch of a four-padded robot with diagonal links connected at the centre of the quadrilateral.

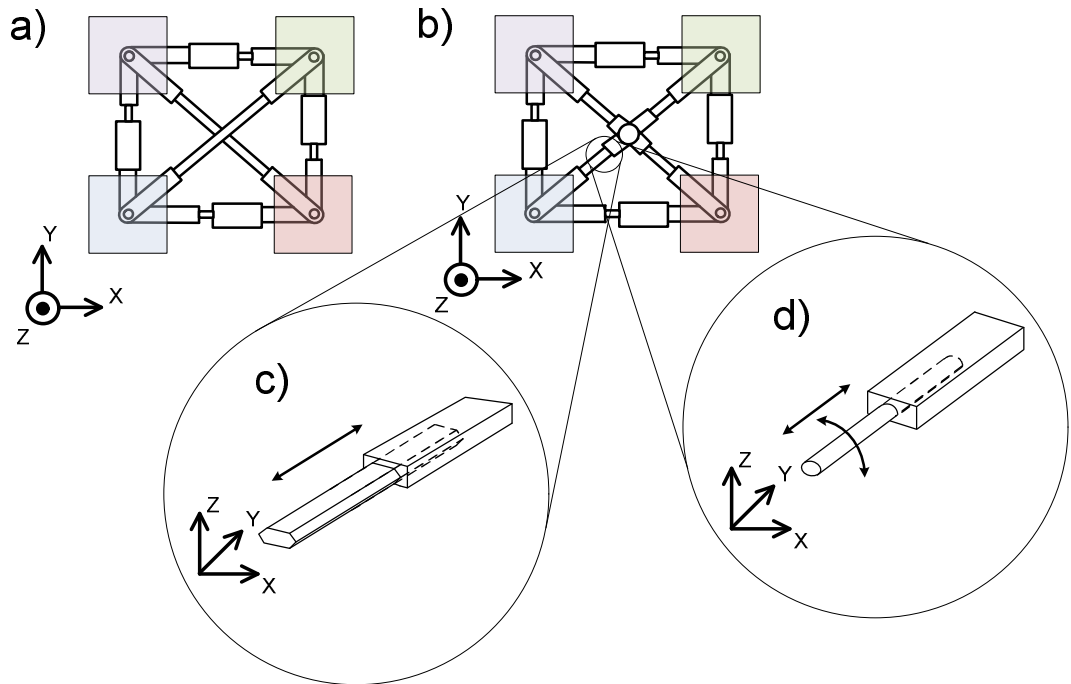


**Figure 165. (a) Sketch of a four-padded robot with diagonal links unconnected at the centre of the quadrilateral, (b) four-padded robot with diagonal links connected at the centre of the quadrilateral, (c) prismatic joint at the connection of the diagonal links, and (d) prismatic and revolute joint at the connection of the diagonal links.**

When the diagonal links are connected at the centre of the quadrilateral, the way the moment is distributed amongst the pads depends on the type of joint used for the connection between the links:

- a prismatic joint connecting the diagonal links enables extension of the links and transmission of moment from the detaching pad to all the supporting pads,
- a prismatic joint and a revolute joint connecting the diagonal links enables extension of the links and transmission of moment between the detaching pad and the supporting pad opposite to the detaching pad.

Figure 165c above shows the prismatic joint at the connection of the diagonal links, and Figure 165d above shows the prismatic and revolute joint at the connection of the diagonal links.

Adding diagonal links to a four-padded robot can be beneficial to support the detaching pad more firmly and further enhance the stability of the robot. These diagonal links require precision manufacturing for the miniature size and were not implemented for the intra-abdominal robot.

## 8.9 An adhesion-reliant robot with more than four adhesive pads

For the design of the intra-abdominal robot with four pads forming a quadrilateral, and the addition of diagonal links to the locomotion mechanism, these design principles were followed:

- symmetry of the configuration of the pads, so that the locomotion sequence of the robot is the same for all directions of the horizontal plane, and
- equal conditions of support and actuation for all the pads of the robot, so that the pads are interchangeable for the controller of the robot.

Keeping symmetry and equal conditions of support and actuation for the pads, more pads can be included in the design of the robot by adding pads to the quadrilateral. In this way, a fifth pad can be added forming a pentagon, a sixth pad can be added forming a hexagon and so on. Diagonal links can also be included in these designs of the robot with more than four pads. In order to illustrate these designs with more than four pads, Figure 166a shows the sketch of a robot with five pads and Figure 166b shows the sketch of a robot with six pads. Figure 166c shows the diagonal links in a five-pads robot and Figure 166d shows the diagonal links in a six-pads robot.

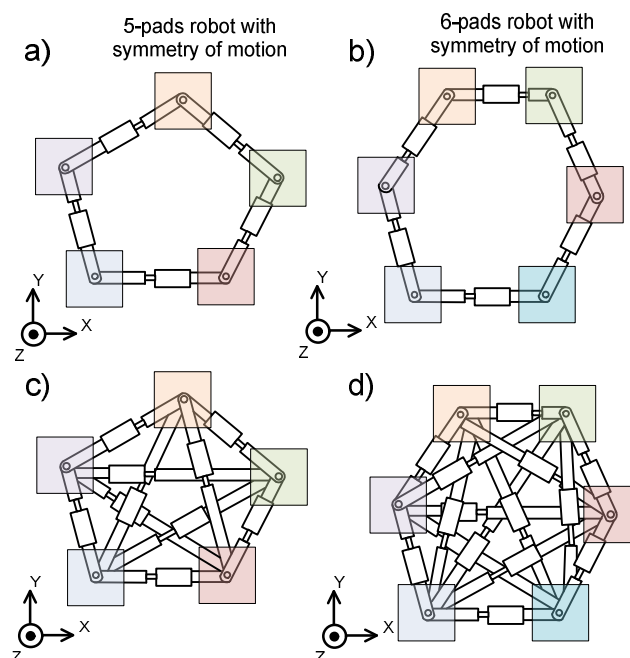


**Figure 166.** (a) Sketch of a robot with five pads, (b) sketch of a robot with six pads, (c) diagonal links for a five-pads robot and (d) diagonal links for a six-pads robot.

Figure 166 shows how the complexity of the locomotion mechanism increases when adding more pads and including diagonal links. If the design

principle of symmetry and equal conditions of support and actuation is not followed, the number of diagonal links can be reduced and pads in alternative positions can be included in the locomotion mechanism. In order to illustrate the variability of these alternative designs for the robot:

- Figure 167a shows the sketch of a six-pads robot with asymmetric links,
- Figure 167b shows a four-padded robot with a central pad,
- Figure 167c shows a six-pads robot with satellite pads, and
- Figure 167d shows an eight-pads robot with an outer ring of four pads and an inner ring of four pads.

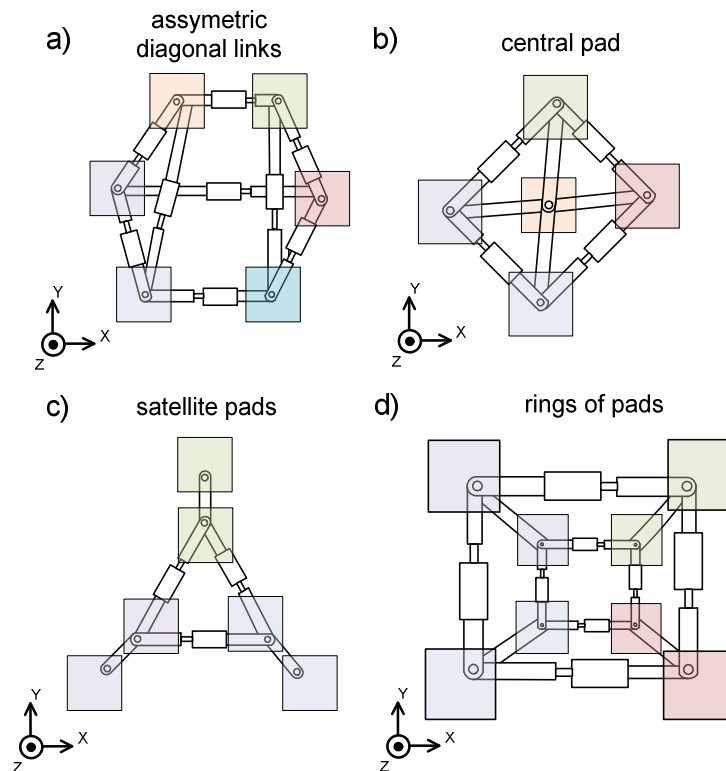


**Figure 167. (a) A robot with asymmetric diagonal links, (b) a robot with a pad in the centre of the mechanism, (c) a robot with satellite pads and (d) a robot with concentric rings of pads.**

In the four-padded intra-abdominal robot, one pad moves at a time in the locomotion sequence because the robot falls down when more than one pad are detached. In a robot with more than four pads, if the robot is stable with more than one pad detached, more than one pad can be moved at a time in the locomotion sequence. In this way, the speed of a robot with more than four pads can be increased.

## 8.9 Discussion and conclusions

The stability criterion defined in Chapter 7 showed how the stability of a robot moving in inverted adhesion-reliant locomotion depends on the forces

applied to the adhesive pads. In order to control the robot, the way forces are transmitted through the locomotion mechanism and how those forces are enhanced or diminished needs to be studied. Such study was carried out in this chapter starting with the analysis of the most basic configuration: an inchworm walker with two pads and two vertical linear motors joined by one horizontal linear motor.

The two-padded configuration showed the way forces are transmitted between a detaching and a supporting pad and set the base of the analysis for more complex configurations. Following the analysis of a two-padded robot, the configurations of three pads in a line and in a triangle were studied because the mechanism of a four-padded robot can be analysed as the superposition of those two three-padded configurations. As the analysis showed, the combination of the two three-padded configurations, in a line and in a triangle, diminishes the moment on the supporting pads, therefore significantly increasing the stability margin of the robot.

This result of the analysis fully agrees with the testing of the robot, given that during the building of the robot it was observed how only a four-padded configuration was able to support the inverted locomotion of the prototype. Four pads were required in the design of the locomotion mechanism in order to keep a strong base of support of three pads while one of the pads moved to the new position. The analysis in this chapter relates that “strong base of support of three pads” to the diminishing of peeling moment taking place in the supporting pads when the force from the motor detaching one pad is transmitted through the mechanism. The chapter also defines control strategies to enhance the stability margin of the pads as much as possible with the actuators of the locomotion mechanism. Such control strategies can be implemented in a further development of the locomotion controller in order to obtain precise control of the attachment and detachment of the pads of the robot.

## **8.10 Summary**

In this chapter, the force and moment applied to the locomotion mechanism of adhesion-reliant robots were analysed, defining control strategies for the locomotion of the robot. The force and moment on the locomotion mechanism of a robot with two pads were analysed first. This analysis considered the actuation of the vertical motor on the detaching pad as well as the actuation of the vertical motor on the supporting pad and the horizontal motor between the pads. Control strategies were defined for the

locomotion mechanism of the two-padded robot in order to reduce the force and moment applied to the supporting pads and thus, increase the stability margin of the robot.

Then, a robot with three pads was analysed for two configurations of the pads: three pads in a line and three pads in a triangle. The analysis considered the actuation of all the vertical motors and horizontal motors in the locomotion mechanism, defining control strategies in order to reduce the force and moment applied to the supporting pads. With the configuration of three pads in a line, the moment in the X direction of the horizontal plane is cancelled for the supporting pad in the middle. With the configuration of three pads in a triangle, the moment in the Y direction of the horizontal plane is cancelled for the supporting pads.

Adding a fourth pad to the robot combines the benefits of three pads in a line and three pads in a triangle. The four pads can be arranged in a quadrilateral and can include diagonal links between the pads. Robot with more than four pads arranged symmetrically or asymmetrically, and moving more than one pad at a time can also be considered.

## **Chapter 9**

### **Conclusions and future work**

#### **9.1 Assessment of the research objectives**

The research aims and their corresponding objectives were defined in the introductory chapter (Chapter 1). This section explains the extent to which the research objectives have been achieved.

1. Review existing literature on robotic surgery, robotic intra-body devices and miniature climbing robots using bio-inspired adhesives.

The literature review of Chapter 2 covered the field of robotic devices used for surgery, from well established commercial applications to state-of-the-art research robots. The review focused on the evolution from the paradigm of floor-mounted robotic arms to the trend of miniaturization to build intra-body robots, internalising their locomotion. In this way, the advantages and desirable improvements to the different developments found in the literature were pointed out. The selection of the design features of the intra-abdominal robot was helped by this review of surgical robots as well as by reviewing current miniature climbing robots using adhesion. This type of robots are particularly relevant to the design of the intra-abdominal robot because they are small and move in inverted locomotion with very similar attachment technology. The chapter finally compared all the reviewed types of robots, highlighting how their features could be considered for the design of the intra-abdominal robot.

2. Design a miniature mechanism to apply a controllable set of forces to the adhesive pads.

In Chapter 3, the environment of the robot was characterised and the safety measures for intra-abdominal locomotion considered in order to define the desirable features for the design of the robot. The advantages and drawbacks of walkers and wheeled robots in this application were also considered. In the light of these considerations and the conclusions of the literature review (Chapter 2), a locomotion methodology of the robot was chosen: a Cartesian walker with four inter-connected adhesive pads. Chapter 4 covered the analysis of this conceptual design, defining the kinematic joints of the mechanism, the workspace of the robot and the

dynamics involved in moving the pads. This fourth chapter also showed how the robot can generate gait and adapt to the environment.

3. Identify actuation and sensor technologies and manufacturing techniques to develop a controllable miniature mechanism.

Actuation and sensing technologies available in the market for miniature size were reviewed in Chapter 5. A linear piezo-electric motor and a linear magnetic encoder were identified as the most suitable actuator and sensor for the design of the robot. The commercial availability and access to manufacturing techniques for the miniature size were explored considering the limitations of a research project. Rapid prototyping was eventually chosen as the manufacturing technique for the locomotion mechanism integrating the motors and sensors previously selected. Chapter 5 also discusses the issues encountered during the manufacturing and assembly of the mechanism due to its miniature size.

4. Build and test a miniature mechanism following the conceptual design of the robot and using the actuation and sensor technologies previously identified.

Chapter 5 explained the whole implementation process, from the first one-axis mechanism to the two prototypes of the robot that were developed. A prismatic joint controlled by the miniature linear motor and encoder (one-axis mechanism) was built in the first place. The mechanism was shown controlling the adhesion of the bio-mimetic pad on rat peritoneum. Then, the first prototype of the robot was built, and its walking performance was preliminary tested using magnetic pads with similar attachment force to the adhesive pads. In order to generate the locomotion sequence of the pads, an open-loop controller and a closed-loop controller of the robot were programmed and tested. Some issues related to the performance of the motors within the mechanism were identified and in order to tackle them a second prototype was built. The second prototype was built and tested using the magnetic pads and the bio-mimetic adhesive pads on pig peritoneum. To further enhance the performance of the robot, some modifications were made to the mechanical design of the second prototype, testing the prototype again. The enhanced second prototype showed a significant improvement of its walking performance.

5. Create engineering models of the mechanical and adhesive interaction of the mechanism and the tissue.

The way the adhesive pad can be detached from the tissue using the locomotion mechanism of the robot was analysed in Chapter 6. The peeling model developed in this chapter combines Kendall's theory of thin film peeling with Euler-Bernoulli's beam theory applied to the bending of the pad. The model predicts the value of force and moment that makes the adhesive pad detach. The prediction of the model is consistent with previous work carried out on the value of force required when peeling the bio-mimetic adhesive pad.

6. Define the main parameters involved in the control of adhesion and develop strategies for stable motion of the robot.

Chapter 7 reviewed the different ways proposed in the literature to define the stability of a walking robot. In the light of this review, this chapter proposed a new stability criterion for adhesion-reliant robots. The stability margin defined according to this criterion can be calculated using the value of detachment force and moment from the peeling model in Chapter 6. The analysis of Chapter 8 focused on the different ways the pads can be arranged and actuated within the locomotion mechanism in order to enhance the stability of the robot. This chapter analysed a configuration of two adhesive pads first and then the arrangements of three pads in a line and three pads in a triangle, showing the benefits of each of them to control adhesion. The chapter showed that these benefits can be combined in a robot with four pads, like the intra-abdominal robot developed throughout the thesis.

## **9.2 Discussion and conclusions**

The development of the intra-abdominal robot presented in this thesis draws on various strands of engineering science and a research methodology driven by the empirical aspects of robotic design. This heterogeneous approach led to a proof-of-concept prototype as well as to the development of the theoretical background required to build a control system specifically tailored to inverted adhesion-reliant locomotion.

In the first place, the locomotion system chosen for the robot is a combination of inchworm locomotion, legged locomotion and amoeboid locomotion. The locomotion system resembles inchworm locomotion because part of the robot moves while part of the robot is anchored. The

robot uses four pads, each of them independently moved by three motors, which can be considered feet like in a walking robot. The design of the robot also draws inspiration from amoeboid locomotion because part of the robot sticks to the surface while part of the robot moves to the new position by deforming the central body of the robot. Secondly, the robot uses a micro-structured surface inspired by tree frogs in order to attach to a wet surface like the peritoneum. The locomotion mechanism peels off the tree frog adhesive pads, which is the method used by tree frogs and geckoes to make detachment of the pads smooth and efficient. In addition to these bio-inspired features, the choice of locomotion and the mechanical design of the locomotion mechanism took into consideration the miniature motors available in the market of a sufficiently small size and low weight. All these elements were combined into the four-padded inchworm Cartesian walker chosen for the final design and preference was given to the implementation and testing of the prototype. The emphasis on building the robot and learning from experimenting with it was decided on the basis of the novelty of handling and controlling a complex miniature robot in inverted adhesion-reliant locomotion. The difficulty of simulating the interaction of the robot with a complex material like biological tissue reinforced the empirical approach to the development of the robotic system.

A number of obstacles to the implementation of a miniature robot with a research budget were experienced and had to be overcome accepting the hindrance they represented to the performance of the robot. The trade-off between a sufficiently accurate manufacturing technique and a cost-effective one meant that the performance of the miniature motors within the mechanism was not optimal. The lack of access to appropriate miniature components for the mechanism, like sufficiently small springs with a sufficiently low value of stiffness constant and bearings of a small enough size, further hindered the performance of the motors within the mechanism. Force sensing technologies of suitable specifications for integration with the hardware and the controller of the robot were out of the financial reach of the project's budget. Apart from an open-loop sequence to coordinate the motion of the motors and provide locomotion to the robot, a control architecture for closed-loop operation was designed and programmed using the information of the position of the linear motors. However, a closed-loop controller could not be developed much further because of the lack of access to appropriate force sensors. The motors employed for the robot were quite a recent development and the options to

integrated their drivers into a complex robotic system were quite limited; this did not help either with the development of the closed-loop strategy.

It was then decided to focus the research efforts on improving the performance of the robot in open loop by modifying the mechanical design of the pieces composing the mechanism. Eventually, the prototype was able to obtain consistent locomotion on a steel surface and stable attachment and motion of the pads on peritoneum. The performance of the final prototype proves the feasibility and suitability of the locomotion system developed for the design of the robot. Nonetheless, the testing of the prototype showed that the robot controller requires feedback on the force applied to the pads in order to move consistently on tissue.

The improvements of the hardware, sensor system and electronics of the robot that would improve the consistency of its locomotion on tissue are commercially available and are therefore easily surmountable with a different budget. However, in order to achieve precise and efficient control of the robot in inverted adhesion-reliant locomotion, overcoming the previous implementation issues is not sufficient. It is also crucial to understand the mechanisms at work during the attachment and detachment cycle of the pad and how the forces applied by the locomotion affect this. This is not a matter of a more accommodating budget but a research question that requires some insight into the interaction between the locomotion mechanism and the adhesive surface in order to be answered. This was the aim of Chapter 6, 7 and 8 in which a peeling model, a stability criterion and control strategies were proposed based on the experience gained with the construction and testing of the prototype. To the best of the author's knowledge this is the first model, stability criterion and control analysis proposed for a robot and environment of the kind studied in this thesis. This novelty is probably due to the unusual combination of features in the locomotion system of the intra-abdominal robot, the complexity of the mechanics of its environment, biological tissue, and the difficulty of inverted adhesion-reliant locomotion.

The peeling model analyses the way the pads are detached under the action of the actuators in the locomotion mechanism. The peeling model manages to give quite an accurate prediction of the uniform load required to peel off the pad and explains how the amount of required force is reduced when applying a peeling force at the edge of the pad. This predictions prove that the model works on premises that represent the interaction between the robot's mechanism and the adhesive pad sufficiently accurately. However, the model falls short when predicting the effect of a force component parallel

to the surface of the tissue (shearing force) and requires careful consideration of the thickness parameter used for the model's formulation. These shortcomings of the model are due to the simplifications made about the characteristics of the tissue in order to keep the mathematical formulation of the model easily manageable.

Stability as traditionally defined for walking robots is not the most suitable method to assess the stability of a robot in inverted adhesion-reliant locomotion. This is because what matters most in this type of locomotion is that there is a sufficient number of pads holding the robot as was observed during testing of the prototype. The definition of the stability criterion in Chapter 7 reflects this principle and enables a direct way to calculate the stability margin of the robot if the force applied on the adhesive pads can be measured.

After modelling the force that causes the pad to detach and using that force to assess the stability margin of the robot, the next question was how can the motors be actuated in order to avoid a fall (maximise the stability margin)? The analysis in Chapter 8 answers this question by determining, first of all, the way force is transmitted between a moving and a detaching pad in a two-padded configuration. Then, the same force analysis is applied to configuration with three pads in a line and in a triangle, showing that a four-padded robot can be analysed as a superposition of those two three-padded configurations. Thus, the stability benefits of the three-padded configurations can be combined in a four-padded robot and the result is a significant enhancement of the stability margin. This enhancement is the result of diminishing the moment on the supporting pads with the configuration of four pads forming a quadrilateral, which is not present in a configuration with fewer pads. As reasoned and observed during the design and implementation stages, the analysis in Chapter 8 shows that four is the minimum number of pads to facilitate stable locomotion in inverted adhesion-reliant locomotion with the locomotion system of the robot.

Drawing from different sources of inspiration and technologies, Chapters 3 and 4 of this thesis present the design of a compact locomotion mechanism with the potential to move inside the human abdomen in inverted adhesion-reliant locomotion. The challenges of implementing such a mechanism are explained in Chapter 5, resulting in a prototype twice the size envisaged for the final device, able to traverse consistently a steel surface and move the pads stably on peritoneal tissue. The first requisite for the robot to operate comfortably inside the abdomen as a surgical assistant is to further

miniaturise the locomotion mechanism, gaining financial access to miniature components and manufacturing techniques that guarantee optimal performance of the motors. Once this is obtained, the controller of the robot needs the appropriate tools to assess the stability of its locomotion sequences and it also needs to know how the actions of the motors in the mechanism are going to affect stability. These tools are derived from a control theory for inverted adhesion-reliant locomotion, the foundations of which are developed in Chapters 6, 7 and 8. These chapters pave the way towards precise control of inverted adhesion-reliant locomotion through the definition of a detachment model of the pad, a stability criterion that uses the model and strategies to enhance the stability of the robot.

### **9.3 Future work**

The current prototype of the robot is approximately twice the size that it needs to be in order to fit comfortably through a 3cm-long SPL incision. The size of the robot is mainly due to the dimensions required for the rapid-prototyped components to keep the strength of the mechanism. The linear motors and magnetic encoders occupy a small portion of the total volume of the robot. The dimensions of the mechanism can be reduced with a manufacturing technique that enables smaller and thinner dimensions, using stronger materials. Rapid prototyping machines able to manufacture in stronger materials with higher manufacturing precision are currently available; some of these machines can manufacture a single piece out of different materials. Micro-machining of hard plastic or metal is also a good option for a smaller scale prototype. However, all these are highly specialised techniques in industry and are difficult to access for a research budget. A more precise manufacturing and assembly technique would also bring the benefit of a smoother fit of the components in the mechanism. This would reduce friction and make the motors move more efficiently, improving their performance and ultimately enhancing the locomotion of the robot. More components can be added to the actuation system in order to enhance the detachment of the pads. A good example of how to improve the actuation system is the peeling mechanism developed in the undergraduate project mentioned in Chapter 5 [169].

The motion of the robot would also improve with bespoke communication between the drivers of the motors and the robot controller. This would allow better coordination of the motors to move the detached pad or to apply force on the pads in a particular way. With a more flexible communication system,

more sensorial information can be added to the control algorithm. Sensors to detect the preload and the detachment force applied to the pads would significantly enhance the control of adhesion and locomotion on the surface of the peritoneum. These sensors need to be accurate for a low range of forces and very compact to be integrated in the locomotion mechanism. Low-force sensing technologies to build miniature on-board sensors are available, but require bespoke integration or a significant investment for a research project. With this sensorial information, the peeling model, stability criterion and control strategies developed in the last chapters of the thesis can be used in order to enhance the performance of the robot, especially on tissue.

The emerging field of soft actuation for robots can be useful to further enhance the performance of the robot. This area of research is currently being explored in the field of bio-mimetics and therefore it agrees with the methodology followed for the development of the intra-abdominal robot. The design of the robot already incorporates a soft component, the backing layer of the adhesive pad, which has proved to be advantageous. Improved versions of the pads used by the robot where the micro-structure is printed on softer materials are under development. Compliance could be a feature of the actuation system as well. In this way, soft robotics can provide many benefits to the operation of the intra-abdominal robot. With soft boundaries of the robot's mechanism the idea of amoeboid locomotion through deformation of the body can be explored further. Compliance of the actuators can also help the insertion of the robot through a small incision. The change of stiffness achievable with soft actuators can be beneficial to peel the pads and attach to the surface of the peritoneum more easily. Actuators with variable stiffness are already used in robotics, for instance, series elastic actuators where a load is moved with the combination of a motor and a spring. However, they are not particularly compact for the miniature scale and soft actuators offer a more elegant solution. Electroactive polymers, for example dielectric elastomers, can be a good future solution to substitute the current piezoelectric motors of the robot. These actuators still need to become easy to control in order to be integrated in a robotic application and they need to use a lower voltage to be safe for intra-body operation.

The capability of the locomotion controller can be substantially enhanced with information on how close the pads are from detachment, how adhesion changes and under what circumstances. Along with the models and

strategies developed in the thesis, navigation and optimisation algorithms can be added to the locomotion controller. Force sensors on the pads can register the adhesion force from every part of the peritoneum to which the robot has attached and create a map of available adhesion. A navigation algorithm could then compute the most stable and/or fastest way to reach a target position. This intelligent controller could also check the changes in available adhesion force and avoid certain areas when planning a path in order to avoid a fall or minimise tissue damage. Learning algorithms and optimisation techniques can be used to integrate the information from the sensors and dynamically calculate the best way to move the pads and reach the target of the robot. These further improvements would make the robot an intelligent and efficient surgical assistant, able to enhance the skills of the surgeon and taking them anywhere in the abdomen with minimal trauma to the patient.

Beyond the improvements that can be made to the mechanism and control algorithm of the robot, the significance of this thesis lies on the development of a locomotion system and theory towards precise control of inverted adhesion-reliant locomotion. Robots have been built for this type of locomotion and some strategies to recover adhesion of the pads have been developed [101]. The modelling and analysis work carried out in this thesis goes one step further by mathematically representing the interaction between robot and adhesive pad and analysing how the stability of the robot can be monitored and enhanced. This can be the foundation for a general theory on the locomotion of robots relying on adhesion to remain stably attached to a surface. A thorough validation of the peeling model can identify all the parameters relevant to different types of surfaces, biological and non-biological, and these can be included in the formulation of the model. Algorithms using the stability criterion and control strategies for inverted adhesion-reliant locomotion can be programmed, tested and improved until precise adhesion control is obtained.

The locomotion system of the robot developed in the thesis is not limited to an inverted surface can be used for all types of terrain. Thus, the design of the robot can be extended to one that can operate in every position: on the ground, an inclined wall and an inverted surface. With the necessary modifications, the application of the robot can also be expanded to make it work in different types of tight and irregular environments, like other body cavities (for instance the colon), amongst rubble, inside pipes and tanks. Some modifications that can be made to the robot to make it work in different

environments are: a mechanism to ease transition from the ceiling or a wall to the ground; another set of adhesive pads at the free end of the vertical motors so that the robot can conveniently stick to the ground if required. For the intra-abdominal application, these modifications could allow the robot to move in all the surfaces of the abdominal cavity, transitioning from the peritoneum to the surface of the abdominal organs and sticking to the abdominal organs to stabilise its motion.

An interesting line of research that could be followed, apropos of the biological context of the project, would be to investigate if there is any relation between the stability criterion proposed in this thesis and animal locomotion. Do animals climbing an inverted surface control their motion using a similar stability criterion? Do they know which feet need to be attached at any time during inverted locomotion and react when one too many of these feet are losing adhesion? If the answer to these questions is positive, the findings on how animals sense and react to loss of adhesion can be fed into a further development of the control system for inverted adhesion-reliant locomotion.

The design of the robot includes elements of amoeboid locomotion which have not been explored before and can be further researched and exploited for robotic locomotion. Some configurations of more pads in alternative designs have been proposed in the thesis; these alternatives can be implemented and tested expanding on how the different connections between the pads affect stability. The amoeba-inspired concept of the quadrilateral changing shape can be expanded to create new designs where a network of adhesive pads are interconnected and coordinated in order to intensify the fluidity and smoothness of motion observed in amoebas. Using the models and control analysis proposed in this thesis, this robotic network of adhesive pads can be used to develop a general theory on how to control the motion and stability of a set of adhesive pads connected by any combination of links and actuators.

## List of references

- [1] Troccaz J. (Eds.), *Medical Robots*, ISBN: 978-1-84821-334-0, Wiley-ISTE, 2012.
- [2] Prescott T.J., Lepora N.F., Mura A., and Verschure P.F.M.J. (Eds.), *Proceedings of the First International Conference in Bio-mimetic and Bio-hybrid Systems (Living Machines 2012)*, Lecture Notes in Artificial Intelligence, vol. 7375, ISBN: 978-3-642-31524-4, Barcelona, Spain, Springer, 2012.
- [3] Lepora N.F., Verschure P.F.M.J., and Prescott T.J., "The State-of-the-Art in Bio-mimetics", in *First International Conference on Bio-mimetic and Bio-hybrid Systems (Living Machines 2012)*, Barcelona, Spain, 2012.
- [4] <http://www.laparoscopicsurgeryinfo.com/the-laparoscopic-gallbladder-surgery-procedure/>, "The Laparoscopic Gallbladder Surgery Procedure," ©Trief and Olk - Laparoscopic Gallbladder Surgery Attorneys, Accessed August 2013.
- [5] <http://www.mayoclinic.com/health/medical/IM03921>, "Oophorectomy (ovary removal surgery)," ©Mayo Foundation for Medical Education and Research, Accessed August 2013.
- [6] Perissat J., Collet D., Belliard R., Desplantez J., and Magne E., "Laparoscopic cholecystectomy: the state of the art. A report on 700 consecutive cases.", *World Journal of Surgery*, vol. 16 (6), pp. 1074-82, 1992.
- [7] Guillou P.J., Quirke P., Thorpe H., Walker J., Jayne D.G., Smith A.M., and others, "Short-term endpoints of conventional versus laparoscopic-assisted surgery in patients with colorectal cancer (MRC CLASICC trial): multicentre, randomised controlled trial", *Lancet*, vol. 365 (9472), pp. 1718-26, 2005.
- [8] G. Taylor, T. Liskiewicz, A. Neville, A. Morina, P. Gaskell, and D. Jayne, "Providing adhesion for a miniature mobile intra-abdominal device based on biomimetic principles", in *3rd Vienna International Conference on Nano-technology (VIENNANO)*, Vienna, Austria, vol. 1, pp. 401-407, 2009.
- [9] G. Taylor, A. Neville, D. Jayne, R. Roshan, T. Liskiewicz, A. Morina, and P. Gaskell, "Wet adhesion for a miniature mobile intra-abdominal device based on biomimetic principles", *Proceedings of the Institution of Mechanical*

*Engineers, Part C: Journal of Mechanical Engineering Science*, vol. 224 (7), pp. 1473-1485, 2010.

[10] R. Roshan, D. G. Jayne, T. Liskiewicz, G. W. Taylor, P. H. Gaskell, L. Chen, A. Montellano López, A. Morina, and A. Neville, "Effect of tribological factors on wet adhesion of a microstructured surface to peritoneal tissue", *Acta Biomaterialia*, vol. 7 (11), pp. 4007-4017, 2011.

[11] S. C. Cowin and S. B. Doty, *Tissue mechanics*, New York, Springer, 2007.

[12] K. Autumn and N. Gravish, "Gecko adhesion: evolutionary nanotechnology", *Philosophical Transactions of the Royal Society A: Mathematical, Physical and Engineering Sciences*, vol. 366 (1870), p. 1575, 2008.

[13] B. Aksak, M. P. Murphy, and M. Sitti, "Gecko inspired micro-fibrillar adhesives for wall climbing robots on micro/nanoscale rough surfaces", in *IEEE International Conference on Robotics and Automation (ICRA)*, Pasadena, California, USA, vol. 1, pp. 3058-3063, 2008.

[14] L. Boesel, C. Greiner, E. Arzt, and A. del Campo, "Gecko Inspired Surfaces: A Path to Strong and Reversible Dry Adhesives", *Advanced Materials*, vol. 22 (19), pp. 2125-2137.

[15] M. Murphy, B. Aksak, and M. Sitti, "Gecko-inspired directional and controllable adhesion", *Small*, vol. 5 (2), pp. 170-175, 2009.

[16] P. Dario, R. Valleggi, M. Carrozza, M. Montesi, and M. Cocco, "Microactuators for microrobots: A critical survey", *Journal of Micromechanics and microengineering*, vol. 2 p. 141, 1992.

[17] G. T. Sibley, M. H. Rahimi, and G. S. Sukhatme, "Robomote: A tiny mobile robot platform for large-scale ad-hoc sensor networks", in *IEEE International Conference on Robotics and Automation (ICRA)*, Washington, DC, USA, vol. 2, pp. 1143-1148, 2002.

[18] M. B. McMickell, B. Goodwine, and L. A. Montestruque, "MICAbot: a robotic platform for large-scale distributed robotics", in *IEEE International Conference on Robotics and Automation (ICRA)*, Taipei, Taiwan, vol. 2, pp. 1600-1605, 2003.

[19] S. A. Stoeter, P. E. Rybski, M. Gini, and N. Papanikolopoulos, "Autonomous stair-hopping with scout robots", in *IEEE/RSJ International Conference on Intelligent Robots and Systems* Laussane, Switzerland, vol. 1, pp. 721-726, 2002.

- [20] G. Caprari, P. Balmer, R. Piguet, and R. Siegwart, "The autonomous micro robot "Alice": a platform for scientific and commercial applications", vol., pp. 231-235, 2002.
- [21] F. Mondada, G. C. Pettinaro, A. Guignard, I. W. Kwee, D. Floreano, J.-L. Deneubourg, S. Nolfi, L. M. Gambardella, and M. Dorigo, "SWARM-BOT: A new distributed robotic concept", *Autonomous Robots*, vol. 17 (2), pp. 193-221, 2004.
- [22] J. Haverinen, M. Parpala, and J. Roning, "A miniature mobile robot with a color stereo camera system for swarm robotics research", in *IEEE International Conference on Robotics and Automation (ICRA)* Barcelona, Spain, vol., pp. 2483-2486, 2005.
- [23] N. O. Perez-Arancibia, K. Y. Ma, K. C. Galloway, J. D. Greenberg, and R. J. Wood, "First controlled vertical flight of a biologically inspired microrobot", *Bioinspiration & Biomimetics*, vol. 6 (3), pp. 036009-20, 2011.
- [24] M. Kovac, J. Germann, C. Hurzeler, R. Y. Siegwart, and D. Floreano, "A perching mechanism for micro aerial vehicles", *Journal of Micro-Nano Mechatronics*, vol. 5 (3), pp. 77-91, 2009.
- [25] M. Kovac, M. Schlegel, J.-C. Zufferey, and D. Floreano, "Steerable miniature jumping robot", *Autonomous Robots*, vol. 28 (3), pp. 295-306, 2010.
- [26] A. Lehman, M. Rentschler, S. Farritor, and D. Oleynikov, "The current state of miniature in vivo laparoscopic robotics", *Journal of Robotic Surgery*, vol. 1 (1), pp. 45-49, 2007.
- [27] N. Patronik, T. Ota, M. Zenati, and C. Riviere, "A miniature mobile robot for navigation and positioning on the beating heart", *IEEE Transactions on Robotics*, vol. 25 (5), pp. 1109-1124, 2009.
- [28] M. Rentschler, J. Dumpert, S. Platt, S. Farritor, and D. Oleynikov, "Mobile in vivo biopsy and camera robot", *Studies in Health Technology and Informatics*, vol. 119 p. 449, 2005.
- [29] A. Menciassi, J. H. Park, S. Lee, S. Gorini, P. Dario, and J.-O. Park, "Robotic solutions and mechanisms for a semi-autonomous endoscope", in *IEEE/RSJ International Conference on Intelligent Robots and Systems (IROS)*, Laussane, Switzerland, vol. 2, pp. 1379-1384, 2002.
- [30] L. Zhang, J. J. Abbott, L. Dong, K. E. Peyer, B. E. Kratochvil, H. Zhang, C. Bergeles, and B. J. Nelson, "Characterizing the swimming

properties of artificial bacterial flagella", *Nano Letters*, vol. 9 (10), pp. 3663-3667, 2009.

[31] SBL02-06 Micro DC Brushless motor - Namiki Precision Jewel Co., <http://www.namiki.net/product/dcmotor/micro.html#micromotor>, Accessed August 2013

[32] Miniature Linear Motion Series PQ12 - Firgelli Technologies Inc., [http://www.firgelli.com/Uploads/PQ12\\_datasheet.pdf](http://www.firgelli.com/Uploads/PQ12_datasheet.pdf), Accessed August 2013

[33] N-310 NEXACT® OEM Miniature Linear Motor/Actuator - Physik Instrumente (PI) GmbH & Co., [http://www.physikinstrumente.com/en/pdf/N310\\_Datasheet.pdf](http://www.physikinstrumente.com/en/pdf/N310_Datasheet.pdf), Accessed August 2013

[34] Piezo LEGS® Linear 6N - PiezoMotor, [http://www.piezomotor.se/documents/150010\\_LL10.pdf](http://www.piezomotor.se/documents/150010_LL10.pdf), Accessed August 2013

[35] [http://www.newscaletech.com/doc\\_downloads/SQL-RV-1-8\\_datasheet.pdf](http://www.newscaletech.com/doc_downloads/SQL-RV-1-8_datasheet.pdf), "SQL-RV-1.8 Reduced Voltage SQUIGGLE RV linear drive system data sheet," New Scale Technologies Inc., Accessed October 2012.

[36] NanoMuscle NM706-Super - Linear Muscle Wire Actuator - Miga Motor Company, <http://store.migamotors.com/nanomuscle-nm706-super-linear-muscle-wire-actuator>, Accessed August 2013

[37] NanoMuscle NM70R-6P - Rotary Memory Metal Actuator - Miga Motor Company, <http://store.migamotors.com/nanomuscle-nm70r-6p-rotary-memory-metal-actuator>, Accessed August 2013

[38] N. Morgan, "Medical shape memory alloy applications--the market and its products", *Materials Science and Engineering A*, vol. 378 (1-2), pp. 16-23, 2004.

[39] J. Pons, *Emerging actuator technologies: a micromechatronic approach*, 0470091975, John Wiley & Sons Inc, 2005.

[40] T. Yih and I. Talpasanu, *Micro and Nano Manipulations for Biomedical Applications*, 1596932546, Artech House, 2008.

[41] M. Kohl, *Shape memory microactuators*, 3540206353, Springer Verlag, 2004.

[42] T. Morita, "Miniature piezoelectric motors", *Sensors and Actuators A: physical*, vol. 103 (3), pp. 291-300, 2003.

- [43] W. Huang, "On the selection of shape memory alloys for actuators", *Materials & Design*, vol. 23 (1), pp. 11-19, 2002.
- [44] M. Shahinpoor and K. Kim, "Ionic polymer-metal composites: I. Fundamentals", *Smart Materials and Structures*, vol. 10 p. 819, 2001.
- [45] M. Behl and A. Lendlein, "Shape-memory polymers", *Materials Today*, vol. 10 (4), pp. 20-28, 2007.
- [46] J. Breguet, R. Perez, A. Bergander, C. Schmitt, R. Clavel, and H. Bleuler, "Piezoactuators for motion control from centimeter to nanometer", vol. 1, pp. 492-497, 2002.
- [47] R. Gilbertson and J. Busch, "A survey of micro-actuator technologies for future spacecraft missions", *Journal of The British Interplanetary Society*, vol. 49 (4), pp. 129-138, 1996.
- [48] SMA products - SAES Getters S.p.A., [http://www.saesgetters.com/sites/default/files/SMA%20products%20datasheets\\_0.pdf](http://www.saesgetters.com/sites/default/files/SMA%20products%20datasheets_0.pdf), Accessed August 2013
- [49] Intracardiac blood pump, <http://www.faulhaber-group.com/n365115/n.html>, Accessed March 2013.
- [50] Abiomed, Impella Heart Pump, <http://www.abiomed.com/>, Accessed March 2013.
- [51] Oleynikov D., Rentschler M., Hadziolie A., Dumpert J., Pratt S.R., and Farritor S., "Miniature robots can assist in laparoscopic cholecystectomy", *Surgical Endoscopy*, vol. 19 pp. 473-476, 2005.
- [52] Farritor S.M., Lehman A.C., and Oleynikov D., "Miniature In Vivo Robots for NOTES", in *Surgical Robotics: Systems Applications and Visions*, Rosen J. and others, Eds., Springer, pp. 123-138, 2011.
- [53] C. Stefanini, A. Menciassi, and P. Dario, "Modeling and experiments on a legged microrobot locomoting in a tubular, compliant and slippery environment", *The International Journal of Robotics Research*, vol. 25 (5-6), p. 551, 2006.
- [54] M. Quirini, R. Webster, A. Menciassi, and P. Dario, "Design of a pill-sized 12-legged endoscopic capsule robot", vol., pp. 1856-1862, 2007.
- [55] M. Quirini, A. Menciassi, S. Scapellato, C. Stefanini, and P. Dario, "Design and fabrication of a motor legged capsule for the active exploration of the gastrointestinal tract", *IEEE/ASME Transactions on Mechatronics*, vol. 13 (2), pp. 169-179, 2008.

- [56] Rentschler M.E., "*In Vivo* Abdominal Surgical Robotics: Tissue Mechanics Modeling, Robotics Design, Experimentation and Analysis", The University of Nebraska, PhD, 2006.
- [57] M. Rentschler, J. Dumpert, S. Platt, K. Iagnemma, D. Oleynikov, and S. Farritor, "An in vivo mobile robot for surgical vision and task assistance", *Journal of Medical Devices*, vol. 1 p. 23, 2007.
- [58] S. Patel, M. Rajadhyaksha, S. Kirov, Y. Li, and R. Toledo-Crow, "Endoscopic laser scalpel for head and neck cancer surgery", in *SPIE 8207 Photonic Therapeutics and Diagnostics VIII*, San Francisco, California, USA, vol., p. 82071S, 2012.
- [59] Patronik N. A., "A Miniature Mobile Robot for Precise and Stable Access to the Beating Heart ", The Robotics Institute, Carnegie Mellon University, PhD thesis, 2008.
- [60] D. Hosokawa, T. Ishikawa, H. Morikawa, Y. Imai, and T. Yamaguchi, "Development of a biologically inspired locomotion system for a capsule endoscope", *The International Journal of Medical Robotics and Computer Assisted Surgery*, vol. 5 (4), pp. 471-478, 2009.
- [61] E. Cheung, M. Karagozler, S. Park, B. Kim, and M. Sitti, "A new endoscopic microcapsule robot using beetle inspired microfibrillar adhesives", vol., pp. 551-557, 2005.
- [62] M. Karagozler, E. Cheung, J. Kwon, and M. Sitti, "Miniature endoscopic capsule robot using biomimetic micro-patterned adhesives", in *The First IEEE/RAS-EMBS International Conference on Biomedical Robotics and Biomechatronics (BioRob)*, Pisa, Italy, vol. 1, pp. 105-111, 2006.
- [63] M. Shahinpoor and K. J. Kim, "Ionic polymer-metal composites: IV. Industrial and medical applications", *Smart Materials and Structures*, vol. 14 (1), p. 197, 2004.
- [64] T. T. Nguyen, N. S. Goo, V. K. Nguyen, Y. Yoo, and S. Park, "Design, fabrication, and experimental characterization of a flap valve IPMC micropump with a flexibly supported diaphragm", *Sensors and Actuators A: physical*, vol. 141 (2), pp. 640-648, 2008.
- [65] BioMetal Helix BMX Series - Toki Corporation, [http://www.toki.co.jp/biometal/download/downloadfiles/BMX\\_eng.pdf](http://www.toki.co.jp/biometal/download/downloadfiles/BMX_eng.pdf), Accessed August 2013

- [66] Bekey G. A., *Autonomous Robots. From Biological Inspiration to Implementation and Control*, Cambridge (Massachusetts) and London (England), The MIT Press, 2005.
- [67] P. González de Santos, E. García, and J. Estremera, *Quadrupedal locomotion: an introduction to the control of four-legged robots*, 184628306X, Springer, 2006.
- [68] McKerrow P., *Introduction to Robotics*, ISBN 0201182408, Addison-Wesley Longman Publishing Co., Inc. Boston, MA, USA, 1991.
- [69] M. Greuter, G. Shah, G. Caprari, F. Tâche, R. Siegwart, and M. Sitti, "Toward micro wall-climbing robots using biomimetic fibrillar adhesives", vol., pp. 39-46, 2006.
- [70] D. J. Todd, *Walking machines: an introduction to legged robots*, Chapman & Hall, 1985.
- [71] M. G. Bekker, *Off-the-road locomotion: research and development in terramechanics*, University of Michigan Press, 1960.
- [72] P. Torrone, "Building The BRAT – entry level bipedal robot", in Make, <http://makezine.com/2006/10/23/building-the-brat-entry-l/>, Accessed August 2013.
- [73] J. M. Conrad, *Stiquito Controlled!: Making a Truly Autonomous Robot*, ISBN 0471716278, Wiley-IEEE Computer Society, 2005.
- [74] F. Michaud, D. Letourneau, M. Arsenault, Y. Bergeron, R. Cadrin, F. Gagnon, M.-A. Legault, M. Millette, J.-F. Pare, and M.-C. Tremblay, "Multi-modal locomotion robotic platform using leg-track-wheel articulations", *Autonomous Robots*, vol. 18 (2), pp. 137-156, 2005.
- [75] K. Daltorio, T. Wei, A. Horchler, L. Southard, G. Wile, R. Quinn, S. Gorb, and R. Ritzmann, "Mini-Whegs TM Climbs Steep Surfaces Using Insect-inspired Attachment Mechanisms", *The International Journal of Robotics Research*, vol. 28 (2), p. 285, 2009.
- [76] P. Dario, P. Ciarletta, A. Menciassi, and B. Kim, "Modelling and experimental validation of the locomotion of endoscopic robots in the colon", *The International Journal of Robotics Research*, vol. 23 (4-5), p. 549, 2004.
- [77] A. S. Boxerbaum, K. M. Shaw, H. J. Chiel, and R. D. Quinn, "Continuous wave peristaltic motion in a robot", *The International Journal of Robotics Research*, vol. 31 (3), pp. 302-318, 2012.

- [78] J. H. Boyle, S. Johnson, and A. A. Dehghani-Sanij, "Adaptive Undulatory Locomotion of a *C. elegans* Inspired Robot", *IEEE/ASME Transactions On Mechatronics*, vol. 18 (2), pp. 439-448, 2013.
- [79] S. Hirose, *Biologically inspired robots: Snake-like locomotion and manipulation*, Oxford, Oxford University Press, 1993.
- [80] J. K. Hopkins, B. W. Spranklin, and S. K. Gupta, "A survey of snake-inspired robot designs", *Bioinspiration & Biomimetics*, vol. 4 (2), pp. 021001-19, 2009.
- [81] G. S. P. Miller, "Snake Robots for Search and Rescue", in *Neurotechnology for Biomimetic Robots*, Ayers Joseph W., Davis Joel L., and R. A., Eds., ISBN 026201193X, Cambridge, Massachusetts, USA, MIT Press, pp. 271-283, 2002.
- [82] Shang J., Noonan D., Payne C., Clark J., Sodergren M. H., Darzi A., and Yang G.-Z., "An Articulated Universal Joint Based Flexible Access Robot for Minimally Invasive Surgery", in *IEEE International Conference on Robotics and Automation (ICRA)*, Shanghai, China, 2011.
- [83] David P. Noonan website at The Hamlyn Centre for Robotic Surgery (Imperial College London), [http://www.doc.ic.ac.uk/~dnoonan/research\\_notes.html](http://www.doc.ic.ac.uk/~dnoonan/research_notes.html), Accessed August 2013
- [84] J. M. Lackie, *Cell movement and cell behaviour*, 0045740356, Allen & Unwin, 1986.
- [85] Bell L. G. E. and Jeon K. W., "Locomotion of *Amoeba Proteus*", *Nature*, vol. 198 pp. 675 - 676, 1963.
- [86] Hong D. W., Ingram M., and Lahr D., "Whole skin locomotion inspired by amoeboid motility mechanisms", *Journal of Mechanisms and Robotics*, vol. 1 (1), 2009.
- [87] Nagabuko A. and S. Hirose, "Walking and climbing of the quadruped wall-climbing robot", in *IEEE International Conference on Robotics and Automation (ICRA)*, San Diego, USA, 1994.
- [88] Balaguer C., Gimenez A., and Jardon A., "Climbing Robots' Mobility for Inspection and Maintenance of 3D Complex Environments", *Autonomous Robots*, vol. 18 pp. 157-169, 2005.

- [89] J. C. Grieco, M. Prieto, M. Armada, and P. Gonzalez de Santos, "A six-legged climbing robot for high payloads", in *IEEE International Conference on Control Applications*, Trieste, Italy, vol. 1, pp. 446-450, 1998.
- [90] Simi M., V. P. Sardi G., Menciassi A., and Dario P., "Magnetic Levitation Camera Robot for Endoscopic Surgery", in *IEEE International Conference on Robotics and Automation (ICRA)*, Shanghai, China, 2011.
- [91] M. Murphy and M. Sitti, "Waalbot: An agile small-scale wall-climbing robot utilizing dry elastomer adhesives", *IEEE/ASME Transactions on Mechatronics*, vol. 12 (3), pp. 330-338, 2007.
- [92] S. Kim, M. Spenko, S. Trujillo, B. Heyneman, V. Mattoli, and M. R. Cutkosky, "Whole body adhesion: hierarchical, directional and distributed control of adhesive forces for a climbing robot", in *IEEE International Conference on Robotics and Automation*, Rome, Italy, vol. 1, pp. 1268–1273, 2007.
- [93] K. Autumn, M. Sitti, Y. Liang, A. Peattie, W. Hansen, S. Sponberg, T. Kenny, R. Fearing, and J. Israelachvili, "Evidence for van der Waals adhesion in gecko setae", *Proceedings of the National Academy of Sciences of the United States of America*, vol. 99 (19), p. 12252, 2002.
- [94] S. Gorb, M. Sinha, A. Peressadko, K. Daltorio, and R. Quinn, "Insects did it first: a micropatterned adhesive tape for robotic applications", *Bioinspiration & Biomimetics*, vol. 2 p. S117, 2007.
- [95] K. Autumn, "Properties, principles, and parameters of the gecko adhesive system", in *Biological adhesives*, Springer Berlin Heidelberg, pp. 225-256, 2006.
- [96] K. Autumn and A. Peattie, "Mechanisms of adhesion in geckos", *Integrative and Comparative Biology*, vol. 42 (6), p. 1081, 2002.
- [97] K. Autumn, Y. Liang, S. Hsieh, W. Zesch, W. Chan, T. Kenny, and R. Fearing, "Adhesive force of a single gecko foot-hair", *Nature*, vol. 405 (6787), pp. 681-685, 2000.
- [98] Gao H., Wang X., Yao H., Gorb S., and Arzt E., "Mechanics of hierarchical adhesion structures of geckos", *Mechanics of Materials*, vol. 37 (2-3), pp. 275-285, 2004.
- [99] O. Unver and M. Sitti, "Tankbot: A Palm-size, Tank-like Climbing Robot using Soft Elastomer Adhesive Treads", *The International Journal of Robotics Research*, 2010.

- [100] S. Kim, M. Spenko, S. Trujillo, B. Heyneman, D. Santos, and M. Cutkosky, "Smooth vertical surface climbing with directional adhesion", *IEEE Transactions on Robotics*, vol. 24 (1), pp. 65-74, 2008.
- [101] M. Murphy, C. Kute, Y. Mengüç, and M. Sitti, "Waalbot II: Adhesion Recovery and Improved Performance of a Climbing Robot using Fibrillar Adhesives", *The International Journal of Robotics Research*, 2011.
- [102] O. Unver, A. Uneri, A. Aydemir, and M. Sitti, "Geckobot: a gecko inspired climbing robot using elastomer adhesives", in *IEEE International Conference on Robotics and Automation (ICRA)* Orlando, Florida, USA, vol. 1, pp. 2329-2335, 2006.
- [103] O. Unver and M. Sitti, "Tankbot: A Miniature, Peeling Based Climber On Rough and Smooth Surfaces", in *IEEE International Conference on Robotics and Automation (ICRA)*, Kobe, Japan, 2009.
- [104] C. Kute, M. P. Murphy, Y. Mengü, and M. Sitti, "Adhesion recovery and passive peeling in a wall climbing robot using adhesives", in *IEEE International Conference on Robotics and Automation (ICRA)*, Anchorage, Alaska, vol. 1, pp. 2797-2802, 2010.
- [105] Barnes W. J. P., Oines C., and Smith J. M., "Whole animal measurements of shear and adhesive forces in adult tree frogs: insights into underlying mechanisms of adhesion obtained from studying the effects of size and scale", *Journal of Computational Physiology*, vol. 192 (11), pp. 1179-91, 2006.
- [106] W. Federle, W. Barnes, W. Baumgartner, P. Drechsler, and J. Smith, "Wet but not slippery: boundary friction in tree frog adhesive toe pads", *Journal of The Royal Society Interface*, vol. 3 (10), p. 689, 2006.
- [107] W. J. P. Barnes, C. Oines, and J. M. Smith, "Whole animal measurements of shear and adhesive forces in adult tree frogs: insights into underlying mechanisms of adhesion obtained from studying the effects of size and scale", *Journal of Comparative Physiology A: Neuroethology, Sensory, Neural, and Behavioral Physiology*, vol. 192 (11), pp. 1179-1191, 2006.
- [108] Smith J. M., Barnes W. J. P., Downie J. R., and Ruxton G. D., "Structural correlates of increased adhesive efficiency with adult size in the toe pads of hylid tree frogs", *Journal of Comparative Physiology A: Neuroethology, Sensory, Neural, and Behavioral Physiology*, vol. 192 (11), pp. 1193-1204, 2006.

- [109] H. Zeng, N. Pesika, Y. Tian, B. Zhao, Y. Chen, M. Tirrell, K. L. Turner, and J. N. Israelachvili, "Frictional adhesion of patterned surfaces and implications for gecko and biomimetic systems", *Langmuir*, vol. 25 (13), pp. 7486-7495, 2009.
- [110] S. Abbott and P. Gaskell, "Mass production of bio-inspired structured surfaces", *Proceedings of the Institution of Mechanical Engineers, Part C: Journal of Mechanical Engineering Science*, vol. 221 (10), pp. 1181-1191, 2007.
- [111] M. P. Reyes and R. S. Fearing, "Macromodel for the mechanics of gecko hair adhesion", in *IEEE International Conference on Robotics and Automation*, Pasadena, California, USA, vol. 1, pp. 1602-1607, 2008.
- [112] T. Kim and B. Bhushan, "The adhesion model considering capillarity for gecko attachment system", *Journal of The Royal Society Interface*, vol. 5 (20), p. 319, 2008.
- [113] C. S. Majidi, "Enhanced Friction and Adhesion with Biologically Inspired Fiber Arrays", University of California at Berkeley, PhD Thesis, 2007.
- [114] P. Dasgupta, "Advanced laparoscopic surgery using the da Vinci robotic system", in *Robotics in Surgery. State of the Art.*, London, 2010.
- [115] J. Gilbert, "Robots in laparoscopic surgery", in *Robotics in Surgery. State of the Art.*, London, 2010.
- [116] FreeHand 2010 Ltd., <http://www.freehandsurgeon.com>, Accessed February 2013.
- [117] P. Finlay and R. McCloy, "The EndoAssist Endoscopic Camera Holder", *Primer of robotic & telerobotic surgery*, p. 42, 2004.
- [118] S. Kommu, P. Rimington, C. Anderson, and A. Rané, "Initial experience with the EndoAssist camera-holding robot in laparoscopic urological surgery", *Journal of Robotic Surgery*, vol. 1 (2), pp. 133-137, 2007.
- [119] M. Alessandrini, A. De Padova, B. Napolitano, A. Camillo, and E. Bruno, "The AESOP robot system for video-assisted rigid endoscopic laryngosurgery", *European Archives of Oto-Rhino-Laryngology*, vol. 265 (9), pp. 1121-1123, 2008.
- [120] B. Kraft, C. Jäger, K. Kraft, B. Leibl, and R. Bittner, "The AESOP robot system in laparoscopic surgery: Increased risk or advantage for

surgeon and patient?", *Surgical Endoscopy*, vol. 18 (8), pp. 1216-1223, 2004.

[121] Intuitive Surgical, Inc. - da Vinci Surgical System, <http://www.intuitivesurgical.com/>, Accessed Accessed February 2013.

[122] Z. Nawrat and P. Kostka, "Polish cardio-robot 'Robin Heart'. System description and technical evaluation", *The International Journal of Medical Robotics and Computer Assisted Surgery*, vol. 2 (1), pp. 36-44, 2006.

[123] G. Hirzinger, "MIROSURGE - An Innovative System for Minimally Invasive Robot Surgery", in *Robotics in Surgery. State of the Art.*, London, 2010.

[124] U. Hagn, R. Konietzschke, A. Tobergte, M. Nickl, S. Jörg, B. Kübler, G. Passig, M. Gröger, F. Fröhlich, and U. Seibold, "DLR MiroSurge: a versatile system for research in endoscopic telesurgery", *International journal of computer assisted radiology and surgery*, vol. 5 (2), pp. 183-193, 2010.

[125] G. Hirzinger, J. Bals, M. Otter, and J. Stelter, "The DLR-KUKA success story: robotics research improves industrial robots", *Robotics & Automation Magazine, IEEE*, vol. 12 (3), pp. 16-23, 2005.

[126] P. Finlay, "Needle Guiding Robots for Minimally Invasive Surgery", in *Robotics in Surgery. State of the Art.*, London, 2010.

[127] G. Deacon, A. Harwood, J. Holdback, D. Maiwand, M. Pearce, I. Reid, M. Street, and J. Taylor, "The Pathfinder image-guided surgical robot", *Proceedings of the Institution of Mechanical Engineers, Part H: Journal of Engineering in Medicine*, vol. 224 (5), pp. 691-713, 2010.

[128] M. Eljamel, "Validation of the PathFinder™ neurosurgical robot using a phantom", *The International Journal of Medical Robotics and Computer Assisted Surgery*, vol. 3 (4), pp. 372-377, 2007.

[129] EndoWrist Instruments, Intuitive Surgical, <http://www.intuitivesurgical.com/products/instruments/>, Accessed Accessed February 2013.

[130] Piccigallo M., Scarfogliero U., Quaglia C., Petroni G., Valdastris P., Menciassi A., and Dario P., "Design of a Novel Bimanual Robotic System for Single-Port Laparoscopy", *IEEE/ASME Transactions on Mechatronics*, vol. 15 (6), December 2010.

[131] Shang J., Payne J. C., Clark J., Noonan D. P., Kwok K.-W., Darzi A., and Yang G.-Z., "Design of a Multitasking Robotic Platform with Flexible

Arms and Articulated Head for Minimally Invasive Surgery", in *IEEE/RSJ International Conference on Intelligent Robots and Systems*, Vilamoura, Algarve, Portugal, 2012.

[132] Lehman A.C., Wood N.A., Dumpert J., Oleynikov D., and Farritor S.M., "Dexterous miniature in vivo robot for NOTES", in *2nd Biennial IEEE/RAS-EMBS Conference on Biomedical Robotics and Biomechanics*, Scottsdale (AZ), USA, vol. 1, pp. 244–249, 2008.

[133] G. Ribaric, "NOTES/new innovations for minimal access surgery", in *1st Leeds International Oncological Engineering Conference*, Leeds, UK, 2011.

[134] Lehman A. C., Dumpert J., Wood N. A., Redden L., Visty A. Q., Farritor S., Varnell B., and Oleynikov D., "Natural orifice cholecystectomy using a miniature robot", *Surgical Endoscopy*, vol. 23 (2), pp. 260-266, 2009.

[135] A. Menciassi, M. Quirini, and P. Dario, "Microrobotics for future gastrointestinal endoscopy", *Minimally Invasive Therapy & Allied Technologies*, vol. 16 (2), pp. 91-100, 2007.

[136] Cosentino F., Tumino E., Passoni G. R., Rigante A., Barbera R., Tauro A., and Cosentino P.E., "Robotic Colonoscopy", in *Colonoscopy*, P. P. Miskovitz, Ed., ISBN: 978-953-307-568-6, InTech, 2011.

[137] B. Kim, S. Lee, J. Park, and J. Park, "Inchworm-like microrobot for capsule endoscope", vol. 1, pp. 458-463, 2005.

[138] Era Endoscopy S.r.l, <http://www.endotics.com/>, Accessed February 2013.

[139] Invendo Medical, <http://www.invendo-medical.com/>, Accessed February 2013.

[140] Given Imaging, Ltd., <http://www.givenimaging.com>, Accessed February 2013.

[141] P. Glass, E. Cheung, H. Wang, R. Appasamy, and M. Sitti, "A motorized anchoring mechanism for a tethered capsule robot using fibrillar adhesives for interventions in the esophagus", in *2nd IEEE RAS & EMBS International Conference on Biomedical Robotics and Biomechanics (BioRob)*, Scottsdale, Arizona, USA, vol. 1, pp. 758-764, 2008.

[142] A. Glukhovskiy and H. Jacob, "The development and application of wireless capsule endoscopy", *The International Journal of Medical Robotics and Computer Assisted Surgery*, vol. 1 (1), pp. 114-123, 2004.

- [143] P. Allen, N. Patronik, M. Zenati, and C. Riviere, "A Mobile Robot Driven by Miniature Onboard Motors for Cardiac Intervention", in *34th Annual Northeast Bioengineering Conference*, Providence, Rhode Island, vol. 9, p. 10, 2008.
- [144] M. Rentschler, J. Dumpert, S. Platt, D. Oleynikov, S. Farritor, and K. Iagnemma, "Mobile in vivo biopsy robot", in *IEEE International Conference on Robotics and Automation (ICRA)*, Orlando, Florida, USA, vol. 1, pp. 4155-4160, 2006.
- [145] M. Rentschler, S. Farritor, and K. Iagnemma, "Mechanical design of robotic in vivo wheeled mobility", *Journal of Mechanical Design*, vol. 129 p. 1037, 2007.
- [146] M. Rentschler, J. Dumpert, S. Platt, K. Iagnemma, D. Oleynikov, and S. Farritor, "Modeling, analysis, and experimental study of in vivo wheeled robotic mobility", *IEEE Transactions on Robotics*, vol. 22 (2), pp. 308-321, 2006.
- [147] M. Rentschler, J. Dumpert, S. Platt, S. Farritor, and D. Oleynikov, "Natural orifice surgery with an endoluminal mobile robot", *Surgical Endoscopy*, vol. 21 (7), pp. 1212-1215, 2007.
- [148] Sliker L. J., Wang X., Schoen J. A., and Rentschler M. E., "Micropatterned Treads for *In Vivo* Robotic Mobility", *Journal of Medical Devices*, vol. 4 2010.
- [149] <http://www.zygotebody.com/>, "Zygote Body," Zygote Body Media Group, Accessed January 2013.
- [150] Gómez-Suárez C, Bruinsma GM, Rakhorst G, Van der Mei HC, and B. HJ., "Hydrophobicity of peritoneal tissues in the rat", *J Colloid Interface Sci*, vol. 253 pp. 470-1, 2002.
- [151] G. Taylor and D. Jayne, "Robotic applications in abdominal surgery: their limitations and future developments", *The International Journal of Medical Robotics and Computer Assisted Surgery*, vol. 3 (1), pp. 3-9, 2007.
- [152] Hu Tie, Allen Peter K. , Hogle Nancy J., and Fowler Dennis L., "Insertable Surgical Imaging Device with Pan, Tilt, Zoom, and Lighting", *The International Journal of Robotics Research*, vol. 28 p. 1373, 2009.
- [153] SILS™ Port - Covidien, [www.covidien.com/hernia/access/silSPORT](http://www.covidien.com/hernia/access/silSPORT), Accessed August 2013.

- [154] E. Leach, R. Peters, and R. Rossiter, "Experimental thermal burns, especially the moderate temperature burn", *Experimental Physiology*, vol. 32 (1), pp. 67-86, 1943.
- [155] D. Henderson, "Simple Ceramic Motor... Inspiring Smaller Products", in *ACTUATOR 2006*, vol. 50, p. 10.
- [156] [http://www.newscaletech.com/doc\\_downloads/NSE-5310\\_Datasheet.pdf](http://www.newscaletech.com/doc_downloads/NSE-5310_Datasheet.pdf), "NSE-5310 Miniature Position Encoder SOIC with Zero Reference and I<sup>2</sup>C Output data sheet," Austria Microsystems AG and New Scale Technologies Inc., Accessed October 2012.
- [157] [http://www.newscaletech.com/app\\_notes/DesignNote\\_QuickTips-for-Integrating-Squiggle-Motors.pdf](http://www.newscaletech.com/app_notes/DesignNote_QuickTips-for-Integrating-Squiggle-Motors.pdf), "Design Note: Quick Tips for Integrating SQUIGGLE Motors," New Scale Technologies Inc., Accessed October 2012.
- [158] Rasso takes one step on a steel ceiling, open-loop controlled, [http://youtu.be/PaW\\_tec9BVQ](http://youtu.be/PaW_tec9BVQ), Accessed October 2012.
- [159] Rasso takes two steps on a steel ceiling, closed-loop controlled, <http://youtu.be/UGOhgKC9Mzc>, Accessed October 2012.
- [160] Rasso takes three steps on a steel ceiling, closed-loop controlled, <http://youtu.be/xFlfPP2ILdc>, Accessed October 2012.
- [161] Rasso (second prototype) moving the pads and taking one step on a steel ceiling, open-loop controlled, <http://youtu.be/eFLDIchJQdc>, Accessed October 2012.
- [162] Rasso (second prototype) crossing a 9cm-long steel plate, open-loop controlled, <http://youtu.be/J-QLk5ephNA>, Accessed October 2012.
- [163] Intra-abdominal robot on fresh porcine peritoneum, [http://youtu.be/nj\\_thwOSUKA](http://youtu.be/nj_thwOSUKA), Accessed May 2013.
- [164] Autotex Datasheet by McDermid Autotype, <http://www.macdermidautotype.com/MacDermid/media/resources/Datasheets/AUTOTEX-PDS-English.pdf>, Accessed April 2013
- [165] Patel P.S., Shepherd D.E., and Hukins D.W., "Compressive properties of commercially available polyurethane foams as mechanical models for osteoporotic human cancellous bone", *BMC Musculoskeletal Disorders*, vol. 9 p. 137, 2008.
- [166] C. Song, A. Alijani, T. Frank, G. Hanna, and A. Cuschieri, "Mechanical properties of the human abdominal wall measured in vivo

during insufflation for laparoscopic surgery", *Surgical endoscopy*, vol. 20 (6), pp. 987-990, 2006.

[167] K. Kendall, "The adhesion and surface energy of elastic solids", *Journal of Physics D: Applied Physics*, vol. 4 (8), p. 1186, 1971.

[168] Beer F. P. and Johnston Jr E. R., *Vector Mechanics for Engineers: Statics*, McGraw-Hill, 2001.

[169] J. Norton, "University of Leeds MECH 3810 Individual Project," Leeds, UK: University of Leeds, 2012.

[170] E. Garcia, J. Estremera, and P. G. De Santos, "A comparative study of stability margins for walking machines", *Robotica*, vol. 20 (6), pp. 595-606, 2002.

[171] R. B. McGhee and A. A. Frank, "On the stability properties of quadruped creeping gaits", *Mathematical Bioscience*, vol. 3 pp. 331-351, 1968.

[172] R. B. McGhee and G. I. Iswandhi, "Adaptive locomotion for a multilegged robot over rough terrain", *IEEE Transactions on Systems, Man and Cybernetics*, vol. SMC-9 (4), pp. 176-182, 1979.

[173] C. Zhang and S. Song, "Gaits and geometry of a walking chair for the disabled", *Journal of Terramechanics*, vol. 26 (3/4), pp. 211-233, 1989.

[174] C. Zhang and C. Song, "Stability analysis of wave-crab gaits of a quadruped", *Journal of Robotic Systems*, vol. 7 (2), pp. 243-276, 1990.

[175] S. Mahalingam and W. L. Whittaker, *Terrain adaptive gaits for walkers with completely overlapping leg workspaces*, Society of Manufacturing Engineers, 1989.

[176] D. A. Messuri, "Optimization of the locomotion of a legged vehicle with respect to maneuverability", The Ohio State University, PhD Thesis, 1985.

[177] S. Hirose, H. Tsukagoshi, and K. Yoneda, "Normalized energy stability margin and its contour of walking vehicles on rough terrain", in *IEEE International Conference on Robotics and Automation*, Seoul, Korea, vol. 1, pp. 181-186, 2001.

[178] P. Nagy, "An investigation of walker/terrain interaction", Carnegie Mellon University, PhD Thesis, 1991.

- [179] P. González de Santos, J. Estremera, E. García, and M. Armada, "Including joint torques and power consumption in the stability margin of walking robots", *Autonomous Robots*, vol. 18 (1), pp. 43-57, 2005.
- [180] J. C. Grieco, "Robots Escaladores. Consideraciones acerca del diseño, estabilidad y estrategias de control", University of Valladolid, PhD Thesis, 1997.
- [181] J. C. Grieco, M. Prieto, M. Armada, and P. Gonzalez de Santos, "A six-legged climbing robot for high payloads", in *Control Applications, 1998. Proceedings of the 1998 IEEE International Conference on*, vol. 1, pp. 446-450, 1998.
- [182] D. E. Orin, "Interactive control of a six-legged vehicle with optimization of both stability and energy", The Ohio State University, PhD Thesis, 1976.
- [183] D. O. Kang, Y. Lee, S. Lee, Y. S. Hong, and Z. Bien, "A study on an adaptive gait for a quadruped walking robot under external forces", in *Proceedings of the IEEE International Conference on Robotics and Automation* vol. 4, pp. 2777-2782, 1997.
- [184] B. Lin and S. Song, "Dynamic modeling, stability and energy efficiency of a quadrupedal walking machine", in *Proceedings of the IEEE International Conference on Robotics and Automation*, Atlanta, Georgia, vol. 1, pp. 367-373, 1993.
- [185] K. Yoneda and S. Hirose, "Three-dimensional stability criterion of integrated locomotion and manipulation", *Journal of Robotics and Mechatronics*, vol. 9(4) pp. 267-274, 1997.
- [186] D. Zhou, K. H. Low, and T. Zielinska, "A stability analysis of walking robots based on leg-end supporting moments", in *Proceedings of the International Conference on Robotics and Automation*, vol. 3, pp. 2834-2839, 2000.
- [187] E. Papadopoulos and D. Rey, "A new measure of tipover stability margin for mobile manipulators", in *Proceedings of the IEEE International Conference on Robotics and Automation*, Minneapolis, Minnesota, vol. 4, pp. 3111-3116, 1996.
- [188] E. Garcia and P. Garcia de Santos, "An improved energy stability margin for walking machines subject to dynamic effects", *Robotica*, vol. 23 (1), pp. 13-20, 2005.

- [189] M. Hardt and O. von Stryk, "Dynamic modeling in the simulation, optimization, and control of bipedal and quadrupedal robots", *Journal of Applied Mathematics and Mechanics/Zeitschrift fur Angewandte Mathematik und Mechanik*, vol. 83 (10), pp. 648-662, 2003.
- [190] J. Foret, O. Bruneau, and J. G. Fontaine, "Dynamics and m-stability of legged robots", *International Journal of Humanoid Robotics*, vol. 2 (1), pp. 1-20, 2005.
- [191] M. Vukobratovic and D. Juricic, "Contribution to the synthesis of biped gait", *IEEE Transactions on Biomedical Engineering*, vol. BME-16 (1), pp. 1-6, 1969.
- [192] M. Vukobratovic and B. Borovac, "Zero-moment point - thirty five years of its life", *International Journal of Humanoid Robotics*, vol. 1 (1), pp. 157-173, 2004.
- [193] K. Harada, S. Kajita, K. Kaneko, and H. Hirukawa, "ZMP analysis for arm/leg coordination", in *Proceedings of the IEEE/RSJ International Conference on Intelligent Robots and Systems (IROS)* vol. 1, pp. 75-81, 2003.
- [194] Saida T., Yokokoji Y., and Y. T., "FSW (feasible solution of wrench) for Multi-legged Robots", in *IEEE Int. Conf. on Robotics and Automation (ICRA)*, 2003.
- [195] A. Goswami, "Postural stability of biped robots and the foot-rotation indicator (FRI) point", *The International Journal of Robotics Research*, vol. 18 (6), pp. 523-533, 1999.

## **Appendix A**

### **List of published conference papers and extended abstracts, and journal papers in preparation**

Part of the research carried out for this thesis has been presented in international conferences and published in the following papers and extended abstracts:

- Conference papers:
  1. Montellano López A., Khazravi M., Richardson R., Dehghani A., Roshan R., Liskiewicz T., Morina A., Neville A., and Jayne D., "Locomotion Selection and Mechanical Design for a Mobile Intra-abdominal Adhesion-reliant Robot for Minimally Invasive Surgery", in Proceedings of the 12th Annual Conference Towards Autonomous Robotic Systems (TAROS), Sheffield, UK, 2011, vol. 6856, pp. 173-182.
  2. Montellano López A., Khazravi M., Richardson R., Dehghani A., Roshan R., Liskiewicz T., Morina A., Neville A., and Jayne D., "Force Characterisation of One Axis for an Adhesive Foot in a Climbing Robot for Minimally Invasive Abdominal Surgery", in Proceedings of the 14th International Conference on Climbing and Walking Robots and the Support Technologies for Mobile Machines (CLAWAR), University Pierre et Marie Curie (UPMC), Paris, France, 2011, pp. 705-714.
- Extended abstracts:
  1. Montellano López A., Richardson R., Dehghani A., Jayne D., and Neville. A., "Ex-vivo walking performance of a bio-inspired intra-abdominal robot for laparoscopic surgery", in Proceedings of the 26th International Conference and Exhibition on Computer Assisted Radiology and Surgery, Pisa, Italy, 2012.
  2. Montellano López A., Richardson R., Dehghani A., Roshan R., Jayne D., and Neville A., "Preliminary Adhesion Control Of A Miniature Intra-Abdominal Robot For Laparoscopic Surgery", in Proceedings of the 5th Hamlyn Symposium on Medical Robotics, London, 2012.
  3. Montellano López A., Richardson R., Dehghani A., Roshan R., Jayne D., and Neville A., "Bio-inspiration for a Miniature Robot Inside the Abdomen", in Proceedings of the 1st International

Conference on Bio-mimetic and Bio-hybrid Systems (Living Machines 2012), Barcelona, Spain, 2012, vol. 7375, pp. 380-381.

Papers 1 and 2 about the design and implementation of the robot contain information from Chapters 2, 3, 4 and 5 of this thesis and correspond to contributions 1 and 2 presented in Chapter 1.

Extended abstract 1 about the performance of the prototype contains information from Chapters 2 and 5 of this thesis and corresponds to contribution 2 presented in Chapter 1.

Extended abstract 2 about the adhesion control of the robot contains information from Chapters 2 and 5 of this thesis and corresponds to contributions 1 and 2 presented in Chapter 1.

Extended abstract 5 about the bio-inspired features of the robot contains information from Chapters 1, 2, 3, 4 and 5 and corresponds to contributions 1 and 2 presented in Chapter 1.

In all the previous papers and extended abstracts the author of this thesis carried out the research and writing while the rest of the authors supervised the work.

Journal papers in the following areas are in preparation at the time of submission of this thesis:

1. Design and implementation of a bio-inspired locomotion mechanism for an intra-abdominal adhesion-reliant robot (from an engineering perspective).
2. Development of the proof-of-concept prototype of a miniature intra-abdominal robot for laparoscopic surgery (from a surgical perspective).
3. Detachment control and stability analysis of adhesion-reliant robots walking in inverted locomotion.
4. Bio-inspiration for a miniature adhesion-reliant robot for intra-abdominal operation.

## Appendix B

### The intra-abdominal robot in the media

The application and bio-inspired design of the intra-abdominal robot drew the attention of the British media and the international media:

1. "Biomimicry: new thinking about design and engineering inspired by nature. Biomimicry case 3: the gecko surgeon" at 3'46", webcast funded by Hyundai, Smoking Pony Productions, Summer 2012.  
Video available in this link: <http://youtu.be/INpi-QJljzM>.
2. The One Show, Series 6, Designed by Nature, BBC1, Tigress Productions, April 2013.  
Video available in this link: <http://youtu.be/XTrogpss6W0>.
3. Slate.com, The Slate Group (The Washington Post Company), April 2013  
Article available in this link (Accessed May 2013):  
[http://www.slate.com/blogs/future\\_tense/2013/04/23/surgical\\_robot\\_inspired\\_by\\_a\\_frog\\_can\\_roam\\_around\\_inside\\_your\\_abdomen.html](http://www.slate.com/blogs/future_tense/2013/04/23/surgical_robot_inspired_by_a_frog_can_roam_around_inside_your_abdomen.html).
4. Yorkshire Evening Post, 2<sup>nd</sup> May 2013  
Scanned image of the article:



*“There is nothing too little for so little a creature as man. It is by studying little things that we attain the great art of having as little misery and as much happiness as possible.”*

*Samuel Johnson*